

**MULTILAYERED POLYELECTROLYTE-COATED SILICA FOR THE REMOVAL OF
TOXIC METAL IONS AND ORGANIC CONTAMINANTS: A NOVEL PROTOCOL**

BY

ZAKARIYAH ABDULKAREEM JAMIU

A Dissertation Presented to the
DEANSHIP OF GRADUATE STUDIES

KING FAHD UNIVERSITY OF PETROLEUM & MINERALS

DHAHRAN, SAUDI ARABIA

In Partial Fulfillment of the
Requirements for the Degree of

DOCTOR OF PHILOSOPHY

In

CHEMISTRY

APRIL 2017

KING FAHD UNIVERSITY OF PETROLEUM & MINERALS
DHAHRAN- 31261, SAUDI ARABIA
DEANSHIP OF GRADUATE STUDIES

This thesis, written by **ZAKARIYAH ABDULKAREEM JAMIU** under the direction of his thesis advisor and approved by his thesis committee, has been presented and accepted by the Dean of Graduate Studies, in partial fulfillment of the requirements for the degree of **DOCTOR OF PHILOSOPHY IN CHEMISTRY**.

sk. Asrof Ali

Dr. Shaikh Asrof Ali
(Advisor)

[Signature]
8/16/2017

Dr. Abdulaziz Al-Saadi
Department Chairman

[Signature]

Dr. Salam A. Zummo
Dean of Graduate Studies



15/6/17

Date

[Signature]

Dr. Hasan Ali Al-Muallem
(Member)

[Signature]

Dr. Mazen Mohammad Khaled
(Member)

[Signature]

Dr. Nisar Ullah
(Member)

[Signature]

Dr. Basheer Chanbasha
(Member)

© ZAKARIYAH ABDULKAREEM JAMIU

2017

Dedicated to my parents

ACKNOWLEDGMENTS

First, I give thanks to Allah, the generally merciful and the especially merciful, for His favors on me by aiding the successful completion of my PhD study. Indeed, all praises are due to Allah! May Allah's peace and blessing be upon His messenger- Muhammad.

I will like to express my profound acknowledgement to my thesis advisor Prof. Shaikh Asrof Ali for his tremendous supports in carrying out the work. He shall be long remembered. Great thanks to my thesis committee members Dr. Hasan Ali Al-Muallem, Dr. Mazen Mohammad Khaled, Dr. Nisar Ullah and Dr. Basheer Chanbasha for their contributions.

Furthermore, I will also like to express my special appreciation to my family- both immediate and extended- for their patience with me during the study. My appreciation also goes to friends and acquaintances from across the board and from Nigerian Community in KFUPM.

Finally, I will also like to appreciate King Fahd University of Petroleum and Minerals and the Chemistry Department for giving me the scholarship opportunity to study in her facilities. The affable nature of the Chairman of Chemistry Department, Dr. Abdulaziz Al-Saadi has been very helpful.

TABLE OF CONTENTS

ACKNOWLEDGMENTS	V
TABLE OF CONTENTS	VI
LIST OF SCHEMES	XIV
LIST OF TABLES.....	XV
LIST OF FIGURES.....	XVIII
ABSTRACT.....	XXIII
ملخص الرسالة.....	XXV
CHAPTER 1 INTRODUCTION.....	1
1.1 Literature Review.....	3
1.2 Objectives	6
1.3 Present State of the Problem	7
1.4 General Description of the Objectives and the Work Plan.....	8
1.4.1 Synthesis of Monomers and their Cyclopolymerization	8
1.4.2 Synthesis of Cross-linked Resins	14
1.4.3 Chemical and Physical Characterization.....	16
1.4.4 Preparation of Solid Supports and Layer-by-Layer (LBL) Assembly	16
1.4.5 Complexation and Metal Interaction Study	17
1.4.6 Adsorption Experiments	18
CHAPTER 2 SYNTHESIS AND APPLICATION OF A PH-TRIGGERABLE CYCLOPOLYMER CONTAINING ASPARTIC ACID RESIDUES	20
Abstract	20

2.1	Introduction.....	21
2.2	Experimental methods.....	25
2.2.1	Materials.....	25
2.2.2	Physical Method for Structural Characterization	25
2.2.3	Synthesis of Monomers.....	26
2.2.4	Synthesis of Polymers.....	29
2.2.5	Physicochemical Characterization	31
2.2.6	Applications	33
2.3	Results and Discussions.....	39
2.3.1	Synthesis and spectroscopic characterization of monomers and polymers.....	39
2.3.2	Solubility behavior	41
2.3.3	Viscosity measurements.....	42
2.3.4	Basicity Constant.....	44
2.3.5	Scale inhibition properties of the synthesized polymers.....	47
2.3.6	Phase diagrams using (PZA 9 + two equivalents of NaOH)–POE–H ₂ O (NaCl) systems.....	50
2.3.7	The Correlation of the Phase Diagrams.....	51
2.4	Conclusions.....	52
 CHAPTER 3 SYNTHESIS AND APPLICATION OF ASPARTIC ACID ALTERNATE COPOLYMERS.....		54
	Abstract	54
3.1	Introduction.....	55
3.2	Experimental Methods.....	57
3.2.1	Materials.....	57
3.2.2	Physical Methods	58
3.2.3	Procedure for 10/SO ₂ Copolymerization and Physical Characterization of 11.....	59

3.2.4	Solubility Measurements.....	63
3.2.5	Potentiometric titrations.....	63
3.2.6	Evaluation of anti-scalant behavior	63
3.2.7	Phase Compositions of PZA 13 (+ 2 equivs NaOH) – UPVE 17– H ₂ O (NaCl) Systems	64
3.3	Results and Discussions.....	66
3.3.1	Synthesis of Polymers and their Characterization.....	66
3.3.2	Solubility Behavior	67
3.3.3	Infrared and NMR Spectroscopy.....	68
3.3.4	Viscosity Measurement	70
3.3.5	Basicity Constant.....	73
3.3.6	Inhibition of CaSO ₄ Scale Formation by the Synthesized Polymer.....	74
3.3.7	Phase Diagrams using [PZA 13 + 2 equivs. NaOH] – UPVA 17 – H ₂ O (NaCl) Systems.....	79
3.3.8	The Correlation of the Phase Diagrams.	80
3.3.9	Poly(N,N-diallylaspartic acid) 6 versus Poly(N,N-diallylaspartic acid-alt-SO ₂) 13: A Comparison of the Homo- and Copolymers.....	83
3.4	Conclusions.....	86
 CHAPTER 4 SYNTHESIS AND APPLICATION OF A CROSS-LINKED RESIN WITH ASPARTIC ACID RESIDUES		
	Abstract	87
4.1	Introduction.....	88
4.2	Experimental.....	90
4.2.1	Chemicals and Materials	90
4.2.2	Physical methods.....	90
4.2.3	Synthesis	91
4.2.4	Adsorption of Pb(II) on CDAP	94

4.2.5	Regeneration of the Resin	94
4.2.6	FTIR Spectroscopy.....	95
4.3	Results and Discussion	95
4.3.1	Synthesis of cross-linked Terpolymer	95
4.3.2	FT-IR Characterization of Monomers and Polymer	96
4.3.3	Thermo-gravimetric measurement	98
4.3.4	Effect of pH on the adsorption.....	99
4.3.5	Effect of initial concentration on the adsorption of Pb(II)	100
4.3.6	Adsorption kinetics	101
4.3.7	Adsorption isotherm models	104
4.3.8	Energy of adsorption.....	106
4.3.9	Regeneration of the Resin	113
4.3.10	Structure and Surface morphology of unloaded and loaded CDAP.....	113
4.3.11	Treatment of real wastewater samples	115
4.4	Conclusion	117
CHAPTER 5 SYNTHESIS AND APPLICATION OF GLUTAMIC ACID-BASED POLYMER KEEPING INTACT THE INTEGRITY OF ALL THE THREE ORIGINAL FUNCTIONALITIES OF THE AMINO ACID		118
Abstract		118
5.1	Introduction.....	119
5.2	Experimental methods.....	122
5.2.1	Materials	122
5.2.2	Physical Methods for Structural Characterization.....	122
5.2.3	Synthesis of monomer and polymer	123
5.2.4	Solubility Measurements.....	126

5.2.5	Potentiometric titrations.....	126
5.2.6	Evaluation of anti-scalant behavior	130
5.3	Results and discussions	131
5.3.1	Synthesis and physical characterization of monomers and polymers	131
5.3.2	IR and NMR spectra	133
5.3.3	Solubility behavior	133
5.3.4	Viscosity measurements	137
5.3.5	Basicity Constants	139
5.3.6	Scale inhibition properties of the synthesized polymers	142
5.4	Conclusion	144
CHAPTER 6 SYNTHESIS AND APPLICATION OF ALTERNATE COPOLYMER OF DIALLYLGLUTAMIC ACID AND SULFUR DIOXIDE		145
Abstract		145
6.1	Introduction.....	146
6.2	Experimental.....	149
6.2.1	Materials	149
6.2.2	Physical Methods for Structural Characteruzation.....	149
6.2.3	Procedure for 4/ SO ₂ copolymerization	150
6.2.4	Conversion of 9 into 11 by NaOH.....	150
6.2.5	Solubility Measurements.....	151
6.2.6	Potentiometric Titrations	151
6.2.7	Evaluation of anti-scalant behavior	154
6.2.8	Phase Compositions of PZA 9 (+ 2 equivs NaOH) – PEG – H ₂ O (NaCl) Systems	154
6.3	Results and Discussions.....	159
6.3.1	Monomers and Polymer Synthesis	159

6.3.2	Infrared and NMR spectra	160
6.3.3	Solubility Behavior	163
6.3.4	Viscosity Measurements.....	163
6.3.5	Basicity Constants	164
6.3.6	Viscometric Titrations	166
6.3.7	Scale inhibition by the synthesized polymer.....	166
6.3.8	Phase diagrams: [PZA 9 + 2 equivs. NaOH] – PEG – H ₂ O (0.6 M NaCl)	168
6.3.9	Correlation of the Phase Diagram.....	170
6.3.10	A comparison of homopolymer 5 and copolymer 9:.....	175
6.4	Conclusions	176
 CHAPTER 7 SYNTHESIS AND APPLICATION OF GLUTAMIC ACID-BASED RESIN.....		177
	Abstract	177
7.1	Introduction.....	177
7.2	Experimental.....	180
7.2.1	Chemical and Materials	180
7.2.2	Physical Methods	180
7.2.3	Synthesis of the starting materials	181
7.2.4	Co(II) adsorption on CDAP resin.....	184
7.2.5	Regeneration experiment.....	184
7.2.6	FTIR spectra	185
7.3	Results and discussion	185
7.3.1	Resin synthesis	185
7.3.2	Characterization of the resins by FT-IR	185
7.3.3	Thermo-gravimetric analysis (TGA).....	189

7.3.4	pH dependency of the adsorption process	190
7.3.5	Initial Co(II) concentration (C _i) versus adsorption capacity	193
7.3.6	Adsorption energy	194
7.3.7	Data analyses	196
7.3.8	Morphology of fresh and Co-loaded CDAP 4 resin	207
7.3.9	Regeneration of the resin	209
7.3.10	Wastewater treatment	210
7.4	Conclusion	213

CHAPTER 8 PREPARATION OF MULTILAYERED POLYELECTROLYTE-COATED SILICA FOR THE REMOVAL OF TOXIC METAL IONS AND ORGANIC POLLUTANTS..... 214

Abstract	214
8.1 Introduction.....	215
8.2 Experimental.....	217
8.2.1 Chemical and Materials	217
8.2.2 Physical Methods	218
8.2.3 Synthesis of the Polymers	220
8.2.4 Synthesis of mesoporous silica SBA-15	221
8.2.5 Boehm Titration	221
8.2.6 Preparation of polyelectrolyte multilayers on silica.....	222
8.2.7 Cd(II) adsorption on modified Silica adsorbent.....	223
8.3 Results and Discussion	224
8.3.1 Preparation of polyelectrolyte multilayers on silica.....	224
8.3.2 Zeta Potential	227
8.3.3 ²⁹ Si CP-MAS NMR Experiments	228

8.3.4	Scanning electron microscopy (SEM) Study	230
8.3.5	Atomic Force Microscopy (AFM) Examination	232
8.3.6	Nitrogen adsorption-desorption.....	232
8.3.7	Thermo-gravimetric Analysis (TGA)	235
8.3.8	Initial concentration (Ci) versus adsorption capacity	237
8.3.9	Energy paramters	240
8.3.10	Data analyses.....	244
8.4	Conclusion	250
REFERENCES.....		252
VITAE.....		295
LIST OF PUBLICATIONS.....		296

LIST OF SCHEMES

Scheme 1.1 Butler's Cyclopolymerization to Water-soluble Polyelectrolytes	8
Scheme 1.2 Cationic Polyelectrolytes	9
Scheme 1.3 Anionic Polyelectrolytes	10
Scheme 1.4 Polyampholytes with Charge Symmetry	11
Scheme 1.5 Hydrophobically modified ionic Polymers	12
Scheme 1.6 pH-triggerable Polyelectrolytes having Residues of Aspartic Acid	13
Scheme 1.7 pH-triggerable Polyelectrolytes having Residues of Glutamic Acid	14
Scheme 1.8 Cross-linked Polymers containing Residue of Aspartic Acid	15
Scheme 2.1 Aspartic acid, polyaspartic acid and metal-ion aspartate complex.	23
Scheme 2.2 Synthesis of cyclopolymers having aspartic acid residues	24
Scheme 3.1 Aspartic acid, polyaspartate and polymer containing aspartic acid residues.	57
Scheme 3.2 Cyclopolymerization protocol in the synthesis of pH-triggerable polymers containing aspartic acid residues	65
Scheme 4.1 Synthesis of Cross-linked Polyzwitterion/anion Polymer	93
Scheme 4.2 Illustration of the resins's latitude in forming complex with metal ions.	114
Scheme 5.1 Synthesis of cyclopolymers containing glutamic acid residues.	121
Scheme 6.1 Glutamic acid, α - and β -poly(glutamic acid) and polymer containing glutamic acid residues	148
Scheme 6.2 Synthesis of cyclopolymers containing glutamic acid residues.	157
Scheme 6.3 Interchain H-bonding leading to increased hydrodynamic volume.	158
Scheme 7.1 Synthesis of pH-triggerable resin	183
Scheme 7.2 Illustration of the resin's latitude in forming complex with Co(II)	209

LIST OF TABLES

Table 2.1 Cyclopolymerization of monomer 4 and 6 to give CPE 7 and PZA 9, respectively.	30
Table 2.2 composition of the Phases of the [POE ^a + PZA 9 ^b] system (2.0 equiv. NaOH, m _{NaCl} of 0.6 mol·kg ⁻¹) at 296 K shown in figure 2.2a.	35
Table 2.3 Protonation of Polymer 11 (Z ⁼) and 10 (ZH [±] -) at 23 °C in Water and 1 M NaCl.	38
Table 2.4 Inhibition percentage over precipitation for different times in the presence of varying concentrations of the polymer 9 in a supersaturated CaSO ₄ solution at 40°C.	49
Table 3.1 Cyclocopolymerization of 10/SO ₂ to copolymer 11 at 63°C for 36 h	69
Table 3.2 Cyclocopolymerization of 5/SO ₂ to copolymer 13 at 63°C for 36 h	69
Table 3.3 Determination of Protonation constants of Polymer 15 (Z ⁼) and 14 (ZH [±] -) at 23 °C in deionized water	76
Table 3.4 Inhibition percentage over precipitation for different times in the presence of varying concentrations of the polymer 13 ^a in 3 CB supersaturated CaSO ₄ solution at 40°C	77
Table 3.5 composition of the Phases of the [UPVA ^a + PZA 8 ^b] system (2.0 equiv. NaOH, 0.6 M NaCl at 296 K shown in figure 3.4c	78
Table 3.6 Basicity constant K ₁ , molar mass and scale efficiency of inhibition of homo- and co-polymer.....	85
Table 4.1 Adsorption kinetic parameters for Lagergren models.....	108
Table 4.2 Intraparticle diffusion parameters	108
Table 4.3 Isotherm constants for adsorption of Pb ²⁺ on CDAP	109
Table 4.4 Thermodynamic and kinetic parameters for Pb ²⁺ adsorption on CDAP	109
Table 4.5 Comparism of the adsorption capacity of the resin and those of various adsorbents in literature for Pb (II) as computed by the linear Langmuir equation.....	110
Table 4.6 Comparison of Pb(II) concentrations in wastewater sample before and after the treatment with the polymer resin	116
Table 5.1 Cyclopolymerization ^a of Monomer 4.....	126

Table 5.2 Protonation of Polymer 8 (Z^-), 7 (ZH^{\pm}) and 6 (ZH_2^{\pm}) at 23 °C in deionized water and 1 M NaCl.	129
Table 5.3 Inhibition percentage over precipitation at different times in the presence of varying amounts of the polymer 6 in a supersaturated $CaSO_4$ solution at 40 °C.	130
Table 6.1 Cyclocopolymerization of 4/ SO_2 at 63°C for 36 h.....	151
Table 6.2 Protonation of Polymer 11 (Z^-) and 9 (ZH^{\pm}) at 23 °C in deionized water.....	153
Table 6.3 Inhibition percentage over precipitation for different times in the presence of varying amounts of the polymer 9 in a supersaturated $CaSO_4$ solution at 40 °C	154
Table 6.4 composition of the Phases of the [$POE^a + PZA^b$] system (2.0 equiv. NaOH, 0.6 M NaCl) at 296 K Shown in figure 7a.....	156
Table 6.5 Values for Parameter A^a in eqs 5 and 6 along with the $rmsd^b$ of the Model from the Experimental Data of the Partition Coefficients	158
Table 6.6 Basicity constants K_i and scale efficiency of inhibition of homo- and co-polymer	168
Table 7.1 Mathematical Equations for all the Models used in this Study.	195
Table 7.2 Thermodynamic and kinetic parameters for Co(II) adsorption on resin 4.....	196
Table 7.3 Isotherm parameters for Co(II) adsorption on CDAP 4	201
Table 7.4 Comparison of the adsorption capacity of the current resin with that of various adsorbents for Co(II) at 298 K.....	202
Table 7.5 Adsorption kinetic parameters for pseudo first and second order models.	206
Table 7.6 Intraparticle diffusion parameters.	206
Table 7.7 Industrial wastewater sample treated with the resin.	212
Table 8.1 Pore diameters (D_p), pore volumes (P_v), surface areas (S_{BET}) and zeta potentials (Z_p) for the mesoporous SBA-15 and its surface modified forms	228
Table 8.2 Comparison of Cd(II) adsorption performance of SBA-15/SBA-15-PDDA-PDE for 12hrs contact time with 50mg adsorbent	239
Table 8.3 Dual Cation/anionic Performance of SBA-15/SBA-15-PDDA-PDEH for Organic Pollutants.....	240
Table 8.4 Mathematical equations for all the models used in this study	241

Table 8.5 Thermodynamic and kinetic parameters for Cd(II) adsorption	243
Table 8.6 Isotherm parameters for Cd(II) adsorption	247
Table 8.7 Comparison of the adsorption capacity of the current adsorbent with that of various adsorbents for Cd(II) at 298 K.....	248
Table 8.8 Adsorption kinetic parameters for pseudo first and second order models	250

LIST OF FIGURES

<p>Figure 2.1 ¹H NMR spectrum of (a) 4 (b) 6, (c) 7, and (d) 9 (+NaCl), (e) bottom layer (system 3, supplementary data : Table S1) in D₂O.....</p>	36
<p>Figure 2.2 ¹³C NMR spectrum of (a) 4, (b) 6, (c) 7, and (d) 9 (+NaCl) in D₂O.</p>	37
<p>Figure 2.3 (a) TGA curve of PZA 9; Utilizing a viscometer, 30 °C: the viscosity behavior of (b) (+) CPE 7 (entry 2, Table 2.1) in (i) ■ salt-free water and (ii) □ 0.1 M NaCl and of (±) PZA 9 (prepared from entry 2, Table 2.1) in (iii) ▲ the presence of one equivalent of NaOH in 0.1 M NaCl; (c) (±) PZA 9 (entry 9, Table 2.1) in (i) ▲ two equivalents of NaOH, salt-free water, (ii) ·one equivalent of NaOH, salt-free water, (iii) Δ two equivalents of NaOH, 0.1 M NaCl, (iv) ◆ 0.1 M HCl, (v) ○ one equivalent of NaOH, 0.1 M NaCl, (vi) ■ 1.5 M NaCl, and (vii) □ 1.0 M NaCl</p>	41
<p>Figure 2.4 Figure 2.4 (a) Plot for the apparent log K₂ versus degree of protonation (̢) in ■ salt-free water (entry 3, Table 2.3) and □ 1 M NaCl (entry 2, Table 2.3); (b) Trends in precipitation of a supersaturated solution of CaSO₄ with addition of (5, 15, and 20 ppm) and absence of PZA 9; (c) phase diagram (■ and □ represent data obtained by, respectively, the NMR and dilution methods) at 296 K of 0.6 M NaCl containing PZA 9 (treated with two equivalents of NaOH)–POE at 296 K; and (d) correlation of phase diagram of PZA 9 (two equivalents of NaOH)–POE–H₂O (0.6 M NaCl).....</p>	46
<p>Figure 3.1 ¹H NMR spectrum of (a) 10, (b) 5, (c) 11, (d) 13 (in the presence of KI), and (e) top layer (System 1, Table 3.5) in D₂O.....</p>	61
<p>Figure 3.2 ¹³C NMR spectrum of (a) 10, (b) 5, (c) 11 and (d) 13 (in the presence of KI) in D₂O.</p>	62
<p>Figure 3.3 (a) TGA curve of PZA 13; Utilizing a viscometer, 30 °C: the viscosity behavior of (b) (+) CPE 11 (entry 4, Table 3.1) in (i) ■ salt-free water and (ii) ● 0.1 M HCl and (iii) ▲ 0.1 M NaCl; (c) (±) PZA 13 (entry 1, Table 3.2) in (i) ■ 1 equivs NaOH, salt-free water, (ii) □ 2 equiv NaOH, salt-free water; (iii) ● 2 equivs NaOH, 0.1 M NaCl, (iv) ○ 1 equivs NaOH, 0.1 M NaCl, (v) ▲ PZA 13 (prepared from entry 4, Table 3.1) 1 equiv NaOH, 0.1 M NaCl.</p>	72

Figure 4.1 IR Spectra of cross-linked resins (a) CPZA 3 (b) CDAP 4 and (c) CDAP 4 loaded with Pb ²⁺	97
Figure 4.2 TGA curve of CDAP 4.....	98
Figure 4.3 Effect of pH on the adsorption of Pb ²⁺ ions.....	100
Figure 4.4 (a) Effect of initial Pb ²⁺ concentrations on percent Pb ²⁺ removal (b) Effect of initial concentrations of Pb ²⁺ on the adsorption capacity.	101
Figure 4.5 (a) Lagergren first-order plots, (b) Pseudo second-order plots and (c) and Weber-Morris intraparticle diffusion plots at 40ppm for the adsorption of Pb ²⁺ on CDAP....	111
Figure 4.6 (a) Arrhenius and (b) Thermodynamic plots for Pb ²⁺ adsorption on CDAP 4.....	112
Figure 4.7 SEM image and the corresponding EDX spectrum of (a) unloaded CDAP 4 and (b) CDAP loaded with Pb ²⁺	115
Figure 5.1 TGA curve of PZA 6.	132
Figure 5.2 ¹ H NMR spectrum using trimethylsilylpropionate-2,2,3,3-d ₄ (TSP) as internal standard of (a) 4, (b) 6 (+NaCl), (c) 8 in D ₂ O.....	135
Figure 5.3 ¹³ C NMR spectrum using trimethylsilylpropionate-2,2,3,3-d ₄ (TSP) as internal standard of (a) 4, (b) 6 (+NaCl), (c) 8 in D ₂ O.....	136
Figure 5.4 The viscosity behavior of sample derived entry 2, Utilizing a viscometer, 30 °C: (i) ■ (=) 8 in deionized water, (ii) □ (± -) 7 in deionized water, (iii) ▲ (=) 8 in 0.1 M NaCl, (iv) Δ in 1.0 M NaCl, (v) * (± -) 7 in 0.1 M NaCl, (vi) ◇ (± -) 7 in 1.0 M NaCl, (vii) ● (±) 6 in 1.5 M NaCl, (viii) ○ (±) 6 in 1.0 M NaCl and (ix) ○ (±) 6 in 0.75 M NaCl.....	138
Figure 5.5 Plot of η versus apparent ■ log K ₁ in deionized water (entry 1, Table 2), □ log K ₂ in deionized water (entry 1, Table 2) and ● log K ₃ in 1 M NaCl (entry 1, Table 2).....	141
Figure 5.6 Trends in precipitation of a supersaturated solution of CaSO ₄ with addition of (5, 10, and 20 ppm) and absence of PZA 6. Inset represents the data for a shorter time scale of 1000 min.....	143
Figure 6.1 TGA curve of PZA 9 (entry 2, Table 6.1).	160

Figure 6.2 ¹ H NMR spectra of (a) 4, (b) 9 (+NaI) and (c) 11 in D ₂ O (referenced using signal of trimethylsilylpropionate-2,2,3,3-d ₄ (TSP) at 0 ppm of as internal standard).....	161
Figure 6.3 ¹³ C NMR spectra of (a) 4, (b) 9 (+NaI) and (c) 11 in D ₂ O (referenced using δ67.4 ppm of dioxane as external standard).....	162
Figure 6.4 (a) The viscosity behavior of sample derived entry 2, Table 1 Utilizing a viscometer, 30 °C: (i) ■ (± -) 10 and (ii) □ (=) 11 in deionized water; (b) (i) □ (=) 11 and (ii) ■ (± -) 10 in 0.1 M NaCl; (c) Plot for the apparent (i) log K ₁ versus degree of protonation (̄) (entry 3, Table 2) and (ii) log K ₂ versus ̄ for PDA 11 (derived from entry 2, Table 1) in deionized water (entry 3, Table 2); (d) Reduced viscosity (̄ _{sp} /C) at 30 °C of a 0.00858 M (i.e. 0.25 g/dL) solution of polymer PZA 9 (ZH ₂ [±]) in deionized water (●) versus equivalent of added NaOH. Distribution curves (dashed lines) of the various ionized species [■ 9 (ZH ₂ [±]), □ 10 (ZH [±] -), Δ 11 (Z ⁼)] calculated using eq 2 (Scheme 2) and pH of the solutions in deionized water at 23°C.....	172
Figure 6.5 Trends in precipitation of a supersaturated solution of CaSO ₄ with addition (5, 10, 15, 30 ppm) and absence of PZA 9 (treated with NaHCO ₃). Inset showing the precipitation behavior in a shorter time scale of 100 min.	173
Figure 6.6 ¹ H NMR spectrum of (a) bottom layer and (b) top layer of (System 5, Table 4) in D ₂ O (+ K ₂ CO ₃).	174
Figure 6.7 (a) Phase diagram [■ and □ represent data obtained by respective NMR and turbidimetric method] at 296 K of 0.6 M NaCl containing PZA 9 (treated with 2 equivs. NaOH)-PEG at 296 K; (b) Correlation of phase diagram of PZA 9 (2 equiv. NaOH)-PEg-H ₂ O (0.6 M NaCl).	175
Figure 7.1 IR Spectra of (a) 3 (b) unloaded 4 and (c) Co(II) loaded 4	187
Figure 7.2 IR Spectra of cross-linked resins (a) original (b) used and (c) regenerated CDAP 4	188
Figure 7.3 TGA curve of resin 4.....	189
Figure 7.4 TGA curves of original, Co-loaded and regenerated CDAP 4 resin.....	190

Figure 7.5 Initial pH-dependency of the adsorption of Co(II).	192
Figure 7.6 Distribution of cobalt ionic species as a function of pH [239]	192
Figure 7.7 (a) Effect of initial Co(II) concentrations on percent Co(II) removal, (b) Effect of initial concentration of Co(II) on the adsorption capacity.	193
Figure 7.8 (a) Arrhenius and (b) Thermodynamic plots for Co (II) adsorption on CDAP 4.....	196
Figure 7.9 (a) Langmuir (b) Freundlich and (c) Temkin adsorption isotherms for Co ²⁺ adsorption on CDAP 4 for various initial concentrations at 298K.	200
Figure 7.10 Comparison of experimental and predicted adsorption isotherms for Co (II) according to: (a) Langmuir–Freundlich model (b) Redlich–Peterson model	202
Figure 7.11 For Co (II) adsorption on resin 4 at 298 K: (a) Lagergren first-order plots, (b) Pseudo second-order plots and Weber-Morris intraparticle diffusion plots: (c) at various concentrations (d) temperatures.	205
Figure 7.12 SEM image and EDX spectrum of (a) unloaded 4 and (b) Co(II) loaded 4.....	208
Figure 7.13 Adsorption/desorption with repeated cycles as a measure of performance and efficiency of the resin.....	210
Figure 8.1 Synthesis of mesoporous materials through cooperative self-assembly	226
Figure 8.2 Modification scheme of SBA 15 mesoporous-silica with PDDA and PDE	227
Figure 8.3 ²⁹ Si CP-MAS NMR spectra of the SBA-15 and its modified forms: SBA-15-PDDA and SBA-15-PDDA-PDE	230
Figure 8.4 SEM images of the SBA-15 and its modified forms: (a) as-fabricated; (b) after first LBL deposition of PDDA; (c) after second LbL deposition of PDE on (b); and (d) 200 nm view of the silica particles in (c).....	231
Figure 8.5 AFM tapping mode images of (a) as-synthesized SBA-15 material; (b) SBA-15 material after LBL deposition of PDDA/PDE	232
Figure 8.6 Nitrogen adsorption–desorption isotherms of SBA-15 and LBL-modified SBA-15.....	234
Figure 8.7 BJH desorption pore size distributions of SBA-15 and LBL-modified SBA-15	235
Figure 8.8 TGA profiles of SBA-15 and LBL-modified SBA-15.....	236

Figure 8.9 Effect of initial Cd(II) concentrations on Cd(II) adsorption capacity.....	238
Figure 8.10 Effect of initial concentration of Cd(II) on the adsorption capacity	239
Figure 8.11 (a) Activation (b) Thermodynamic Energy plots for the hybrid adsorbent.....	243
Figure 8.12 (a) Langmuir (b) Freundlich and (c) Temkin adsorption isotherms for Cd(II) adsorption.....	246
Figure 8.13 (a) Lagergren first-order plots and (b) Pseudo second-order plots at 298 K for various initial concentrations	249

ABSTRACT

Full Name : [Zakariyah Abdulkareem Jamiu]
Thesis Title : [Multilayered Polyelectrolyte-coated Silica for the Removal of Toxic Metal Ions and Organic Contaminants: A Novel Protocol]
Major Field : [Chemistry]
Date of Degree : [April 2017]

A number of pH-triggerable ionic polymers with different type of charges and their densities on the polymer backbone have been prepared through Butler's cyclopolymerization process using N,N-diallylaspartic and N,N-diallylglutamic acid hydrochloride salt monomers. SO₂ spacer was introduced in similar polymerization protocol to obtain their respective copolymers. These cationic, anionic, and zwitterionic polymers having reactive groups on the pendants have been utilized to explore the complexation behavior between the synthesized polycation and polyanion. The basicity constants, viscosity and solubility behaviors of the polymers were determined. Anti-scaling behavior of some of the polymers were evaluated by studying their inhibition effects on the precipitation of CaSO₄ from its supersaturated solution. These pH-triggerable homo- and co-polymers have demonstrated to be effective anti-scaling agents reaching up to 100% for the duration of the study. Furthermore, the aqueous two-phase systems (ATPSs) of the pH-triggerable polymers and polyoxyethylene have been studied. The transformation of these water-soluble polymers to insoluble forms within a workable pH window makes them a special kind of recyclable ATPSs for advanced application in the separation of protein and other biomolecules.

Novel resins of these polymers were equally obtained by Butler's cyclopolymerization of the respective monomers with the aid of cross-linker 1,1,4,4-tetraallylpiperazinium dichloride and with or without sulfur dioxide. The resins were found to be effective generally in the removal of toxic metal pollutants with Pb(II) and Co(II) as specific examples.

Finally, these novel cationic, anionic, and zwitterionic polymers having reactive groups on the pendants have been utilized for the formation of multilayer coating on silica adsorbents by layer-by-layer (LBL) assembly. The efficiency and binding capacity of the polyelectrolyte complexes have been examined. The mechanically and thermally stable coated multilayered polyelectrolyte complex having relatively large surface areas have been used for the effective removal of toxic cadmium metal ions from aqueous solutions. In addition, some of the ionic polymers were also hydrophobically modified before LBL assembly. This has imparted the new material with the ability to attract and remove organic contaminants (methylene blue and eriochrome black T) from model and industrial wastewaters. Overall, the solid adsorbents coated with the synthesized ionic polymers containing interesting blends of carboxylate as well as trivalent nitrogens have imparted excellent complexation properties in water treatment processes.

ملخص الرسالة

الاسم الكامل: زكريا عبد الكريم جاميو

عنوان الرسالة: متعدد الطبقات من بوليميرات متعددة الشحنة المغلفة للسيليكا لإزالة الأيونات المعدنية السامة والملوثات العضوية: بروتوكول مميز ومبتكر

التخصص: الكيمياء

تاريخ الدرجة العلمية: أبريل 2017

حُضر عدد من البوليميرات الأيونية المتأثرة بالحموضة مع نوع مختلف من الشحنات وكثافتها على السلسلة الأساسية للبوليمير من خلال عملية بوتلر في البلمرة الحلقية باستخدام N,N-diallylaspartic وملح N,N-diallylglutamic acid hydrochloride كمنوميرات.

أدخل ثنائي أكسيد الكبريت كفاصل في بروتوكول بلمرة مماثل للحصول على البوليميرات المرافقة. وقد استخدمت هذه البوليميرات الحاوية على متعلقات موجبة الشحنة و سالبة الشحنة ومتعددة الشحنة لاستكشاف السلوك المعقد بين متعدد الشحنات السالبة ومتعدد الشحنات الموجبة.

حُدثت ثوابت القلوية و اللزوجة وسلوكيات الذوبان للبوليميرات. فُيُم سلوك منع التكلُّس لبعض البوليميرات من خلال دراسة آثار تثبيطها لترسيب كبريتات الكالسيوم من محلول فوق مشبع. وقد أثبتت هذه البوليميرات (المتجانسة والمشاركة) فعاليتها كعملاء لمنع التكلُّس بنسبة 100% خلال مدة هذه الدراسة. وعلاوة على ذلك تمت دراسة أنظمة ثنائية الطور المائي (ATPSs) للبوليميرات المتأثرة بالحموضة و البولي أوكسي اثيلين. التحول لهذه البوليميرات القابلة للذوبان بالماء الى اشكال غير قابلة للذوبان ضمن مجال محدد من الباهاء أكسيها نوع خاص من إعادة التدوير (ATPSs) للتطبيقات المتقدمة في فصل البروتين والجزيئات الحيوية الأخرى.

حُصل على راتنجات مبتكرة بواسطة عملية بوتلر في البلمرة الحلقية للمنوميرات المتوافقة بمساعدة الرابط 1,1,4,4-tetraallylpiperazinium dichloride و مع أبو بدون ثنائي أكسيد الكبريت. وُجد أن هذه الراتنجات فعالة عموماً في إزالة الملوثات المعدنية السامة كالرصاص (II) و الكوبالت (II).

و أخيراً أستخدمت هذه البوليميرات الفريدة ذات المتعلقات الموجبة الشحنة و السالبة الشحنة و متعددة الشحنة لتشكيل طلاء متعدد الطبقات على سطح الغمزاز السلكا بواسطة التركيب طبقة طبقة. فُحصت كفاءة و سعة معقدات متعدد الشحنات. و استخدم متعدد الشحنات المطلي على السلكا للحصول على مساحة سطحية كبيرة والذي يعتبر ثابت حرارياً و ميكانيكياً في إزالة شوارد معدن الكاديوم السامة من المحاليل المائية. بالإضافة إلى ذلك، عُدلت خواص الكره للماء لبعض البوليميرات الشارديّة قبل عمليّة التجميع طبقة طبقة. وقد أعطى هذا الإجراء الأخير القدرة على جذب وإزالة الملوثات العضوية كـ methylene blue و erichrome black T من مخلفات المياه الصناعيّة.

عموماً فإن معالجة وتعديل الممتزات الصلبة بالبوليميرات الأيونية المصنعة الحاوية على مزيج من زمر الكربوكسيلات و النتروجينات ثلاثية التكافؤ قد أعطت خصائص تعقيد في عمليات معالجة المياه.

CHAPTER 1

INTRODUCTION

The wastewater reuse has long been a potential intervention strategy in addressing water scarcity in the eastern Mediterranean countries such as Saudi Arabia [1]. Wastewater containing toxic materials is a matter of great concern due to its negative impact on the environment and human health. Non-renewable ground water aquifers [2], the source of over 80% of Saudi Arabia's water supply, is estimated to contain only about 15-25 year-supply [3]. In response to the alarming statistics of rapid population growth, increased urbanization, and more stringent health based regulations [4,5], wastewater recycling came to the limelight and it has the potential to reduce total ground water withdrawals as a future water supply option in countries like Saudi Arabia.

In recent time, concerted efforts have led to the development of promising techniques such as adsorption [6], precipitation [7], dialysis [8], ion exchange [9], reverse osmosis [10] and extraction [11] for the removal of metal contaminants from non-usable water resources. Among all these developed systems, the adsorption process is one of the most widely used processes which involves the use of various solid adsorbents like activated carbon [12], organic ion exchange polymers [12], and numerous chemically anchored organic functionalities on silica gel [12,13], clays [14], and mesoporous silica [15–18]. New understanding of mechanisms on the physicochemical sorption processes for the removal of organic and inorganic contaminants in wastewater has facilitated the

optimization of sorbent properties [19,20]. Energy of adsorption of organic contaminants to the adsorbed surface is governed by hydrophobic, dispersion, and weak dipolar forces between the adsorbent and the adsorbed species [21].

The use of adsorption process in purification technology is extremely important; but this process is still inconvenient for highly contaminated aqueous sample purification due to its limited density of surface active sites, the activation energy of sorptive bonds, the slow kinetics and non-equilibrium of sorption in heterogeneous systems, and the mass transfer rate to the sorbent surface [22]. Moreover, this technology removes metals and other organic contaminants non-specifically, which constitutes a great difficulty to recover the metal and reuse. The method of ion exchange to remove heavy metals in wastewater is expensive which limits its application [23]. These limitations and drawbacks associated with these current technologies have led to an unprecedented need for new technologies, which can selectively and efficiently remove heavy metals and organic contaminants from aqueous resources.

This research proposal will develop a reusable multilayer adsorbent system using various novel polyelectrolytes with a hope to create high surface area to volume ratio to overcome many of these present intrinsic limitations. The polyelectrolytes will have the ability to form stable ionic cross-linked polyelectrolyte complexes, and can capture heavy metals by their accessible metal anchoring ligands and organic components by physical attractive forces. In addition, one can easily recover heavy metals from the multilayer polyelectrolyte adsorbents and can be reused.

To achieve this proposed research goal, we will synthesize a series of cationic, anionic, zwitterionic, and ampholytic polymers using Butler's cyclopolymerization protocol involving a variety of specialty diallylammonium salt monomers [24–26]. The ionic polymers, most of which are pH-triggerable, and have different type of charges and their densities on the polymer backbone, and reactive group on the pendent will ultimately be utilized for the formation of multilayer coating on silica adsorbents by layer-by-layer [27–29]. The materials having large surface areas coated with polyelectrolytes and their hydrophobically modified counterparts will be exploited in removing toxic metal ions and organic contaminants from aqueous solutions. Although it is not within the scope of the current work, these polyelectrolytes may as well serve to remove metal in the anionic form (as in arsenate, chromate, etc). The current proposal will ultimately build a novel technology for water treatment.

1.1 Literature Review

The interaction of oppositely charged polyelectrolytes to form polyelectrolyte complexes is a topic of considerable interest [30,31]. Polyelectrolyte complexes have the potential to be used in a wide variety of applications including: separation membranes [32,33], immobilization of enzymes [34], drug carriers [35], gene delivery tools [36] and protein purification [37]. Combining solutions of oppositely charged polyelectrolytes can lead to formation of layer-by-layer assemblies [30,38]. Substrate with polyelectrolyte complexes is typically achieved by either layer-by-layer assembly or complex coacervation. The layer-by-layer assembly, introduced by Decher [29] involves sequential deposition of polyanions

and polycations, and allows excellent control of the thickness and composition of the layers [30].

The polyelectrolytes can be easily attracted by the oppositely charged multivalent ions such as Ca^{2+} , Ba^{2+} , Sr^{2+} , Pb^{2+} , Cu^{2+} etc, and form stable ionically cross-linked connections by inter-chain ionic bonding resulting in the formation of a three-dimensional cross-linked network [39,40]. The heavy metals are toxic, non-biodegradable and can accumulate in the human body causing a variety of diseases and disorders [41–43].

Adsorption process is one of the most attractive techniques in removing toxic metal ions due to the availability of different types of low-cost and environment-friendly adsorbents [44,45]. The use of biopolymers as adsorbents has been described in a recent published book [46], which reports the use of chitosan-based bio-adsorbents for the separation and recovery of pollutants from wastewater. In recent years, chitosan based derivatives were successfully utilized for removal of anions from waste water [47,48]. Chitosan intercalated montmorillonite having improved pore-structure has been prepared and used as adsorbent for dyes [49]. Qi and Su have evaluated the sorption of Pb(II) onto chitosan nanoparticles (40–100 nm) prepared by ionic gelation of chitosan and tripolyphosphate [50]. The contributions of carbon-based nanomaterials have been critically assessed for broad range of environmental applications such as sorbents for environment pollution prevention [51].

Inorganic and/or organic polymer hybrid adsorbents have been widely investigated; their efficacies in metal ion removal have been attributed to the formation of a stronger chemical bonding between M^{n+} and, for instance, amine motifs in the hybrid materials [52–54]. Recently, researchers have focused on the syntheses of zwitterionic cross-linked

inorganic and/or organic hybrid materials for the removal of heavy metal ions via electrostatic effects [55,56]. Considerable attention has been given to synthesize chelating agents containing amino methyl phosphonate motif owing to its extraordinary chelating properties in extracting heavy metal ions from waste water [57].

The removal of heavy metal ions from aqueous solution has involved the use of various solid adsorbents like activated carbon, organic ion exchange polymers [12], and numerous chemically anchored organic functionalities on silica gel [12,58], clays and mesoporous silica [13–16]. The applications of activated carbon in water and waste water treatment include reduction in organic contaminant [59], polycyclic aromatic hydrocarbons [60], or naphthalene [61]. Zeolites are effective sorbents and ion-exchange media for metal ions [58]. Zeolite NaY nanocrystals were hydrothermally grown on polyelectrolyte-coated three dimensionally ordered macroporous activated zirconia [62].

Amine (NH_2) group grafted on a mesoporous SBA-15 silica surface has been shown to increase the efficiency for adsorption of heavy metal ions [63]. Due to the regular pore system and controllable pore size, mesoporous silica is acknowledged as supports of adsorption for the extremely large surface areas and shape selective properties [64]. Recent articles described the synthesis of MCM-41 (LUS-type) silica membranes having its surface functionalized with aminopropyl and sulfonate groups to separate valuable and/or toxic metal species from aqueous media [65,66]. The functionalized mesoporous silica (e.g. SBA-15) was found to increase effectiveness for the removal of Cu(II) from aqueous solution due to the chelating nature of the porphyrin-bridging group [67]. A review article [68] described the use of mesoporous silica and organically-modified silica-based materials

for removal of inorganic (such as heavy metal species, toxic anions, radionuclides) and a wide range of organic pollutants from aqueous solution.

1.2 Objectives

The proposed study will have the following objectives:

- I. To design, synthesize and characterize a variety of ionic polyelectrolytes/and or their SO₂ copolymers as outlined in Schemes 1-7.
- II. To study their polyelectrolyte properties, especially their ability to form polyelectrolyte complexes (PEC's) with each other.
- III. To study their use in the formation of multilayers, including the effects of polyelectrolyte composition and concentration on morphology, and strength of the resultant coated substrates.
- IV. To study the interaction of the individual polyelectrolyte and resultant multilayered polyelectrolyte coated substrates with heavy metal ions (e.g. Pb(II), Co(II), Cd(II), etc.,) and their feasibility for effective removal of organic contaminants from aqueous samples.
- V. To synthesize some cross-linked resins for comparative study with the multilayered polyelectrolyte coated substrates.

1.3 Present State of the Problem

Currently the method of ion exchange is comprehensively employed to remove heavy metals in water bodies, but the process appears to be expensive which limits its application [23]. This situation prompted researchers to explore other methods like direct sorption. Direct sorption of organic contaminants to the adsorbed surface is usually driven by fundamental hydrophobic, dispersion, and weak dipolar forces that determine sorption energies in conventional systems [21]. While the adsorption process is revolutionary in terms of uses, this process is still inconvenient for highly contaminated aqueous sample purification due to its limited density of surface active sites, the activation energy of sorptive bonds, the slow kinetics and non-equilibrium of sorption in heterogeneous systems, and the mass transfer rate to the sorbent surface [22].

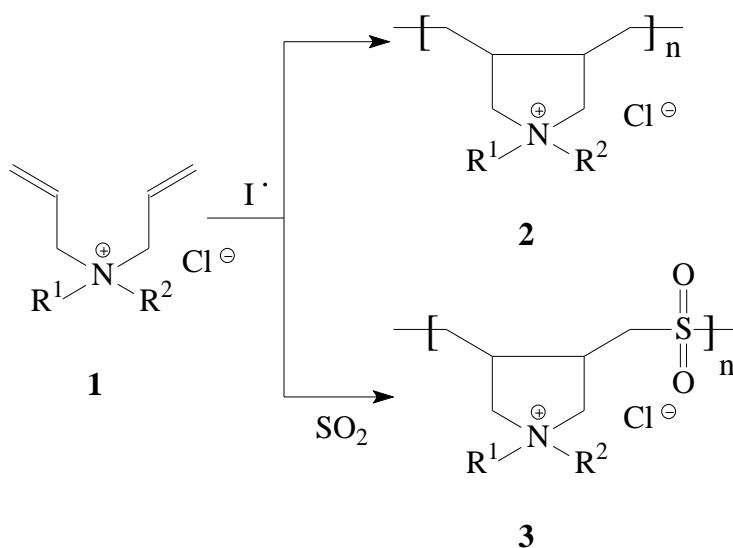
Moreover, this technology removes metals and other organic contaminants non-specifically, which constitutes a great difficulty to recover the metal and reuse. These limitations and draw backs associated with these current technologies have led to an unprecedented need for new technologies, which can selectively and efficiently remove heavy metals and organic contaminants from aqueous resources.

In this study, coated solid materials having relatively large surface areas will be used for the removal of toxic heavy metal ions and organic contaminants from aqueous solutions. Some of the polymers will be hydrophobically modified so as to attract and remove organic contaminants from industrial and non-usable waste water.

1.4 General Description of the Objectives and the Work Plan

1.4.1 Synthesis of Monomers and their Cyclopolymerization

A variety of ionic polymers **2** and/or copolymer **3** will be synthesized via Butler's cyclopolymerization [24,25,69] of diallylammonium salts monomers **1** as depicted in Scheme 1.1.



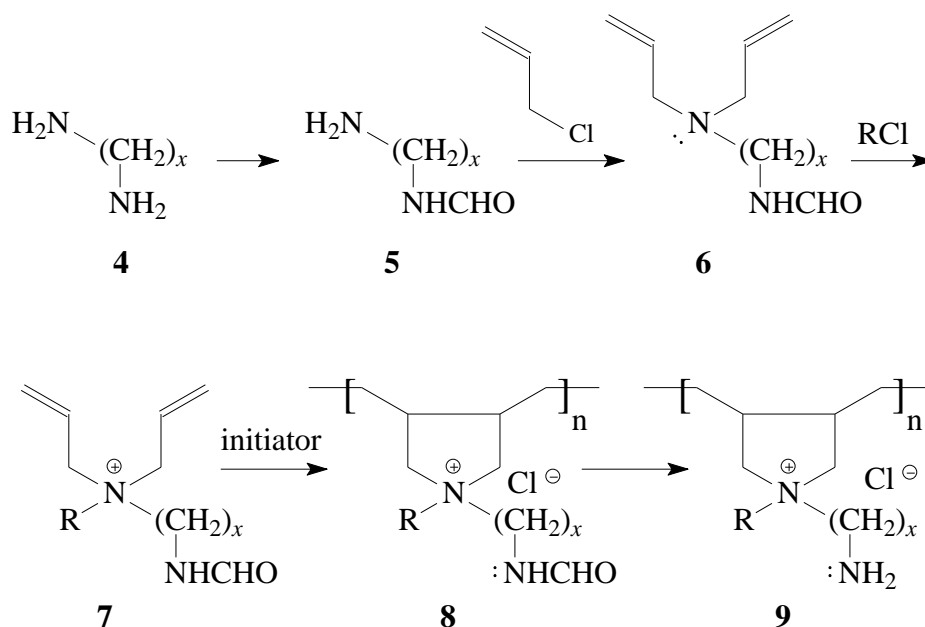
Scheme 1.1 Butler's Cyclopolymerization to Water-soluble Polyelectrolytes

The hydrophilic monomers required for the cyclopolymerization will be synthesized and subjected to undergo homocyclopolymerization or cocyclopolymerization with SO_2 or a hydrophobic comonomer as presented in Schemes 1.2 - 1.7.

Polymers **8** and **9** will be synthesized in our laboratory (Scheme 1.2). Specialty monomer **10** will be synthesized from the diamine **4** of suitable hydrocarbon spacer 'x'.

The diamine, after selective protection of one end with formyl group, will be elaborated to give the required monomer **7**. A similar synthetic procedure has been reported recently [70].

Monomer **7** on cyclopolymerization will lead to polymer **8**, which upon hydrolysis will be converted into polymer **9**. The interesting polymer **9** will have cationic backbone as well as a basic ligand NH_2 in the pendent, which may potentially play dual role as ligand NH_2 as well as cation NH_3^+ , which will be of tremendous importance to bind the metal ions and cross-linked with oppositely charged reactive polyelectrolytes (*vide infra*).

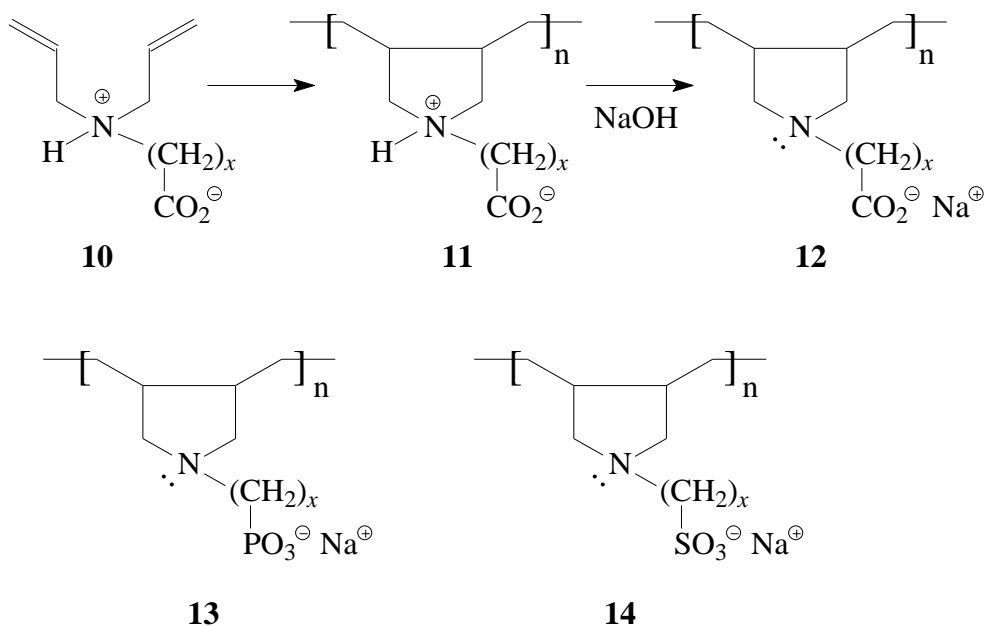


Scheme 1.2 Cationic Polyelectrolytes

While polymerization of carbo-, phospho- or sulfo-betaine (zwitterions) (M^\pm) monomers having charges of both algebraic signs in the same molecular framework leads to

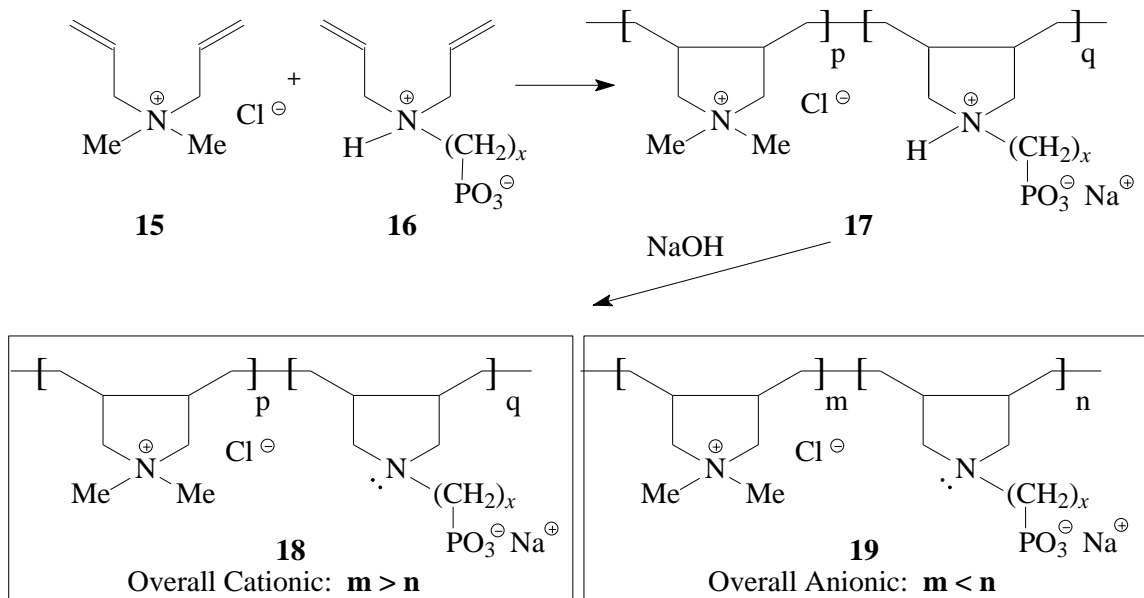
polybetaines (polyzwitterions) [25,26], the presence of both M^+ and M^- with varying proportions in the same polymer chain constitutes a polyampholyte with or without charge symmetry. Cyclopolymerization reaction of zwitterionic diallylammonium monomers or their copolymerizations with sulfur dioxide has been an efficient method for the synthesis of polyzwitterions [71–74].

A series of anionic polyelectrolytes **12-14** (Scheme 1.3) of suitable 'x' value will be synthesized using procedures as described [72,75,76]. For instance, zwitterionic monomer **10** will be converted to its zwitterionic polymer **11** which on basic treatment would generate the pH-triggerable anionic polyelectrolyte **12**.



Scheme 1.3 Anionic Polyelectrolytes

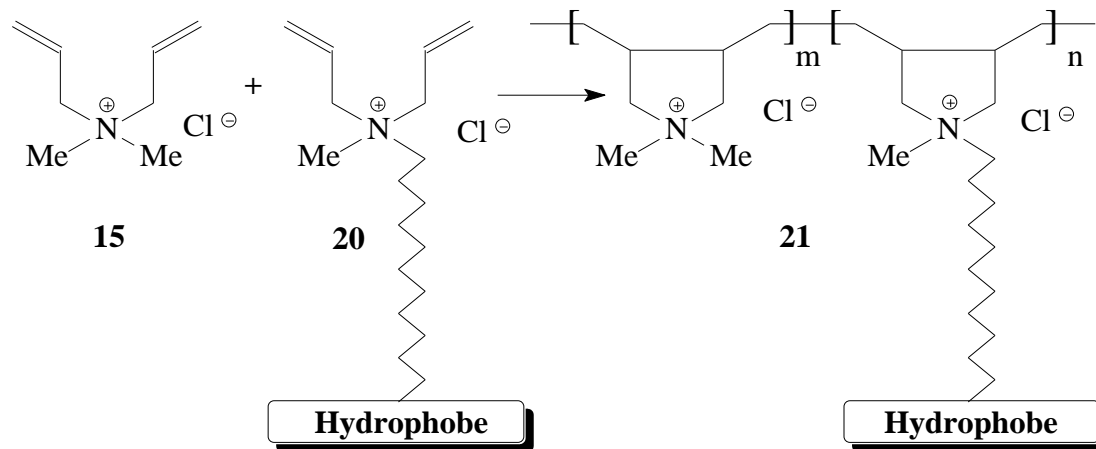
Scheme 1.4 outlines the synthesis of a novel series of polyampholytes using copolymerization of cationic monomer **15** and zwitterionic monomer **16**. The resulting cationic/zwitterionic copolymer **17** upon treatment with NaOH will be converted into polyampholytes with or without charge symmetry. Polyampholytes **18** and **19** will have excess cationic and anionic charges in the polymer backbone. This charge imbalance is expected to have implications in their adsorption behaviors on the solid surfaces.



Scheme 1.4 Polyampholytes with Charge Symmetry

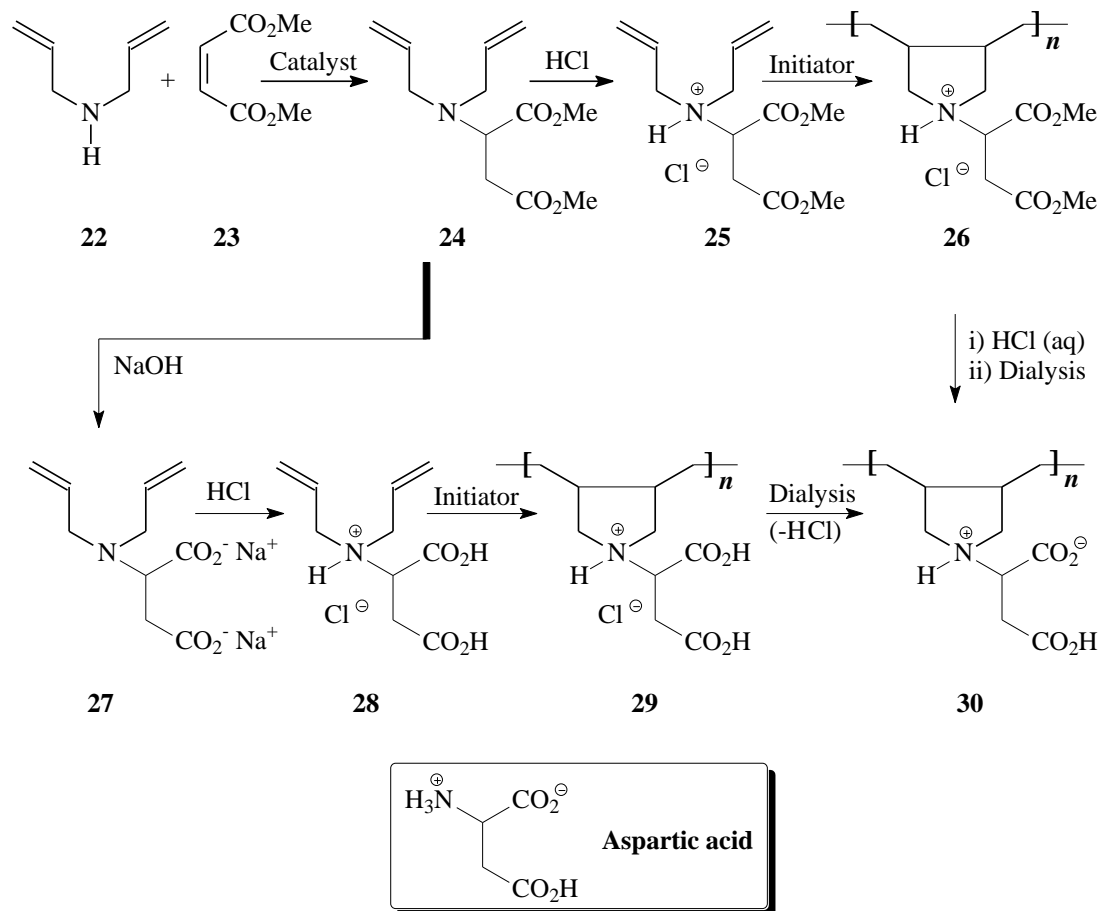
There are several reports [77–81], which describe the synthesis of associating ionic copolymers **21** prepared by Butler’s cyclocopolymerization of hydrophilic monomers **15** with a few mol% of hydrophobic monomers **20** (Scheme 1.5). The hydrophobically modified cationic polymers and completely hydrophilic anionic polymers may have an

intriguing property to control the thickness and smoothness of the surface and durability of multilayer complexes, which ultimately help us to further improve the efficacy in the removal of target organic contaminants.

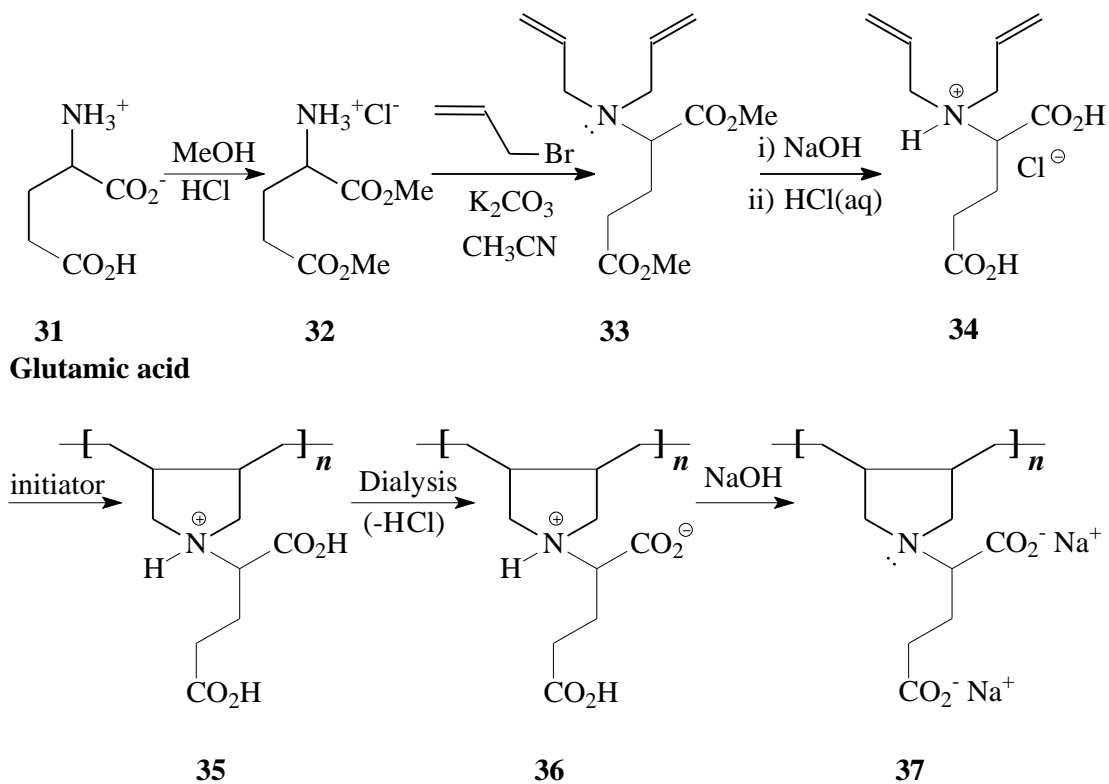


Scheme 1.5 Hydrophobically modified ionic Polymers

Butler's cyclopolymerization protocol will be utilized to synthesize a novel series of pH-triggerable polyelectrolytes having residues of aspartic and glutamic acid as outlined in Schemes 1.6 and 1.7, respectively.



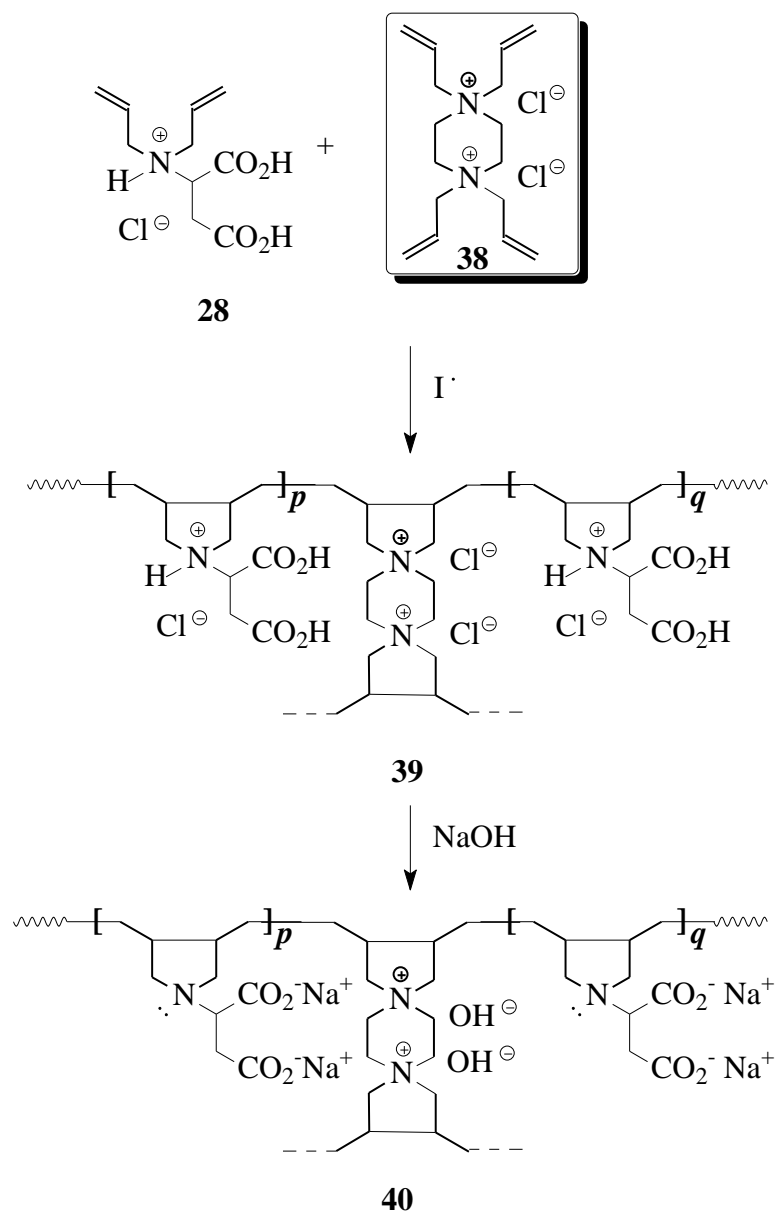
Scheme 1.6 pH-triggerable Polyelectrolytes having Residues of Aspartic Acid



Scheme 1.7 pH-triggerable Polyelectrolytes having Residues of Glutamic Acid

1.4.2 Synthesis of Cross-linked Resins

To the best of our knowledge, the following synthesis of the resins (scheme 1.8) would represent the first examples of cross-linked polymers (containing residue of aspartic acid) by the cyclopolymerization protocol involving monomers having unquenched nitrogen valency. The cross-linker **38** will be prepared as described [82]. The monomer **28** will be prepared as described in Scheme 1.6.



Scheme 1.8 Cross-linked Polymers containing Residue of Aspartic Acid

1.4.3 Chemical and Physical Characterization

The structural composition of the resulting polymers will be determined by Nuclear Magnetic Resonance spectroscopy (NMR) and Fourier transform infrared spectroscopy (FT-IR). IR spectra will be recorded on a Perkin Elmer 16F PC FTIR spectrometer. ^1H and ^{13}C NMR spectra will be measured in CDCl_3 or D_2O using TMS or Dioxane (in case of D_2O) as internal standard on a JEOL LA 500 MHz NMR spectrometer operating at 500.00 MHz and 125.65 MHz respectively. Elemental analysis will be carried out on a EURO EA Elemental Analyzer to identify all the new compounds. All melting points will be determined in a calibrated Electrothermal- IA9100- Digital Melting point apparatus.

The molecular weight and their distributions will be measured by gel permeation chromatography (GPC) and/ or viscometric technique. Appearance and strength of the complexes will be observed by microscopic technique such as scanning electron microscopy (SEM). Concentration of removed/ effluent heavy metal in sample will be determined by suitable spectroscopic technique such as atomic absorption spectrometry.

1.4.4 Preparation of Solid Supports and Layer-by-Layer (LBL) Assembly

Polyelectrolyte multilayer structures will be constructed on the surface of the solid supports using layer-by-layer method [29]. The nature of the first deposited layer will depend on the point of zero charge (PZC) of the solid support; subsequent layers will be deposited using polyelectrolyte of an alternate charge. Multiple layers of polyelectrolyte of alternate charges will be deposited using aqueous solutions containing 0.1 M NaCl with a

liquid/solid volume ratio of 50 at ambient temperature. After each deposition step the sample will be centrifuged, washed with water, filtered, and dried at room temperature.

The solids proposed for this work is mesoporous silica of the SBA-15 type. SBA-15 materials will be synthesized via co-condensation from aqueous solution containing surfactant and silica precursors. Pluronic-123 [EO₂₀PO₇₀EO₂₀, Aldrich] will be used as structure directing agent while tetraethyl orthosilicate [TEOS, Sigma-Aldrich] is the silicon precursor. In a typical synthesis, appropriate amount of Pluronic-123 will be dispersed in hydrochloric acid (HCl) solution. The dispersion is then stirred at room temperature for about an hour. Stirring at 308K will be continued for another 1 h before the addition of the required amount of TEOS. The mixture will then be allowed to ripe for 5-8 min before aging it at 363K without stirring, for 24 h. The solid product will then be recovered by filtration, dried at 373K, and then calcined at 823K for 4 h.

1.4.5 Complexation and Metal Interaction Study

Polyelectrolyte complexes of a synthetic polyanion with a polycation will be studied in aqueous solution as a function of charge ratio, total polymer loading, polymer molecular weight, and ionic strength. It is hoped that they form solid, gels, liquid complexes (coacervate), or soluble complexes depending on the condition used, which preliminary would guide us to choose a suitable combination for the construction of multilayers.

The key to this approach is that they will form a complex by simultaneous interactions between oppositely charge polyelectrolyte. It is further hoped that in case of covalently cross-linked polyelectrolytes, the ionic interactions will occur instantly followed by

covalent cross-linking, which will be achieved by using complementary reactive groups that are attached to two different polyelectrolytes. The reactive groups are polymer-bound and constitute a few mol%, as such they should not reduce the binding efficiency of the resultant polyelectrolyte-complex (e.g. 33, Scheme 7) and target metal from metal contaminated samples.

A model study will also be undertaken to explore the complexation behavior between the polycation and polyanion in presence of gelling and non-gelling ions in order to understand the complexation quality, efficiency and binding capacity of the polyelectrolyte complexes.

Solid substrates such as alumina, silica and/or carbon (activated) will be sequentially (LBL) coated [27–29] with oppositely charged polyelectrolytes in order to better understand the polyelectrolytes interaction with substrates, hydrophilicity, hydrophobicity and strength of the complexes. The LBL will primarily build up by anchoring the solid adsorbents with oppositely charged polyelectrolytes. The mechanically and thermally stable polyelectrolyte complexes will eventually be exposed to model metal cations/anions such as Pb(II), Cd(II), Hg(II), arsenate, chromate, etc., and organic contaminants in order to study the efficiency as well as selectivity for effective removal of various metals and organics from aqueous samples.

1.4.6 Adsorption Experiments

Adsorption experiments will be carried out as described in earlier work [83–86]. The procedure for the adsorption experiments of the polyelectrolyte coated materials for metal ions can be described briefly as follows: a mixture of the polyelectrolyte coated material (50 mg) in an aqueous solution (20 mL) having certain concentration of metal ions will be

stirred using a magnetic stir-bar at different pH for 24 h. The material will then be filtered and carefully washed with deionized water. The combined filtrate will be analyzed by ICP-MS to determine the amount of metal ions remained. The adsorption capacity (q) in mg/g can be calculated using Eq. (1):

$$q = \frac{(C_0 - C_f)V}{W} \quad (1)$$

Where C_0 and C_f are the initial and final concentrations of metal ions in mg/L, respectively, W is the weight of the polymer in g, and V is the volume of the solution in L.

For adsorption kinetic studies, the coated sample will be stirred in a solution containing metal ions for different adsorption times at a preferred pH. The adsorption isotherm will be constructed by changing the concentration of metal ions at 25°C for 24 h. Based on the adsorption data from experiments carried out at different temperatures, the activation energy for the adsorption process and thermodynamic parameters ΔG , ΔH and ΔS for metal removal will be calculated.

CHAPTER 2

SYNTHESIS AND APPLICATION OF A pH- TRIGGERABLE CYCLOPOLYMER CONTAINING ASPARTIC ACID RESIDUES

Abstract

The reaction between diallylamine and dimethyl maleate afforded the Michael addition product dimethyl *N,N*-diallylaspartate $[(\text{CH}_2=\text{CH}-\text{CH}_2)_2\text{NCH}(\text{CO}_2\text{Me})\text{CH}_2\text{CO}_2\text{Me}]$ **I**, which upon treatment with dry HCl and ester hydrolysis with aqueous HCl gave its hydrochloride salt $[(\text{CH}_2=\text{CH}-\text{CH}_2)_2\text{NH}^+\text{CH}(\text{CO}_2\text{Me})\text{CH}_2\text{CO}_2\text{Me Cl}^-]$ **II** and *N,N*-diallylaspartic acid hydrochloride $[(\text{CH}_2=\text{CH}-\text{CH}_2)_2\text{NH}^+\text{CH}(\text{CO}_2\text{H})\text{CH}_2\text{CO}_2\text{H Cl}^-]$ **III**, respectively. The new monomers **II** and **III** underwent cyclopolymerization to give, respectively, cationic polyelectrolytes (CPEs) poly(**II**) and poly(**III**). Under the influence of pH, triprotic acid (+) poly(**III**) was equilibrated to water-insoluble diprotic polyzwitterionic acid (\pm) **IV**, water-soluble monoprotic poly(zwitterion-anion) ($\pm -$) **V**, and its conjugate base polydianion (=) **VI**. The protonation constants of the carboxyl group and trivalent nitrogen in **VI** have been determined. A 20-ppm concentration of **IV** is effective in inhibiting the precipitation of CaSO_4 from its supersaturated solution with a $\approx 100\%$ scale efficiency of inhibition for a duration of 50 h at 40 °C. The aqueous two-phase systems (ATPSs) of **VI** and polyoxyethylene have been studied. The transformation of water-

soluble **VI** to insoluble **IV** makes it a recycling ATPS as it can be recycled by precipitation at a lower pH.

2.1 Introduction

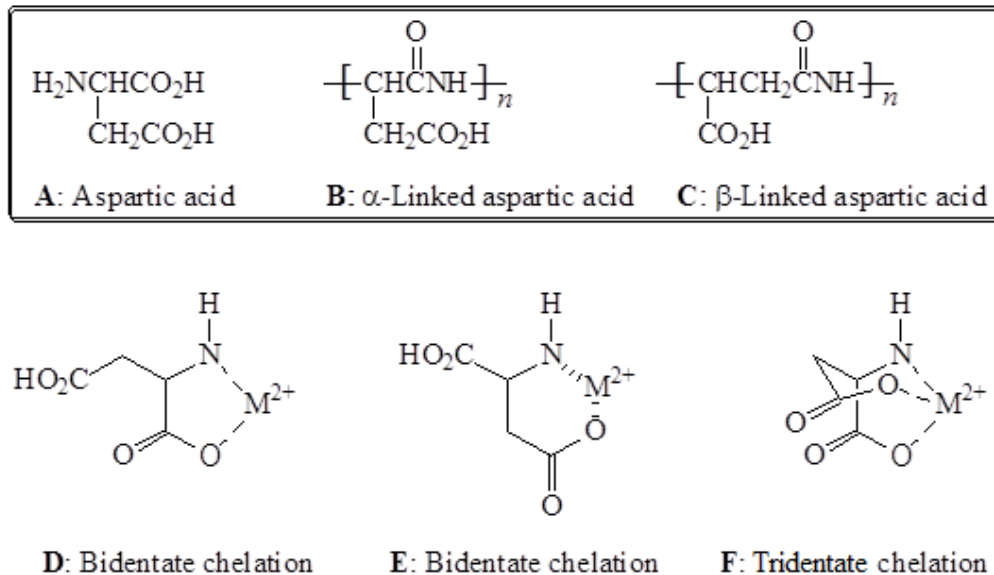
The environmentally friendly and biodegradable poly(aspartic acid) and its derivatives have found innumerable industrial applications [87]. They offer advantageous features that render them suitable for use as corrosion inhibitors [88], antiscalants [89], super-swelling material in diaper and food packaging [90], detergents and dispersants [87], carriers for drug delivery [91], hydrogels [92], etc. The ever-expanding list of applications also includes industrial, medical, and agricultural applications to replace many non-biodegradable traditional polyanionic materials such as polyacrylates [93]. While the naturally occurring poly(aspartic acid) (PASP) (**A**) consists of α -linked L-aspartic acid (**B**) as fragments of larger proteins [94], the repeating unit of the synthetic counterpart exists as randomly distributed isomeric forms having α ($\approx 30\%$) (**B**) and β links ($\approx 70\%$) (**C**) (Scheme 2.1) [88]. The use of PASP as a green scale inhibitor is attractive because of its biodegradability. For a supersaturated solution of 800 ppm of Ca^{2+} in the form of CaCO_3 generated in situ from NaHCO_3 and CaCl_2 , PASP at a concentration of 6 ppm imparted a 90% inhibition of CaCO_3 scale for 10 h at 30°C [95]. The reversible formation of a gel using electrostatic attraction between a cationic poly(diallyldimethylammonium chloride) and anionic polyacrylate/polyaspartate has been exploited in enhancing the retention of a scale inhibitor within a hydrocarbon-producing system [96]. PASP with lower molar

masses has been shown to impart better scale inhibition than polymers with higher molar masses. PASP with molar masses ranging from 1000 to 2000 g mol⁻¹ imparted an efficiency of inhibition of 80% in supersaturated 0.1 M Na₂SO₄ and CaCl₂ solutions at 30 °C for 24 h [89].

The ability of the PASP to scavenge metal ions makes it an effective antiscalant. Note that, in the peptide bonds of PASP (**B** and **C**), the nitrogen loses its basic character whereas each repeating unit consists of a single anionic center in the pendant carboxylate motif. The objective of the current work is to obtain a polymer in which the basic character of the nitrogen in aspartic acid will be retained in addition to the two anionic centers in the carboxylates. The presence of the amino acid residues in the polymer is thus anticipated to enhance the chelating ligand properties of every repeating unit. The metal ion-binding properties of aspartic acid are well known [97–99]. Aspartic acid is known to act as a bidentate (**D**, **E**) or a tridentate ligand (**F**) forming complexes with almost all metal ions via its three binding sites (Scheme 2.1) [100,101]. The ability of aminopolycarboxylates to form strong complexes with metal ions makes them useful in a wide variety of chemical, medical, and environmental applications [102].

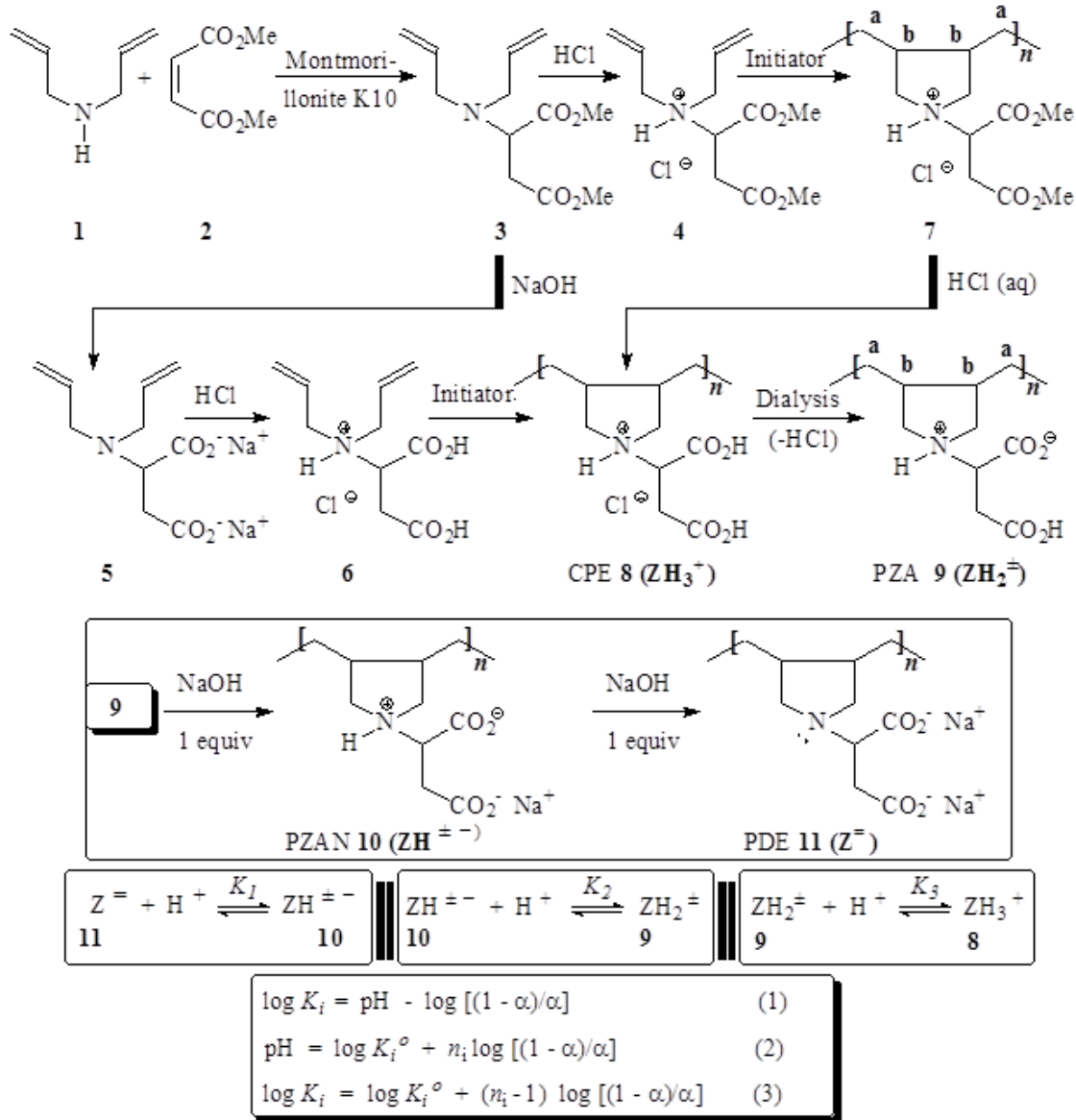
For the synthesis of an aminopolycarboxylate, we intend to apply Butler's [24,25,103,104] cyclopolymerization protocol, which is instrumental in converting diallylammonium salts into a variety of industrially significant cyclopolymers. Herein, we report the synthesis and polymerization of aspartic acid-derived diallyl monomers **4** and **6** to generate new pH-triggerable cyclopolymer **9**, which could be valuable in numerous industrial applications, for instance, in the field of corrosion and scale inhibition, chelation of metal ions, etc. (Scheme 2.2). In this study, the use of the cyclopolymerization protocol

to obtain polymer **9** containing the residues of aspartic acid with all its basic centers intact is demonstrated for the first time. We anticipate exciting solution properties of the cyclopolymer, which would be tested for its antiscalant behavior. For environmental reasons, we aim to look for aqueous two-phase systems (ATPSs) containing pH-triggerable zwitterionic polymers that may be introduced potentially to the field of biotechnology for downstream separation of biomolecules [105,106]. We intend to use cyclopolymer **9** as a component to build a recyclable ATPS, in which the biomimicking **9** can be easily recycled by precipitation at its isoelectric point. The current work would also pave the way to synthesize polymer-based chelating adsorbents containing amine and carboxylate functionalities [107,108].



Scheme 1. Aspartic acid, polyaspartic acid acid and metal ion-aspartate complex

Scheme 2.1 Aspartic acid, polyaspartic acid and metal-ion aspartate complex.



Scheme 2.2 Synthesis of cyclopolymers having aspartic acid residues

2.2 Experimental methods

2.2.1 Materials

The following reagents were used as received: diallylamine, dimethyl maleate, *t*-butylhydroperoxide (TBHP) (70% in water), and montmorillonite K10 from Fluka AG (Buchs, Switzerland); ammonium persulfate (APS); and 2,2'-azobis-(2-methylpropionamide) dihydrochloride (AMPD) from Sigma-Aldrich. For dialysis, a membrane (Spectra/Por) with a molecular weight cutoff (MWCO) of 6000–8000 was purchased from Spectrum Laboratories, Inc. (Rancho Dominguez, CA, USA). 2,2'-Azobisisobutyronitrile (AIBN) purchased from Fluka AG (Buchs, Switzerland) was crystallized (C₂H₅OH–CHCl₃). Poly(oxyethylene) (POE) with a molar mass of 35,000 g mol⁻¹ was purchased from Merck-Schuchardt OHG (Hohenbrunn, Germany).

2.2.2 Physical Method for Structural Characterization

An elemental analyzer (Perkin Elmer Series II Model 2400) and a Fourier transform infrared (FTIR) spectrometer (Perkin Elmer 16F PC) were utilized for elemental analyses and IR spectroscopy. The nuclear magnetic resonance (NMR) spectra were recorded using a 500-MHz JEOL LA spectrometer. The ¹H signal of tetramethyl silane (TMS) at δ 0 ppm in CDCl₃, the residual proton resonance of D₂O at δ 4.65 ppm, and the dioxane ¹³C peak at δ 67.4 were used as internal standards. TGA was conducted using an SDT analyzer (Q600: TA Instruments, New Castle, DE, USA) in a nitrogen atmosphere. An Ubbelohde viscometer (viscometer constant = 0.005317 mm² s⁻²) was utilized to measure viscosities using CO₂-free water under N₂. The pH of the solutions was measured using a Sartorius

pH meter PB 11. The conductivity measurements were carried out using an Orion Versa Star conductivity meter.

To determine the molecular weight, a gel permeation chromatography (GPC) assay was conducted at 34 °C using PL-GPC 220 (Agilent Technologies) equipped with a refractive index (RI) detector and two mixed bed columns (PL-aquagel-OH mixed-H, 8 μm , 300 \times 7.5 mm). High-performance liquid chromatography (HPLC)-grade water containing 0.003 M NaN_3 was used as eluent (flow rate: 1.0 mL min^{-1}). A sample solution of 0.100 w/v% was prepared in water. The resulting solution (50 μl) was injected into the GPC columns. The equipment was calibrated using polyethylene oxide/glycol standards.

2.2.3 Synthesis of Monomers

a. Dimethyl N,N-diallylaspartate (**3**)

A mixture of dimethyl maleate **2** (60.2 g, 417 mmol), montmorillonite K10 (21 g), methanol (23 cm^3), and diallylamine (120 g, 1.23 mol) was stirred at 40 °C for 72 h [109]. The catalyst was filtered off and washed with dichloromethane (75 cm^3). After concentration, the residual liquid was distilled (bp_{2 mbar Hg}, 101 °C) to yield new tertiary amine **3** (93.5 g, 93%). The following data were obtained: (found: C, 59.6; H, 7.9; and N, 5.8%. $\text{C}_{12}\text{H}_{19}\text{NO}_4$ requires C, 59.73; H, 7.94; and N, 5.80%; and ν_{max} (neat): 3079, 3006, 2982, 2953, 2844, 1747, 1733, 1641, 1438, 1357, 1295, 1258, 1166, 1074, 998, 923, 846, and 788 cm^{-1} . δ_{H} (CDCl_3) 2.60 (1H, dd, J 7.2, 15.7 Hz), 2.83 (1H, dd, J 7.2, 15.7 Hz), 3.08 (2H, dd, J 7.3, 14.3 Hz), 3.26 (2H, dd, J 4.9, 14.3 Hz), 3.68 (3H, s), 3.72 (3H, s), 4.01 (1H, t, J = 7.6 Hz), 5.15 (4H, m), 5.74 (2H, m); δ_{C} (CDCl_3) 34.86 (1C, $\underline{\text{C}}\text{H}_2\text{CO}_2\text{Me}$), 51.52 (1C, $\underline{\text{Me}}$), 51.79 (1C, $\underline{\text{Me}}$), 53.90 (2C, N- $\underline{\text{C}}\text{H}_2$), 58.48 (1C, N- $\underline{\text{C}}\text{H}$), 117.42 (2C, = $\underline{\text{C}}\text{H}_2$), 136.10

(2C, =CH), 171.70 (1C, CO₂Me), 172.36 (1C, CO₂Me), (CDCl₃ 77.13 ppm middle C). DEPT 135 NMR spectrum confirmed the ¹³C assignments.

b. Dimethyl N,N-diallylaspartate hydrochloride (4)

Moisture-free gaseous HCl was bubbled through a magnetically stirred, salt–ice-cooled solution of **3** (45 g, 186 mmol) in diethyl ether (200 cm³) until no further precipitation of hydrochloride salt **4** was observed on the clear supernatant liquid. The chloride salt was dissolved in methanol and precipitated in ether. Amine salt **4** was vacuum-dried at 50 °C (49 g, 95%, white). The following data were obtained: Mp 94.5–95.6 °C (closed capillary); (Found: C, 51.7; H, 7.4; N, 4.9%. C₁₂H₂₀ClNO₄ requires C, 51.89; H, 7.26; N, 5.04%); ν_{\max} (KBr): 3431, 2954, 2909, 2852, 1737, 1644, 1439, 1359, 1335, 1227, 1199, 1105, 1054, 999, 954, 941, 861, 842, and 787 cm⁻¹. The NMR spectra are shown in Figs. 2.1 and 2.2. δ_{H} (D₂O) 3.10 (2H, m), 3.64 (3H, s), 3.69 (2H, dd, *J* 7.6, 13.2 Hz), 3.73 (3H, s), 3.88 (2H, dd, *J* 6.5, 13.2 Hz), 4.68 (1H, t, *J* 6.4 Hz), 5.50 (4H, m), 5.80 (2H, m), (HOD: 4.65; δ_{C} (D₂O) 30.44 (1C, CH₂CO₂Me), 54.00 (1C, Me), 54.97 (1C, Me), 55.91 (2C, N-CH₂), 59.46 (1C, N-CH), 126.38 (2C, =CH), 128.26 (2C, =CH₂), 168.90 (1C, CO₂Me), 171.99 (1C, CO₂Me), (dioxane: 67.40 ppm). DEPT 135 NMR spectrum confirmed the ¹³C assignments.

c. N,N-diallylaspartic acid hydrochloride (6)

A mixture of **3** (40 g, 166 mmol) in water (115 cm³) containing NaOH (13.8 g, 345 mmol, 2.08 equivalent) was stirred at 23 °C for 6 h, by which time the ¹H NMR signals of the methoxy protons disappeared. Upon acidification with concentrated HCl (50 g, 506 mmol), the hydrolyzed reaction mixture containing **6** and NaCl was lyophilized by freeze-

drying, and the freeze-dried product was triturated with ethanol (80 cm³), filtered to remove NaCl, and washed with ethanol (30 cm³). Ethanol was expelled from the filtrate by roto-evaporation at 25 °C, and the residue was vacuum-dried at 60 °C for 3 h to yield 6 in the form of a white solid (40.7 g, 98%). The following data were obtained: Mp 159.5–160.0 °C (ethanol/ether) (closed capillary); and Found: C, 47.8; H, 6.7; N, 5.5%. C₁₀H₁₆ClNO₄ requires C, 48.10; H, 6.46; N, 5.61%); ν_{\max} . (KBr): 3409, 2987, 2838, 1732, 1643, 1458, 1425, 1240, 1192, 1097, 997, 956, 846, and 632 cm⁻¹. The NMR spectra are shown in Figs. 2.2 and 2.3. δ_{H} (D₂O) 2.93 (1H, dd, *J* 7.9, 17.0 Hz), 2.97 (1H, dd, *J* 4.6, 17.0 Hz), 3.63 (2H, dd, *J* 7.9, 13.5 Hz), 3.82 (2H, dd, *J* 6.5, 13.5 Hz), 4.44 (1H, dd, *J* 4.6, 7.9 Hz), 5.47 (4H, m), 5.77 (2H, m), (HOD: 4.65); δ_{C} (D₂O) 30.80 (1C, CH₂CO₂H), 55.75 (2C, N-CH₂), 60.39 (1C, N-CH), 126.68 (2C, =CH), 127.84 (2C, =CH₂), 170.84 (1C, CO₂H), 173.68 (1C, CO₂H), (dioxane: 67.40 ppm). DEPT 135 NMR spectrum confirmed the ¹³C assignments.

A solution of 4 (4 mmol) in water (4 cm³) was hydrolyzed using NaOH (5.5 mmol) as described previously. The resulting solution of 5 was added dropwise to methanol to obtain its precipitate as a white powder, which was filtered and vacuum-dried at 60 °C (95%). Salt 5 was found to be insoluble in methanol or acetone. ν_{\max} . (KBr): 3464 (weak), 3077, 2977, 2939, 2827, 1599, 1408, 1324, 1257, 1179, 1132, 1071, 998, 918, 876, 789, 754, 676, and 535 cm⁻¹. δ_{H} (D₂O) 2.27 (2H, dd, *J* 6.1, 15.0 Hz), 2.45 (2H, dd, *J* 8.4, 15.0 Hz), 3.00 (2H, dd, *J* 7.4, 13.9 Hz), 3.17 (2H, dd, *J* 6.1, 13.9 Hz), 3.55 (1H, dd, *J* 6.1, 8.4 Hz), 5.08 (4H, m), 5.75 (2H, m), (HOD: 4.65); δ_{C} (D₂O) 39.12 (1C, CH₂CO₂Na), 54.58 (2C, N-CH₂), 64.15 (1C, N-CH), 119.51 (2C, =CH₂), 135.98 (2C, =CH), 180.09 (1C, CO₂Na), 181.12 (1C, CO₂Na), (dioxane: 67.40 ppm). DEPT 135 NMR spectrum confirmed the ¹³C assignments.

2.2.4 Synthesis of Polymers

a. Polymerization of Monomer 4

After purging with N₂, a solution of monomer 4 and an initiator in water (or dimethyl sulfoxide (DMSO)) in a round-bottom (RB) flask was stirred at the specified temperature (Table 2.1). The polymerization with AIBN, AMPD, or TBHP undertaken in a closed flask, whereas the reaction in water using APS was conducted under N₂ in a flask fitted with a condenser. At the end, the transparent viscous content in the flask was added slowly to acetone with stirring to precipitate polymer 7, which was redissolved in methanol and reprecipitated in acetone (repeated three times). Mp (closed capillary): slight phase change around 195 °C with color darkening on further heating; it became dark brown to black around 280 °C but with no noticeable melting or decomposition up to 400 °C. Found: C, 51.6; H, 7.5; and N, 4.9. C₁₂H₂₀ClNO₄ requires C, 51.89; H, 7.26; and N, 5.04. ν_{max} (KBr): 3437, 3215, 3022, 2958, 1748, 1632, 1441, 1407, 1221, 1059, 996, 854, and 599 cm⁻¹. The NMR spectra are shown in Figs. 2.1 and 2.2.

b. Acidic hydrolysis of the CPE 7

A solution of CPE 7 (4.0 g, 14.4 mmol) (entry 2, Table 2.1) in 6 M HCl (50 cm³) was stirred at 70 °C for 96 h; the disappearance of the methoxy signals in the proton NMR spectrum confirmed the completion of the ester hydrolysis. The homogenous solution containing 8 was dialyzed against deionized water. After depletion of HCl, polymer 9 started to separate out in the dialysis bag, and the heterogeneous mixture was freeze-dried to obtain the polymer (3.1 g, 86 %). Mp (closed capillary): changed to liquid at 240–245 °C, became dark brown on further heating, but did not char to 400 °C. (Found: C, 56.0; H, 7.2; N, 6.4%. C₁₀H₁₅NO₄ requires C, 56.33; H, 7.09; N, 6.57%); ν_{max} (KBr): 3412 (br),

2951, 2629, 1732, 1634, 1406, 1232, 1050, 842, and 630 cm^{-1} . D₂O-insoluble polymer **9** became soluble in the presence of NaCl; the resulting solution was used to record NMR spectra (Figs. 2.1 and 2.2).

c. Polymerization of **6**

An aqueous solution of monomer **6** in a Round Bottom flask fitted with a condenser was heated to 90 °C under N₂. The required amount of initiator APS was added at 90 °C, and the reaction mixture was stirred (Table 2.1: entries 8–10). An exothermic reaction occurred within seconds after the addition of APS; after the elapsed time, the polymerization mixture was dialyzed against deionized water. The polymer was initially soluble in water, then became cloudy, and finally separated as a jelly. The total mixture was then freeze-dried to obtain white polymer **9**, which is similar to the polymer obtained above via hydrolysis of CPE **7** (*vide supra*).

Table 2.1 Cyclopolymerization of monomer **4** and **6** to give CPE **7** and PZA **9**, respectively.

Entry	4 (mmol)	Solvent (wt%)	Initiator ^a (mg/mmol 4)	Temp (°C)	Time (h)	Yield (%)	Intrinsic Viscosity ^b (dL g ⁻¹)
Monomer 4							
1	10	DMSO (47)	A (50)	65	48	41	0.0159
2	30	Water (25)	B (40)	85	0.5	83	0.0129
3	10	Water	B (30)	95	0.5	71	0.0163

		(20)					
4	10	Water	B (20)	90	1.5	45	0.0321
		(20)					
5	15	Water	B (10)	85	1.5	38	0.101
		(25)					
6	10	Water	C (10)	85	60	32	0.0345
		(25)					
7	10	Water	D (10)	85	60	35	0.0372
		(25)					
Monomer 6							
8	30	Water	B (40)	90	0.25	67	0.0556
		(25)					
9	30	Water	B (30)	90	0.25	75	0.0583
		(25)					
10	30	Water	B (30)	90	0.25	72	0.0498
		(30)					

^aA= azobisisobutyronitrile; B= ammonium persulfate; C=AMPD; D= *t*-butylhydroperoxide

^bViscosity of 1-0.25 % in 0.1 M NaCl (entries 1-7) and 1.0 M NaCl (entries 8-10) at 30 °C was measured with an Ubbelohde Viscometer ($K=0.005317 \text{ mm}^2/\text{s}^2$).

2.2.5 Physicochemical Characterization

a. Solubility Measurements

The critical (minimum) salt concentration (CSC) values were determined by titrating a 1% w/w aqueous solution of PZA **9** containing salts or HCl at a higher concentration than their

CSC values at 23 °C with deionized water. The average of the triplicate results of the CSCs were determined to be 0.640 M NaCl, 0.360 M NaBr, 0.228 M NaI, and 0.0224 M HCl with approximate accuracies of $\pm 1\text{--}2\%$.

b. Potentiometric Titrations

The potentiometric titration used to determine protonation constants (K) is described elsewhere [72,110]. In each trial, a certain number of millimoles of PZA **9** (ZH_2^\pm) in CO_2 -free water (200 cm^3) was titrated by gradual addition of $0.05\text{--}0.15\text{ cm}^3$ of NaOH solution as described in Table 2.2. PZA **9** was insoluble in salt-free water (200 cm^3); it remained attached to the wall of the flask as a sticky material. However, it was soluble in 0.1222 M HCl (3 cm^3), and the solution was then diluted to 200 cm^3 using deionized water to give a cloudy suspension, which was then titrated with 0.0981 N NaOH. Upon the addition of a certain volume of the titrant, a clear solution was obtained which was then titrated with further addition of NaOH solution to determine the protonation constants. Note that the polymer was soluble in 1 M NaCl which is higher than the CSC value. The $\log K_1$, $\log K_2$ and $\log K_3$ represent the protonation constants of the most basic center in **11** (Z^-), **10** (ZH^\pm), and **9** (ZH_2^\pm), respectively. After each addition of the titrant, the recorded pH values were used to calculate $\log K$ s at each pH value by the Henderson–Hasselbalch equation (Eq. (2); Scheme 2.2). The degree of protonation (α) of **11**, **10** and **9** is the respective ratio $[\text{ZH}^\pm]_{\text{eq}}/[\text{Z}]_0$, $[\text{ZH}_2^\pm]_{\text{eq}}/[\text{Z}]_0$ and $[\text{ZH}_3^+]_{\text{eq}}/[\text{Z}]_0$, respectively, where $[\text{ZH}^\pm]_{\text{eq}}$, $[\text{ZH}_2^\pm]_{\text{eq}}$ and $[\text{ZH}_3^+]_{\text{eq}}$ represent the corresponding concentrations at equilibrium of **10**, **9** and **8**. $[\text{Z}]_0$ represents the initial polymer concentration in terms of repeating units. Because of the solubility problem of PZA **9**, $\log K_3$ associated with the equilibration $\text{9} (\text{ZH}_2^\pm) + \text{H}^+ \rightleftharpoons (\text{ZH}_3^+) \text{8}$ could not be determined in salt-free water.

The relationship between the protonated species during the first step of titration of (ZH_2^\pm) **9** with NaOH to determine $\text{Log } K_2$ was given by $[\text{ZH}_2^\pm]_{\text{eq}} = [\text{Z}]_0 + C_{\text{H}^+} - C_{\text{OH}^-} - [\text{H}^+] + [\text{OH}^-]$, where C_{OH^-} represents the concentration of added NaOH. The equilibrium $[\text{H}^+]$ and $[\text{OH}^-]$ values were determined from the pH values [29-31]. C_{H^+} represents the concentration of HCl (3.0 cm^3 of 0.1222 M) added initially to disperse PZA **9** in salt-free water. It is to be noted that no HCl was added in the titration in 1 M NaCl since the polymer is soluble in salt-added water. Continuing the titration, $\log K_1$ were calculated using titrant volume after subtracting one-equivalent volume from the total volume.

2.2.6 Applications

a. Evaluation of anti-scaling behavior

The precipitation and inhibition of calcium sulfate (gypsum) scale formation were evaluated at $40 \pm 1 \text{ }^\circ\text{C}$ in a supersaturated solution of 2598 mg L^{-1} of Ca^{2+} and 6300 mg L^{-1} of SO_4^{2-} in the presence of newly synthesized antiscalant **9** (Table 2.1, entry 9) ($x \text{ ppm}$) using the procedure described elsewhere [103]. Induction time was assigned as the time when a rapid decrease in conductivity indicated the beginning of precipitation of $\text{CaSO}_4 \cdot 2\text{H}_2\text{O}$ (Table 2.3). Visual inspections for any turbidity were performed.

b. Phase Composition of PZA **9** (+ two equivalents of NaOH)-POE-H₂O (NaCl) Systems

(i) The tie-lines by ^1H NMR spectroscopy

The stock solutions of 20 wt\% each of PZA **9** (Table 2.1, entry 9) (treated with 2.0 equivalents of NaOH) and POE in 0.6 M NaCl were used to make several known total

systems ($\approx 7 \text{ cm}^3$) of compositions (A_{total}) in 0.6 M NaCl at 296.0 K (Fig. 2.4c, Table 2.2). The resultant ATPSs were analyzed by ^1H NMR spectroscopy as described elsewhere [111]. Figure 2.1e presents the ^1H NMR spectra of the bottom layer of system 3 (Table 2.2), which is overwhelmingly rich in polydianion (PDE) **11** (i.e., PZA **9** + 2 equivalents of NaOH). The area (A) of the ^1H NMR signals appearing in the range $0.6 \leq \delta \leq 3.5$ ppm belongs to the thirteen protons of each repeating unit of **11**, whereas the area (B) under the singlet at $\delta = 3.6$ ppm accounts for the four protons of POE. The area ratio of single H of POE and PZA resulted in the mole ratio $n_{\text{POE}}/n_{\text{PZA}}$ of $(B/4)/(A/13)$. The molar mass of the repeating unit of PZA **9** and POE (i.e., $\text{CH}_2\text{CH}_2\text{O}$) are taken to be 213.23 and 44.05 $\text{g}\cdot\text{mol}^{-1}$, respectively. After determining the weight fraction (w) in each phase (presented as Table 2.2) as described [103], the tie-lines were constructed.

(ii) Binodals by Dilution Method

For the PZA **9**/POE systems, the binodal was constructed using the dilution method as described elsewhere [29]. Thus, 0.6 M NaCl solution was added in portions to several two-phase systems with known compositions (A_{total}), and after centrifugation more NaCl solution was added dropwise until the systems became homogeneous; the compositions before the last drop added gave the binodal points (presented as in Table 2.2).

Table 2.2 Composition of the Phases of the [POE^a + PZA **9**^b] System (2.0 equiv. NaOH, m_{NaCl} of 0.6 mol·kg⁻¹) at 296 K shown in Figure 2.2a.

NMR method							
System	Total system		Top phase		Bottom phase		Volume ratio ^c
	POE $w \times 100$	PZA $w \times 100$	POE $w \times 100$	PZA $w \times 100$	POE $w \times 100$	PZA $w \times 100$	
1	7.09	6.39	15.8	0.497	0.121	11.5	0.87
2	5.69	5.92	12.7	0.711	0.270	10.1	0.82
3	4.78	5.39	10.5	0.822	0.422	8.98	0.79
4	3.86	3.78	5.51	2.30	0.865	6.44	1.8

Dilution method				
System	Total system (two-phase)		Total system (one-phase)	
	POE $w \times 100$	PZA $w \times 100$	POE $w \times 100$	PZA $w \times 100$
a	13.3	6.63	4.69	2.33
b	9.94	10.0	3.13	3.15
c	6.63	13.3	2.11	4.23

^apoly(oxyethylene) of molar mass 35,000 g mol⁻¹. ^bPZA **9** (+ 2 equiv. NaOH). ^cVolume ratio of top and bottom phase.

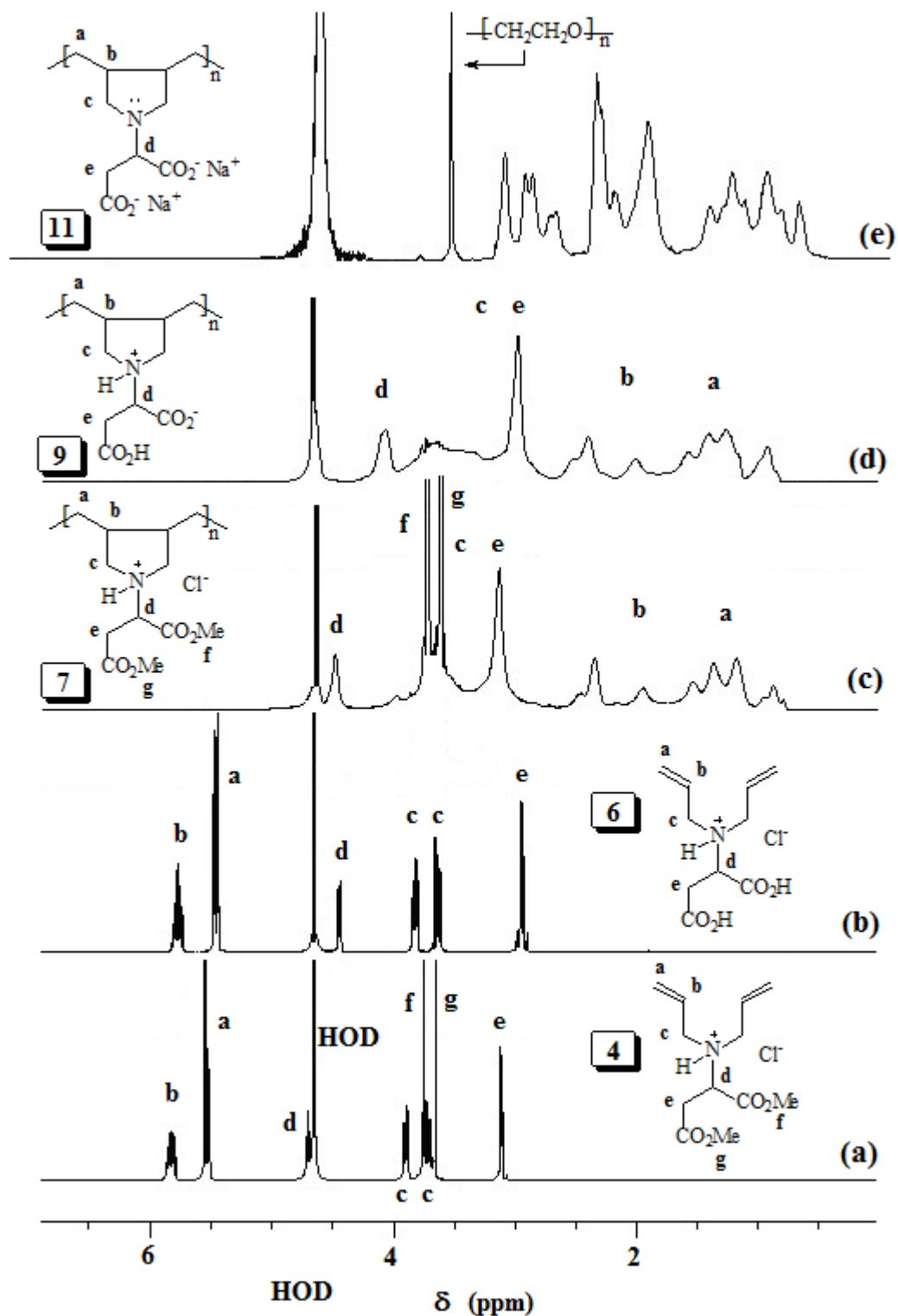


Figure 2.1 ^1H NMR spectrum of (a) 4 (b) 6, (c) 7, and (d) 9 (+NaCl), (e) bottom layer (system 3, supplementary data : Table S1) in D_2O .

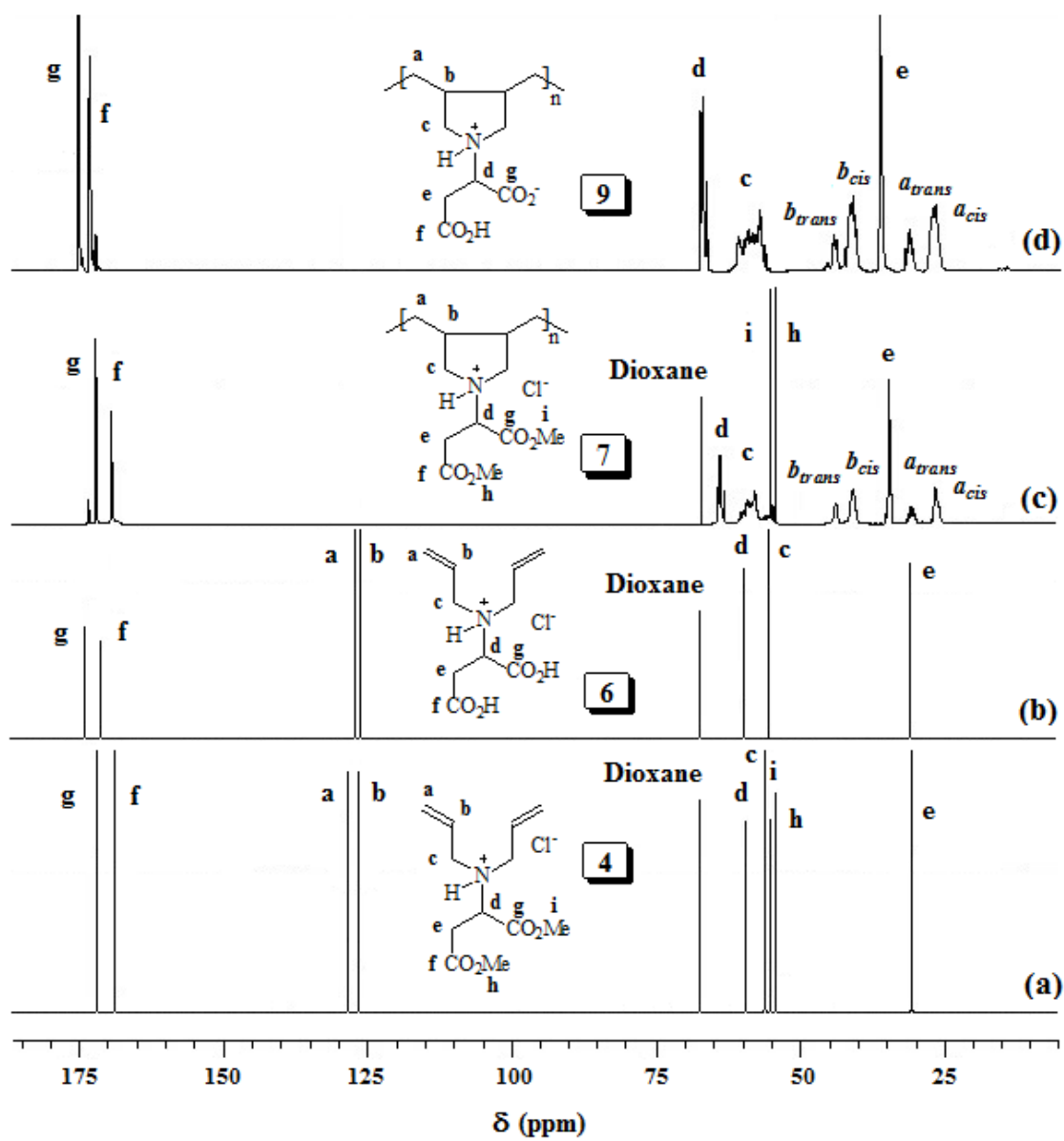


Figure 2.2 ^{13}C NMR spectrum of (a) 4, (b) 6, (c) 7, and (d) 9 (+NaCl) in D_2O .

Table 2.3 Protonation of Polymer 11 (Z=) and 10 (ZH± -) at 23 °C in Water and 1 M NaCl.

run	ZH ₂ [±] (mmol)	C _T ^a (mol dm ⁻³)	α-range	pH-range	Points ^b	Log K _i ^{o c}	n _i ^c	R ² , ^d
Polymer 9 deionized water								
1	0.2828 (ZH ₂ [±])	-0.0981	0.91-0.54	9.74-10.98	28	11.01	1.30	0.9931
2	0.3288 (ZH ₂ [±])	-0.0981	0.90-0.47	9.94-11.16	24	11.10	1.20	0.9970
3	0.3761 (ZH ₂ [±])	-0.0981	0.90-0.41	9.98-11.28	24	11.17	1.23	0.9904
Average						11.09 (8)	1.24 (5)	
Log K ₁ ^e = 11.09 + 0.24 log [(1-α)/α] For the reaction: Z = + H ⁺ $\xrightleftharpoons{K_1}$ ZH ^{± -}								
1	0.2828 (ZH ₂ [±])	-0.0981	0.80-0.20	3.29-5.98	26	4.59	2.17	0.9986
2	0.3288 (ZH ₂ [±])	-0.0981	0.80-0.15	3.25-6.12	25	4.44	2.05	0.9983
3	0.3761 (ZH ₂ [±])	-0.0981	0.78-0.20	3.43-5.85	32	4.55	2.11	0.9995
Average						4.53 (8)	2.11 (6)	
Log K ₂ ^e = 4.53 + 1.11 log [(1-α)/α] For the reaction: ZH ^{± -} + H ⁺ $\xrightleftharpoons{K_2}$ ZH ₂ [±]								
Polymer 9 in 1.0 M NaCl								
1	0.2823 (ZH ₂ [±])	-0.0981	0.91-0.26	8.84-10.42	24	9.97	1.15	0.9977
2	0.3283 (ZH ₂ [±])	-0.0981	0.95-0.27	8.53-10.38	28	9.93	1.16	0.9972
Average						9.95 (3)	1.16 (1)	
Log K ₁ ^e = 9.95 + 0.16 log [(1-α)/α] For the reaction: Z = + H ⁺ $\xrightleftharpoons{K_1}$ ZH ^{± -}								
1	0.2823 (ZH ₂ [±])	-0.0981	0.62-0.19	3.31-4.89	17	3.69	1.78	0.9965
2	0.3283 (ZH ₂ [±])	-0.0981	0.66-0.23	3.08-4.58	19	3.64	1.74	0.9962
Average						3.66 (4)	1.76 (3)	
Log K ₂ ^e = 3.66 + 0.76 log [(1-α)/α] For the reaction: ZH ^{± -} + H ⁺ $\xrightleftharpoons{K_2}$ ZH ₂ [±]								

^a (-)ve values represent titrations with NaOH.

^b Number of data points.

^c Standard deviations in the last digit are given under the parentheses .

^d R = Correlation coefficient.

^e log K_i = log K_i^o + (n_i - 1) log [(1 - α)/α].

^fTitration was done in the presence of added 0.1222 M HCl (3-4 cm³) to reach the required values of the α.

2.3 Results and Discussions

2.3.1 Synthesis and spectroscopic characterization of monomers and polymers

The Michael addition of diallylamine (**1**) to dimethyl maleate (**2**) resulted in an excellent yield (93%) of the *N,N*-diallyl derivative of dimethyl aspartate **3** (Scheme 2.2). Protonation with gaseous HCl yielded the cationic monomer **4** (94%), whereas hydrolysis of **3** with NaOH led to **5**, which upon acidification readily furnished cationic monomer **6** (98% from **3**). Monomers **4** and **6** underwent cyclopolymerization in the presence of various initiators to give cationic polyelectrolyte (CPE) **7** and polyzwitterionic acid (PZA) **9**, respectively (Table 2.1). CPE **7** (from entry 2) was hydrolyzed to yield CPE **8**, which upon dialysis was converted into PZA **9** when HCl was depleted.

The TGA curve of PZA **9** is shown in Fig. 2.3a; the sharp loss of 21% in the temperature range 150–265 °C was caused by the release of one of the CO₂ units, whereas the gradual loss of 13% and sharp loss of 33% in the temperature ranges 265–385 and 385–460 °C, respectively, were associated with the respective decarboxylation and the degradation of the nitrogenated organic fraction.

The IR band at 1748 cm⁻¹ confirmed the presence of COOMe in CPE **7**. The symmetric and antisymmetric stretching of COO⁻ in the dipolar form **9** appeared at, respectively, 1406 and 1634 cm⁻¹ similar to those observed for simple amino acids [112], whereas the absorption for the C=O stretch of COOH appeared at 1732 cm⁻¹.

The ¹H and ¹³C NMR spectra of monomers **4** and **6**, and polymers **7** and **9** are displayed in Figs. 2.1 and 2.2, respectively. The low molecular weights of the polymers

and the absence of any residual alkene in the NMR spectra of the polymers suggested the presence of the chain termination process by abstraction of an allylic proton of the monomer [113] as well as by the coupling process [114]. After hydrolysis, the OCH₃ signals in **7** completely disappear in the NMR spectra of **9**. Integration of the relevant carbon signals [115,116] revealed a 3:1 *cis/trans* ratio of the ring substituents at C_{b,b} (Scheme 2.2).

Efforts to determine the molar masses of polymers **8–11** by GPC failed due to strong adsorption to the column materials. Similar difficulties associated with polymers containing amine and carboxy motifs (CO₂⁻/CO₂H) have been reported [117]. Presumably, the CO₂⁻/CO₂H groups are adsorbed in **8–11** strongly, thereby resulting in erratic values of molar masses. However, CPE **7** containing ester groups (CO₂Et) from entries 2 and 3 (Table 2.1) were determined to have \overline{M}_w of 22,000 and 25,500 g mol⁻¹, respectively, with a polydispersity index (PDI) of 2.2.

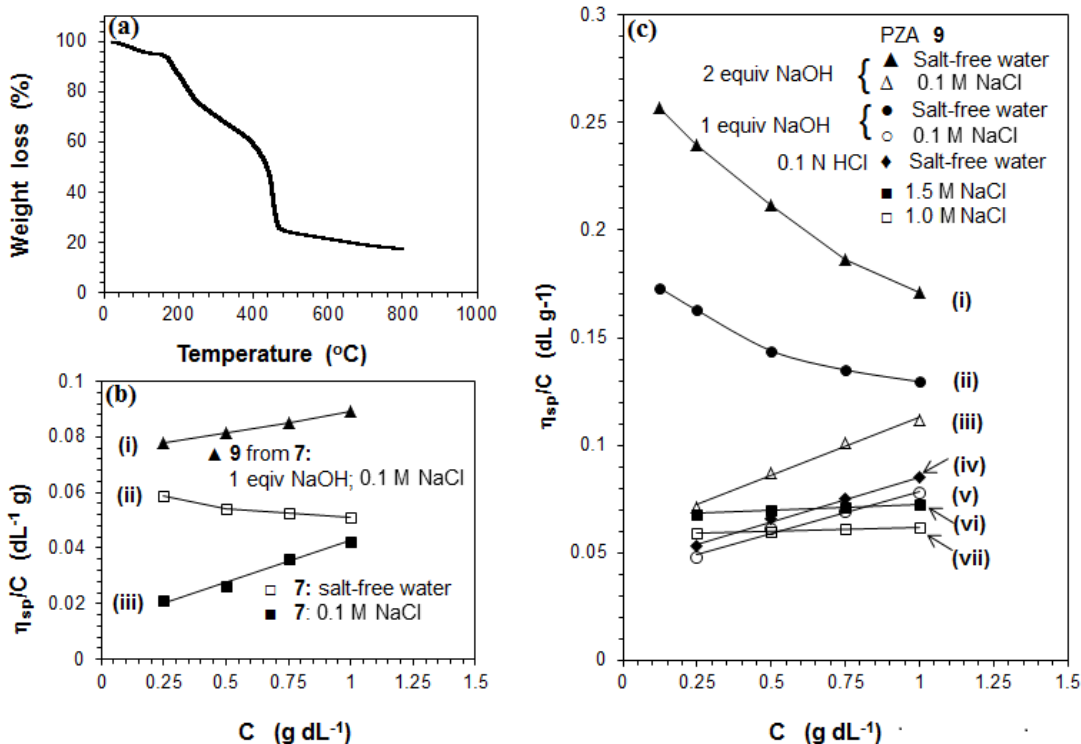


Figure 2.3 (a) TGA curve of PZA 9; Utilizing a viscometer, 30 °C: the viscosity behavior of (b) (+) CPE 7 (entry 2, Table 2.1) in (i) ■ salt-free water and (ii) □ 0.1 M NaCl and of (±) PZA 9 (prepared from entry 2, Table 2.1) in (iii) ▲ the presence of one equivalent of NaOH in 0.1 M NaCl; (c) (±) PZA 9 (entry 9, Table 2.1) in (i) ▲ two equivalents of NaOH, salt-free water, (ii) ● one equivalent of NaOH, salt-free water, (iii) △ two equivalents of NaOH, 0.1 M NaCl, (iv) ◆ 0.1 M HCl, (v) ○ one equivalent of NaOH, 0.1 M NaCl, (vi) ■ 1.5 M NaCl, and (vii) □ 1.0 M NaCl

2.3.2 Solubility behavior

CPEs 7 and 8 as well as poly(zwitterion–anion) (PZAN) 10 and polydianionic electrolyte (PDE) 11 are water-soluble as expected of any polyelectrolyte. The anionic portion in (±) 10 dictates the water solubility, whereas the electroneutral (±) 9 was found to be insoluble in water like the majority of known polyzwitterions [74,75,118,119]. However, the water-solubility of (±) 9 is promoted by the CSCs of added salts of small molar masses. For various salts, the CSCs at 23 °C were determined to be 0.640 M NaCl, 0.360 M NaBr,

and 0.228 M NaI. The most polarizable (soft) iodide is the most effective in neutralizing ionic cross-links, thereby disrupting the intragroup, intrachain, and interchain attractive interactions [25]. Zwitterionic (\pm) **9** was found to be soluble in 0.0224 M HCl as a result of its transformation to a backbone comprising a mixture of repeating units of (\pm) **9** and cationic (+) **8**. It has been revealed that addition of NaOH to an aqueous mixture of (\pm) **9** during potentiometric titrations leads to its solubility at a point where the backbone composition of the repeating units of (\pm) **9**/ $(\pm -)$ **10** becomes <80:20. Increasing the anionic portion thus leads to solubility in deionized water.

2.3.3 Viscosity measurements

The viscosity data for CPE **7** (entry 2, Table 2.1) and its hydrolyzed sample **9** are presented in Fig. 2.3b. In deionized free water, the viscosity plot for (+) **7** was typical of polyelectrolytes, that is, concave upwards (Fig. 2.3b-ii), whereas the plot became linear in 0.1 M NaCl (Fig. 2.3b-iii). ($\pm -$) PZAN **10** (i.e., (\pm) **9** in the presence of one equivalent of NaOH) displayed an intrinsic viscosity $[\eta]$ of 0.0743 dL g⁻¹ (Fig. 2.3b-i), while its precursor CPE **7** with an identical degree of polymerization was found to have a lower $[\eta]$ of 0.0129 dL g⁻¹ (Fig. 2.3b-iii).

The viscosity data of PZA (\pm) **9** (entry 9, Table 2.1) and its corresponding ($\pm -$) PZAN **10** and (=) PDE **11**, obtained by treating **9** with one and two equivalents of NaOH, respectively, are displayed in Fig. 2.3(c). In deionized water, dianionic **11** has higher reduced viscosities than that of zwitterionic–anionic **10** ((Fig. 2.3c-i vs. c-ii)); this is expected as the polymer chain of the former experiences greater repulsion among negative charges, thereby leading to an expanded coil with higher hydrodynamic volume. In 0.1 M

NaCl, linear plots marked iii and v revealed the $[\eta]$ values of 0.059 and 0.0398 dL g⁻¹ for **11** and **10**, respectively. CPE (+) **8** (i.e., (±) **9** + HCl) was shown to have a $[\eta]$ value of 0.0437 dL g⁻¹ in 0.1 M HCl ((Fig. 2.3c-iv)).

The antipolyelectrolytic behavior of (±) **9** is confirmed by the increase of $[\eta]$ with increase in the concentration of NaCl (cf. Fig. 2.3c-vi vs. c-vii); $[\eta]$ values were determined to be 0.0583 and 0.0667 dL g⁻¹ in 1.0 and 1.5 M NaCl, respectively. The strong binding ability of N⁺ to Cl⁻ than the binding of CO₂⁻ to Na⁺ is expected to impart an overall negative charge on the zwitterionic dipole [118,120,121]. The repulsion among the dipole centers with excess negative charges leads to increasing viscosity with increasing NaCl concentration.

Monomer **4** and **6** gave CPE (±) **7** and PZA (±) **9**, respectively. The polymers obtained via two pathways were correlated by the conversion of **7** to water-insoluble **9** (Section 2.4.2). PZA (±) **9** thus obtained from the two different pathways was transformed into PZAN (± -) **10** by treatment with one equivalent of NaOH. The polymer solutions of PZAN (± -) **10** derived from CPE (+) **7** of molar mass 22,000 g mol⁻¹ (entry 2, Table 2.1) and from PZA (±) **9** (entry 9, Table 2.1) were determined to have $[\eta]$ of 0.0743 and 0.0398 dL g⁻¹, respectively, in 0.1 M NaCl. Using these $[\eta]$ values and molar mass of CPE (+) **7** as 22,000 g mol⁻¹, Mark-Houwink equation ($[\eta] = KM^a$) helped us to calculate the approximate molar mass of PZA (±) **9** (entry 9, Table 2.1) as 10,080 g mol⁻¹; the value of a was assumed to be 0.8. Thus, the viscosity values indicate the relatively higher molecular weights of the polymers from monomer **4** than from monomer **6**. The solution properties of ionic polymers with balanced or imbalanced charges have been described mathematically [121–124] in terms of excluded volume, which increases with the increase

in the charge imbalances. For electroneutral (\pm) **9**, the minimum excluded volume leads to a collapsed polymer chain and hence insolubility in deionized water. However, in salt-added water, PZA **9** becomes soluble because of the zwitterionic dipoles acquiring a net negative charge (*vide supra*), the magnitude of which increases with the increase in NaCl concentration (cf. Fig. 2.3c-vi vs. c-vii).

2.3.4 Basicity Constant

The apparent basicity constants of anionic centers are described by Eq. (3) (Scheme 2.2) where $\log K_i^o = \text{pH}$ at degree of protonation $\alpha = 0.5$ and $n_i = 1$ in the case of sharp basicity constants. The pH versus $\log [(1-\alpha)/\alpha]$ plots enabled us to determine ' n_i ' and $\log K_i^o$ as the slope and intercept, respectively. In deionized water, the basicity constants $\log K_1$ (i.e., $\text{p}K_1$ of the conjugate acid) and $\log K_2$ (i.e., $\text{p}K_2$) were determined to be 11.09 and 4.53, respectively (Table 2.2), whereas the corresponding values in 1 M NaCl were found to be 9.95 and 3.66. In deionized water, $\log K_3$ (i.e., $\text{p}K_3$) involving the equilibrium **9** (ZH_2^\pm) + $\text{H}^+ \rightleftharpoons (\text{ZH}_3^+)$ **8** cannot be determined owing to the solubility problem associated with zwitterionic (\pm) **9**. During titration, it was revealed that a polymer backbone consisting of <80% zwitterionic (ZH_2^\pm) **9** and >20% zwitterionic–anionic ($\text{ZH}_2^\pm^-$) **10** remained water soluble, whereas higher percentages of the zwitterionic fraction impart insolubility.

The “apparent” [125] nature of all the basicity constants is reflected by the n_i values that were found to be >1. A measure of the polyelectrolyte index n is shown in Fig. 2.4a. A strong polyelectrolyte effect is reflected by a greater value of n associated with a greater variation of K with α . A decrease of $\text{p}K_2$ (involving (ZH^\pm^-) **10** + $\text{H}^+ \rightleftharpoons (\text{ZH}_2^\pm)$ **9**) with increasing α is a result of a gradual decrease in the overall negative charges, which induces

protonation. For pK_2 , the n_2 values were determined to be 2.11 and 1.76 in deionized water and 1 M NaCl, respectively, whereas the corresponding n_1 values for pK_1 (involving (Z^-) **11** + $H^+ \rightleftharpoons (ZH^{+ -})$ **10**) were found to be 1.24 and 1.16. The greater n_2 values confirm the consequence of the entropy effects [125,126]: as water-soluble $(\pm -)$ **10** is the most hydrated and water-insoluble (\pm) **9** is the least hydrated, a greater number of water molecules from the repeating unit of **10** is released as it is transformed to **9**. In comparison, both $(=)$ **11** and $(\pm -)$ **10** are hydrated; the former is slightly more hydrated as a result of its greater charge imbalance. As a result, the number of water molecules released for each protonation of the repeating unit is greater during the transformation from $(\pm -)$ **10** to (\pm) **9** than from $(=)$ **11** to $(\pm -)$ **10** transformation. The differences in the degree of hydration is reflected in n_2 values being $>n_1$. As the exothermic enthalpy changes (ΔH°) do not change with the increase in the degree of protonation, α , the ΔG° values are thus dictated by the contribution of the entropy term [126].

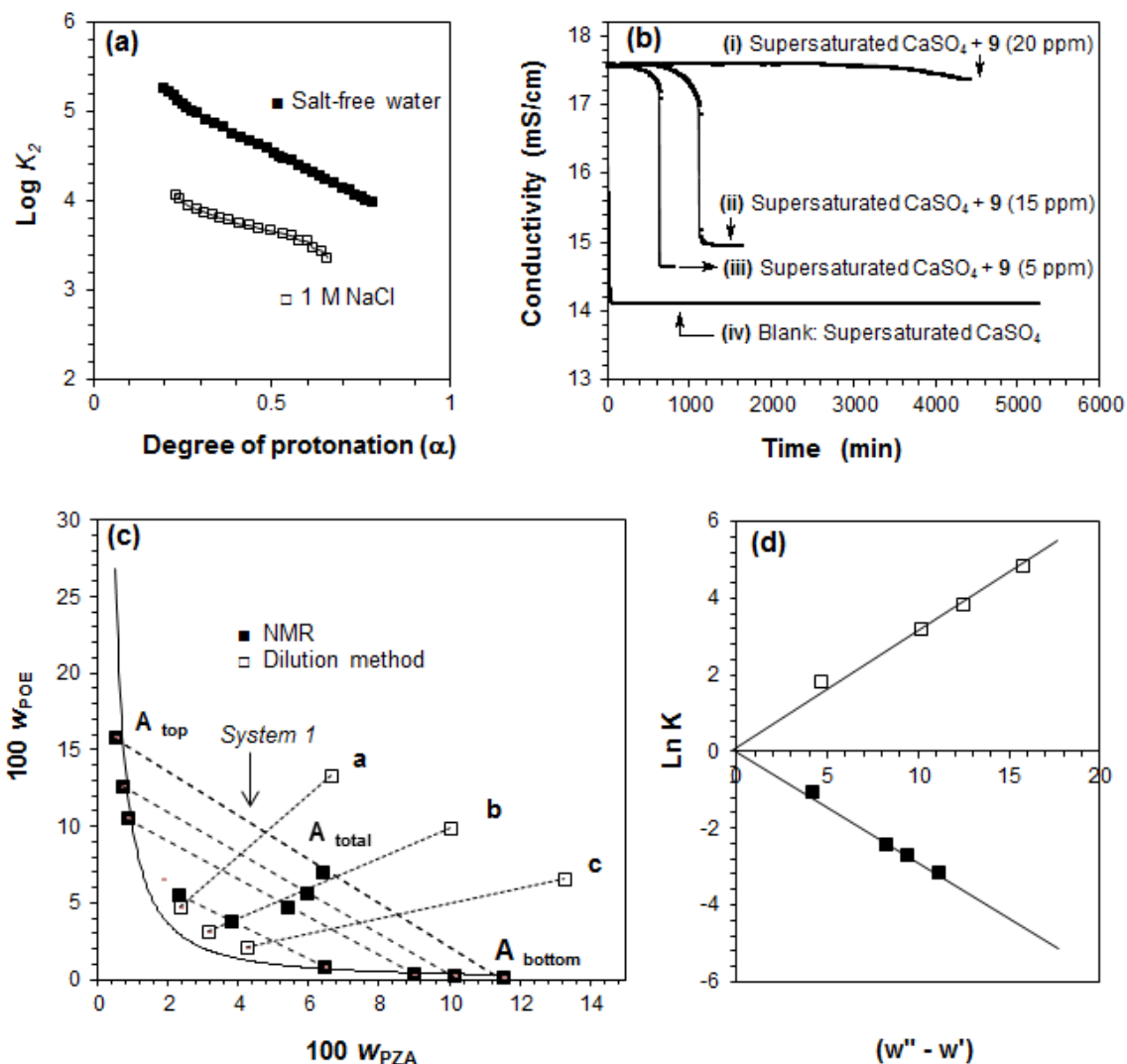


Figure 2.4 Figure 2.4 (a) Plot for the apparent $\text{log } K_2$ versus degree of protonation (\square) in \blacksquare salt-free water (entry 3, Table 2.3) and \square 1 M NaCl (entry 2, Table 2.3); (b) Trends in precipitation of a supersaturated solution of CaSO_4 with addition of (5, 15, and 20 ppm) and absence of PZA 9; (c) phase diagram (\blacksquare and \square represent data obtained by, respectively, the NMR and dilution methods) at 296 K of 0.6 M NaCl containing PZA 9 (treated with two equivalents of NaOH)–POE at 296 K; and (d) correlation of phase diagram of PZA 9 (two equivalents of NaOH)–POE–H₂O (0.6 M NaCl).

2.3.5 Scale inhibition properties of the synthesized polymers

In the Reverse Osmosis (RO) process, the inlet stream is feed water and outlet streams are product water and reject brine. If the dissolved salts in the reject brine stream become supersaturated, then scaling occurs. The percent inhibition (PI) of scaling is calculated using Eq. (4):

$$\% \text{ Scale Inhibition} = \frac{[Ca^{2+}]_{inhibited(t)} - [Ca^{2+}]_{blank(t)}}{[Ca^{2+}]_{inhibited(t_0)} - [Ca^{2+}]_{blank(t)}} \times 100 \quad (4)$$

where $[Ca^{2+}]_{inhibited(t_0)}$ is the initial concentration at time zero, and $[Ca^{2+}]_{inhibited(t)}$ and $[Ca^{2+}]_{blank(t)}$ are the concentrations in the inhibited and blank solution (without antiscalant) at time t , respectively.

For the current work, the scaling behavior of a supersaturated solution of $CaSO_4 \cdot 2H_2O$ containing 2598 ppm of Ca^{2+} and 6300 ppm of SO_4^{2-} in the presence of various concentrations of the synthesized antiscalant was investigated. The PI of **9** at concentrations of 5, 10, and 15 ppm is given in Table 2.3. The precipitation of $CaSO_4$ is indicated by a sudden drop in conductivity as in the absence of antiscalant (Fig. 2.4b-iv: blank). To our satisfaction, the presence of 20 ppm of **9** registered a 99 % scale inhibition for about 3000 min as calculated using Eq. (4). In the presence of a meager 5 ppm of antiscalant, it registered a 99% scale inhibition for a duration of 200 min. Usually a residence time of ≈ 30 min is required for the brine in the osmosis chamber. As shown in Fig. 2.4b, in the presence of **9**, the onset of precipitation is preceded by an induction period. Later on, the crystal growth recommences with a measurable rate observed by a sharp drop in conductivity. The duration of the induction periods depends on the concentration of the antiscalants; at a time scale of >4400 min, no induction was observed at the inhibitor

concentration of 20 ppm. Inhibition or retardation of crystal growth depends on the efficacy of an antiscalant [127] to scavenge metal cations and alter the crystal morphology at the time of nucleation [128]. The results presented in this study clearly show that the new polymer is able to prolong the induction period, and thus the fouling of membranes by CaSO_4 scale may be minimized.

Table 2.4 Inhibition percentage over precipitation for different times in the presence of varying concentrations of the polymer 9 in a supersaturated CaSO₄ solution at 40°C.

Entry	Sample (ppm)	Percent inhibition at times (min) of						Induction time (min)
		200	700	1500	3000	4000	4400	
1	5	99	15	–	–	–	–	630
2	15	100	99	25	–	–	–	1100
3	20	100	100	100	99	96	94	– ^a

^a No induction observed on the studied time range

2.3.6 Phase diagrams using (PZA 9 + two equivalents of NaOH)–POE– H₂O (NaCl) systems

The binodal and the tie-lines in the phase diagram of POE-PDE **11** (i.e., PZA **9** + two equivalents of NaOH) with 0.6 M NaCl in Fig. 2.4c are constructed by the dilution method and the ¹H NMR technique, respectively. The top and bottom phase remained rich in POE and PZA, respectively. The phases in equilibrium are connected by tie-lines; A_{total} and A_{bottom} represent the compositions of the total systems, the top phase, and the bottom phase, respectively. As the volume ratio (or the mass ratio) of the top and bottom phases $V_{\text{top}}/V_{\text{bottom}}$ is equated to the ratio of the length of the tie-line segments $(A_{\text{total}}-A_{\text{bot}})/(A_{\text{total}}-A_{\text{top}})$, a two-phase system with a suitable volume ratio can be constructed for a separation process. Single- and two-phase regions are demarcated by a binodal curve, which provides information about the suitability of the polymers for the downstream separation process.

The high water content makes an ATPS economical, environmentally friendly, harmless to biomaterials, and biocompatible. The effective and environmentally friendly use of ATPSs calls for a recycling method after the back-extraction of the biomacromolecules [129]. Although the use of nonionic polymers as components of ATPSs is well documented, the application of ionic polymers is scarce [106]. For this work, we have chosen biomimicking polyzwitterion acid PZA **9** (Scheme 2.2) for the construction of an ATPS containing POE as the second polymer component. Protein partitioning in ATPS composed of a pH-triggerable copolymer and POE has been demonstrated [106]. The use of inexpensive POE is well documented in the literature, which helped us utilize POE as the second polymer component in the current work [105,106,129]. The presence

of three pH-triggerable functionalities (N and CO₂⁻) in the current polymers is expected to impart pH-triggerable solution behavior; insolubility at lower pH values may help recycling the polymers by pH-controlled precipitation. We intend to use the current ATPS in the separation of several important proteins.

2.3.7 The Correlation of the Phase Diagrams

A Florey–Huggins theory-based correlation of the phase diagrams developed by Diamond and Hsu [130] to check the consistency of the tie-lines is given by Eqs. (5) and (6):

$$\ln K_1 = A_1 (w''_1 - w'_1) \quad (5)$$

and

$$\ln K_2 = A_2 (w''_2 - w'_2) \quad (6)$$

where the subscripts 1 and 2 represent polymer 1 (PZA **9** + NaOH) and polymer 2 (POE), respectively. The polymer weight percentages in the top and bottom phase are denoted as w'' and w' , respectively. The polymer molar masses and their interactions with water dictate the magnitude of the slopes A_1 and A_2 , whereas K_1 and K_2 represent the partition coefficient (C_t/C_b) of the polymer. The excellent linear least square fits of the data in Fig. 2.4d indicate that the phase behavior can be reasonably well described with the Diamond and Hsu model. Thus, this simple model requires only a single-phase composition to calculate A_1 and A_2 , thereby helping avoid extensive phase equilibrium determination.

Using Eqs. (6) and (7), a linear regression of $\ln K$ versus $w''_i - w'_i$, with zero intercept value afforded the parameters A_1 and A_2 . The root-mean-square deviation (rmsd) was

calculated using the experimental K_{exp} and the calculated partition constants K_{cal} by Eq. (7) [131]:

$$\text{rmsd} = \sqrt{\frac{\sum_{i=1}^N (K_{\text{exp}} - K_{\text{calc}})_i^2}{N-1}} \quad (7)$$

where the parameters A_i ($A_1 = -0.284$, $A_2 = 0.315$) and rmsd values ($(\text{rmsd})_1 = 0.0283$, $(\text{rmsd})_2 = 6.41$) of the correlation model for the partition coefficients using N number of tie-lines (Fig. 2.4d) ascertain that the Diamond and Hsu equations (Eqs. (5) and (6)) are helpful in correlating the experimental data of the current work.

2.4 Conclusions

New monomers **4** and **6** with residues of aspartic acid have been developed in excellent yields. The pH-triggerable polymer **8** represents the first example of a cyclopolymer containing residues of aspartic acid (an amino acid) as pendants. The solution properties of the pH-triggerable polymers **8–11** have been studied. The basicity constants for several basic centers have been determined; the data would be especially useful when considering the use of polymers as scavengers of toxic metal ions and inhibitors of metal corrosion. PZA **9** is shown to be a potential antiscalant additive in RO plants, as it imparted excellent scale inhibition at a meager concentration of 5–20 ppm. As discussed in the introduction section, polymers with lower molar masses may impart even better scale inhibition. The ATPSs of POE–(NaOH-treated PZA)–water (NaCl) may have industrial significance as the water-insolubility of the ionic polymer at lower pH values will permit its effective removal from solution. Note that the current work may not be

compared to the precedent literature on the topics covered in the article; the objective here is to introduce aspartic acid in a new role: that is, to synthesize a new aspartic acid-derived polymer and investigate its applicability. The polymer has already demonstrated remarkable antiscalant behavior.

CHAPTER 3

Synthesis and Application of Aspartic Acid Alternate

Copolymers

Abstract

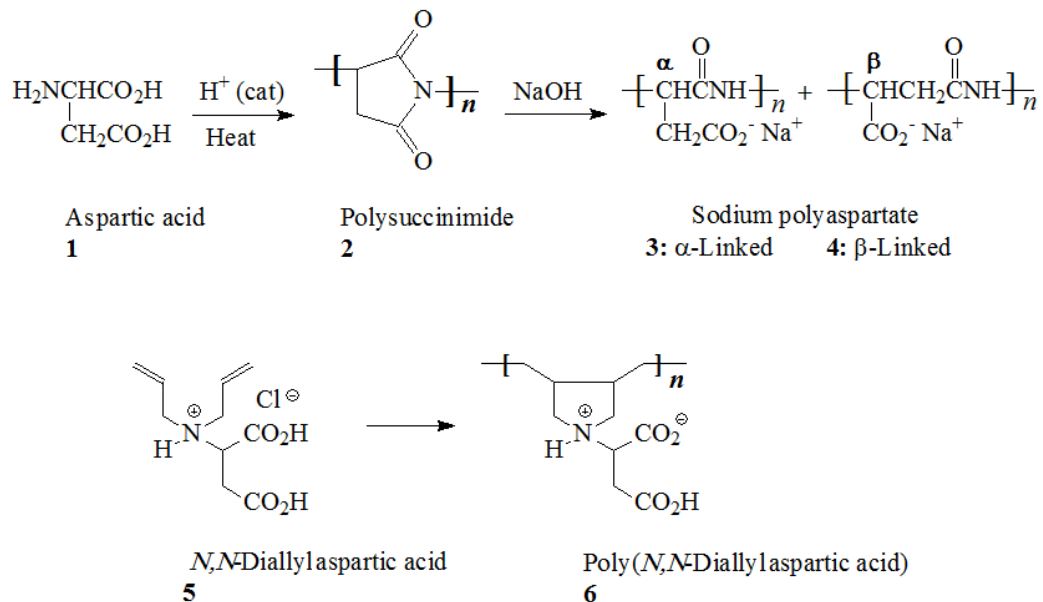
Monomer pairs: Dimethyl N,N-diallylaspartate hydrochloride $[(\text{CH}_2=\text{CH}-\text{CH}_2)_2\text{NH}+\text{CH}(\text{CO}_2\text{Me})\text{CH}_2\text{CO}_2\text{Me Cl}^-]$ (I)/ SO_2 and N,N-diallylaspartic acid hydrochloride $[(\text{CH}_2=\text{CH}-\text{CH}_2)_2\text{NH}+\text{CH}(\text{CO}_2\text{H})\text{CH}_2\text{CO}_2\text{H Cl}^-]$ (II)/ SO_2 , underwent alternate cyclocopolymerization to give cationic polyelectrolytes (CPEs) poly(I-alt- SO_2) (III) and poly(II-alt- SO_2) (IV), respectively, in very good yields. (+) III upon acid hydrolysis was converted to cationic (+) IV bearing in each repeating unit the triprotic acid residues $[(\text{NH}^+\dots(\text{CO}_2\text{H})_2]$ of aspartic acid hydrochloride. Under the influence of pH, (+) IV has been equilibrated to water-insoluble diprotic polyzwitterionic acid (\pm) V, water-soluble monoprotic poly(zwitterion-anion) ($\pm -$) VI and finally its conjugate base polydianion ($=$) VII. Basicity constants of CO_2^- and amine group have been determined. The pH-triggerable polymer has been demonstrated to be an efficient antiscalant against CaSO_4 scaling. For potential separation and purification of biomolecules, a recyclable aqueous two-phase system (ATPS) has been constructed using water-soluble ($=$) VII and urethanized polyvinyl alcohol; the ionic polymer can be recycled by precipitating it as (\pm) V at a lower pH.

3.1 Introduction

Aspartic acid (**1**) is one of the 23 proteinogenic amino acids, the building blocks of proteins; it plays an important role in the citric acid cycle, or Krebs cycle, during which many other important amino acids are synthesized (Scheme 3.1) [132]. Aspartic acid also plays a crucial role in generating cellular energy and as such, gets its reputation as a treatment for chronic fatigue. Poly(aspartic acid) (PASA) is a biodegradable water-soluble poly(amino acid) which may replace many non-biodegradable polymers [133]. Even though PASA has been found in nature as fragments of larger proteins [94], to our knowledge, it is yet to be isolated as a pure homo polymeric material from any natural source [134]. Polyaspartate (PASP), a 30:70 mixture of α - and β -linked amino acid (**3** and **4**), is currently produced on the industrial scale by thermal polymerization process leading through polysuccinimide (**2**) intermediate (Scheme 3.1) [88]. PASP and its derivatives are biodegradable [93] and environmentally friendly; as such, they are attractive alternatives to polyacrylic acid as corrosion inhibitors [88], antiscalant in desalination processes [89] and chelator of metal ions in waste water treatment. They have also found applications in manufacturing super-swelling material in diaper products and food packaging [90], biodegradable detergent and dispersant [87]. Recent research has also paved the way to use PASA-based pH-sensitive hydrogel for controlled drug release [135].

Note that in the peptide bonds in PASP, the nitrogen loses its basic character while each repeating unit consists of a single anionic center in the pendant carboxylate motifs. Keeping in view of the broad interest in this material from biomedical and material research community, diallyl derivative **5** of aspartic acid was cyclopolymerized using Butler's cyclopolymerization protocol [24–26,136] to obtain low molecular weight polymer **6** in

which the basic character of the nitrogen and the two anionic centers in the carboxylates are preserved [137]. However, attempts to obtain homopolymer **6** having high molar masses were unsuccessful. It has been reported earlier that diallylammonium salts having pendant carboxyl functionality give low molecular weight homopolymers in lower yields even in the presence of excessive amount of initiators [76]. No rationale was provided to account for the difficulty associated with the presence of carboxyl moiety. The objective of the current work is to apply copolymerization protocol [76] to obtain **5**/SO₂ copolymer **12** (Scheme 3.2) which would allow us to study the effect of SO₂ spacer on its pH-triggerable solubility behavior, basicity constant of the metal chelation centers and antiscalant properties. We intend to exploit the pH-dependent solubility behavior of **12** to develop recyclable aqueous two-phase system (ATPS) for potential application in bioseparation technology [106,138]. The titled alternate copolymer would represent the first example of its kind containing the residues of an important amino acid, i.e. aspartic acid. The current work would pave the way to utilize Butler's cyclopolymerization protocol [83] to synthesize aspartic acid-based cross-linked adsorbents for scavenging toxic metal ions from wastewater.



Scheme 3.1 Aspartic acid, polyaspartate and polymer containing aspartic acid residues.

3.2 Experimental Methods

3.2.1 Materials

For dialysis, membrane (Spectra/Por) with a MWCO of 6000-8000 was purchased from Spectrum Laboratories, Inc. (Rancho Dominguez, CA, USA). 2,2'-Azobisobutyronitrile (AIBN) from Fluka AG (Buchs, Switzerland) was crystallized from C₂H₅OH/CHCl₃ mixture. Dimethylsulfoxide (DMSO) was dried over calcium hydride overnight and then distilled under reduced pressure at a boiling point of 64-65°C (4 mmHg).

Polyvinyl alcohol (PVA) **16** with a \overline{M}_n of 72,000 g mol⁻¹ and a degree of hydrolyzation of 0.975-0.995 mole fraction was purchased from Fluka Chemie AG (Buchs, Switzerland). Partly urethanized PVA (UPVA) **17** (urethanized to the extent of 0.13 mole fraction) of

\overline{M}_n of 69,000 g mol⁻¹ was synthesized by heating a PVA **16**/urea in 1:1 mole ratio as described (Scheme 3.2) [139,140]. Dimethyl *N,N*-diallylaspartate (**9**) upon treatment with dry HCl gave hydrochloride salt **10**, while its hydrolysis with NaOH followed by acidification with HCl afforded *N,N*-diallylaspartic acid hydrochloride **5** [137].

3.2.2 Physical Methods

Perkin Elmer Series II (Model 2400) was used to carry out elemental analysis, and IR spectra were recorded on a Perkin Elmer 16F PC FTIR spectrometer. The NMR spectra were taken in a JEOL LA 500 MHz spectrometer using the residual proton resonance of D₂O at δ 4.65 ppm as an internal standard and dioxane ¹³C peak at δ 67.4 ppm as an external standard. TGA conducted using an SDT analyzer (Q600: TA instruments, USA) in a nitrogen atmosphere. Viscosities were measured in a Ubbelohde viscometer (viscometer constant = 0.005317 mm²/s²) using CO₂-free water under N₂ at 30.0 ± 0.1 °C. pH of the solutions was measured by a Sartorius pH meter PB 11. Conductivity measurements were carried out using an Orion Versa Star meter Thermoscientific (Beverly, MA, USA). PL-GPC 220 from Agilent Technologies equipped with a Refractive Index (RI) detector and two mixed bed columns (PL-aquagel-OH mixed-H 8 μm, 300 × 7.5 mm) was used to determine molecular weight. A 50 μl portion of a 0.100 w/v % aqueous solution of the polymer was injected into the GPC columns, and HPLC grade water containing 0.003 M NaN₃ was used as eluent at a flow rate of 1.0 mL/min.

3.2.3 Procedure for 10/SO₂ Copolymerization and Physical Characterization of 11

Table 3.1 describes the polymerization conditions. For instance, for the experiment under entry 4, SO₂ (2.56 g, 40 mmol) was absorbed in a monomer **10** (11.1 g, 40 mmol)/DMSO (12 g) solution in a Round bottom flask (50 mL). The initiator AIBN (0.120 g) was added and the mixture was stirred under N₂ at 63 °C for 36 h. The transparent reaction mixture was precipitated in acetone. The white polymer was grinded using mortar and pestle, filtered and washed with hot acetone. Copolymer **11** was then dried for 4 h at 60 °C in vacuum to a constant weight (11.8 g, 86%). Mp. (Closed capillary): slight phase change was noticed around 170 °C, became darker on further heating, turned brown at 285 °C and black at 325 °C with no further changes up to 400 °C. (Found: C, 41.9; H, 6.1; N, 4.0; S, 9.2. C₁₂H₂₀NO₆SCl requires C, 42.17; H, 5.90; N, 4.10; S, 9.38%); ν_{\max} (KBr): 3438, 2962, 2920, 1745, 1635, 1446, 1376, 1307, 1227, 1126, 1052, 1002, 857, 775 and 514 cm⁻¹. The ¹H and ¹³C NMR spectra are displayed in Figs. 3.1 and 3.2.

a. Acidic Hydrolysis of Copolymer 11

A solution of copolymer **11** (entry 4, Table 3.1) (10.3 g, 30 mmol) in 6 M HCl (120 cm³) was stirred at 65 °C for 72 h to complete the hydrolysis of the ester groups as checked by the absence of the methoxy proton signals. During the hydrolysis, polymer gradually precipitated from the initially clear solution. The entire mixture was dialyzed against deionized water for 48 h to remove HCl. The white polymer was grinded using mortar and pestle, filtered, washed with liberal excess of water and vacuum-dried at 55 °C to obtain copolymer **13** (7.4 g, 89%) as a white powder. Its spectral data are identical to that of the polymer obtained *via* **5**/SO₂ copolymerization described below.

b. Monomer **5**/SO₂ Copolymerization

The conditions for the copolymerization is described in Table 3.2. For instance, SO₂ (1.28 g, 20 mmol) was absorbed in a solution of monomer **5** (5.0 g, 20 mmol) in DMSO (5.0 g) in a Round bottom flask (25 mL). Initiator AIBN (0.100 g) was then added under N₂ to the homogeneous solution; the mixture in Round bottom flask was stirred at 63 °C for 36 h. The immovable gel was soaked in water for 24 h, and the white polymer was grinded with mortar and pestle, filtered and washed with excess water to obtain copolymer **13**, which was vacuum-dried at 60 °C to a constant weight. Its spectral data are identical to that of the polymer obtained *via* hydrolysis of the diester polymer **11** (*vide supra*). The thermal decomposition: turned tan on heating, became dark brown at 290 °C, and darker on further heating up to 400 °C with evolution of gas at 330 °C. (Found: C, 43.0; H, 5.6; N, 4.9, S, 11.2. C₁₀H₁₅NO₆S requires C, 43.32; H, 5.45; N, 5.05; S 11.56%); ν_{\max} . (KBr): 3459, 3041, 2977, 2920, 1728, 1628, 1386, 1305, 1127, 862, 780, 669 and 512 cm⁻¹. The ¹H, ¹³C NMR spectra and TGA curve are displayed in Figs. 3.1, 3.2 and 3.3a, respectively.

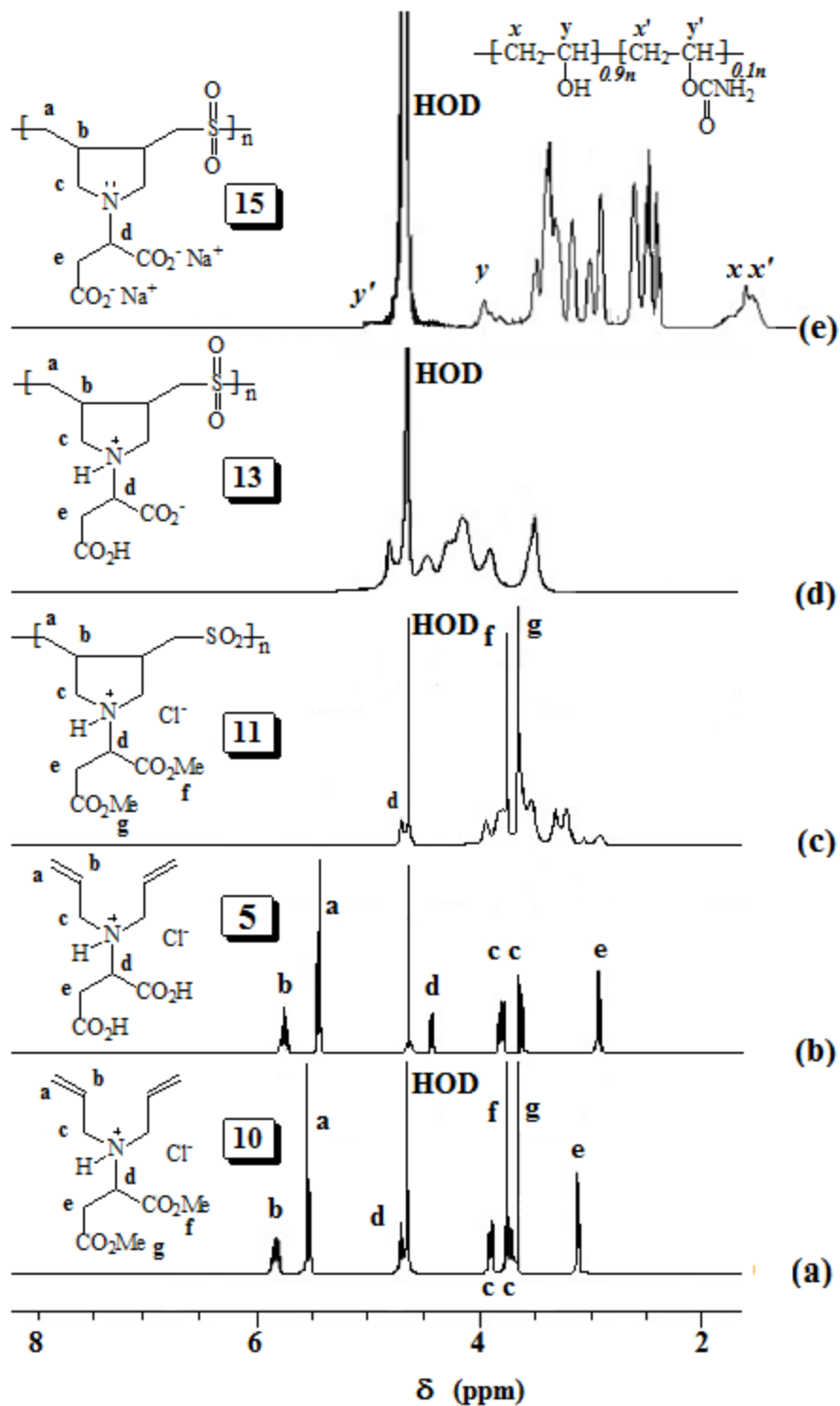


Figure 3.1 ^1H NMR spectrum of (a) 10, (b) 5, (c) 11, (d) 13 (in the presence of KI), and (e) top layer (System 1, Table 3.5) in D_2O .

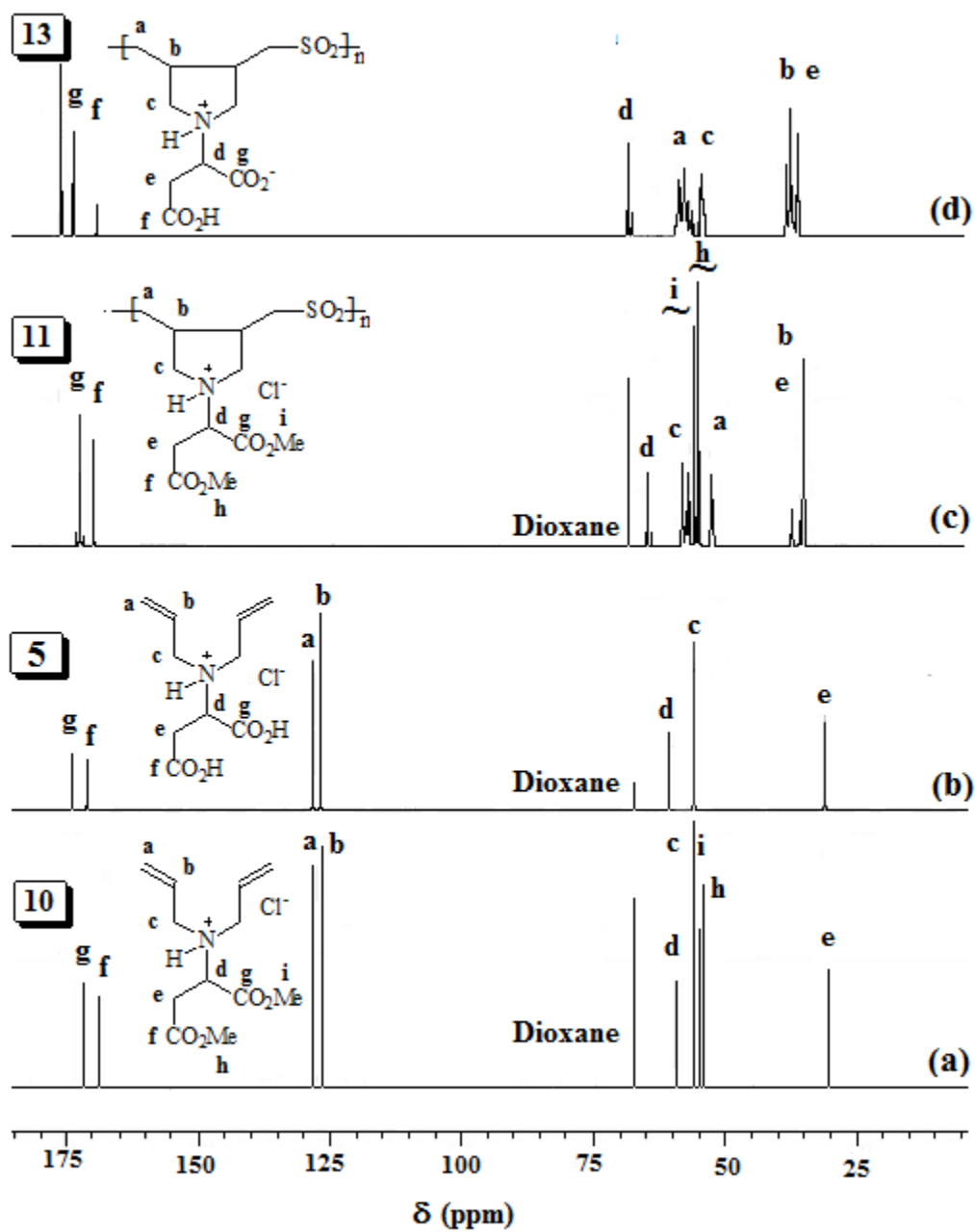


Figure 3.2 ^{13}C NMR spectrum of (a) 10, (b) 5, (c) 11 and (d) 13 (in the presence of KI) in D_2O .

3.2.4 Solubility Measurements

The Critical (minimum) Salt Concentration (CSC) values were determined by titrating a 1% w/w aqueous solution of PZA **13** containing salts at a higher concentration than their CSC values at 23 °C with deionized water. The average of the triplicate results of the CSCs were determined to be 4.73 M NaBr and 2.90 M NaI with approximate accuracies of $\pm 2-3\%$. The polymer was found to be insoluble in the presence of any concentration of NaCl or HCl (0 – 12 M).

3.2.5 Potentiometric titrations

Protonation constants (K) were determined using potentiometric titration as described elsewhere [72]. In each trial, a certain mmol of PZA **13** (ZH_2^\pm) was dissolved in a known amount of 0.1106 M NaOH (2.50 equivalent), then diluted to 200 cm³ using CO₂-free water (Table 3.3). After each addition of 0.05-0.15 cm³ of 0.1222 M HCl, the recorded pH values were used to calculate the log K_i s by the Henderson-Hasselbalch Eq. (2) (Scheme 3.2). Because of the solubility problem of PZA **13**, log K_3 associated with the equilibration **13** (ZH_2^\pm) + H⁺ \rightleftharpoons (ZH_3^+) **12** could not be determined in deionized water.

3.2.6 Evaluation of anti-scalant behavior

Newly synthesized antiscalant **13** (dissolved using 1 equiv. NaHCO₃, Table 3.2, entry 1) (20 and 30 ppm) was used to study the disruption of formation calcium sulfate scale at 40 °C \pm 1 °C in a supersaturated solution of 2598 mg/L of Ca²⁺ and 6300 mg/L of SO₄²⁻ [103]. The induction time, defined as the time at which a rapid decrease in conductivity occurs, indicates the beginning of CaSO₄ precipitation (Table 3.4).

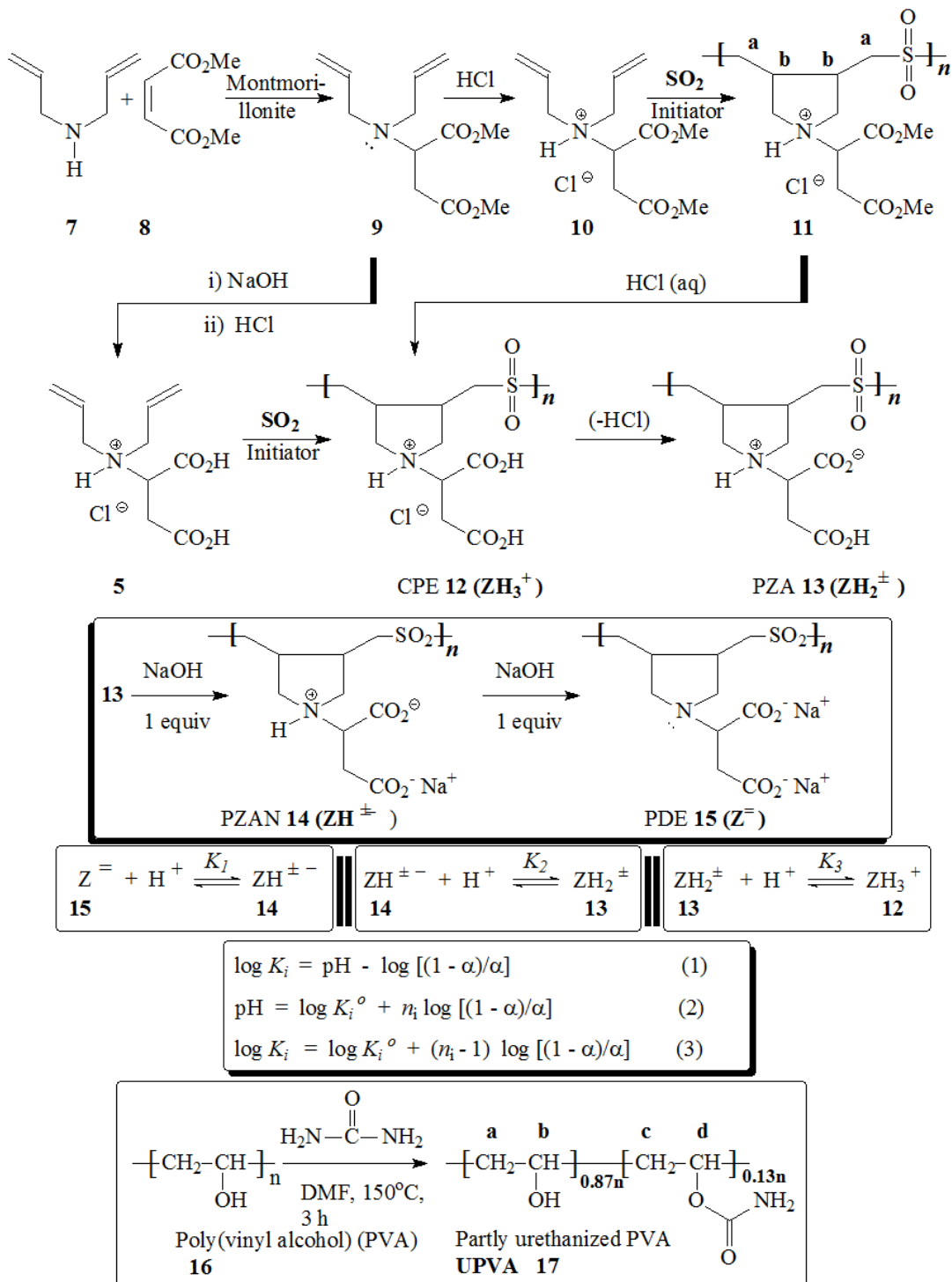
3.2.7 Phase Compositions of PZA **13** (+ 2 equivs NaOH) – UPVE **17**– H₂O (NaCl) Systems

a. The Tie-lines by ¹H NMR Spectroscopy

The stock solutions (20 wt%) of PZA **13** (Table 3.2, entry 1: treated with 2.0 equivalents of NaOH) and UPVE **17** in 0.6 M NaCl were used in certain compositions to make several ATPSs of total volume $\approx 7 \text{ cm}^3$ in a calibrated cylinder using diluents of 0.6 M NaCl. After mixing and centrifuging (ca. 5 min), the separated layers were equilibrated at 23 °C for 24 h. Volumes of the top and bottom layers were recorded and their densities measured. The ¹H NMR of the phases after exchanging H₂O with D₂O were taken to determine the molar ratios of the polymers in each phase. Fig. 3.1e displays the NMR spectrum of top phase of system 1 (Table 3.5); the thirteen protons of the PZA **13** (+NaOH) appeared as NMR signals in the range $2.3 \leq \delta \leq 3.7$ ppm having area integration of **A**, while the two-proton signals for UPVA **17** is displayed around δ 1.7 ppm having an area of **B**. Integration of the signals thus provided the mole ratios of the polymers **13/17** in each phase as $(\mathbf{A}/13)/(\mathbf{B}/2)$. The molar mass of the repeat unit of PZA **13** and UPVA **17** are taken as 277.3 and 49.6 g mol⁻¹, respectively. After determining the weight fraction (w) in each phase as described [20], the tie lines were constructed.

b. Binodals by Turbidity Method

The binodal data for the **13-17**-water (NaCl) systems at 23 °C were obtained by turbidimetric method using a procedure described elsewhere [20].



Scheme 3.2 Cyclopolymerization protocol in the synthesis of pH-triggerable polymers containing aspartic acid residues.

3.3 Results and Discussions

3.3.1 Synthesis of Polymers and their Characterization

Dimethyl *N,N*-diallyl aspartate (**9**), the Michael addition product from diallyamine (**7**)-dimethyl maleate (**8**), on treatment with gaseous HCl gave cationic monomer **10**, which upon hydrolysis with NaOH followed by acidification afforded the hydrochloride salt of *N,N*-diallyl aspartic acid (**5**) (Scheme 3.2).

Monomers **10** and **5** underwent cyclocopolymerization in the presence of initiator AIBN to give cationic polyelectrolyte (CPE) **11** (Table 3.1) and polyzwitterionic acid (PZA) **13** (Table 3.2), respectively, in very good to excellent yields. The change in initiator concentration from 3 mg/mmol monomer (Table 3.1, entry 1) to 4 and 5 mg/mmol (entries 2 and 3) did not change either the yield or the intrinsic viscosity in 0.1 M HCl. However the presence of higher amount of solvent DMSO (0.30 g/mmol monomer in entry 4 vs. 0.25 g/mmol monomers in entries 1-3) afforded the polymer in the highest yield (Table 3.1, entry 4). The amount of initiator also did not have any considerable effect on the yield and viscosity values of PZA **13** (Table 3.2). The polymers in Tables 1 and 2 were correlated by hydrolyzing CPE **11** (from entry 4) to CPE **12** which upon dialysis was converted into PZA **13** upon depletion of HCl (Scheme 3.2).

Three major weight losses were revealed in the TGA curve of PZA **13** (Fig. 3.3a). The first slow weight loss of 8% up to 100 °C resulted from the release of moisture trapped in the polymer. The polymer remained stable in the temperature range 100-150 °C, thereafter, second sharp loss of 23% in the temperature range 150-300 °C resulted from the release of SO₂. The third steep loss of 40% in the temperature range 300-430 °C was associated with

the decarboxylation and the degradation of the nitrogenated organic fraction. At 800 °C, the residual mass was found to be 17%.

Efforts to determine the molar masses of PZA **13** by GPC failed due to strong adsorption to the column materials. Similar difficulty associated with polymers containing amine and carboxy motifs have been reported [117]. However, CPE **11** from entries 3 and 4 (Table 3.1) were determined to have \overline{M}_w of 58,500 and 56,000 g mol⁻¹, respectively, with a PDI of 2.2.

3.3.2 Solubility Behavior

CPE **11** as well as poly(zwitterion-anion) (PZAN) ($\pm -$) **14** and polydianionic electrolyte (PDE) ($=$) **15** are water-soluble as expected of any polyelectrolyte or polymer backbone with a charge imbalance in favor of either of the algebraic signs. It is the anionic portion in ($\pm -$) **14** that promotes water-solubility. It is worth mentioning that in 0.1 M NaCl, a 0.25 w/w% of (+) **11** remained homogeneous, while at a concentration of 0.125 w/w%, it became a cloudy suspension rather than precipitation. The dilution is expected to shift the equilibrium: $(R')_2R''NH^+ (\mathbf{11}) \rightleftharpoons (R')_2R''N: + H^+$ towards right thereby increasing the fractional contribution of the water-insoluble neutral amine $(R')_2R''N:$ on the polymer chain. However, in deionized water, 0.125 w/w% polymer remained soluble by shifting the equilibrium to the left since the ammonium salt is a weaker acid in deionized water than in 0.1 M NaCl [22]. As expected of majority of electroneutral (\pm) polymers [74,118,119,141], zwitterionic **13** was found to be insoluble in deionized water but soluble in the presence of minimum critical salt concentrations (CSCs) of 4.73 M NaBr and 2.90 M NaI. The I⁻ being more polarizable than Br⁻ is more effective in neutralizing the ionic crosslinks thereby disrupting the intragroup, intra- and interchain attractive interactions [25]. Such large CSC

values indicate the remarkable strength of the zwitterionic interactions. It is quite surprising that the polymer was found to be insoluble in the presence of any concentration of NaCl or HCl (0.1 – 12 M). We find no rationale behind the insolubility in the presence of HCl which is expected to push zwitterionic (\pm) **13** towards CPE (+) **12**. It has been revealed during potentiometric titrations that addition of NaOH to an aqueous mixture of (\pm) **13** led to its solubility at a point where the backbone composition of repeat unit of (\pm) **13**/ $(\pm -)$ **14** becomes less than 90:10. Increasing the anionic portion thus leads to solubility in water.

3.3.3 Infrared and NMR Spectroscopy

The carbonyl frequency of the ester group in CPE **11** is confirmed by the presence of IR band at 1745 cm^{-1} . The strong bands around 1306 and 1126 cm^{-1} were assigned to the respective asymmetric and symmetric vibrations of SO_2 unit in **11** as well as in **13**. The symmetric and anti-symmetric stretching of COO^- in the dipolar form **13** appeared at respective 1386 cm^{-1} and 1628 cm^{-1} similar to those observed for simple amino acids [112], while the absorption for the C=O stretch of COOH appeared at 1728 cm^{-1} .

The ^1H and ^{13}C NMR spectra of monomers **5** and **10**, and polymers **11** and **13**, displayed in Figs. 3.1 and 3.2, respectively, reveal the absence of any residual alkene in the polymers as a consequence of faster intramolecular cyclization than intermolecular propagation in the cyclopolymerization protocol. The chain termination process by abstraction of an allylic proton of the monomer [113], as well as coupling process [114], would also lead to the absence of residual alkene in the polymers.

Table 3.1 Cyclocopolymerization of 10/SO₂ to copolymer 11 at 63°C for 36 h

Entry	Monomer (mmol)	SO ₂ (g) (mmol)	DMSO (g)	AIBN ^a (mg)	Yield (%)	η_{sp}/C^b dL/g
1	10	10	2.5	30	71	0.212
2	10	10	2.5	40	73	0.230
3	10	10	2.5	50	75	0.223
4	40	40	12	120	86	0.195

^a azobisisobutyronitrile.

^b Intrinsic viscosity of 1-0.125 % polymer solution in 0.1 M HCl at 30 °C was measured with an Ubbelohde Viscometer ($K=0.005317 \text{ mm}^2/\text{s}^2$).

Table 3.2 Cyclocopolymerization of 5/SO₂ to copolymer 13 at 63°C for 36 h

Entry	Monomer (mmol)	SO ₂ (g) (mmol)	DMSO (g)	AIBN ^a (mg)	Yield (%)	$[\eta]^b$ dL/g
1	20	20	5.0	80	71	0.585
2	20	20	5.0	100	73	0.573

^a azobisisobutyronitrile.

^b Intrinsic viscosity of 1-0.125 % polymer solution in the presence of 1 equiv. NaOH in 0.1 N NaCl at 30 °C was measured with an Ubbelohde Viscometer ($K=0.005317 \text{ mm}^2/\text{s}^2$).

3.3.4 Viscosity Measurement

Viscosity data for CPE (+) **11** (entry 4, Table 3.1) are plotted in Fig.3b-i. In deionized water, the viscosity plot for **11** was not typical of polyelectrolytes (i.e. concave upwards) (Fig. 3.3b-i); with decreasing concentration, the reduced viscosity decreases as a result of increasing presence of the neutral amine form in the mobile equilibrium: $(R')_2R''NH^+$ (**11**) $\rightleftharpoons (R')_2R''N: + H^+$ (*vide supra*). The viscosity plots move downwards in 0.1 M NaCl as compared in deionized water owing to the shielding of the cationic charges by Cl^- ions [Fig. 3.3b-iii]. The straight-line plot changes direction downwards at lower concentrations; the solution became a cloudy suspension at 0.125 w/w% as a result of the presence of excessive amount of the neutral amine. The reduced repulsive charges on the polymer chain therefore decreases the hydrodynamic volumes, hence decreases the viscosity values. The viscosity plot becomes normal in 0.1 M HCl (Fig. 3.3b-ii); added H^+ forces CPE **11** to be in the cationic form. The equilibrium mentioned above is shifted towards left, and Cl^- ions shield the positive nitrogens so as to give normal linear plot. A comparison between Fig. 3.3b-ii and Fig. 3.3b-iii confirms that the higher viscosity in 0.1 M HCl than in 0.1 M NaCl is a result of the higher cationic charge density in the polymer chain in the former medium.

PZA (\pm) **13** is water-insoluble; however in the presence of 1 and 2 equivs. NaOH it is converted into ($\pm -$) PZAN **14** and ($=$) PDE **15**, respectively. The viscosity plots of **14** (Fig. 3.3c-i) and **15** (Fig. 3.3c-ii) are concave upwards in deionized water as expected of polyelectrolytes, while they became linear in 0.1 M NaCl (Figs.3.3c-iii and iv). It is surprising to note that dianionic ($=$) **15** has lower viscosity values (Fig. 3.3c-ii) than that of zwitterionic/anionic ($\pm -$) **14** (Fig. 3.3c-i) in deionized water as confirmed by careful triplicate measurements under N_2 . As per expectation, ($=$) **15** should have higher viscosity

values as a result of greater repulsions among its repeating units having higher negative charge density. The expected trend is observed in 0.1 M NaCl (Figs.3c-iii versus iv) but not in deionized water. One possible rationale behind these findings is that in deionized water, the shorter distance between the positive nitrogens in the neighboring zwitterionic dipoles in (\pm -) **14** leads to greater repulsions than the repulsions experienced among more distant negative oxygens in the neighboring repeating units of dianions (=) **15**. In 0.1 M NaCl, the Cl⁻ ions effectively neutralizes the positive nitrogens in (\pm -) **14** permitting the greater negative charges in (=) **15** to dictate the viscosity values. In order to correlate two polymers (+) **11** (Table 3.1) and (\pm) **13** (Table 3.2), obtained *via* respective monomers **10** and **5**, diester **11** was hydrolyzed to **13** (Scheme 3.2). The intrinsic viscosities of (\pm -) **14** [i.e. (\pm) **13** + 1 equiv NaOH] prepared from Table 3.1 (entry 4) and Table 3.2 (entry 1) were determined to be 0.354 and 0.585 dL g⁻¹, respectively (*cf.* Fig. 3.3c-iv vs. 3.3c-v). Using Mark-Houwink equation ($[\eta] = KM^a$) with an approximate ‘a’ value of 0.8, the sample from Table 3.2 (entry 1) is estimated to have a Mw of 105,000 g mol⁻¹ as calculated from the known Mw of 56,000 g mol⁻¹ for the sample of Table 3.1 (entry 4) and the $[\eta]$ values of 0.354 and 0.585 dL g⁻¹ as presented above. The diester monomer **10** was thus found to give polymers (Table 3.1) with lower molar masses as compared to its hydrolysed counterpart **5** (Table 3.2), presumably as a result of higher steric crowding of the ester group (during cyclization) than its hydrolysed counterpart.

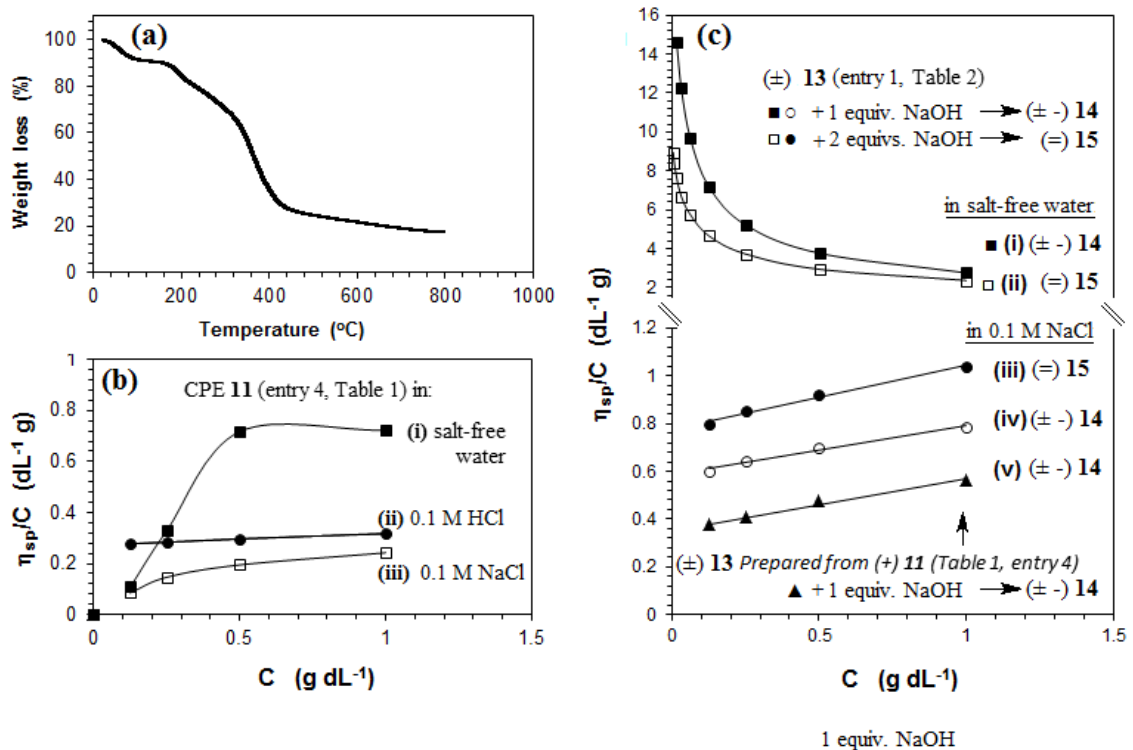


Figure 3.3 (a) TGA curve of PZA 13; Utilizing a viscometer, 30 °C: the viscosity behavior of (b) (+) CPE 11 (entry 4, Table 3.1) in (i) ■ salt-free water and (ii) ● 0.1 M HCl and (iii) ▲ 0.1 M NaCl; (c) (±) PZA 13 (entry 1, Table 3.2) in (i) ■ 1 equivs NaOH, salt-free water, (ii) □ 2 equiv NaOH, salt-free water; (iii) ● 2 equivs NaOH, 0.1 M NaCl, (iv) ○ 1 equivs NaOH, 0.1 M NaCl, (v) ▲ PZA 13 (prepared from entry 4, Table 3.1) 1 equiv NaOH, 0.1 M NaCl.

3.3.5 Basicity Constant

Basicity constants K_1 , K_2 and K_3 describes the protonation of repeat units in (=) **15**, (\pm -) **14** and (\pm) **13**, respectively. Unlike small molecules, the K_i of a repeat unit is ‘apparent’[125], it depends on the type of charge and its density in the neighbouring units, and as such it varies with the degree of protonation (α). The K_i s of anionic centers is described by Eq. (3) (Scheme 3.2) where $\log K_i^o = \text{pH}$ at $\alpha = 0.5$ and $n_i = 1$ in the case of sharp basicity constants. Using Eq. (2), the pH vs. $\log [(1-\alpha)/\alpha]$ plots enabled us to determine the ‘ n_i ’ and $\log K_i^o$ as the slope and intercept, respectively, as described elsewhere [72]. In deionized water, basicity constants $\log K_1$ and $\log K_2$ were determined to be 9.91 and 5.33, respectively, while the corresponding n_1 and n_2 were found to be 1.71 and 1.35 (Table 3.3). $\log K_3$ involving the equilibrium: **13** (ZH_2^\pm) + $\text{H}^+ \rightleftharpoons (\text{ZH}_3^+)$ **12** could not be determined owing to the water-insolubility of the component polymers. It was revealed during titration that a polymer backbone consisting of less than 90% zwitterionic (ZH_2^\pm) **13** and more than 10% zwitterionic-anionic ($\text{ZH}_2^\pm^-$) **10** remained water-soluble while higher percentages of zwitterionic fraction impart insolubility.

Any value of n_i (i.e. polyelectrolyte index) other than 1 leads to variation of K with α (Fig. 3.4a). The n_i values greater than 1 lead to the decrease of K with α . A strong polyelectrolyte effect is reflected by a greater value of n associated with a greater variation of K with α . A gradual decrease of average negative charge density per repeating unit with increasing α reduces the electrostatic field that induces protonation. It is worth mentioning that $\log K$ of a base is the $\text{p}K_a$ of its conjugate acid.

3.3.6 Inhibition of CaSO₄ Scale Formation by the Synthesized Polymer

In Reverse Osmosis (RO) process, the inlet feed water stream is divided into product water and reject brine which may become supersaturated with salts that may lead to scaling thus reducing the efficiency of the desalination membrane. The percent inhibition (PI) of scaling is calculated using Eq. (5):

$$\% \text{ Scale Inhibition} = \frac{[\text{Ca}^{2+}]_{\text{inhibited}(t)} - [\text{Ca}^{2+}]_{\text{blank}(t)}}{[\text{Ca}^{2+}]_{\text{inhibited}(t_0)} - [\text{Ca}^{2+}]_{\text{blank}(t)}} \times 100 \quad (5)$$

where $[\text{Ca}^{2+}]_{\text{inhibited}(t_0)}$, $[\text{Ca}^{2+}]_{\text{inhibited}(t)}$ and $[\text{Ca}^{2+}]_{\text{blank}(t)}$ are the Ca^{2+} concentrations at time zero and t in the inhibited and blank solution (without antiscalant), respectively.

For the current work, the scaling behavior of a supersaturated solution of CaSO₄ containing 2598 ppm of Ca²⁺ and 6300 ppm of SO₄²⁻ in the presence of 30 and 20 ppm of synthesized antiscalant **13** was investigated, and the results of % scale inhibition are given in Table 3.4. The effectiveness of an antiscalant depends on its ability to scavenge metal cations [89] and interfere with crystal formation at the time of nucleation [128]. In the absence of antiscalant, the precipitation of CaSO₄ is indicated by a sudden drop in conductivity (Fig. 3.4b-iii: Blank). To our satisfaction, the presence of 20 and 30 ppm **13** registered scale inhibitions of 98 and 99%, respectively for about 30 min as calculated using Eq. (5). In the presence of 30 ppm antiscalant, it registered a 97.5 % scale inhibition at a time of 1500 min. Usually, a residence time of ≈ 30 min is required for the brine in osmosis chamber. At the inhibitor concentration of 20 ppm, an induction period of 70 min is followed by a sharp drop in conductivity which indicates an accelerated growth of CaSO₄

crystal (Fig. 3.4b-ii). However, at the time scale of over 3000 minutes, no induction was observed at the inhibitor concentration of 30 ppm.

In the presence of an antiscalant, crystals having irregular shapes and loose structures of smaller fragments are formed. Involvement of the antiscalant into the nucleation process during the induction period leads to the prevention of the normal growth of $\text{CaSO}_4 \cdot 2\text{H}_2\text{O}$ by poisoning the active growing sites in the crystal. This leads to the increase in the internal stress of the distorted crystals, thereby resulting in crystal fractures and prevention of deposition of microcrystalline [128]. Later on, after all the antiscalant molecules are adsorbed into growing crystal, the crystal growth can resume at a rate comparable to that of the un-poisoned systems. So, the induction period depends on the concentration of the antiscalant; at a higher concentration (30 ppm versus 20 ppm), it is able to prolong the induction period and may thus minimize the fouling of membranes by $\text{CaSO}_4 \cdot 2\text{H}_2\text{O}$.

Table 3.3 Determination of Protonation constants of Polymer 15 (Z^-) and 14 ($ZH^{\pm-}$) at 23 °C in deionized water

run	ZH_2^{\pm} (mmol)	C_T^a (mol dm ⁻³)	α -range	pH-range	Points ^b	Log $K_i^{\circ c}$	n_i^c	$R^2,^d$
Polymer 13 in Salt-Free water^e								
1	0.2171 (ZH_2^{\pm})	+0.1222	0.44–0.90	10.25–8.30	19	9.95	1.68	0.9984
2	0.2528 (ZH_2^{\pm})	+0.1222	0.33–0.90	10.51–8.34	27	9.88	1.73	0.9897
3	0.2885 (ZH_2^{\pm})	+0.1222	0.32–0.92	10.55–8.13	23	9.91	1.71	0.9915
Average						9.91 (4)	1.71 (3)	
Log $K_1^f = 9.91 + 0.71 \log [(1-\alpha)/\alpha]$						For the reaction: $Z^- + H^+ \xrightleftharpoons{K_1} ZH^{\pm-}$		
1	0.2171 (ZH_1^{\pm})	+0.1222	0.15–0.81	6.40–4.62	20	5.39	1.38	0.9925
2	0.0.2528 (ZH_2^{\pm})	+0.1222	0.11–0.83	6.49–4.45	24	5.30	1.31	0.9940
3	0.2885 (ZH_2^{\pm})	+0.1222	0.17–0.89	6.25–4.05	30	5.31	1.35	0.9988
Average						5.33 (5)	1.35 (4)	
Log $K_2^f = 5.33 + 0.35 \log [(1-\alpha)/\alpha]$						For the reaction: $ZH^{\pm-} + H^+ \xrightleftharpoons{K_2} ZH_2^{\pm}$		

^a (+)ve values describe titrations with HCl.

^b Number of data points.

^c Standard deviations in the last digit are given under the parentheses.

^d R = Correlation coefficient.

^e Known amount of polymer PZA 13 (ZH_2^{\pm}) was dissolved in a known amount of 0.1106 M NaOH (2.50 equivalent), then diluted to 200 cm³ using salt-free water.

^f $\log K_i = \log K_i^{\circ} + (n_i - 1) \log [(1 - \alpha)/\alpha]$.

Table 3.4 Inhibition percentage over precipitation for different times in the presence of varying concentrations of the polymer 13^a in 3 CB supersaturated CaSO₄ solution at 40°C

Entry	Sample (ppm)	Percent inhibition at times (min) of						Induction time (min)
		10	20	30	60	90	1500	
1	20	98.5	98.5	98	92	14	–	70
2	30	99.5	99.3	99	98	98	97.5	– ^b

^a Dissolved in water with the aid of minimum amount of NaHCO₃.

^b No induction observed on the studied time range.

Table 3.5 composition of the Phases of the [UPVA^a + PZA 8^b] system (2.0 equiv. NaOH, 0.6 M NaCl at 296 K shown in figure 3.4c

NMR method							
System	Total system		Top phase		Bottom phase		Volume ratio ^c
	PZA <i>w</i> × 100	UPVA <i>w</i> × 100	PZA <i>w</i> × 100	UPVA <i>w</i> × 100	PZA <i>w</i> × 100	UPVA <i>w</i> × 100	
1	1.62	3.33	2.29	0.342	0.101	10.1	2.4
2	1.31	3.20	1.89	0.406	0.139	8.78	1.9
3	1.10	2.76	1.59	0.491	0.169	7.41	1.8
4	0.557	3.54	1.11	0.645	0.196	5.63	0.5

Turbidity method					
System	Binodal data		System	Binodal data	
	PZA <i>w</i> × 100	UPVA <i>w</i> × 100		PZA <i>w</i> × 100	UPVA <i>w</i> × 100
a	0.176	3.15	f	0.521	0.805
b	0.206	2.37	g	0.543	0.573
c	0.231	1.62	h	0.967	0.114
d	0.269	1.32	i	1.11	0.0892
e	0.442	1.08	j	3.04	0.0726

^a Urethenized poly(vinyl alcohol).

^b PZA 8 (+ 2 equiv. NaOH).

^c Volume ratio of top and bottom phase.

3.3.7 Phase Diagrams using [PZA 13 + 2 equivs. NaOH] – UPVA 17 – H₂O (NaCl) Systems.

The turbidity method was used to construct the binodal, while ¹H NMR technique was utilized for the tie lines in phase diagram of UPVE 17 - PDE 15 (i.e., PZA 13 + 2 equiv NaOH) - 0.6 M NaCl in Fig. 3.4c. The A_{total} represents the composition of a total system, which splits into PZA-rich top (A_{top}), and UPVA-rich bottom (A_{bottom}) phases. The three compositions are connected by a tie line where volume ratio (or the mass ratio) of the top and bottom phases V_{top}/V_{bottom} is equated to the ratio of the tie-line length: $(A_{total}-A_{bot})/(A_{total}-A_{top})$ [138], Variation in the A_{total} is helpful in the construction of ATPS with a suitable volume ratio.

A binodal curve demarcates a single- and two-phase region, and thus provides information about the suitability of the polymers for industrial separation process. Its position closer to the axes makes the ATPS more economical, since it will require lower amount of polymers for phase separation to occur. For the current ATPS, the phase separation occurs at total polymer concentrations of $\approx 5\%$ which is excellent from industrial point of view. At higher polymer concentrations, ATPS systems become more expensive. For bioseparation, the high water content is expected to make this ATPS biocompatible and benign to biomaterials. One of the most gratifying aspects of the current ATPS is the solubility behavior of the component polymer PZA 13. Environmentally friendly use of ATPSs in separation and purification of biomolecules demands a way to their recycling [138], which is possible with the current polymer 13, since at lower pH values, it is practically insoluble in water. Though outnumbered by construction and use of non-ionic ATPSs, application of ionic polymers in protein separation has also been documented

[106]. PZA **13** containing aspartic acid residues with pH-triggerable functionalities (N and CO₂⁻) is anticipated to impart pH responsive behaviors in selective separation and purification of biomolecules like proteins.

3.3.8 The Correlation of the Phase Diagrams.

Eqs. (6) and (7), based on Florey-Huggins theory, were developed by Diamond and Hsu [130] to check the consistency of the tie-lines.

$$\ln K_1 = A_1 (w''_1 - w'_1) \quad (6)$$

and

$$\ln K_2 = A_2 (w''_2 - w'_2) \quad (7)$$

where the subscripts 1 and 2 represent polymer 1 (UPVA) and polymer 2 (PZA **13** + NaOH), while w'' and w' denote the polymer weight percent in the top and bottom phase, respectively. The magnitude of the slopes A_1 and A_2 reflect the effects of polymer molar masses and their interactions with water. The concentration ratio of the polymers in the top and bottom layer (C_t/C_b) represents the partition coefficient K_1 and K_2 . The simple model thus describes the phase behavior reasonably well as shown by the good least square linear fits of the data in Fig. 3.4d. A linear regression of $\ln K$ versus $w''_i - w'_i$, with zero intercept value afforded the parameters A_1 and A_2 . The root mean-square deviation (rmsd) was calculated using the experimental K_{exp} and the calculated partition constants K_{cal} by Eq. (8) [131]:

$$\text{rmsd} = \sqrt{\frac{\sum_{i=1}^N (K_{\text{exp}} - K_{\text{calc}})_i^2}{N-1}} \quad (8)$$

where the parameters A_i ($A_1 = -0.371$, $A_2 = 1.51$) and rmsd values [$(\text{rmsd})_1 = 0.0257$, $(\text{rmsd})_2 = 2.87$] of the correlation model for the partition coefficients using N number of tie lines (Fig. 3.4d) ascertain that Eqs. (6) and (7) are helpful in correlating the experimental data of the current work. The simple model thus requires only a single phase composition to calculate A_1 and A_2 , thereby helps to avoid extensive phase equilibrium determination.

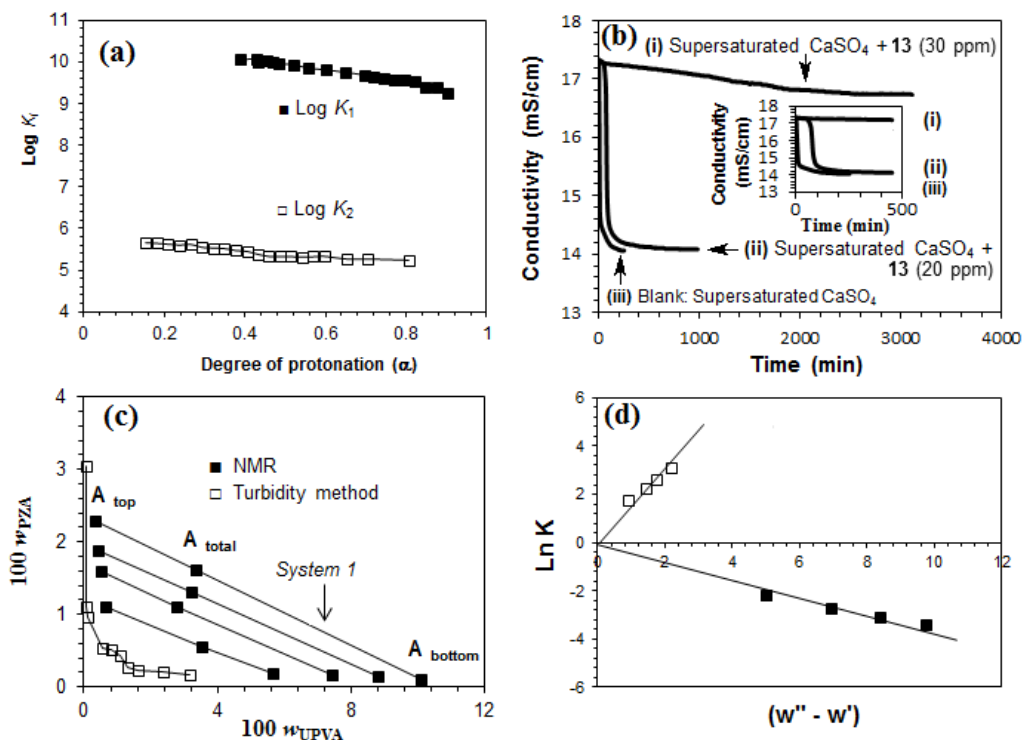


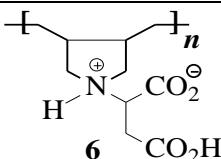
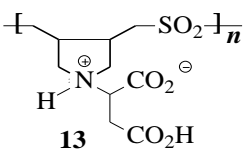
Figure 3.4 (a) Plot for the apparent $\log K_i$ versus degree of protonation (\square) \blacksquare (K_1 , entry 1, Table 3.3) \square (K_2 , entry 1, Table 3.3); (b) Trends in precipitation of a supersaturated solution of CaSO_4 with addition of (20, 30 ppm) and absence of PZA 13 (+1 equiv. NaHCO_3); (c) Phase diagram [\blacksquare and \square represent data obtained by respective NMR and turbidity method] at 296 K of PZA 13 (treated with 2 equivs. NaOH)-UPVA- H_2O (0.6 M NaCl) at 296 K; (d) Correlation of phase diagram of PZA 13 (2 equiv. NaOH)-UPVA- H_2O (0.6 M NaCl).

3.3.9 Poly(N,N-diallylaspartic acid) **6** versus Poly(N,N-diallylaspartic acid-*alt*-SO₂) **13**: A Comparison of the Homo- and Copolymers

Several properties of homopolymer poly(diallyl aspartate) (**6**) and copolymer poly(diallyl aspartate-*alt*-SO₂) (**13**) are summarized in Table 3.6. The presence of electron-withdrawing SO₂ unit has decreased the log K_1 i.e. log [basicity constant] of the amine nitrogen by 1.2 unit as compared to the homopolymer. Since $\log K_1 = pK_{NH^+}$, the conjugate acid **14** of copolymer **13** is thus more acidic than its homopolymer counterpart. The presence of SO₂ is also expected to increase the acidity of diester copolymer **11**; its increased dissociation to the neutral amine form led to its insolubility in dilute aqueous mixture (*vide supra*). Butler's cyclopolymerization protocol gave copolymers having much higher molar masses than the corresponding homopolymers (Table 3.6). Homopolymer **6** imparted much higher scale inhibition than copolymer **13**; at a 20 ppm concentration, the inhibition of CaSO₄ scale formation after the elapse of 1500 min was found to be 100 and 14%, respectively. It is to be noted, in this respect, that PASP (**3/4**) (Scheme 3.1) with lower molar masses has been shown to impart better scale inhibition than the polymer with higher molar masses. PASP with molar masses in the range 1000-2000 g mol⁻¹ imparted an efficiency of inhibition of 80% in a supersaturated 0.1 M Na₂SO₄ and CaCl₂ solutions at 30 °C for 24 h [7]. Therefore it is logical to conclude that the better scale inhibition by homopolymer **6** as compared to copolymer **13** must be a consequence of its lower molar mass. In future endeavor, attempts would be made to obtain homo- and copolymers with molar masses as low as possible in order to achieve better scale inhibition efficiencies. Polymers with smaller sizes can interfere more effectively with the nucleation and growth of scale.

There is a great difference in the solubility behaviors of the homo- and copolymers. The copolymer has higher CSC values for various salts i.e., higher amount of salts are required to promote its water-solubility (Table 3.6). As a result of electron-withdrawal by SO₂ unit, the positive charge on the nitrogens in copolymer **13** is more dispersed, hence less hydrated. The enhanced zwitterionic attraction in **13** in the absence of interference by hydration demands greater amount of salts for its disruption to promote solubility. It is interesting to note that the copolymer is practically insoluble in the presence of any amount of added HCl or NaCl, thereby making it a suitable polymer component in a pH-controlled recyclable ATPS.

Table 3.6 Basicity constant K_1 , molar mass and scale efficiency of inhibition of homo- and co-polymer

Polymer	$pK_{NH^+}^a$ or $\log K_1$	Mw (g mol ⁻¹)	Scale inhibition ^b (%)	CSC ^c			
				NaCl (M)	NaBr (M)	NaI (M)	HCl (M)
 <p>6</p>	11.1	10,100	100	0.640	0.360	0.228	0.0224
 <p>13</p>	9.91	105,000	14	Insolu- ble ^d	4.73	2.90	Insolu- ble ^d

^a in deionized water at 23 °C.

^b after 1500 min using 20 ppm polymer in a supersaturated solution of CaSO₄ (aq) at 40 °C.

^c Critical salt concentration required to promote solubility at 23 °C.

^d Insoluble in the presence of any concentration of NaCl or HCl.

3.4 Conclusions

Monomers **5** and **10** containing residue of aspartic acid have been cyclopolymerized with SO₂ to obtain alternate copolymers PZA **13** (i.e. **5**-alt-SO₂) and CPE **11** (i.e. **10**-alt-SO₂) in very good yields. PZA **13** is practically insoluble in water or aqueous HCl or NaCl, while soluble only in the presence of high concentrations of NaBr and NaI. The addition of NaOH transforms PZA (\pm) **13** to water-soluble PZAN (\pm -) **14** and PDE (=) **15**, which has been used as a component polymer in the construction of a recyclable ATPS. The interesting solubility behaviour envisages its use at a higher pH value and recycling by precipitating at a lower pH. The basicity constant K for the ligand centres in the following equilibria: (=) **15** + H⁺ \rightleftharpoons (\pm -) **14** and (\pm -) **14** + H⁺ \rightleftharpoons (\pm) **13** have been determined; the data would be of great value for proper utilization of the polymer as a scavenger of toxic metal ions and inhibitor of metal corrosion.

The potential of PZA **13** as an antiscalant has been demonstrated; it imparted excellent CaSO₄-scale inhibition. The interesting pH-dependent solubility behaviour for the current polymers could well be exploited in forming blend films containing zwitterion structure units for potential application in membrane separation [142]. Work is currently underway in our laboratory to utilize current monomers to synthesize aspartic acid-based cross-linked resin as chelating adsorbents for the removal of toxic materials.

CHAPTER 4

Synthesis and Application of a Cross-linked Resin with Aspartic Acid Residues

Abstract

In this work, a unique cross-linked polyzwitterion/anion having aspartic acid residue was synthesized via butler's cyclopolymerization protocol involving *N,N*-diallylaspartic acid hydrochloride, 1,1,4,4-tetraallylpiperazinium dichloride and sulfur dioxide in the presence of azoisobutyronitrile. The structure and morphology of the polymer were characterized by using FTIR, TGA, EDX and SEM. The adsorption performance of the resin was evaluated using lead Pb(II) as model. The effect of various parameters such as contact time, pH, initial concentration and temperature were investigated to arrive at optimum conditions. Optimum pH of 6.0 and dosage of 1.5g L⁻¹ were obtained. The mechanism of adsorption was investigated using kinetic, diffusion, isotherm and thermodynamic models. The adsorption kinetic data were described well by the pseudo-second order model with R² of 0.999. The activation energy (E_a) of the adsorption process was calculated as 39.29 kJ mol⁻¹. The negative ΔG° values indicate a spontaneous adsorption process while the negative ΔH° (-43.87 KJ/mol) suggests an exothermic reaction. Adsorption data were described well by the Langmuir and Temkin models. EDX analysis confirmed the adsorption of Pb²⁺ on the polymer. The overall results suggest that the polymer could be

employed as an efficient adsorbent for the adsorption of toxic Pb^{2+} from polluted aqueous solutions

4.1 Introduction

Heavy metals are released into the surface and ground water because of various activities such as electroplating, and pigment and paint manufacturing. Because of their toxicity and tendency to bioaccumulation, the removal of metals from industrial effluents before discharge into the environment is required to mitigate any impact on plants, animals and humans [143]. Lead is one of the most toxic metals that are widely used in various industries, such as battery and glass manufacturing, metal plating and finishing, printing and tanning. The permissible levels of lead in drinking and waste water are 0.005 mg/L and 0.05mg/L, respectively [144].

Several conventional methods, such as chemical precipitation as hydroxides, carbonates or sulfides and subsequent liquid-solid separation, sorption, membrane processes, and reverse osmosis, electrolytic recovery and liquid-liquid extraction, are used for the removal of pollutants [145]. However, these technologies are either expensive for the treatment and disposal of the secondary toxic sludge or ineffective when the toxic metal is present in wastewaters at low concentrations [146].

Alternatively, adsorption is one of the preferred methods for the treatment of wastewater because of its efficiency and simplicity. A successful adsorption process depends on the adsorption performance of the adsorbents. Various conventional adsorbents have been reported for the removal of lead from wastewaters including activated carbon, clay, metal oxides nanoparticles and nanomaterials [145,147–149]. However, small particle size of

nanoparticle results in the difficulty of separation from solution, which limits the application in water treatment. The new adsorbents requested by the industry should have high capacity, rapid adsorption kinetics and operational stability at elevated temperatures in the presence of steam and other reaction components. The new adsorption processes may then take advantage of such materials.

Among these, polymers could represent the best candidate displaying a pronounced chemical versatility given by the great number of chemical functionalities or motifs present in their structures. Recently, researchers have focused on the syntheses of zwitterionic cross-linked inorganic and/or organic hybrid polymer materials for the removal of heavy metal ions via electrostatic effects [42,55,150]. Considerable attention has been given to synthesize chelating agents containing amino methyl phosphonate motif owing to its extraordinary chelating properties in extracting heavy metal ions from wastewater. More recently, a porous resin with Schiff base chelating groups for removal of heavy metal ions from aqueous solutions has been developed [151].

The objective of the current work was to synthesize a novel functionalized resin as sorbent for removal of Pb^{2+} ions as a model case from aqueous solution. The cross-linked polymer is anticipated to retain the metal chelating character of the nitrogen in addition to the two anionic centers in the carboxylates in aspartic acid. In this respect, we intend to apply Butler's homo-[24–26,152] and co-cyclopolymerization [71,77,153] protocol, which is instrumental in converting diallylammonium salts into a plethora of industrially significant cyclopolymers, whose pyrrolidine ring-embedded architecture is considered to be the eighth most important structural type [154,155]. Butler's cyclopolymer poly(diallyldimethylammonium chloride) has numerous publications and patents (> 1000).

Water purification and personal care formulation remain the important areas of its application [24]. With this in mind, herein we report the cycloaterpolymerization of diallyl monomer **1**, cross-linker **2** and SO₂ to generate a novel pH-triggerable cross-linked cycloaterpolymer **4** (Scheme 4.1). The cycloaterpolymerization protocol was used for the first time to obtain resin **4** containing the residues of aspartic acid with all its basic centers intact.

4.2 Experimental

4.2.1 Chemicals and Materials

Azoisobutyronitrile (AIBN) from Fluka AG was purified by crystallization from a chloroform–ethanol mixture. Dimethylsulfoxide (DMSO) was dried over calcium hydride overnight and then distilled under reduced pressure at a boiling point of 64–65°C (4 mm Hg). Standard solution (1000 mg/L) of Pb (II), hydrochloric acid, nitric acid and sodium hydroxide were obtained from Sigma–Aldrich. The lead standard solution was utilized to prepare the required initial concentrations by dilution. All solvents used were of analytical grade.

4.2.2 Physical methods

Field emission scanning electron microscope (FESEM) was used to characterize the surface morphology of the polymer before and after the adsorption of lead. Energy-dispersive X-ray spectroscopy (EDX) equipped with a detector model X-Max was employed to obtain the elemental spectrum and to get elemental analysis of the pristine polymer and Pb(II)-loaded polymer. PerkinElmer 2400 Series II CHNS/O Elemental Analyzer was also used for the elemental analysis. Thermo Scientific iCE 3000 flame

atomic absorption spectrometer (FAAS) equipped with a 10 cm air-acetylene burner was used to monitor the concentration of Pb(II). The concentrations of some metal ions in real wastewater samples was analysed by inductively coupled plasma mass spectrometry (ICP-MS) model ICP-MS XSERIES-II Thermo Scientific. IR spectra were recorded on a Perkin–Elmer 16F PC FTIR spectrometer. ¹H and ¹³C spectra were measured on a JEOL LA 500 MHz spectrometer using HOD signal at δ4.65 and dioxane signal at 67.4 ppm as internal standards, respectively. TGA conducted using a thermal analyzer SDT Q600, V20.9 Build 20 manufactured by TA instruments, USA. The temperature was raised at a uniform rate of 10°C/min. The analyses were made over a temperature range of 20–700°C in an air-atmosphere flowing at a rate of 100 mL/min. The specific surface area and pore size distribution were determined by the Brunauer-Emmett-Teller (BET) and Barrett-Joyner-Halenda (BJH) methods, respectively.

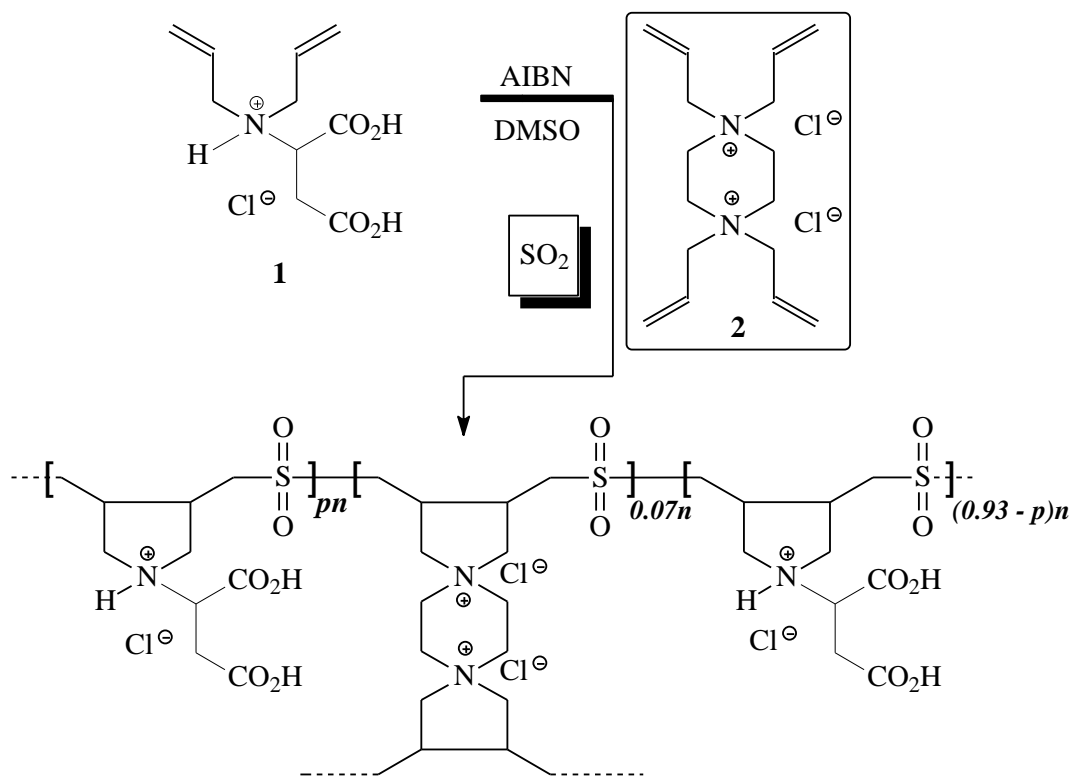
4.2.3 Synthesis

To the best of our knowledge, the following synthesis of the resins would represent the first example of cross-linked cyclopolymer containing the residues of aspartic acid by the cyclopolymerization protocol involving monomers having unquenched nitrogen valency. The cross-linker **2** was prepared as described [82]. Monomer **1** containing the residue of aspartic acid was prepared via Michael addition of diallylamine to dimethyl maleate followed by hydrolysis of the Michael adduct in aqueous NaOH and neutralization with aqueous HCl.

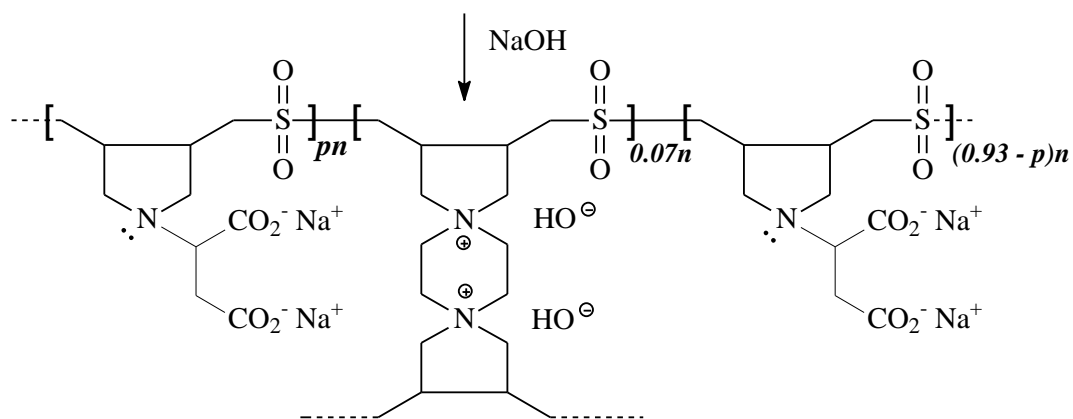
a. General procedure for the terpolymerization of **1** and **2** with sulfur dioxide.

To a solution of monomer **1** (6.06 g, 24.2 mmol), cross-linker **2** [82] (0.582 g, 1.82 mmol) in DMSO (9.1 g) in a round bottom flask (50 ml), was absorbed SO₂ (1.78 g, 27.8 mmol)

(from a cylinder) by gentle blowing it over the stirred surface of the solution (scheme 4.1). After the initiator AIBN (105 mg) was added, the reaction mixture was stirred at 60°C under N₂ for 24 h. Within 3-5 h, the magnetic stir-bar stopped moving; the reaction mixture became a transparent swelled gel. At the end of the elapsed time, the swelled gel of the cross-linked polyzwitterionic acid (CPZA) **3** was soaked in water (48 h) with replacement of water several times. The swelled gel in water ($\approx 65 \text{ cm}^3$) was agitated with NaOH (1.6 g, 40 mmol) at room temperature for 5 h followed by further addition of NaOH (1.6 g, 40 mmol) and stirring for 1 h to ensure complete exchange with Na⁺. The CPZA **3** in acid form is less expanded owing to the zwitterionic form while the anionic form in resin CDAP **4** is highly expanded in the above alkaline mixture. The resin **4** was dropped onto acetone (200 ml), filtered, vacuum-dried at 60°C to a constant weight (7.7 g, 90%). (Elemental analysis Found: C, 38.1; H, 4.6; N, 4.4; S, 9.5%). A terpolymer from monomer **1** in disodium form C₁₀H₁₃NNa₂O₄ (93 mol%) and monomer **2** in the hydroxide form C₁₆H₃₀N₂O₂ (7 mol%) and SO₂ (100 mol%) requires C, 38.65; H, 4.41; N, 4.62; S, 9.93).



3: Crosslinked polyzwitterionic acid (CPZA)



4: Crosslinked dianionic polyelectrolyte (CDAP)

Scheme 4.1 Synthesis of Cross-linked Polyzwitterion/anion Polymer

4.2.4 Adsorption of Pb(II) on CDAP

The experiments were carried out as follow. A 30mg of adsorbent CDAP was added in 20mL of aqueous Pb²⁺ solution of specific concentration and then stirred for period of 2, 5, 10,15, 20, 30, 40, 50, 60, 90 and 120 minutes respectively at 298K. This study was done with different initial Pb²⁺ concentrations ranging from 10 to 100mgL⁻¹ while maintaining the adsorbent amount of 1.5 g L⁻¹. The resultant solution was filtered using a filter paper and the filtrate was analyzed by atomic absorption spectroscopy to determine the amount of Pb²⁺ uptake. The pH of the solution was also measured during course of adsorption. The effect of pH was studied at 298K with an initial Pb²⁺ concentration of 40mgL⁻¹. The kinetic and thermodynamic behaviors were studied in a similar manner with initial Pb²⁺ concentration of 40mgL⁻¹ at 298, 313 and 333K respectively. The amount of Pb²⁺ adsorbed by the adsorbent CDAP was computed using the following equation.

$$q_t = \frac{(C_i - C_t)V}{W} \quad (1)$$

Here, C_i and C_t are the initial and final concentrations of Pb²⁺ ions in mg L⁻¹ respectively; V is the volume of solution in L with which the resin of weight W in gram is contacted and q_t is the adsorption capacity in mg g⁻¹

4.2.5 Regeneration of the Resin

Adsorption experiments were performed by stirring 30mg of the resin in aqueous 20ml Pb²⁺ solution for 120 minutes. The amount of Pb²⁺ uptake was determined as described above. The loaded resin was then filtered and vacuum-dried at 60°C to a constant weight. It was then quantitatively transferred to a stirring 1M HNO₃ (20ml) for 120minutes for the desorption experiment. The regenerated resin was washed and dried and the amount of

desorbed Pb^{2+} was determined in a similar way to the adsorption. The efficiency of desorption process was calculated by taking the ratio of the desorbed amount to that of the adsorbed amount of Pb^{2+} . The re-usability of the regenerated resin was tested in a similar way to the adsorption experiment. All experiments were done in triplicates.

4.2.6 FTIR Spectroscopy

The FT-IR spectra of the resin before and after adsorption experiments were examined. Unloaded resin (30 mg) was contacted with $40\text{mgL}^{-1}\text{Pb}^{2+}$ concentration at adsorbent amount of 1.5 g L^{-1} for 120 minutes at a pH of 6.0. It was filtered and vacuum-dried until constant weight was achieved.

4.3 Results and Discussion

4.3.1 Synthesis of cross-linked Terpolymer

Monomer **1**, cross-linker **2** and SO_2 underwent cyclooligomerization to give cross-linked polyzwitterionic acid **3** (CPZA) which upon basification with NaOH afforded the cross-linked dianionic polyelectrolyte (CDAP) **4** in an excellent overall yield of 90% (Scheme 4.1). Resin **4** has the unquenched nitrogen valency, which can act as a chelation center along with the two carboxylate motifs. The synthesis represents the first example of a cross-linked cyclopolymer containing the residues of the versatile aspartic acid. The three basic centers (N and CO_2^-) in aspartic acid with different basicity constant is anticipated to impart interesting chelation properties in sequestering toxic metal ions.

4.3.2 FT-IR Characterization of Monomers and Polymer

The IR spectrum of cross-linked polyzwitterionic acid **3** (CPZA) shows strong bands at 1727 cm^{-1} and 1631cm^{-1} which are usually attributed to the asymmetric and symmetric stretchings of COOH [76] fig. 4.1a. These bands were also observed for monomer 1 (spectrum not shown here). The resin **3** (CPZA) also contains bands at 1304 cm^{-1} and 1125 cm^{-1} which have been assigned in literature to asymmetric and symmetric bands of SO_2 [156]. In the unloaded cross-linked dianionic polyelectrolyte **4** CDAP, the C=O stretch shift dramatically to 1578.7 cm^{-1} and 1406.8 cm^{-1} for asymmetric and symmetric vibrations respectively because it is now in COO^- form (fig. 4.1b). After Pb^{2+} adsorption fig. 4.1c, an appreciable increase in the intensity and broadness of the COO^- bands is noted [157]. At CPZA, the band at 854.9 cm^{-1} is assigned to C-H bond vibration in the ring while the band at 639 cm^{-1} is assigned to N-H out of plane vibration [158]. The band at 878 cm^{-1} at CDAP, and the band at 875 cm^{-1} at Pd adsorbed CDAP, are assigned to C-H bond vibration in the ring. The slight shift could be attributed to the interaction between the nitrogen pair of electron with lead metal ion leading to distortion of electron cloud in the neighboring C-H bond.

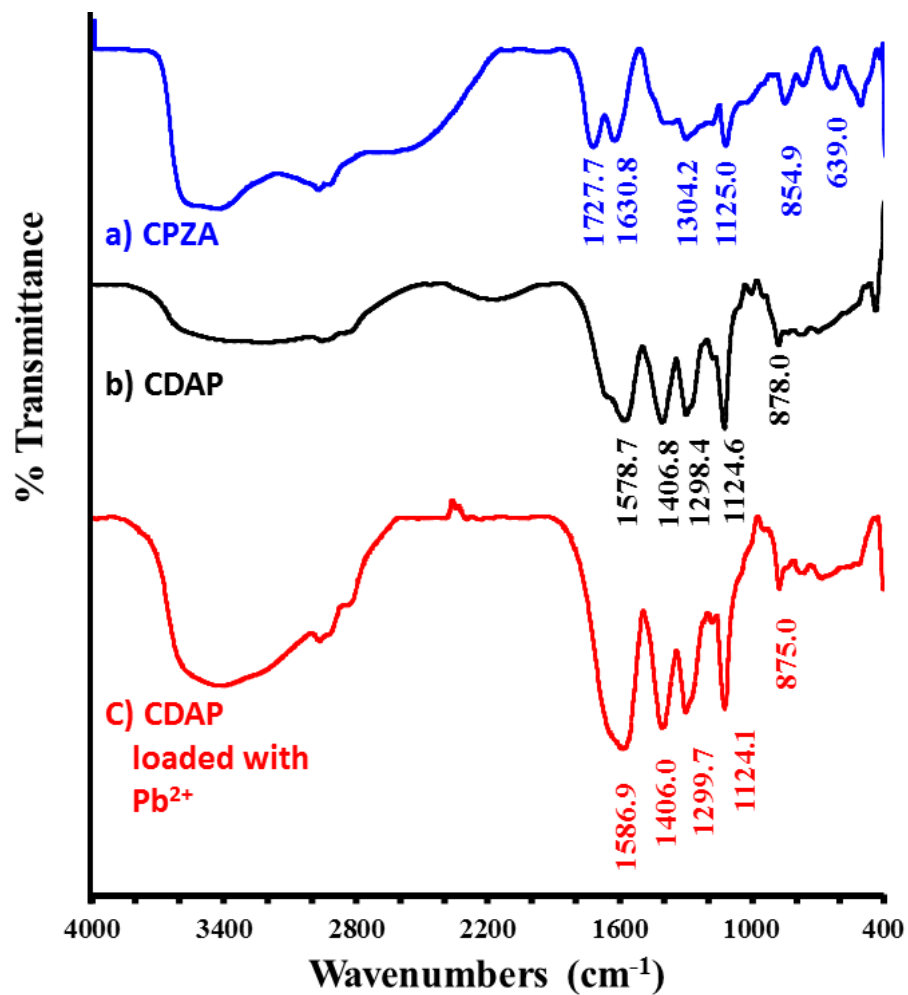


Figure 4.1 IR Spectra of cross-linked resins (a) CPZA 3 (b) CDAP 4 and (c) CDAP 4 loaded with Pb²⁺

4.3.3 Thermo-gravimetric measurement

Figure 4.2 shows the TGA curve of 4 (CDAP) with three distinct weight loss steps. The first slow but gradual weight loss of about 20% is attributed to the removal of moisture and water molecules embedded inside the cross-linked polymer. The second dramatic loss of about 25% around 320°C is attributed to the loss of SO₂ due to polymer degradation. The third slow and gradual loss of 15% is attributed to the combustion of nitrogenous organics with the release of NO_x, CO₂ and H₂O gases [156]. At 700°C, the residual mass was found to be 40%.

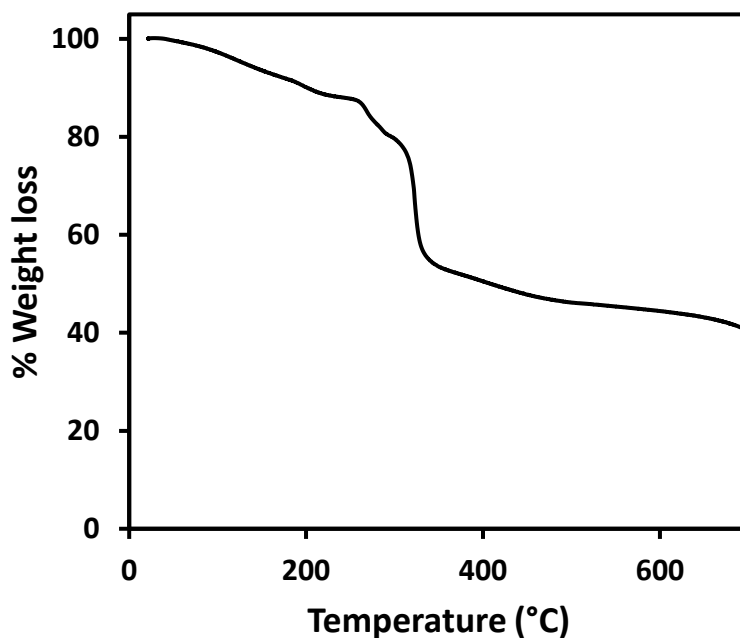


Figure 4.2 TGA curve of CDAP 4

4.3.4 Effect of pH on the adsorption

The relationship between the initial pH of solution and the percentage removal of Pb^{2+} is depicted in figure 4.3. In the pH range of 3 - 9, the Pb^{2+} uptake was monitored by contacting the resin with 40mgL^{-1} lead (Pb^{2+}) solution for 15 minutes at room temperature. The percentage Pb^{2+} removal initially increased from 91.5% to 95.8% as the pH increased from 3 to 6. Further increase of pH to 9 saw a gradual decrease of Pb^{2+} uptake as percentage Pb^{2+} dropped to 94.9%. Therefore, the optimum pH is 6. It has been established that solution pH plays a critical role in metal ion adsorption process due to its influence on both the nature of the metal ions in solution and the state of the functional groups on the surface of the adsorbents [25]. Studies have identified three forms of lead species: Pb^{2+} , $\text{Pb}(\text{OH})^+$ and $\text{Pb}(\text{OH})_2$ in the pH range 2.0-8.0. The distribution of these species as calculated by MINEQL software shows that Pb^{2+} is the preponderant species at pH between 1 and 6 and that its hydrolysis to $\text{Pb}(\text{OH})^+$ and $\text{Pb}(\text{OH})_2$ starts as pH increases while $\text{Pb}(\text{OH})_2$ dominates at the pH higher than 6.0 [159,160]. Under low pH: (1) competition ensued between H^+ and Pb^{2+} and (2) the functional groups on the surface of the resin are in protonated forms which do not favor coordination with Pb^{2+} species as they are repelled by the electrostatic force. Thus, the Pb^{2+} absorption capacity of the resin is decreased [160]. As the pH is increased, this competition reduces and the functional groups on the resin are becoming less protonated, thereby making them more available for coordination with Pb^{2+} . This accounts for increased percentage removal that peaked pH 6.0. Beyond pH 6.0, there is deprotonation as basicity increases, and the functional groups are in anionic forms that should encourage greater coordination with Pb^{2+} . However, this didn't increase the percent Pb^{2+} removal as lead are now being hydrolysed into $\text{Pb}(\text{OH})^+$ and $\text{Pb}(\text{OH})_2$ thereby reducing

the amount of free Pb^{2+} available for complexation. The rest of the adsorption experiments were carried out at the optimum pH of 6.0.

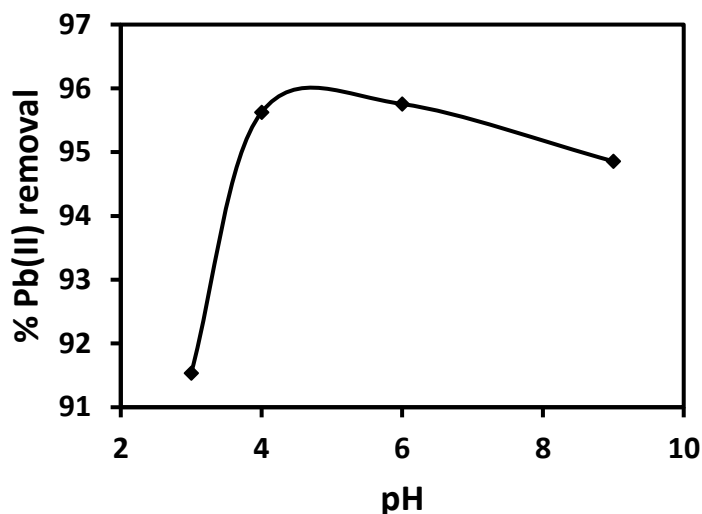


Figure 4.3 Effect of pH on the adsorption of Pb^{2+} ions

4.3.5 Effect of initial concentration on the adsorption of Pb(II)

Figure 4.4(a) depicts the effect of initial concentration of Pb^{2+} on the percentage Pb^{2+} removal by CDAP 4. It can be seen that the percentage removal for the Pb^{2+} rapidly increases from 0 to about 25 minutes contact time and thereafter slowly until it reaches equilibrium. This is due to the fact that the adsorption kinetic depends on the surface area of the adsorbent which is largely uncovered at the start of the experiment (0 contact time). Therefore, the rate of adsorption at the early time increases rapidly until it reaches a point where the remaining fewer adsorption sites are competed for by lead ions. Hence the rate of adsorption slows down until it reaches equilibrium [161]. This situation is observed for all the initial concentration of lead ranging from 10-100 ppm. The effect of the amount of

adsorbate was also investigated and it was observed that the adsorption capacity of CDAP 4 increases as the concentration of Pb^{2+} is raised from 10 up till 100 ppm (fig. 4(b)).

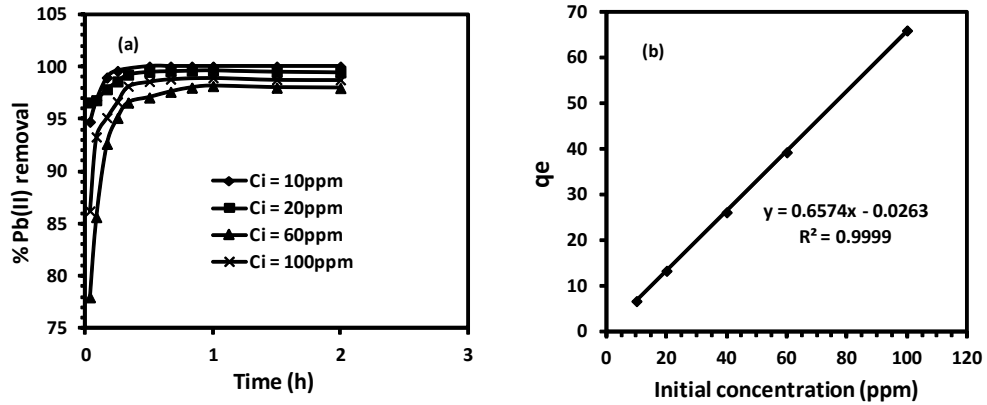


Figure 4.4 (a) Effect of initial Pb^{2+} concentrations on percent Pb^{2+} removal (b) Effect of initial concentrations of Pb^{2+} on the adsorption capacity.

4.3.6 Adsorption kinetics

The dynamics of the interaction at the solid-solution interface during the adsorption of Pb^{2+} from aqueous solution can be described in terms of models. These kinetic models study the rate-controlling mechanism of the adsorption process that comprises of chemical reaction, mass transfer and diffusion control systems. Two kinetic models namely Pseudo first-order and Pseudo second-order have been used in this work to analyze the adsorption data of Pb^{2+} adsorption on CDAP.

A. Pseudo first-order (Lagergren) kinetics

Pseudo first-order relates the adsorption rate of solute to adsorption capacity of the adsorbent. The linear form of the equation is given by the following equation [161].

$$\log(q_e - q_t) = \log q_e - \left(\frac{k_1 t}{2.303}\right) \quad (2)$$

Where q_e and q_t are the amounts of Pb^{2+} adsorbed in (mg g^{-1}) at equilibrium time and at any time, t , respectively and k_1 is the first order rate constant in (h^{-1}). A linear plot of $\log(q_e - q_t)$ versus t yields a straight line for the pseudo first-order kinetics from which k_1 and $q_{e,\text{cal}}$ are calculated. Figure 4.5(a) shows the combined Lagergren plots for the various initial concentrations of Pb^{2+} used for the kinetic studies when adsorbent amount is kept at 1.5gL^{-1} . The kinetic parameters extracted from these plots are displayed in table 4.1. Judging from the fittings, it can be seen that there is generally good linearity of Lagergren Pseudo first-order plots as R^2 ranges from 0.95 to 0.99 for all the plots (table 4.1). The rate constants k_1 are determined to vary between 2.7 to 16.38 h^{-1} . There is a general downward trend of k_1 as initial concentrations increase. However, considering the equilibrium adsorption capacities reveal a sharp disagreement between the experimentally observed $q_{e,\text{exp}}$ and that derived from Lagergren pseudo first-order plots, $q_{e,\text{cal}}$, as shown in table 4.1. This is understood to mean that even though, the model fits Pb^{2+} adsorption data quite fairly, it is not suitable for estimation of $q_{e,\text{cal}}$ as it is not a true first order equation where the intercept of the plot of $\log(q_e - q_t)$ versus t should be equal to $\log q_e$ as in equation 3 [162].

b. Pseudo second-order kinetics

The failure of Lagergren first-order kinetic model to correctly estimate the equilibrium adsorption capacity q_e drives us to pseudo second-order kinetic model for analysis of the dynamics. The linear form of the pseudo second order model [163] can be written as:

$$\frac{t}{q_t} = \frac{1}{k_2 q_e^2} + \frac{t}{q_e} \quad (3)$$

Here, k_2 ($\text{g mg}^{-1} \text{ h}^{-1}$) is pseudo second order rate constant, q_e and q_t are the adsorption capacities at equilibrium and at any time t respectively. A plot of t/q_t against t , figure 4.5(b), gave linear relationship allowing for the calculation of q_e and k_2 as displayed in table 4.1. The initial adsorption rate is also presented as $h = k_2 q_e^2$. As can be seen from figure 4.5 (b) and table 4.1, pseudo second-order model gave an excellent fitting for the adsorption data with the square of regression coefficient of unity for all the experiments. Interestingly, the calculated equilibrium adsorption capacities, $q_{e,\text{cal } 2}$, show very nice agreement with the experimentally observed, $q_{e,\text{exp}}$ table 4.1. While this is an evidence that pseudo second order model describes very well the adsorption process taking place between CDAP 4 and Pb^{2+} ions, it also means that such adsorption process might be of chemical nature [163].

c. Intra-particle diffusion

The Weber-Morris intraparticle diffusion was used as a model to evaluate the diffusion contribution of Pb^{2+} adsorption within the resin. A plot of q_t against $t^{1/2}$ (equation 5) should give a straight line if the mechanism of the adsorption is controlled by the diffusion of the adsorbate ions within the particle in the pore of the adsorbent [164,165]. The diffusion process may take place in the external, macropore and micropore surfaces leading to multi-linear plots [166] suggesting that other processes might play roles in the adsorption [167].

$$q_t = k_{id} t^{1/2} + x_i \quad (4)$$

where q_t is the adsorption capacity at any time t , k_{id} is the intraparticle diffusion rate constant (mg/g hr.) and x_i is a constant that takes into account the boundary layer thickness.

It can be seen from figure 4.5(c) that the diffusion model exhibits three distinct parts for the duration of the study at different temperatures. The effects of temperature on the Weber-Morris parameters are displayed in table 4.2. At 298K, from the start of the process, the first and second straight portions of the curve with steep slopes reflect the easy diffusion of Pb^{2+} ion inside the macropores of the CDAP resin while the third part, indicates the slow diffusion within the micropore [166]. It is informative to note that the third part shows a gradual approach to equilibrium which is an indication of a concentration dependent diffusion process [168]. This result is in agreement with pseudo-second order kinetic model. Experiments conducted at 313 and 333K show similar behavior but with gradual decrease in k_{id} and their regression coefficients (see figure 4.5 (c) and table 4.2). Obviously, this is an indication of the exothermic behavior of the adsorption process which slows down the diffusion mechanism as temperature rises.

4.3.7 Adsorption isotherm models

Isotherm models are used to explain the nature of adsorption sites, their interaction and the number of layer that may be formed on them. Among many models in literature, Langmuir, Freundlich and Tempkin isotherms were used for this study.

a. Langmuir Isotherm

The basic assumptions in Langmuir isotherm are that the adsorption is a monolayer type on a homogenous surface where the adsorption at one site is completely independent of the other [169]. It can be expressed in linear form as follows:

$$\frac{C_e}{q_e} = \frac{C_e}{Q_m} + \frac{1}{Q_m b} \quad (5)$$

Where Q_m is the quantity of adsorbate required to form a single monolayer on a unit mass of the adsorbent (mg g^{-1}), Q_e is the amount adsorbed on a unit mass of adsorbent (mg g^{-1}) at equilibrium concentration C_e (mgL^{-1}) and b is an equilibrium constant that takes care of the apparent energy of adsorption. A plot of C_e/q_e against C_e yielded a straight line in agreement with Langmuir isotherm giving the isotherm parameters as depicted in table 4.3. The high R^2 of about 0.99 is an indication of the suitability of this isotherm in explaining the equilibrium adsorption of Pb^{2+} onto the resin. It thus clarifies that it is a monolayer adsorption.

Comparison of adsorption capacities from the Langmuir isotherm of the current adsorbent for the removal of Pb(II) with those of other adsorbents reported in the literature is displayed in Table 4.5. Quite interestingly, the present resin compare favorably with those of other adsorbents.

Additional analysis was also made by using the dimensionless equilibrium parameter R_L which is a measure of the favorability of adsorption. R_L values are found to range from 0.09 to 0.90, which means that it is favorable adsorption process.

b. Freundlich Isotherm

Freundlich isotherm describes multilayer adsorption taking place on a heterogeneous surface. As in many systems, the heat of adsorption decreases with increasing extent of adsorption but this model unifies the energy [170]. The linear form is given as follows:

$$\log q_e = \log k_f + \frac{1}{n} \log C_e \quad (6)$$

k_f is the Freundlich constant and n is the heterogeneity factor which is a measure of deviation from linearity. Table 4.3 shows a high n of about 2 which is far from unity and R^2 of 0.93. These collectively prove that Freundlich isotherm does not correctly describe this adsorption.

c. Temkin Isotherm

Temkin isotherm takes into consideration the interaction between adsorbate and adsorbent with the consequence that the heat of adsorption of all the molecules in the layer decreases linearly with further coverage. It also assumes that the distribution of adsorbate is uniform [171]. The linear form is given as follows:

$$q_e = \frac{RT}{b} \ln A + \frac{RT}{b} \ln C_e \quad (7)$$

Where T is the absolute temperature in Kelvin (K), R is the molar gas constant (8.314J mol⁻¹ K⁻¹), A represent the equilibrium binding constant (L g⁻¹) corresponding to maximum binding energy and b (Jmol⁻¹) is related to the heat of adsorption. The intercept and slope from the plot of q_e versus $\log C_e$ enabled us to determine A and b as displayed in table 4.3. Judging from the high value of the coefficient of determination $R^2 = 0.9948$, it can be concluded that Temkin isotherm model describe this equilibrium very well. This indicates the possibility of adsorbent-adsorbate interaction and the adsorption process is simply a function of surface coverage.

4.3.8 Energy of adsorption

The activation energy of adsorption can be computed from the Arrhenius equation presented as follows:

$$\ln k_2 = \frac{E_a}{2.303 RT} + \text{constant} \quad (8)$$

Where E_a (kJmol^{-1}) is the activation energy, k_2 ($\text{g mg}^{-1} \text{h}^{-1}$) is the second order rate constant as shown in table 4.1 and R is the molar gas constant ($8.314 \text{J mol}^{-1} \text{K}^{-1}$) and T is the temperature of the solution in Kelvin. Plotting $\ln k_2$ against $1/T$ (figure 4.6(a)) gave a linear relation whose slope (E_a/R) allowed us to determine activation energy of adsorption table 4. From the table 4.4, the activation energy is 39.29kJmol^{-1} , which is low and therefore, is an indication of the favorability of the adsorption process.

Studies on adsorption thermodynamics have employed the ratio of q_e/C_e as the distribution constants K in the Vant-Hoff equation to derive the adsorption thermodynamic parameters [172]. The modified equation is given as follows:

$$\ln \left(\frac{q_e}{C_e} \right) = -\frac{\Delta H}{RT} + \frac{\Delta S}{R} \quad (9)$$

$$\Delta G = \Delta H + T\Delta S \quad (10)$$

Where, all the letters and symbols have their usual meanings. A plot of $\log (q_e/C_e)$ versus $1/T$ is depicted in figure 4.6(b) and the thermodynamic parameters extracted from the plot are shown in table 4.4. Looking at table 4.3, it is evident that as temperature climbs up from 298 to 333K, the free energy change ΔG becomes less negative meaning that as an exothermic process, it is not favored at higher temperatures. The ΔH of -43.87kJmol^{-1} also corroborates this observation. The negative change in entropy ΔS of $-110.11 \text{J mol}^{-1} \text{K}^{-1}$ suggest a significant fall in randomness at solution-solid interface during adsorption.

Table 4.1 Adsorption kinetic parameters for Lagergren models

Concentration (ppm)	$q_{e,exp}$ ($mg\ g^{-1}$)	Pseudo 1st order			Pseudo 2nd order			
		k_1 (h^{-1})	$q_{e,cal}$ ($mg\ g^{-1}$)	R^2	$q_{e,cal}$ ($mg\ g^{-1}$)	k_2 ($g\ mg^{-1}\ h^{-1}$)	h^a ($mg\ g^{-1}\ h^{-1}$)	R^2
10	6.63	16.4	0.606	0.9854	6.70	55.7	2.50×10^3	1.000
20	13.3	10.1	0.908	0.9450	13.3	56.7	1.00×10^4	1.000
40	26.5	2.70	1.595	0.9562	26.3	8.10	5.60×10^3	0.9999
60	39.2	6.93	8.383	0.9541	39.4	3.23	5.01×10^3	1.000
100	59.4	4.97	3.964	0.9640	59.5	2.82	9.98×10^3	1.000

^a Initial adsorption rate, $h = k_2 q_e^2$

Table 4.2 Intraparticle diffusion parameters

Intraparticle diffusion model			
Temperature	k_{id}	x_i	R^2
(K)	($mg\ g^{-1}\ h^{-1}$)	($mg\ g^{-1}$)	
298	2.12	24.7	0.9812
313	0.998	25.15	0.9807
333	0.413	25.14	0.9804

Table 4.3 Isotherm constants for adsorption of Pb²⁺ on CDAP

Adsorption Isotherms	Isotherm Parameters		R ²
Langmuir	Q _m	64.5 mg g ⁻¹	0.9943
	b	2.07 L mg ⁻¹	
Freundlich	k _f	34.2	0.9323
	n	2.23	
Temkin	A	34.8 Lg ⁻¹	0.9948
	b	221 J mol ⁻¹	

Table 4.4 Thermodynamic and kinetic parameters for Pb²⁺ adsorption on CDAP

Temp (K)	ΔG (kJ mol ⁻¹)	ΔH (kJmol ⁻¹)	ΔS (Jmol ⁻¹ K ⁻¹)	E _a (kJmol ⁻¹)
298	-11.1			
313	-9.41	-43.9	-110	39.3
333	-7.20			

Table 4.5 Comparison of the adsorption capacity of the resin and those of various adsorbents in literature for Pb (II) as computed by the linear Langmuir equation

Sorbent Materials	Adsorption	
	Capacity (mg/g)	Ref
Commercial silica	3.9	[173]
Zeolites: Chabazite	6.0	[174]
Activated carbon	6.68	[175]
Porous lignin-based sphere	27.1	[176]
Diethylenetriamine-bacterial cellulose	31.4	[177]
Ethylenediamine modified cellulose	50.0	[178]
Porous lignin xanthate resin	62.6	[179]
Ferrihydrite	366	[180]
Lignocellulosic materials	66	[181]
Modified orange peel	210	[182]
Sulfured orange peel	164	[183]
Nanoribbon	74.6	[184]
Current Resin	64.5	This work

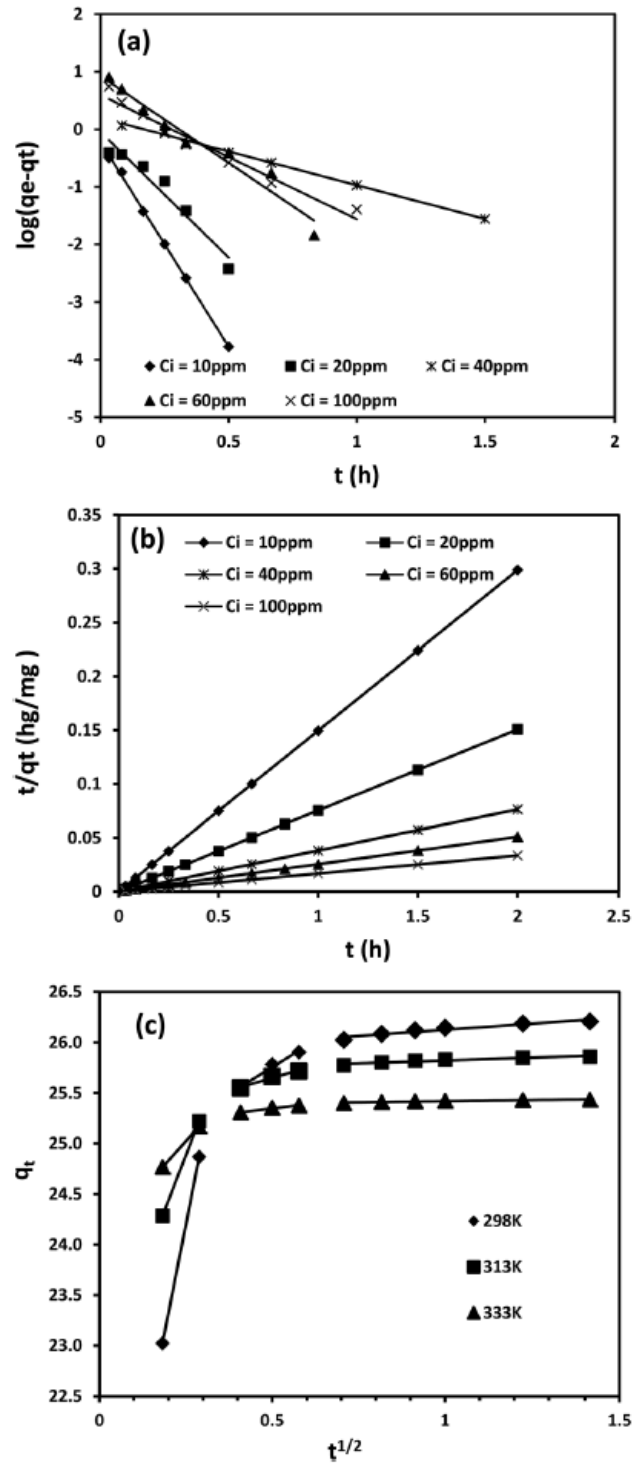


Figure 4.5 (a) Lagergren first-order plots, (b) Pseudo second-order plots and (c) and Weber-Morris intraparticle diffusion plots at 40ppm for the adsorption of Pb^{2+} on CDAP

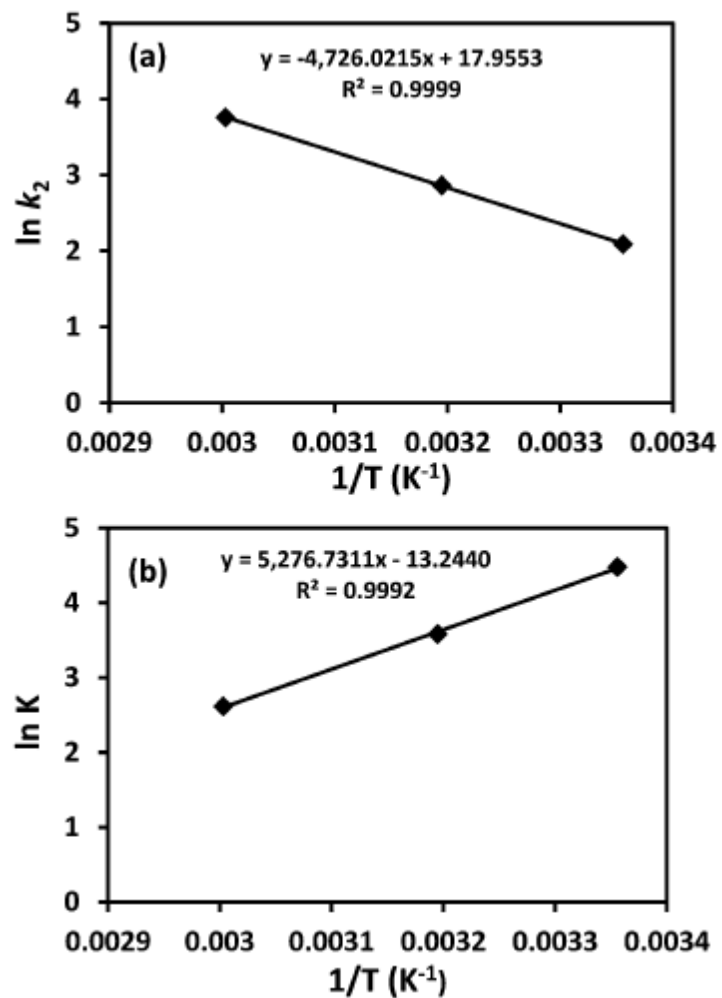


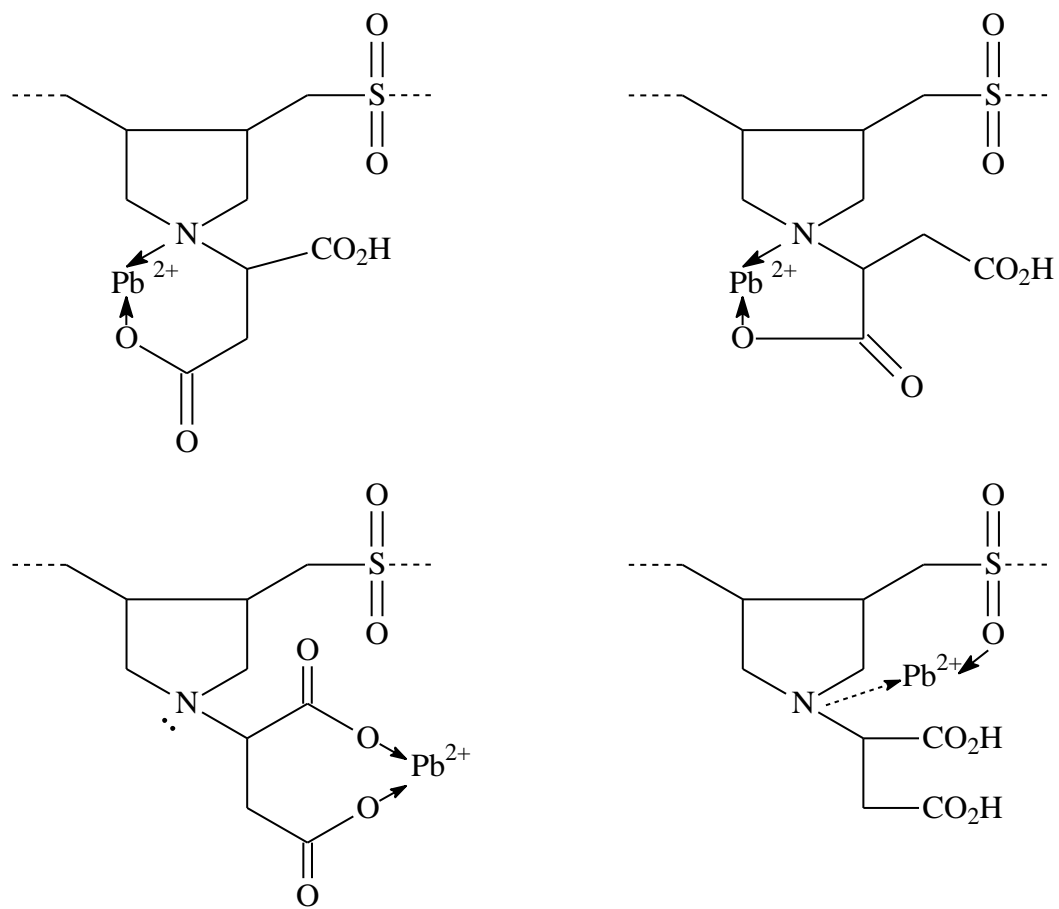
Figure 4.6 (a) Arrhenius and (b) Thermodynamic plots for Pb²⁺ adsorption on CDAP 4

4.3.9 Regeneration of the Resin

The re-usability and safe disposal of the used resin are key factors in enhancing the environmental friendliness of the resin. The result indicated that the efficiency of regeneration stands at 70% . The percentage lead uptake of the regenerated resin stands at 20% as against fresh resin which stands at 95%.

4.3.10 Structure and Surface morphology of unloaded and loaded CDAP

A scanning electron microscope (SEM) and energy dispersive X-ray (EDX) analysis were performed for examining the surface morphology and the structure of the polymer before and after the adsorption, Fig.8. The EDX spectrum recorded for lead-loaded polymer adsorption (figure 4.7b) indicates the main characteristic peaks for Pb(II) at 2.34 and 10.55 keV in addition to the peaks of the other elements of the polymer structure figure (8a). This confirms the binding of Pb(II) to the surface of the polymer. SEM images are depicted in the figures. The surface area and the pore size of the unloaded CDAP as determined by BET are 0.1627m²/g and 15.099 Å respectively. The low surface area of this efficient adsorbent may mean that chemisorption rather than just physisorption governs the adsorption process whereby Pb²⁺ ions are captured by carboxylate and sulfonate groups by chelation. As noted earlier, the increase in broadness and intensity of the IR bands of COO⁻ after Pb²⁺ adsorption (fig. 4.1c) is a strong evidence of the attraction of the resin for Pb²⁺ ions. Evidences of interactions from IR and EDX analyses allow us to propose the following mechanism to explain the latitude of this resin for metal chelation (scheme 4.2). Though scheme 4.2 allows us to visualize the various 5, 6, and 7-membered interactions that are possible for this kind of structures, however, it is too early to conclude on any one as more investigations are needed.



Scheme 4.2 Illustration of the resins's latitude in forming complex with metal ions.

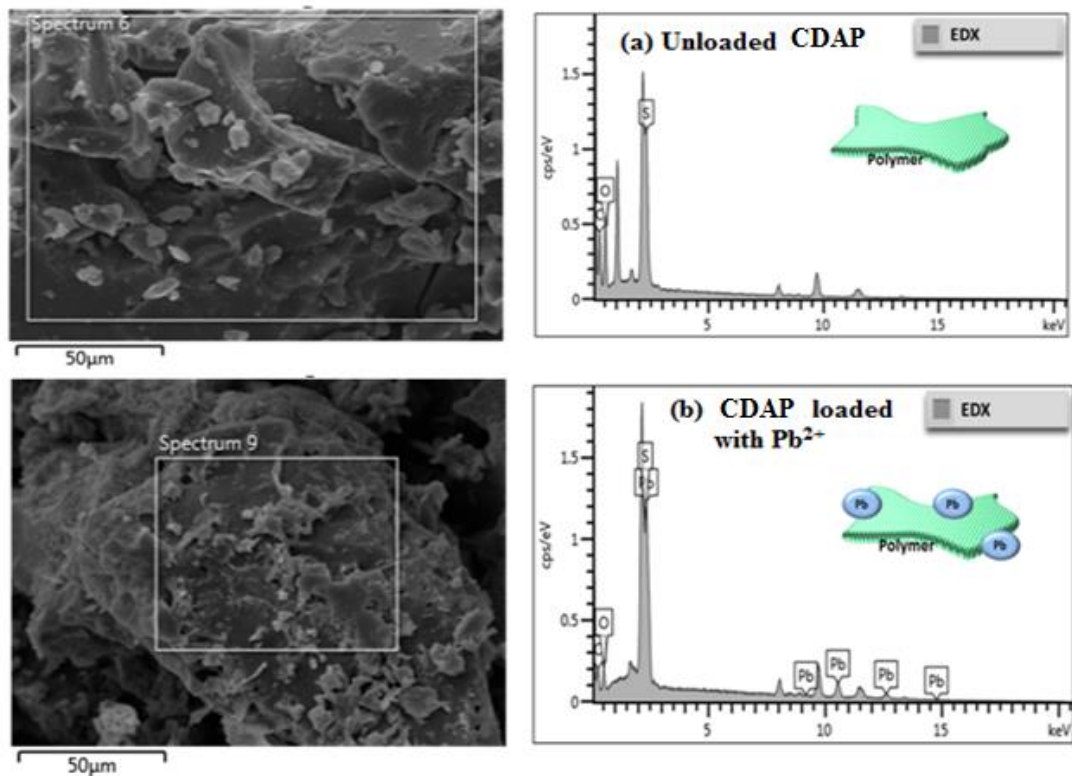


Figure 4.7 SEM image and the corresponding EDX spectrum of (a) unloaded CDAP 4 and (b) CDAP loaded with Pb²⁺

4.3.11 Treatment of real wastewater samples

Sample of industrial wastewater collected from the industrial unit in dammam was used to study the effect of real wastewater matrix and to evaluate practical application of the polymer. The samples were spiked with 0.0 and 20 mg/L Pb(II), and then treated with polymer under the optimum conditions. Table 4.6 presents the ICP results of the analysis of wastewater sample and wastewater sample after being treated with the prepared polymer. It also presents the analysis of wastewater sample after being spiked with 20 ppm Pb(II) and then treated with the prepared polymer. The results indicated that the efficiency of the polymer for the adsorption of Pb(II) is hardly be influenced by the real wastewater matrix. This indicates the high efficiency and capability of polymer to be regarded as a

potential adsorbent for high efficient and renewable adsorbent for Pb(II) ions from aqueous solutions.

Table 4.6 Comparison of Pb(II) concentrations in wastewater sample before and after the treatment with the polymer resin

Metal	Original sample ($\mu\text{g L}^{-1}$)	Original sample spiked with 20000 ($\mu\text{g L}^{-1}$) Pb(II) and then treated with the adsorbent (polymer)
Pb	0.453	357.2
Co	0.362	0.213
Cu	857.14	418.20
As	8.14	3.351
Mo	36.12	10.4
Cd	1.17	0.087
Hg	213.11	133.4

MDL: the method detection limit

4.4 Conclusion

In this work, a novel polymer was synthesized by the cyclopolymerization protocol involving monomers having unquenched nitrogen valency to get a novel functionalized resin. FTIR, EDX, TGA and SEM characterization techniques were used to confirm the structural and morphological properties of the polymer. The polymer displays an outstanding capability to remove Pb(II) ions. The optimum pH value for Pb(II) removal was 6. The contact time has an effect upon Pb²⁺ adsorption. The linearity of the plots t/q_t vs. t implies the adsorption followed the pseudo-second order rate kinetics with high adsorption capacity. Fitting the data to Langmuir, Freundlich and Temkin models show that the Langmuir and Temkin models give a better correlation coefficient with R² of 0.99. Thermodynamic parameters were evaluated; the negative values of ΔG_0 indicate the spontaneity and the negative values of ΔH_0 (-43.87 KJ/mol) showed the exothermic nature of Pb(II) sorption on the polymer. Therefore, the polymer adsorbent could be considered as a potential adsorbent of high efficient for Pb (II) removal.

CHAPTER 5

Synthesis and Application of Glutamic Acid-based Polymer

keeping intact the integrity of all the three original

functionalities of the amino acid

Abstract

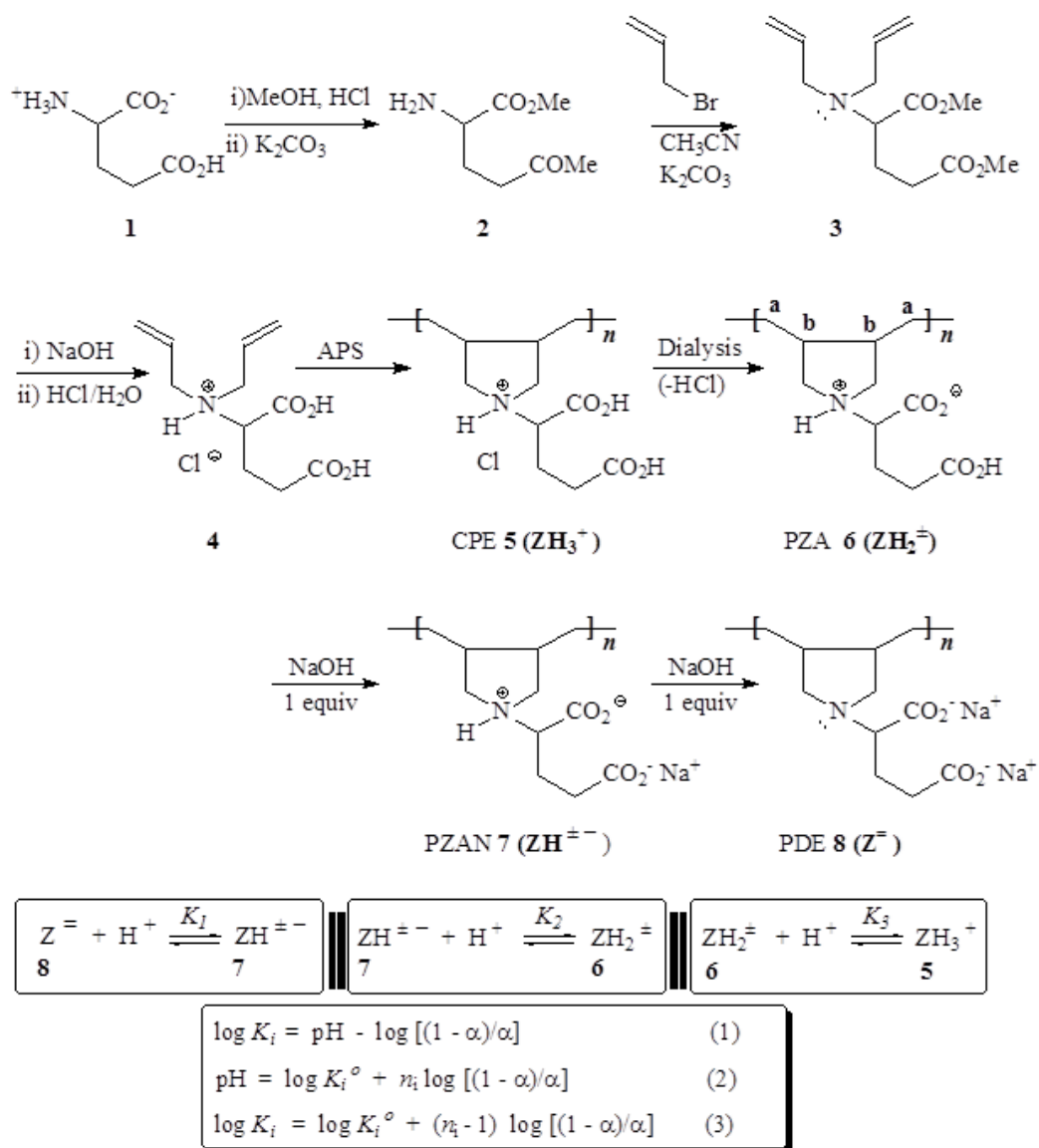
Dimethyl glutamate on treatment with allyl bromide afforded dimethyl *N,N*-diallylglutamate which upon alkaline ester hydrolysis followed by acidification with aqueous HCl gave *N,N*-diallylglutamic acid hydrochloride $[(\text{CH}_2=\text{CH}-\text{CH}_2)_2\text{NH}^+\text{CH}(\text{CO}_2\text{H})(\text{CH}_2)_2\text{CO}_2\text{H Cl}^-]$ **I**. Using Butler's cyclopolymerization protocol, new monomer **I** underwent ammonium persulphate- initiated polymerization to give pyrrolidine ring-embedded linear cyclopolymer **II** i.e., $[-\text{CH}_2(\text{C}_4\text{H}_6)\text{NH}^+\{\text{CH}(\text{CO}_2\text{H})(\text{CH}_2)_2\text{CO}_2\text{H Cl}^-\}\text{CH}_2-]_n$ retaining the integrity of all the three functionalities of glutamic acid. Under the influence of pH, the repeating units of triprotic acid (+) in **II** were equilibrated to those of water-insoluble diprotic polyzwitterionic acid (\pm) **III**, water-soluble monoprotic poly(zwitterion-anion) ($\pm -$) **IV** and its conjugate base polydianion ($=$) **V**. The critical salt concentration required to promote water-solubility of (\pm) **III** has been determined to be 0.548 M NaCl, 0.271 M NaBr, 0.133 M NaI. The basicity constants of the carboxyl groups and trivalent nitrogen in ($=$) **V** have been determined. A 5-ppm and a 20-ppm concentrations of **III** are effective in

inhibiting the precipitation of CaSO_4 from its supersaturated solution with a $\approx 100\%$ scale efficiency of inhibition at 40°C for a duration of over 3 and 16 h, respectively.

5.1 Introduction

Glutamic acid, one of the 20-23 proteinogenic amino acids, is a non-essential amino acid. Its salt, known as glutamate, one of the most abundant molecules in the brain, is an important neurotransmitter in neural activation [185]. Glutamate is involved in cognitive functions such as learning and memory in the brain [186] and a key compound in cellular metabolism [187]. Free glutamic acid, present in a wide variety of foods, is responsible for umami, one of the five basic taste of the human sense of taste. Owing to its biodegradable, non-toxic and non-immunogenic properties, poly (γ -glutamic acid) (\square -PGA) $-\{ \text{NHCH}(\text{CO}_2\text{H})\text{CH}_2\text{CH}_2\text{CO} \}_n$, a biopolymer produced on the industrial scale by *Bacillus subtilis*, has unlimited potential for future application in foods, pharmaceuticals, healthcare, water treatment and other fields [188]. PGA is widely used as a drug delivery system in cancer treatment [189]. A novel bio-based hydrogels, prepared by cross-linking microbial \square -PGA with glucose, has shown extremely high water absorption of 3000 g/g [190]. Many medical applications (especially drug delivery) have exploited poly (\square -glutamic acid) (\square -PGA) $-\{ \text{NHCH}(\text{CH}_2\text{CH}_2\text{CO}_2\text{H})\text{CO} \}_n$, which is synthesized chemically as its microbial production is difficult [191]. For numerous biochemical reactions, enzymes work only in the presence of certain metal ions. In this context, the metal ion complexes of many amino acids including L-glutamic acid have been investigated [97,192,193]. Like aspartic acid-derived polymer, corresponding polymers

from glutamic acid have the potential to act as polychelator to scavenge toxic metal ions from contaminated water resources [194]. Keeping in view the tremendous importance of glutamic acid and its abundant availability, we intend to synthesize a glutamic acid-based monomer that could lead to polymers keeping intact the unquenched valence of the nitrogen. Note that in proteins or PGA, the basic character of the nitrogen is lost in the peptide or amide bond. In the current endeavor, monomer **4**, a pH-triggerable triprotic acid with unquenched nitrogen valence would be subjected to walk through Butler's cyclopolymerization protocol [24–26,71,153] to yield macromolecules bearing residues of glutamic acid (Scheme 5.1). Interesting solution properties of the new polymer are anticipated and its use as an antiscalant will be tested. It is worth mentioning in this context that the cyclopolymerization protocol has efficiently transformed many a diallylammonium salt into a variety of industrially significant cyclopolymers whose architecture is considered to be one of the most important structural type [154,155]. The polymer derived from diallyldimethylammonium chloride alone has over 1000 patents and numerous publications especially in the area of water purification [12].



Scheme 5.1 Synthesis of cyclopolymers containing glutamic acid residues.

5.2 Experimental methods

5.2.1 Materials

L-Glutamic acid from Fluka AG (Buchs, Switzerland) and diallylamine and ammonium persulfate (APS) from Sigma-Aldrich were used as received. For dialysis, a membrane (Spectra/Por) MWCO of 6000–8000 was purchased from Spectrum Laboratories, Inc. (Rancho Dominguez, CA, USA). Sodium 3-Trimethylsilylpropionate-2,2,3,3-d₄ (TSP-deuterated), used as an NMR internal standard, was purchased from Marck Sharp & Dohme Canada Ltd, Montreal, Canada.

5.2.2 Physical Methods for Structural Characterization

An elemental analyzer (Perkin Elmer Series II Model 2400) and a Fourier transform infrared (FTIR) spectrometer (Perkin Elmer 16F PC) were utilized for elemental analyses and IR spectroscopy. The nuclear magnetic resonance (NMR) spectra were recorded using a 500-MHz JEOL LA spectrometer. The ¹H signal of tetramethylsilane (TMS) at 0 ppm in CDCl₃, TSP-deuterated at 0 ppm in D₂O and the dioxane ¹³C peak at 67.4 ppm in D₂O were used as internal standards. TGA was done using an SDT analyzer (Q600: TA Instruments, New Castle, DE, USA) in a nitrogen atmosphere. An Ubbelohde viscometer (viscometer constant = 0.005317 mm² s⁻²) was utilized to measure viscosities using CO₂-free water under N₂. The pH of the solutions was measured using a Sartorius pH meter PB 11. The conductivity measurements were carried out using an Orion Versa Star meter (Thermoscientific, Beverly, MA, USA).

5.2.3 Synthesis of monomer and polymer

a. Dimethyl glutamate (2)

To a mixture of glutamic acid (1) (59 g, 0.4 mol) in methanol (500 mL) was adsorbed dry HCl (25 g, 0.68 mol) at 0°C. The clear mixture was then stirred at room temperature for 3 days or until the esterification was complete as indicated by ¹H MMR spectrum. High temperature was avoided to minimize the formation of cyclization product (lactam). After removal of the solvent at 25 °C, the hydrochloride salt of amine 2 was dissolved in water (100 mL) and carefully neutralized with K₂CO₃ at 0 °C; the aqueous mixture was then saturated with anhydrous K₂CO₃ and immediately extracted with CHCl₃ (5×100 mL). After drying and concentration, the residual amine 2 (61 g, 87%) was immediately used for the subsequent reaction with allyl bromide. Amine 2: δ_H (CDCl₃) 1.49 (2 H, br s, NH₂), 1.85 (1 H, m), 2.08 (1 H, m), 2.48 (2 H, t, *J* 7.3 Hz), 3.48 (1H, dd, *J* 5.2, 8.2 Hz), 3.68 (3 H, s), 3.73 (3H, s).

b. Dimethyl N,N-diallylglutamate (3)

Allylbromide (85 g, 0.70 mol) was added dropwise to a stirred mixture of amine 3 (55 g, 0.314 mol) and anhydrous K₂CO₃ (87 g, 0.63 mol) in acetonitrile (300 mL) at 40-50°C for a period of 30 min. The resultant mixture was then stirred at 60 °C for 18 h. After removal of the solvent, the residue was taken up in water (200 mL) and extracted with ether (3×100 mL). The organic layer was dried, concentrated and distilled using a vigreux distilling column to obtain diallyamine derivative 3 as a colourless liquid (69 g, 86%); bp 0.2 mbar Hg 91 °C. (Found: C, 61.0; H, 8.1; N, 5.4%. C₁₃H₂₁NO₄ requires C, 61.16; H, 8.29; N, 5.49%); □_{max}. (neat): 3078, 3002, 2977, 2953, 2844, 1738, 1642, 1437, 1364, 1258, 1201, 1164, 1120, 1074, 995, 923, and 793 cm⁻¹; δ_H (CDCl₃) 1.85-2.10 (2H, m), 2.42 (2H, m), 3.03

(1H, dd, *J* 7.8, 14.5 Hz), 3.32 (1H, dd, *J* 4.6, 14.5 Hz), 3.47 (1H, dd, *J* 5.8, 9.8 Hz), 3.67 (3H, s), 3.70 (3H, s), 5.15 (4H, m), 5.73 (2H, m); δ_C (CDCl₃) 24.45, 30.65, 51.08, 51.50, 53.29, 60.52, 117.18, 136.42, 173.13, 173.69 (TMS: 0.00 ppm).

c. N,N-Diallylglutamic acid hydrochloride (4)

A heterogeneous mixture of **3** (54 g, 0.21 mol) in water (150 mL) containing NaOH (19.6 g, 0.49 mol, 2.33 equivalents) was stirred at room temperature for 24 h. Upon complete hydrolysis of the two ester groups, as monitored by observing the ¹H NMR signals of the methoxy protons, the reaction mixture was neutralized with concentrated HCl (80 g, 37 w/w%, 0.81 mol). The aqueous mixture was then freeze-dried; the residual mixture was triturated with acetone (300 mL), heated to boiling and filtered to remove NaCl. The solid NaCl was washed with hot acetone (100 mL). The combined filtrate was concentrated, and the residual thick liquid was dissolved in boiling acetone and kept inside a freezer to obtain white crystals of **4** (49.8 g, 91%). A D₂O solution containing **4** (100.0 mg) and EtOH (20.0 mg) was subjected to ¹H NMR analysis which helped us to determine the molar mass of the salt as 261.5 g mol⁻¹ as against the calculated molar mass of 263.72 g mol⁻¹ thereby confirming the structure of **4** as the hydrochloride salt as depicted in Scheme 5.1. Mp 103 -105 °C (acetone). (Found: C, 49.8; H, 6.9; N, 5.2%. C₁₁H₁₈ClNO₄ requires C, 50.10; H, 6.88; N, 5.31%); ν_{\max} (KBr): 3410, 2954 (br) 1727, 1635, 1454, 1425, 1304, 1223, 1179, 1097, 996, 954, 843, 796, and 619 cm⁻¹; δ_H (D₂O) 1.98 (1H,m), 2.09 (1H, m), 2.39 (1H, m), 2.47 (1H, m), 3.65 (1H, dd, *J* 7.3, 13.5 Hz), 3.74 (1H, dd, *J* 7.1, 13.5 Hz), 3.91 (1H, dd, *J* 3.5, 10.2 Hz), 5.41 (4H, m), 5.72 (2H, m) (HOD: 4.65); δ_C (D₂O) 21.56, 30.66, 54.91, 62.93, 126.33 (=CH), 127.84(=CH₂), 171.04, 176.66 (external dioxane: 67.40 ppm). DEPT 135 NMR analysis confirmed the ¹³C spectral assignments.

d. Cyclopolymerization of monomer **4**

As described in Table 5.1, a solution of monomer **4** (7.90 g, 30 mmol) and water (2.63 g) was heated under N₂ to 85 °C in a 50-mL round bottom flask fitted with a condenser. Initiator APS (0.75 g) was added at 85 °C to the stirred solution in one portion. Exothermic polymerization ensued; after continued stirring at 85-90 °C for 15 min, the mixture was cooled to 20°C. Resultant polymer cationic polyelectrolyte (CPE) **5** was transferred to a dialysis bag with the help of 4 M HCl (10 mL) and dialyzed against deionized water for 24 h. The homogeneous solution become cloudy during dialysis owing to the transformation of CPE **5** to polyzwitterionic acid (PZA) **6** and finally started to precipitate. The entire mixture was freeze-dried to obtain PZA **6** as a white powder. (Found: C, 57.8; H, 7.7; N, 6.6%. C₁₁H₁₇NO₄ requires C, 58.14; H, 7.54; N, 6.16%); $\nu_{\max.}(\text{KBr})$ 3418 (br), 3028, 2942, 2688, 1720, 1620, 1454, 1399, 1214, 1064, 885, 810, 767 and 656 cm⁻¹.

Table 5.1 Cyclopolymerization^a of Monomer **4**.

Entry No.	Monomer (mmol)	Water (% w/w)	APS ^a (g)	Temp (°C)	Time (min)	Yield (%)	[η] ^b (dL g ⁻¹)
1	30	25	1.2	85	15	85	0.0557
2	30	25	0.75	85	15	81	0.0640

^aPolymerization reactions took place in aqueous solution of monomer **4** in the presence of ammonium persulfate (APS) at 85 °C to give polymer of **6**, ^bViscosity of 1-0.25 % solution of **6** in 0.75 M NaCl at 30.0 ± 0.1°C was measured with Ubbelohde Viscometer ($K=0.005317 \text{ mm}^2 \text{ s}^{-2}$).

5.2.4 Solubility Measurements

The critical (minimum) salt concentration (CSC) values were determined by titrating a 1% w/w aqueous solution of PZA **6** containing salts or HCl at a higher concentration than their CSC values at 23 °C with deionized water. The average of the triplicate results of the CSCs were determined to be 0.548 M NaCl, 0.271 M NaBr, 0.133 M NaI, and 0.0104 M HCl with approximate accuracies of ±1–2%.

5.2.5 Potentiometric titrations

The potentiometric titration used to determine protonation constants (K) is described elsewhere. [72,110]. In each trial, a certain millimole (in terms of repeating unit (RU)) of PZA **6** (ZH_2^{\pm}) in CO₂-free water (200 mL) was titrated by gradual addition of 0.05–0.15 mL of 0.0978 M NaOH or 0.1222 M HCl as described in Table 5.2. After each addition of the titrant, the recorded pH values were used to calculate $\log K_i$ at each pH value by the Henderson–Hasselbalch equation (Equation (2), Scheme 5.1). Because of the solubility

problem of PZA **6**, $\log K_3$ associated with the equilibration: **6** (ZH_2^\pm) + $\text{H}^+ \rightleftharpoons$ (ZH_3^+) **5** could not be determined in deionized water.

Since PZA **6** is insoluble in deionized water (200 mL), it was dissolved in 0.0978 M NaOH (8-11 mL) and then diluted to 200 mL using deionized water. The clear solution was then titrated with 0.1222 M HCl to determine the protonation constants. The $\log K_1$, $\log K_2$ and $\log K_3$ represent the protonation constants of the most basic center in polydianion (PDE) **8** (Z^-), polyzwitterion-anion (PZAN) **7** (ZH^\pm), and **6** (ZH_2^\pm), respectively. After each addition of 0.05–0.15 mL of the titrant, the recorded pH values were used to calculate the $\log K_i$ s at each pH value by the Henderson-Hasselbalch Equation (2) (Scheme 5.1). The degree of protonation (α) of **8**, **7** and **6** is calculated by $[\text{ZH}^\pm]_{\text{eq}}/[\text{Z}]_0$, $[\text{ZH}_2^\pm]_{\text{eq}}/[\text{Z}]_0$ and $[\text{ZH}_3^+]_{\text{eq}}/[\text{Z}]_0$, respectively, where $[\text{ZH}^\pm]_{\text{eq}}$, $[\text{ZH}_2^\pm]_{\text{eq}}$ and $[\text{ZH}_3^+]_{\text{eq}}$ represent the corresponding concentrations at equilibrium of the protonated species **7**, **6** and **5**. $[\text{Z}]_0$ represents the initial polymer concentration in terms of RUs. $\log K_3$ associated with the equilibration **6** (ZH_2^\pm) + $\text{H}^+ \rightleftharpoons$ (ZH_3^+) **5** could not be determined in deionized water because of the insolubility of PZA **6**. Note that $\log K_3$ was determined in 1 M NaCl which is higher than the CSC value for **6**. Because of addition of 8-11 mL of 0.0978 M NaOH, which is more than two equivalents of the RUs in **6** (ZH_2^\pm), the polymer is converted to its dianionic form **8** (Z^-) by neutralization with two equivalents of NaOH. By considering the excess NaOH as added OH^- , the concentration of the protonated species **7** [ZH^\pm] during the first step of titration of **8** (Z^-) with HCl to determine $\log K_1$ was given by $[\text{ZH}^\pm]_{\text{eq}} = \text{C}_{\text{H}^+} - \text{C}_{\text{OH}^-} - [\text{H}^+] + [\text{OH}^-]$, where C_{OH^-} represents the concentration of the added ‘excess NaOH’. The equilibrium $[\text{H}^+]$ and $[\text{OH}^-]$ values were determined from the pH values, whereas C_{H^+} represents the concentration of added HCl during titrations. Continuing the titration, $\log K_2$

and $\log K_3$ were calculated using titrant volume after subtracting one-equivalent and two-equivalent volume, respectively, from the total volume. In few instances, 0.1222 M HCl (8 mL) was added to **6** (ZH_2^+) to convert it to **5** (ZH_3^+) to attain a suitable value of α_3 (See Table 5.2, footnote). The solution was then titrated with 0.0978 M NaOH to determine $\log K_3$ using equation: $[ZH_3^+]_{eq} = [Z]_o + C_{H^+} - C_{OH^-} - [H^+] + [OH^-]$, where C_{H^+} represents the concentration of added 'excess HCl', and C_{OH^-} represents the concentration of added NaOH during titrations. Note that 1 equivalent of HCl is required to transform **6** (ZH_2^+) to **5** (ZH_3^+); as such the added excess C_{H^+} was calculated after subtracting 1 equivalent from the total added HCl.

Table 5.2 Protonation of Polymer 8 (Z^-), 7 (ZH^{\pm}) and 6 (ZH_2^{\pm}) at 23 °C in deionized water and 1 M NaCl.

run	ZH_2^{\pm} (mmol)	C_T^a (mol dm ⁻³)	α -range	pH-range	Points ^b	Log $K_i^{o,c}$	n_i^c	R^2, d
Polymer 6 in Salt-Free water								
1	0.2658 ^f (ZH_2^{\pm})	+0.1222	0.38–0.90	11.27–8.80	26	10.91	2.24	0.9956
2	0.3080 ^f (ZH_2^{\pm})	+0.1222	0.38–0.92	11.20–8.51	24	10.93	2.17	0.9920
3	0.3529 ^f (ZH_2^{\pm})	+0.1222	0.41–0.90	11.28–8.80	19	10.98	2.15	0.9949
Average						10.94 (4)	2.19 (5)	
Log $K_1^e = 10.94 + 1.19 \log [(1-\alpha)/\alpha]$ For the reaction: $Z^- + H^+ \xrightleftharpoons{K_1} ZH^{\pm-}$								
1	0.2658 ^f (ZH_2^{\pm})	+0.1222	0.17–0.90	6.44–3.68	38	5.24	1.75	0.9974
2	0.3080 ^f (ZH_2^{\pm})	+0.1222	0.13–0.92	6.57–3.57	41	5.25	1.78	0.9935
3	0.3529 ^f (ZH_2^{\pm})	+0.1222	0.11–0.90	6.93–3.67	53	5.27	1.86	0.9971
Average						5.25 (2)	1.80 (6)	
Log $K_2^e = 5.25 + 0.80 \log [(1-\alpha)/\alpha]$ For the reaction: $ZH^{\pm-} + H^+ \xrightleftharpoons{K_2} ZH_2^{\pm}$								
Polymer 6 in 1.0 M NaCl								
1	0.2640 ^f (ZH_2^{\pm})	+0.1222	0.30–0.88	10.38–8.72	19	9.94	1.34	0.9971
2	0.3124 ^f (ZH_2^{\pm})	+0.1222	0.29–0.88	10.48–8.73	28	9.93	1.38	0.9977
Average						9.94 (1)	1.36 (2)	
Log $K_1^e = 9.94 + 0.36 \log [(1-\alpha)/\alpha]$ For the reaction: $Z^- + H^+ \xrightleftharpoons{K_1} ZH^{\pm-}$								
1	0.2640 ^f (ZH_2^{\pm})	+0.1222	0.11–0.85	5.80–3.57	35	4.54	1.37	0.9980
2	0.2645 ^g (ZH_2^{\pm})	-0.0978	0.88–0.11	3.47–5.78	29	4.58	1.30	0.9972
Average						4.56 (2)	1.34 (3)	
Log $K_2^e = 4.56 + 0.34 \log [(1-\alpha)/\alpha]$ For the reaction: $ZH^{\pm-} + H^+ \xrightleftharpoons{K_2} ZH_2^{\pm}$								
1	0.2640 ^f (ZH_2^{\pm})	+0.1222	0.16–0.75	2.88–2.31	15	2.51	0.48	0.9869
3	0.2645 ^g (ZH_2^{\pm})	-0.0978	0.54–0.09	2.53–3.12	16	2.55	0.54	0.9928
2	0.2646 (ZH_2^{\pm})	+0.1222	0.15–0.68	3.08–2.47	14	2.62	0.55	0.9891
Average						2.56 (6)	0.52 (5)	
Log $K_3^e = 2.56 - 0.48 \log [(1-\alpha)/\alpha]$ For the reaction: $ZH_2^{\pm} + H^+ \xrightleftharpoons{K_3} ZH_3^+$								

^a (+)ve values describe titrations with HCl; (-)ve values describe titrations with NaOH

^b Number of data points.

^c Standard deviations in the last digit are given under the parentheses .

^d R = Correlation coefficient.

^e $\log K_i = \log K_i^o + (n_i - 1) \log [(1 - \alpha)/\alpha]$.

^{f,g} Titration was carried out in the presence of added 0.0978 M NaOH (8-11 mL) and 0.1222 M HCl (8 mL), respectively, to attain the required values of the α .

5.2.6 Evaluation of anti-scalant behavior

The precipitation and inhibition of calcium sulfate (gypsum) scale formation were evaluated at 40 ± 1 °C in a supersaturated solution of CaSO₄ containing 2598 mg L⁻¹ of Ca²⁺ and 6300 mg L⁻¹ of SO₄²⁻ in the presence of newly synthesized antiscalant **6** (*x* ppm) (Table 5.1, entry 2) using the procedure described elsewhere [103]. The concentrations of the ions are three times concentrations found in the reject brine of a Reverse Osmosis plant [195]. Induction time was assigned as the time when a rapid decrease in conductivity indicated the beginning of precipitation of CaSO₄ (Table 5.3). Visual inspections for any turbidity were performed.

Table 5.3 Inhibition percentage over precipitation at different times in the presence of varying amounts of the polymer 6 in a supersaturated CaSO₄ solution at 40 °C.

Entry	Sample (ppm)	Percent inhibition at times (min) of						Induction time (min)
		200	300	500	1000	2000	3000	
1	5	99	97	87	9.6	–	–	500
2	10	100	100	100	90	11	–	1200
3	20	100	100	100	100	98	96	– ^a

^a No induction observed on the studied time range

5.3 Results and discussions

5.3.1 Synthesis and physical characterization of monomers and polymers

L-Glutamic acid (**1**) was esterified to dimethyl glutamate (**2**) which upon alkylation with allyl bromide afforded dimethyl *N,N*-diallylglutamate (**3**) in excellent yield (Scheme 5.1). Alkaline hydrolysis of tertiary amine **3** followed by acidification gave new monomer *N,N*-diallylglutamic acid hydrochloride (**4**) in 91% yield. Note that the monomer retains the unquenched nitrogen valency as well as the two carboxyl groups of the glutamic acid. Monomer **4** underwent APS-initiated cyclopolymerization to give CPE **5** which upon depletion of HCl during dialysis was transformed to its water-insoluble zwitterionic form: PZA **6** in over 80% yields (Table 5.1).

The TGA curve of PZA **6** is shown in Figure 5.1; a loss of 5% up to 110 °C and a further loss 3% occurred in the range 110-200°C was due to the loss of trapped moisture. An accelerated loss of 25% in the range 200-290°C resulted from the release of one of the CO₂ units, while the gradual loss of 35% in the range 290-470°C was associated with the removal of the remaining glutamate pendant. At 800°C, remaining mass of 19% belonged to some nitrogenated organic fraction. As can be seen from the TGA plot, the polymer remained stable up to 200°C.

A gel permeation chromatography (GPC) assay was conducted at 34 °C using PL-GPC 220 (Agilent Technologies) equipped with a refractive index (RI) detector and two mixed bed columns (PL-aquagel-OH mixed-H, 8 µm, 300 × 7.5 mm) and using 0.003 M NaN₃ as eluent (flow rate: 1.0 mL min⁻¹).-Efforts to determine the molar masses of the polymers **5-**

8 by the GPC failed owing to strong adsorption to the materials of the column; the erratic values of high molar masses do not reconcile with their quite low intrinsic viscosity values (Table 5.1). Similar difficulty associated with polymers containing amine and carboxy motifs have been reported [117].

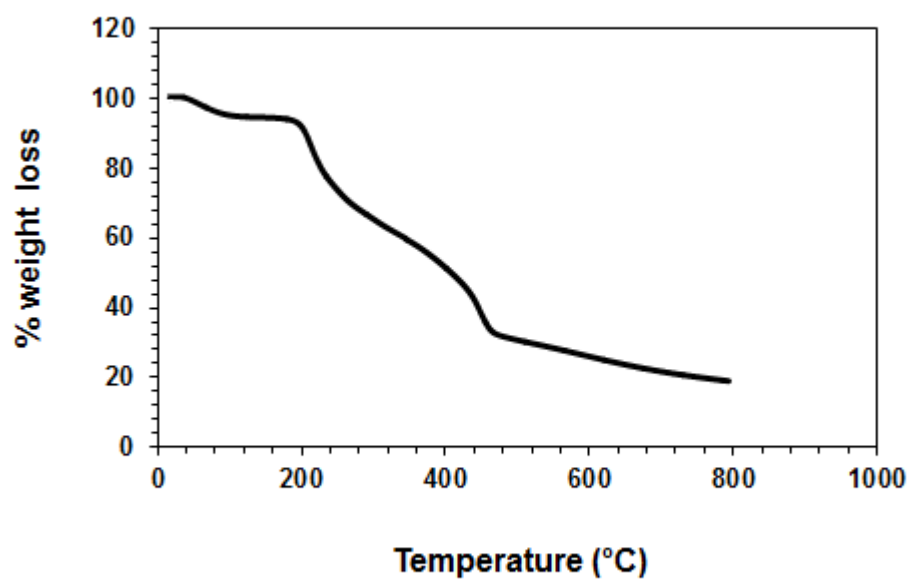


Figure 5.1 TGA curve of PZA 6.

5.3.2 IR and NMR spectra

The symmetric and anti-symmetric stretching of COO^- in the dipolar form (\pm) **6** appeared at respective 1399 cm^{-1} and 1620 cm^{-1} similar to those observed for simple amino acids [119], while the absorption for the $\text{C}=\text{O}$ stretch of COOH appeared at 1720 cm^{-1} .

As evident from the NMR spectra of monomer **4**, polymers **6** and **8** (Figures 3 and 4), the absence of the protons or carbons of the alkene motifs in the polymers' spectra suggests the chain termination to occur via coupling process [114]. The low molar masses as reflected by the lower intrinsic viscosities also point towards chain termination process by abstraction of an allylic proton of the monomer to give stable nonpropagating allyl radicals [113]. Integration of the relevant carbon signals [116,152] revealed a 70:30 cis/trans ratio of the ring substituents at $\text{C}_{b,b}$ (Scheme 5.1; Figure 5.3c).

5.3.3 Solubility behavior

The electroneutral (\pm) **6** was water-insoluble like the majority of known polyzwitterions [74,118,119] but soluble in the presence of various salts of small molar masses. For various salts, the CSCs at $23\text{ }^\circ\text{C}$ were determined to be 0.548 M NaCl , 0.271 M NaBr , 0.133 M NaI . Iodide ions, being the most polarizable (soft), effectively neutralizes the ionic crosslinks so as to disrupt the intragroup, intra- and interchain attractive interactions.[14] Zwitterionic (\pm) **6** was found to be soluble in 0.0104 M HCl as a result of shifting the mobile equilibrium: $(\pm)\text{ } \mathbf{6} + \text{H}^+ \rightleftharpoons (+)\text{ } \mathbf{5}$ towards right where the zwitterionic interactions required for water-insolubility vanishes. PZAN **7** and PDE **8** are water-soluble as expected of any polyelectrolyte; anionic portion in (\pm -) **7** overcomes the zwitterionic interactions so as to impart water-solubility. It has been revealed during potentiometric titrations that the

addition of HCl to an aqueous solution of (=) **8** led to its insolubility at a point where the backbone composition of repeat units of (\pm -) **7**/ (\pm) **6** becomes less than 10:90. Thus increasing the zwitterionic portion to more than 90% thus leads to the polymer's insolubility in deionized water.

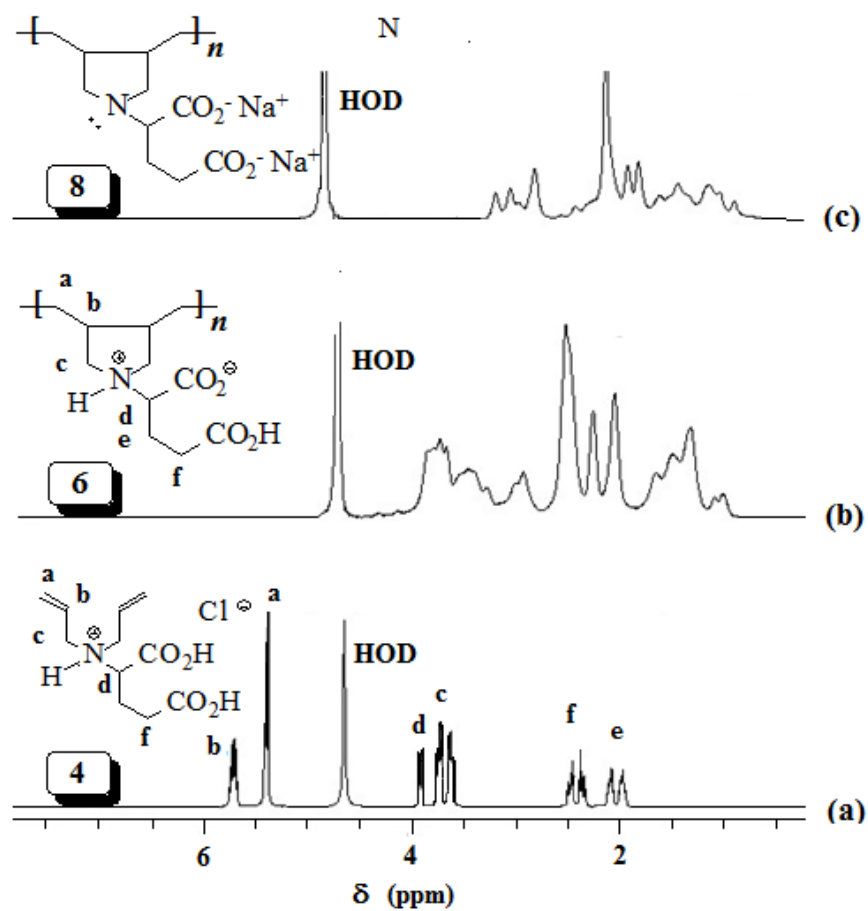


Figure 5.2 ^1H NMR spectrum using trimethylsilylpropionate-2,2,3,3- d_4 (TSP) as internal standard of (a) 4, (b) 6 (+NaCl), (c) 8 in D_2O .

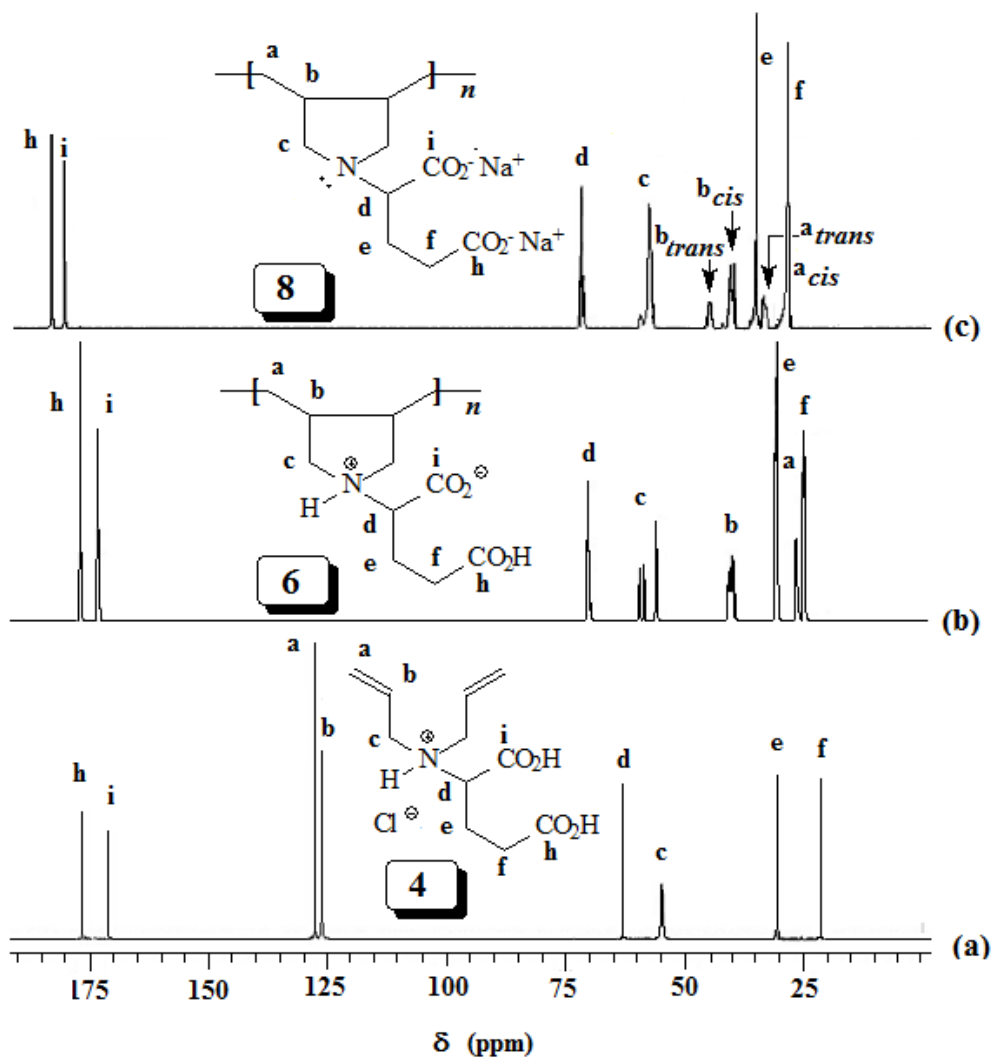


Figure 5.3 ^{13}C NMR spectrum using trimethylsilylpropionate-2,2,3,3- d_4 (TSP) as internal standard of (a) 4, (b) 6 (+NaCl), (c) 8 in D_2O .

5.3.4 Viscosity measurements

Viscosity data for (\pm) **6**, (\pm -) **7** and (=) **8** (entry 2, Table 5.1) are given in Figure 5.4. The viscosity plots for (\pm -) **7** and (=) **8** in deionized water were concave upwards like any polyelectrolytes (Figure 5.4i, ii); whereas, the plots become linear in the presence of NaCl in the concentration range 1-0.25 g dL⁻¹ (Figure 5.4iii-vi). At lower concentrations, the linearity cannot be maintained; the viscosity falls off as a result of movement of the mobile equilibrium: (=) **8** or (\pm -) **7** + H⁺ \rightleftharpoons (\pm -) **7** or (\pm) **6** towards right. As per general rule of hydrolysis, the degree of transformation of **8** to **7** (or **7** to **6**) increases with decreasing concentration; overall decrease in the charge imbalance on the polymer chains decreases thereby leading to lesser electrostatic repulsions hence lesser viscosity values. Only the linear portion of the plots is extrapolated to obtain the intrinsic viscosities. Note that by virtue of having larger negative charge density, (=) **8** has higher viscosity values both in deionized water as well as in NaCl-added solutions. As expected, the viscosity values are lower in 1.0 M NaCl than in 0.1 N NaCl as result of the greater shielding of the backbone and pendant charges in the former medium. Antipolyelectrolyte behavior of (\pm) **6** is confirmed by the increase of $[\eta]$ with increase in the concentration of NaCl (*cf.* Figure 5.4 vii- ix). The zwitterionic dipole has an overall excess negative charge by virtue of more effective binding of the N⁺ by Cl⁻ than the binding of CO₂⁻ by Na⁺. The repulsion among the dipole centres with excess negative charges leads to increasing viscosity with increasing NaCl concentration [118,120,121].

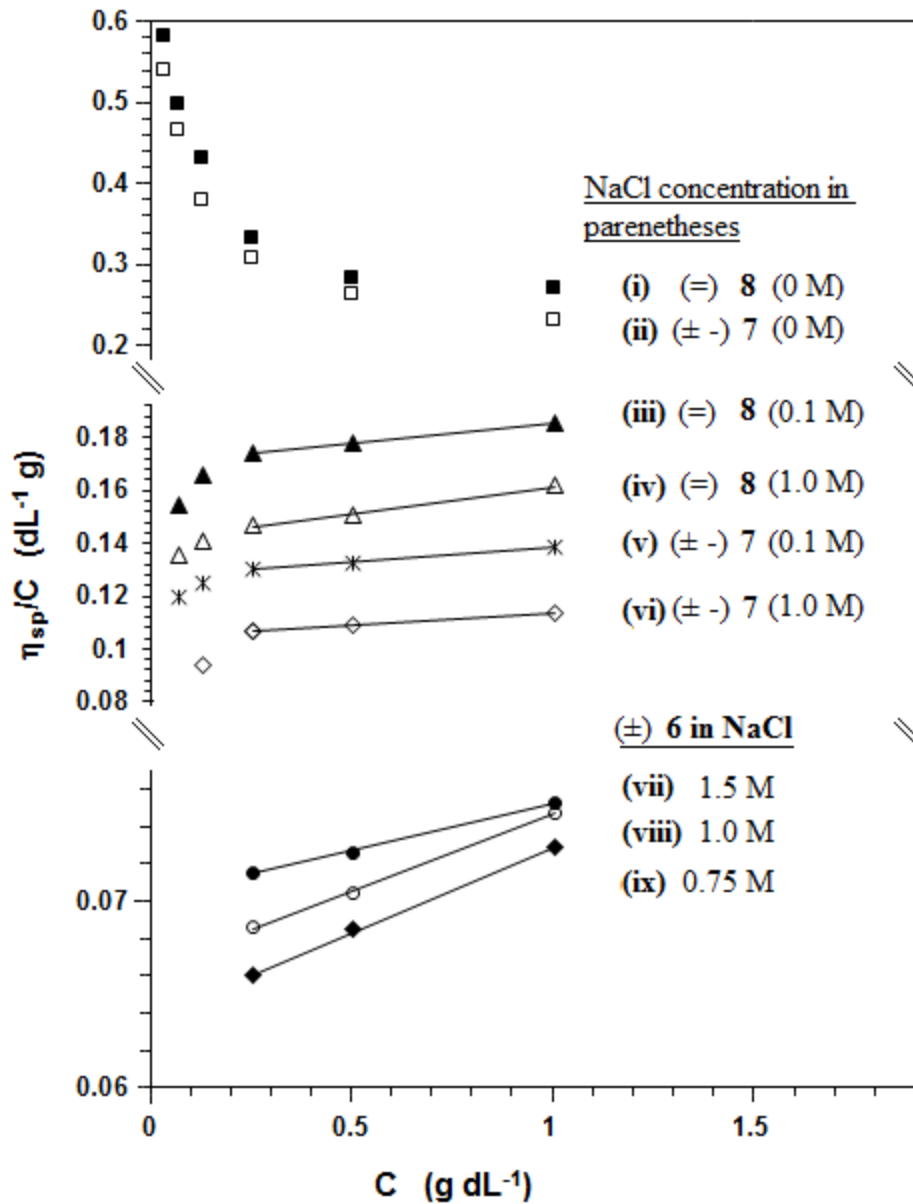


Figure 5.4 The viscosity behavior of sample derived entry 2, Utilizing a viscometer, 30 °C: (i) ■ (=) 8 in deionized water, (ii) □ (± -) 7 in deionized water, (iii) ▲ (=) 8 in 0.1 M NaCl, (iv) △ in 1.0 M NaCl, (v) * (± -) 7 in 0.1 M NaCl, (vi) ◇ (± -) 7 in 1.0 M NaCl, (vii) ● (±) 6 in 1.5 M NaCl, (viii) ○ (±) 6 in 1.0 M NaCl and (ix) ○ (±) 6 in 0.75 M NaCl.

5.3.5 Basicity Constants

The linear regression of pH vs. $\log [(1-\alpha)/\alpha]$ led us to determine the ' n_i ' and $\log K_i^o$ as the slope and intercept, respectively using Equation 2 (Figure 5.5). The apparent basicity constants of anionic centers is described by Equation 3 where $\log K_i^o = \text{pH}$ at $\alpha = 0.5$ and $n_i = 1$ in the case of sharp basicity constants. In deionized water, basicity constants $\log K_1$ of the amine group in (=) **8**, which is the $\text{p}K_1$ of its conjugate acid (\pm -) **7**, and $\log K_2$ of the terminal CO_2^- in (\pm -) **7** (i.e. $\text{p}K_2$ of its conjugate acid in (\pm) **6**) were determined to be 10.94 and 5.25, respectively, in deionized water (Table 5.2) and 9.94 and 4.56 in 1 M NaCl. In deionized water, $\log K_3$ (i.e. $\text{p}K_3$) involving the equilibrium: **6** (ZH_2^{\pm}) + $\text{H}^+ \rightleftharpoons (\text{ZH}_3^+)$ **7** cannot be determined owing to the solubility problem associated with zwitterionic (\pm) **6** (*vide supra*). In 1.0 M NaCl, which is higher than the CSC value for the polyzwitterion, $\log K_3$ was determined to be 2.56 (Table 5.2).

For $\log K_1$ and $\log K_2$, the n_i values, which are a measure of polyelectrolyte effect, are found to be greater than 1. The n_1 values of 2.19 and 1.36 in deionized water and 1.0 M NaCl, respectively, and the corresponding n_2 values of 1.80 and 1.34 reflect the greater polyelectrolyte effect in the former medium. In deionized water, charge centers in polymer (=) **8** or (\pm -) **7** are expected to be more hydrated than in 1.0 M NaCl where greater numbers of water molecules are busy to fill up the hydration shells of Na^+ and Cl^- ions. The average number of hydrated water molecules per RU in deionized water is therefore greater than in 1.0 M NaCl. The higher $\log K_1$, $\log K_2$, n_1 and n_2 values in deionized water are the consequences of the entropy driven [126] protonation step; during which it releases more water of hydration in deionized water than in 1 M NaCl. The variations of $\log K_i$ s with α , shown in Figure 5.5, reflect their "apparent" [125] nature since instead of remaining

constant, they either decrease or increase with the increase in α . An increase in α in the polymer chains decreases the overall negative charges that induces protonation thereby resulting in a decrease of $\log K_1$ and $\log K_2$. In both cases of protonation in deionized water and as well as in 1 M NaCl, the exothermic enthalpy changes (ΔH° s) remain constant with increasing α , and the (ΔG° s) become less negative as a result of progressive decrease in the (+)ve ΔS° s. With each protonation, the (-)ve charge density in the polymer backbone decreases thereby decreasing the average negative charge density and the number of hydrated water molecules associated with the next RU to be protonated. In other words, a RU being protonated releases less water molecules from its hydration shell than that of the unit protonated in the previous step [120]. The continuous decrease of positive ΔS° with α leads to lesser negative ΔG° s, hence a gradual decrease in $\log K$ values.

However, this was found not to be the case with $\log K_3$, [involving $(\text{ZH}_2^\pm) \mathbf{6} + \text{H}^+ \rightleftharpoons (\text{ZH}_3^+)$ **5**]: It is shown to be increasing with the increase in α and associated with an ‘ n ’ value of 0.52. An n value of less than 1 is considered as diagnostic of a compact conformation. Polyzwitterion (\pm) **6**, being the most parked and least hydrated as confirmed by the viscosity data (Figure 5.4), continuously expands during the progressive increase in α ; thus making an easier access of the incoming protons to the more exposed COO^- groups. With each protonation of the COO^- in $(\text{ZH}_2^\pm) \mathbf{6}$, the charge imbalance in favor of the positive charges on the polymer chain increases, hence the number of water molecules to be released in the next protonation from the hydration shell of each unit also increases. This behavior seems to be general in all cases in which the basic COO^- group is in the α position to the nitrogen [196,197].

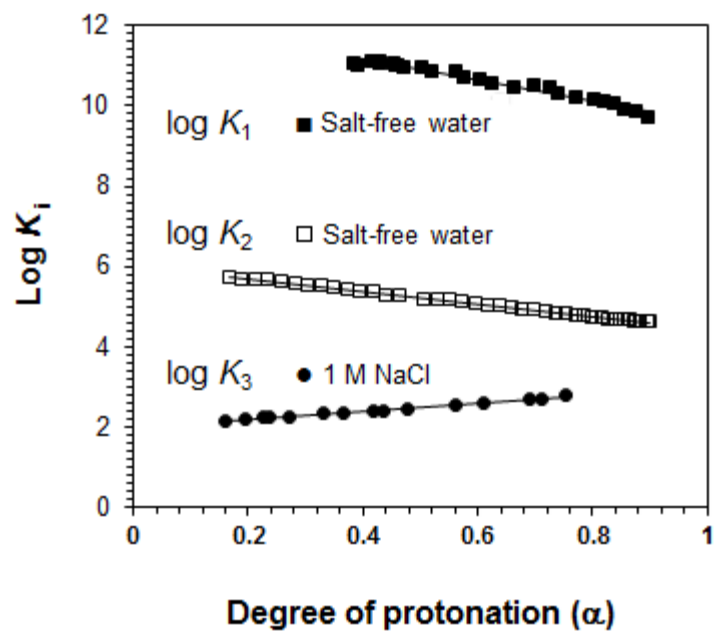


Figure 5.5 Plot of \square versus apparent \blacksquare $\log K_1$ in deionized water (entry 1, Table 2), \square $\log K_2$ in deionized water (entry 1, Table 2) and \bullet $\log K_3$ in 1 M NaCl (entry 1, Table 2).

5.3.6 Scale inhibition properties of the synthesized polymers

In Reverse Osmosis (RO) process, scaling of inorganic salts like CaSO_4 and CaCO_3 damages the smooth functioning of membranes. The scaling occurs when the concentration of the relevant ions in the inlet stream of feed water are supersaturated in the reject brine after producing the product water in the outlet stream. The percent inhibition (PI) of scaling is calculated using the following Equation 4:

$$\% \text{ Scale Inhibition} = \frac{[\text{Ca}^{2+}]_{\text{inhibited}(t)} - [\text{Ca}^{2+}]_{\text{blank}(t)}}{[\text{Ca}^{2+}]_{\text{inhibited}(t_0)} - [\text{Ca}^{2+}]_{\text{blank}(t)}} \times 100 \quad (4)$$

where $[\text{Ca}^{2+}]_{\text{inhibited}(t_0)}$ is the initial concentration at time zero, $[\text{Ca}^{2+}]_{\text{inhibited}(t)}$ and $[\text{Ca}^{2+}]_{\text{blank}(t)}$ are the concentrations in the inhibited and blank solution (without antiscalant) at time t , respectively.

For the current work, a supersaturated solution of CaSO_4 containing 2598 ppm of Ca^{2+} and 6300 ppm of SO_4^{2-} in the presence of various concentration of the synthesized antiscalant was investigated by following the conductivity of the solutions. Percent inhibition (PI) of **6** at concentrations of 5, 10 and 20 ppm is given in Table 5.3. A sudden drop in the conductivity in the absence of antiscalant indicates the precipitation of CaSO_4 (Figure 5.6iv: Blank). Satisfactorily, the presence of 20 ppm of **6** imparted a 100% scale inhibition for about 1000 min, while it was 98 and 96% at the time of 2000 and 3000 min, respectively as calculated using Equation 4. Note that the presence of a meager 5 ppm of the antiscalant was able to register a 99 % scale inhibition at a time of 200 min. This is efficient enough since an usual residence time of ≈ 30 min is required for the feed water to stay in the osmosis chamber. An induction period is observed before the onset of quick precipitation; a sharp drop in conductivity happens at a time of 500 and 1200 min in the presence of 5

and 10 ppm of the antiscalant, respectively. Note that at the time scale of 3000 min, no induction period was observed for the antiscalant concentration of 20 ppm; it still imparted 96% inhibition. The new antiscalant has thus demonstrated its efficacy to scavenge metal ions and disrupt the nucleation and crystallization processes [128,198], hence it could be used as a potential antiscalant to minimize the fouling of membranes by CaSO₄ scale.

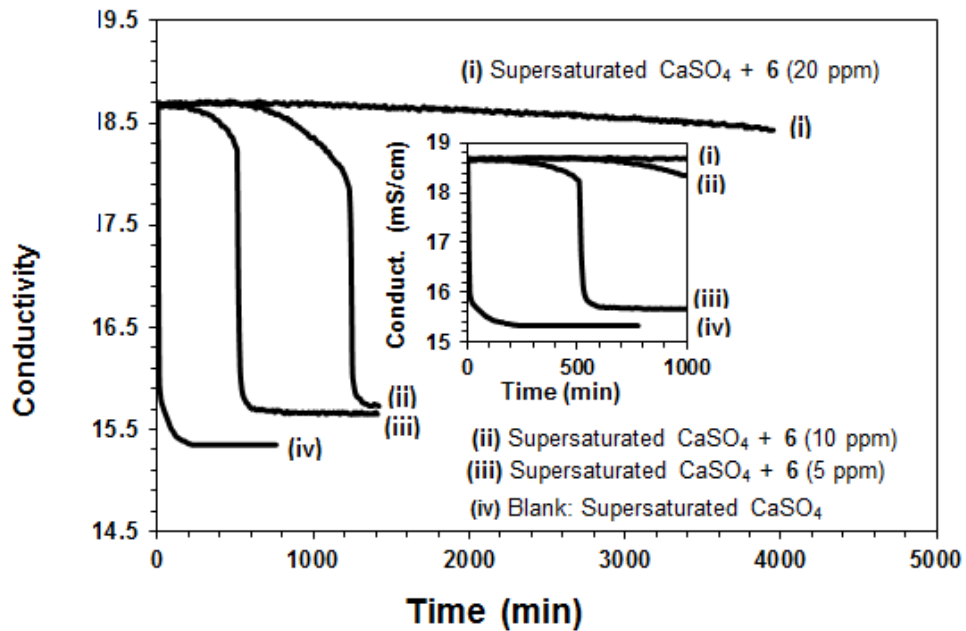


Figure 5.6 Trends in precipitation of a supersaturated solution of CaSO₄ with addition of (5, 10, and 20 ppm) and absence of PZA 6. Inset represents the data for a shorter time scale of 1000 min.

5.4 Conclusion

A new monomer **4** containing glutamic acid residues has been developed and polymerized in excellent yields using Butler's cyclopolymerization protocol to a pH-triggerable polymer **5** which represents the first example of a cyclopolymer containing residues of glutamic acid (an amino acid) as pendants. The solution properties of the pH-triggerable polymers **5-8** having backbone charges (+), (\pm), ($\pm -$), and (=), respectively, along with the CSC required to promote water-solubility of zwitterionic (\pm) **6** have been studied. The basicity constants for the nitrogen and the anionic centers in (=) **8** have been determined; the data would be of great value to utilize and understand its ability to act as scavengers of toxic metal ions and inhibitor of metal corrosion. PZA **6** has demonstrated remarkable efficiency as a potential antiscalant additive in RO plants; it has been found to be an effective antiscalant even at a meager concentration of 5 ppm. Polymeric aminomethylphosphonic acids, prepared using Butler's cyclopolymerization protocol, has been utilized as chelating agents for separation of transition metal ions [57,199]; the current work involving the corresponding polymer of aminoalkyldicarboxylic acid also hold the similar prospects for utilization as polychelatogenes. Glutamic acid has the three pK_a values of 2.1, 4.07, 9.47 while the corresponding values for a RU in **5** were determined to be 10.94, 5.25 and ≈ 2.5 . The conjugate bases being more stronger in the RU would make it a better chelating ligand. Work is currently underway in our laboratory to utilize the current monomer to synthesize cross-linked polymers retaining all three functionalities (i.e. amine and two carboxyl groups) which would act as chelating adsorbents for the removal of toxic materials [84].

CHAPTER 6

Synthesis and Application of Alternate Copolymer of

Diallylglutamic acid and Sulfur dioxide

Abstract

Monomer *N,N*-diallylglutamic acid hydrochloride $[(\text{CH}_2=\text{CH}-\text{CH}_2)_2\text{NH}^+\text{CH}(\text{CO}_2\text{H})\text{CH}_2\text{CH}_2\text{CO}_2\text{H Cl}^-]$ (**I**)/ SO_2 , underwent cyclopolymerization to afford alternate cationic polyelectrolyte (CPE) poly(**I**-*alt*- SO_2) (**II**) in very good yields. Upon depletion of HCl during soaking in water, water-soluble triprotic (+) **II** was transformed to water-insoluble diprotic zwitterionic (\pm) **III** containing residues of glutamic acid in each repeating unit. Upon treatment with 1 and 2 equivalents of NaOH, polyzwitterions (\pm) **III**, was converted into water-soluble monoprotic poly(zwitterion-anion) (\pm -) **IV** and fully deprotonated polydianion (=) **V**, respectively. Basicity strengths of the chelation centers of CO_2^- and nitrogen in (=) **V** have been determined. The polymer has demonstrated its effectiveness as an antiscalant in the inhibition of CaSO_4 scaling. Keeping in view the pH-dependent solubility of the polymers, a recyclable aqueous two-phase system (ATPS) comprising of (=) **V** and polyethylene glycol has been constructed for potential purification of biomolecules. After its use, the ATPS can be recycled by precipitating the ionic polymer in the form of (\pm) **III** at a lower pH.

6.1 Introduction

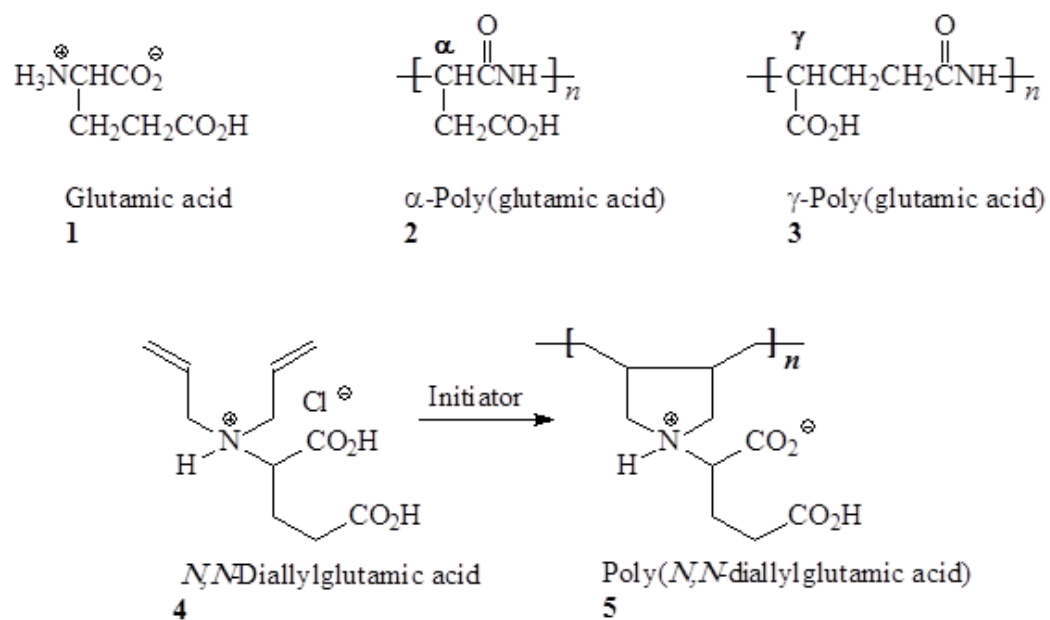
Glutamic acid is a non-essential amino acid that is used in the biosynthesis of proteins (Scheme 6.1). Its side chain CO_2H with a $\text{p}K_a$ of 4.1 exists almost entirely in the CO_2^- form at physiological pH range 7.35-7.45. The carboxylate anion in glutamate is an important excitatory neurotransmitter in neural activation [185,200]. All meats, fish, dairy products, wheat, etc., are excellent sources of glutamic acid. Glutamate, an abundantly available molecule in the brain, is involved in learning and memory [186], it is also a key compound in cellular metabolism [187]. A series of disodium sulphonamides of glutamic acid complexes with copper(II), nickel(II) and ruthenium(III) ions, have demonstrated good anticancer activities [201].

The biodegradable, non-toxic and non-immunogenic properties of naturally occurring poly- γ -glutamic acid (γ -PGA) have rendered its use in the food, medical and wastewater industries (Scheme 6.1) [188,202,203]. γ -PGA has been utilized in many medical applications including drug delivery [202] and cancer treatment [189]. γ -Glutamic acid enhances calcium absorption in the small intestine and increases the solubility of Ca^{2+} , suggesting its chelating ability [204,205]. Glutamic acid-derived polymers have the potential to act as polychelator to scavenge toxic metal ions [194]. The cross-linking of microbial γ -PGA with glucose has led to a hydrogel which has been shown to be a super adsorbent of water (3000 g g^{-1}) [190]. A biodegradable PGA/gadolinium chelate has been evaluated as a contrast agent for magnetic resonance imaging (MRI); this is an important development since most of the currently evaluated macromolecular contrast agents are not biodegradable [206]. The recently developed Fe_3O_4 -PGA nanoparticle has been shown to hold great promise to be used as a contrast agent for MRI of tumors [207]. γ -PGA-

functionalized alumina nanoparticles (γ -PAN) has been evaluated for cytotoxicity towards human prostate cancer cell PC-3; the study provides a basis for further screening of the promising material for future biomedical applications [208].

The abundant availability of inexpensive glutamic acid has led us to synthesize and cyclopolymerize [24–26] diallylglutamic acid **4** to obtain poly(diallylglutamic acid) **5** which retained all three original functionalities of the amino acid (Scheme 6.1) [209]. Note that the nitrogen in the peptide bond in PGA loses its basic character while retaining only one of the original carboxylate motifs of the amino acid. Glutamic acid and materials derived from it are of tremendous importance for biomedical and material research. We anticipated to use **5** as a polymer component in developing a recyclable aqueous two-phase system (ATPS) for its utilization in bioseparation [106,138]. However, failure to synthesize **5** having high molar mass and its solubility behavior (*vide infra*) impeded the development of a recyclable ATPS in which its pH-controlled solubility would permit precipitating out and hence reuse the polymer.

The current work envisages the application of copolymerization protocol [210] to obtain **4**/SO₂ alternate copolymer poly(**4-alt**-SO₂) **8** (Scheme 6.2) with the anticipation that its high molar mass and pH-dependent solubility behavior would permit us to develop a recyclable ATPS. The study would also permit us to evaluate the effects of SO₂ spacer on the basicity constants of various ligand centers and antiscalant properties. The current study would pave the way to synthesize cross-linked adsorbents containing the metal chelating centers of glutamic acid for the removal of toxic metal ions [83,210].



Scheme 6.1 Glutamic acid, α - and γ -poly(glutamic acid) and polymer containing glutamic acid residues.

6.2 Experimental

6.2.1 Materials

L-Glutamic acid from Fluka AG (Buchs, Switzerland) was used as received. Sodium 3-Trimethylsilylpropionate-2,2,3,3-d₄ (TSP-deuterated), an NMR internal standard, was purchased from Merck Sharp & Dohme Canada Ltd, Montreal, Canada. 2,2'-Azobisisobutyronitrile (AIBN) from Fluka AG (Buchs, Switzerland) was crystallized from C₂H₅OH/CHCl₃ mixture. Calcium hydride-dried dimethylsulfoxide (DMSO) was distilled at a boiling point of 64-65°C (4 mmHg). Poly(ethylene glycol) (PEG) of number average molecular weight (\overline{M}_n) of 35000 was purchased from MERCK-Schuchardt.

Dimethyl *N,N*-diallylglutamate (**7**), synthesized from dimethyl glutamate (**6**), was hydrolyzed with NaOH and acidified with HCl to obtain *N,N*-diallylglutamic acid hydrochloride **4** as described [211].

6.2.2 Physical Methods for Structural Characteruzation

A Perkin Elmer (Series II Model 2400) elemental analyzer and a Fourier transform infrared (FTIR) spectrometer (Perkin Elmer 16F PC) were utilized for elemental analyses and IR spectroscopy, respectively. The nuclear magnetic resonance (NMR) spectra were recorded using a 500-MHz JEOL LA spectrometer. Tetramethylsilane (TMS) in CDCl₃ and TSP-deuterated in D₂O were used as internal standards with ¹H signal at 0 ppm. The ¹³C chemical shifts in D₂O were referenced against ¹³C peak of external standard dioxane at 67.4 ppm. A pH meter (Sartorius PB 11) and an Orion Versa Star pH meter were used to measure pH and conductivity, respectively. Viscosity was measured under N₂ in an Ubbelohde viscometer (constant = 0.005317 mm² s⁻²) using polymer solution prepared in

CO₂-free water. An SDT analyzer (Q600: TA Instruments) was utilized to carry out TGA under N₂.

6.2.3 Procedure for 4/ SO₂ copolymerization

The conditions of polymerizations are summarized in Table 6.1. For instance, initiator AIBN was added under N₂ to a homogeneous mixture of monomer **4** (3.96 g, 15 mmol) and SO₂ (960 mg, 15 mmol) in DMSO (3.75 g) in a 25 mL-Round bottom flask. After stirring the contents in the closed flask at 60 °C for 48 h, the viscous polymer mixture was precipitated in water, filtered and vacuum-dried at 60 °C to a constant weight of copolymer polyzwitterion acid (PZA) **9**. Thermal decomposition: Stable up to 240 °C, slight phase change and expansion between 240 and 245 °C, turned tan at 280 °C with evolution of gas which continue up to 400 °C leaving behind dark particles. (Found: C, 45.0; H, 6.1; N, 4.7; S, 10.8. C₁₁H₁₇NO₆S requires C, 45.35; H, 5.88; N, 4.81; S, 11.01%); ν_{\max} (KBr): 3400 (v br), 2978, 1724, 1625, 1405, 1306, 1126, 878, 812, 767, 640 and 512 cm⁻¹.

6.2.4 Conversion of 9 into 11 by NaOH

A mixture of PZA **9** (1.46 g, 5.0 mmol) in water (10 cm³) at 0 °C was treated with NaOH (0.4 g, 10 mmol). Another portion of NaOH (0.2 g, 5 mmol) was added and the solution was quickly dropped onto acetone (75 cm³). The resultant white polydianion electrolyte (PDE) **11** was filtered and washed with MeOH/acetone 1:1 mixture. The polymer was vacuum-dried till constant weight (1.6 g, 91%). Thermal decomposition: Stable up to 290 °C, slight phase change and expansion between 290 and 325 °C, turned tan at 330 °C with evolution of gas which continued up to 400 °C leaving behind dark particles. ν_{\max} (KBr): 3400 (v br), 2962, 2829, 1579 (v br), 1448, 1409, 1300, 1123, 891, 827, 786, and 514 cm⁻¹.

¹. (Found: C, 37.1; H, 4.9; N, 3.9; S, 8.8. C₁₁H₁₅NNa₂O₆S·1H₂O requires C, 37.40; H, 4.85; N, 3.96; S, 9.07%);

Table 6.1 Cyclocopolymerization of 4/SO₂ at 63°C for 36 h

Entry	Monomer (mmol)	SO ₂ (g) (mmol)	DMSO (g)	AIBN ^a (mg)	Yield (%)	[η] ^b dL/g
1	15	15	3.75	45	48	0.873
2	2×15	2×15	2×3.75	2×75	82	1.03
3	15	15	3.75	105	87	1.22

^a Azobisisobutyronitrile. ^b Intrinsic viscosity of 1-0.0625% polymer **9** treated with 2 equivalents NaOH in 0.1 M NaCl at 30 °C was measured with an Ubbelohde Viscometer (K=0.005317 mm²/s²).

6.2.5 Solubility Measurements

An aqueous solution of PZA **9** (1% w/w) containing NaBr or NaI or HCl were titrated with salt-free water at 23 °C until turbidity appeared. Triplicate measurements gave critical (minimum) salt concentration (CSC) of 2.16 M NaBr, 0.581 M NaI, and 8.59 M HCl. PZA **9** was found to be practically insoluble in any possible concentration of NaCl,

6.2.6 Potentiometric Titrations

The procedure for the determination of basicity constants (*K*) is described elsewhere [72,110]. A certain millimole (in terms of repeating unit (RU)) of water-insoluble PZA **9** (ZH₂[±]) was dissolved by treating with 3 equivalents of NaOH using a 0.0978 M NaOH,

then diluted with CO₂-free water to 200 mL, which thus contained a solution of PDE **11** in the presence of 1 equivalent excess NaOH. For water-soluble PDE **11**, its solution was directly prepared in deionized water (200 mL). The solutions were then titrated by gradual addition of 0.1222 M HCl (0.05–0.15 mL) as described in Table 6.2. The pH values, recorded after each addition of the titrant, were used to calculate log K_i by the Henderson–Hasselbalch equation (2) (Scheme 6.2). The insolubility of PZA **9** did not permit the determination of log K_3 associated with the equilibration: **9** (ZH_2^{\pm}) + H⁺ \rightleftharpoons (ZH_3^+) **8**.

The log K_1 and log K_2 represent the basicity constants of the basic centers in PDE **11** (Z^-) and polyzwitterion-anion (PZAN) **10** ($ZH^{\pm -}$), respectively. The degree of protonation (α) of **11** and **10** is calculated by $[ZH^{\pm -}]_{eq}/[Z]_o$, and $[ZH_2^{\pm}]_{eq}/[Z]_o$, respectively, where $[ZH^{\pm -}]_{eq}$ and $[ZH_2^{\pm}]_{eq}$ represent the corresponding equilibrium concentrations of the protonated species **10** and **9**. $[Z]_o$ represents the initial polymer concentration in terms of RUs.

Following the addition of 8–11 mL of 0.0978 M NaOH, which is more than two equivalents of the RUs in **9** (ZH_2^{\pm}), the polymer is converted to its dianionic form **11** (Z^-) by neutralization with two equivalents of NaOH. By considering the excess NaOH as added OH⁻, the concentration of the protonated species **10** $[ZH^{\pm -}]$ during the titration of **11** (Z^-) with HCl to determine log K_1 was given by $[ZH^{\pm -}]_{eq} = C_{H^+} - C_{OH^-} - [H^+] + [OH^-]$, where C_{OH^-} represents the concentration of the added ‘excess NaOH’. The equilibrium concentrations of $[H^+]$ and $[OH^-]$ were determined using the pH values, whereas C_{H^+} represents the concentration of added HCl during titrations. Continuing the titration, log K_2 was calculated using titrant volume after subtracting one-equivalent, from the total volume.

Table 6.2 Protonation of Polymer 11 (Z^-) and 9 (ZH^\pm) at 23 °C in deionized water

run	ZH_2^\pm (mmol)	C_T^a (mol dm ⁻³)	α -range	pH-range	Points ^b	Log $K_i^{o,c}$	n_i^c	$R^2,^d$
Polymer 9 (ZH^\pm) or 11 (Z^-) in Salt-Free water								
1	0.2007 (Z^-)	+0.1222	0.23–0.91	10.37–7.26	22	9.35	2.09	0.9942
2	0.2066 ^f (ZH_2^\pm)	+0.1222	0.18–0.88	10.83–7.60	22	9.30	2.07	0.9945
3	0.2413 ^g (ZH_2^\pm)	+0.1222	0.15–0.88	10.80–7.50	24	9.33	2.04	0.9950
Average						9.33 (3)	2.07 (3)	
Log $K_1^e = 9.33 + 1.07 \log [(1-\alpha)/\alpha]$						For the reaction: $Z^- + H^+ \xrightleftharpoons{K_1} ZH^\pm$		
1	0.2007 (Z^-)	+0.1222	0.16–0.66	6.36–4.93	17	5.40	1.45	0.9934
2	0.2066 ^f (ZH_2^\pm)	+0.1222	0.12–0.75	6.60–4.74	20	5.45	1.40	0.9943
3	0.2413 ^g (ZH_2^\pm)	+0.1222	0.09–0.87	6.85–4.20	23	5.49	1.46	0.9953
Average						5.45 (5)	1.44 (3)	
Log $K_2^e = 5.45 + 0.44 \log [(1-\alpha)/\alpha]$						For the reaction: $ZH^\pm + H^+ \xrightleftharpoons{K_2} ZH_2^\pm$		
^a (+)ve values describe titrations with HCl. ^b Number of data points. ^c Standard deviations in the last digit are given under the parentheses. ^d R = Correlation coefficient. ^e $\log K_i = \log K_i^o + (n_i - 1) \log [(1 - \alpha)/\alpha]$. ^{f,g} Titration was carried out in the presence of 6.43 and 7.50 mL of added 0.0978 M NaOH, respectively, to solubilize and attain the required values of the α .								

6.2.7 Evaluation of anti-scalant behavior

The inhibition of CaSO₄ scale formation were evaluated using supersaturated solution of CaSO₄ containing Ca²⁺ (2600 ppm) and SO₄²⁻ (6300 ppm) in the presence of newly synthesized antiscalant **9** (*x* ppm) (Table 6.1, entry 2) (treated with minimum quantity of NaHCO₃ to dissolve it) at 40 ± 1 °C using the procedure described elsewhere [103]. The concentrations of the ions are three times the concentrations found in the reject brine of a Reverse Osmosis plant [195]. A rapid decrease in conductivity happened at the induction time indicating the beginning of precipitation of CaSO₄ (Table 6.3). Visual inspections for any turbidity were performed.

Table 6.3 Inhibition percentage over precipitation for different times in the presence of varying amounts of the polymer 9 in a supersaturated CaSO₄ solution at 40 °C

Entry	Sample (ppm)	Percent inhibition at times (min) of							Induction time (min)
		30	60	90	120	150	500	1000	
1	5	94	67	15	8.1	7.1	7.3	6.4	60
2	10	98	91	82	71	38	8.5	8.5	90
3	20	99	99	99	98	98	77	12	600
4	30	100	100	100	100	100	100	99	– ^a

^a No induction observed on the studied time range

6.2.8 Phase Compositions of PZA **9** (+ 2 equivs NaOH) – PEG – H₂O (NaCl) Systems

a. The tie-lines by ¹H NMR spectroscopy

Several ATPSs of volume ≈ 7 cm³ having varying compositions of component polymers

PZA **9** (+2.0 equivalents of NaOH) (Table 6.1, entry 2) and PEG were prepared in calibrated cylinders using their stock solutions (20 wt%) in 0.6 M NaCl and 0.6 M NaCl as the diluents. After centrifuging and equilibrating at 23 °C for 24 h, volume and density of the top and bottom layers were measured. The composition of the polymers in the phases were determined by ^1H NMR spectra of the D_2O exchanged phases in the presence of K_2CO_3 (*vide infra*).

b. Binodals by turbidity method

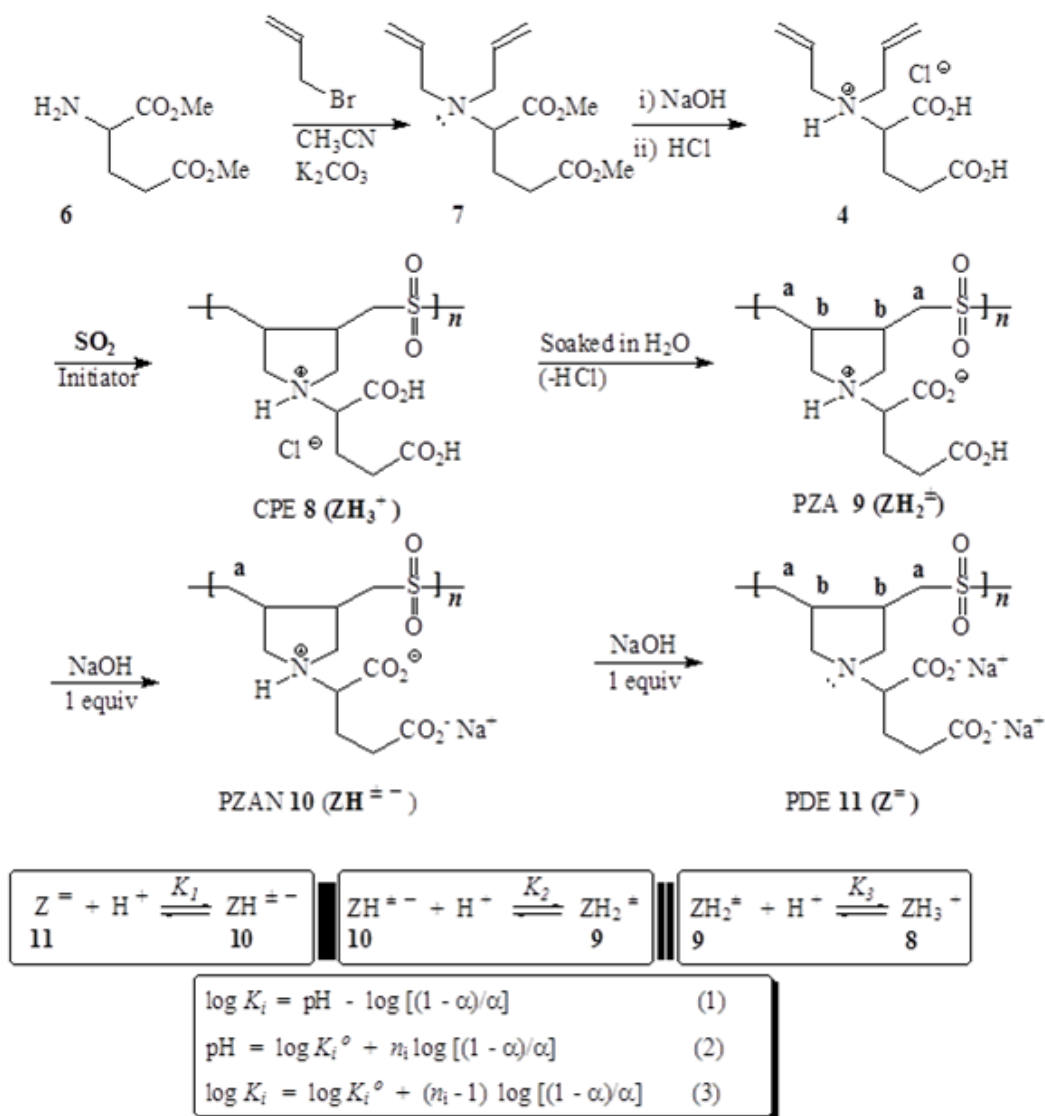
The binodal of the PZA **9** (+ 2 equivs NaOH) – PEG – H_2O (0.6 M NaCl) system was constructed by turbidimetric method at 23 °C as described elsewhere [139].

Table 6.4 composition of the Phases of the [POE^a + PZA^b] system (2.0 equiv. NaOH, 0.6 M NaCl) at 296 K Shown in figure 7a

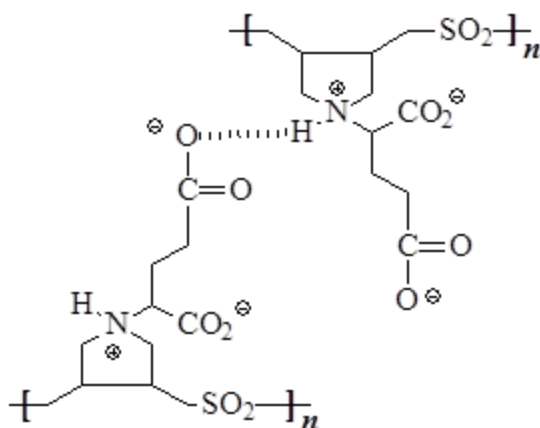
NMR method							
System	Total system		Top phase		Bottom phase		Volume ratio ^c
	PEG <i>w</i> ×100	PZA <i>w</i> ×100	PEG <i>w</i> ×100	PZA <i>w</i> ×100	PEG <i>w</i> ×100	PZA <i>w</i> ×100	
1	3.07	4.46	7.70	0.101	0.128	7.14	0.634
2	3.68	3.15	6.76	0.182	0.254	6.43	1.06
3	2.48	3.63	5.56	0.282	0.354	5.83	0.683
4	2.67	2.65	4.84	0.282	0.454	5.02	1.01
5	1.94	2.81	3.66	0.557	0.831	4.13	0.619

Turbidity method					
System	Binodal data		System	Binodal data	
	PEG <i>w</i> ×100	PZA <i>w</i> ×100		PEG <i>w</i> ×100	PZA <i>w</i> ×100
a	0.332	4.25	h	2.48	0.823
b	0.457	3.55	i	2.92	0.657
c	0.603	2.97	j	3.32	0.553
d	0.897	2.37	k	3.88	0.451
e	1.38	1.74	l	4.58	0.380
f	1.70	1.40	m	6.06	0.254
g	2.05	1.09			

^a Poly(oxyethylene) of molar mass 35000 kg mol⁻¹. ^b 9. ^c Volume ratio of top and bottom phase.



Scheme 6.2 Synthesis of cyclopolymers containing glutamic acid residues.



Scheme 6.3 Interchain H-bonding leading to increased hydrodynamic volume.

Table 6.5 Values for Parameter A^a in eqs 5 and 6 along with the rmsd^b of the Model from the Experimental Data of the Partition Coefficients

Entry	System	PZA ^c		PEG ^d	
		A_1^a	rmsd	A_2^a	rmsd
1	POE + PZA + 2.0 equiv. NaOH	-0.581	0.00587	0.537	3.28

^a A_i is the slope of the linear regression of $\ln K_i$ versus $w''_i - w'_i$, with zero intercept value (eqs 5 and 6). ^bRoot mean-square deviation. ^cPZA **9**. ^dPoly(oxyethylene) of molar mass 35.0 kg·mol⁻¹.

6.3 Results and Discussions

6.3.1 Monomers and Polymer Synthesis

Dimethyl glutamate (**6**) upon alkylation with allyl bromide afforded dimethyl *N,N*-diallylglutamate (**7**) which upon alkaline hydrolysis followed by acidification gave monomer *N,N*-diallylglutamic acid hydrochloride (**4**).²⁵ Monomer **4** underwent AIBN-initiated cyclopolymerization with SO₂ to give CPE (+) **8** which upon depletion of HCl during soaking in water was transformed to its water-insoluble zwitterionic form: PZA (±) **9** in 87% yield (Table 6.1, entry 3). Increasing concentration of the initiator increases both the yields and viscosities of the polymer. The intrinsic viscosities of water-insoluble (±) **9** was measured in 0.1 M NaCl in the presence of two equivalents of NaOH which converts it to water-soluble PDE (=) **11** and are reported in Table 6.1. An analytical sample of **11** was prepared by treating PZA **9** (Table 6.1, entry 2) with excess NaOH in 91% yield. Note that both the monomer and polymers retain the unquenched nitrogen valency as well as the two carboxyl groups of the glutamic acid.

The TGA curve of PZA **9** is shown in Figure 6.1; a minor loss of 6% up to 200 °C is attributed to the loss of trapped moisture. An accelerated loss of 24% in the range 200-250°C could be accounted by the loss of the SO₂ units; note that the calculated mass of SO₂ amounts to 22.0%. The gradual loss of 48% in the range 250-800°C may be associated with the removal of the glutamate pendant containing CO₂ units. At 800°C, remaining mass of 22% belonged to some nitrogenated organic fraction. As can be seen from the TGA plot, the polymer remained stable up to 200°C.

Attempts to determine the molar masses of polymer **11** were unsuccessful owing to the strong adsorption aided by the chelating ligands amine and carboxy of the polymer to the materials of the GPC column [117].

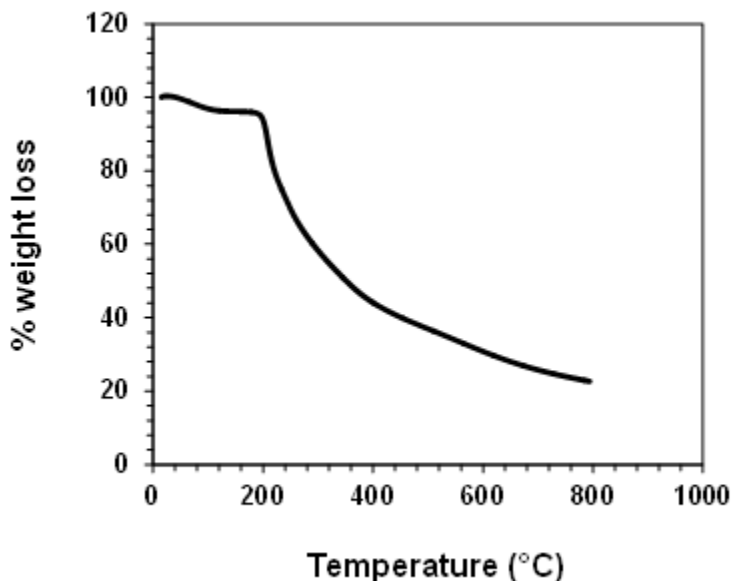


Figure 6.1 TGA curve of PZA 9 (entry 2, Table 6.1).

6.3.2 Infrared and NMR spectra

The presence of SO_2 in the backbone of polymers **9** and **11** was confirmed by the appearance of strong IR bands at ≈ 1305 and 1125 cm^{-1} assigned to its asymmetric and symmetric stretching, respectively. For the dipolar motifs [112] in (\pm) **9**, the symmetric and asymmetric vibrations of COO^- and the $\text{C}=\text{O}$ stretching of COOH were revealed at 1405, 1625 and 1724 cm^{-1} , respectively. The absorption bands at 1409 and 1579 cm^{-1} were attributed to the symmetric and asymmetric stretching of COO^- in (=) **11**, respectively.

The NMR spectra (Figs. 2 and 3) of monomer **4** and polymers **9** and **11** revealed the absence of residual double bonds in the macromolecules. The finding suggests that the chain termination happened via degradative chain transfer to the monomer [113] as well as by coupling process [114]. Integration of the relevant carbon signals revealed a 67:33 *cis/trans* ratio of the ring substituents at C_{b,b} (Scheme 6.1; Figure 6.3c) [116,152].

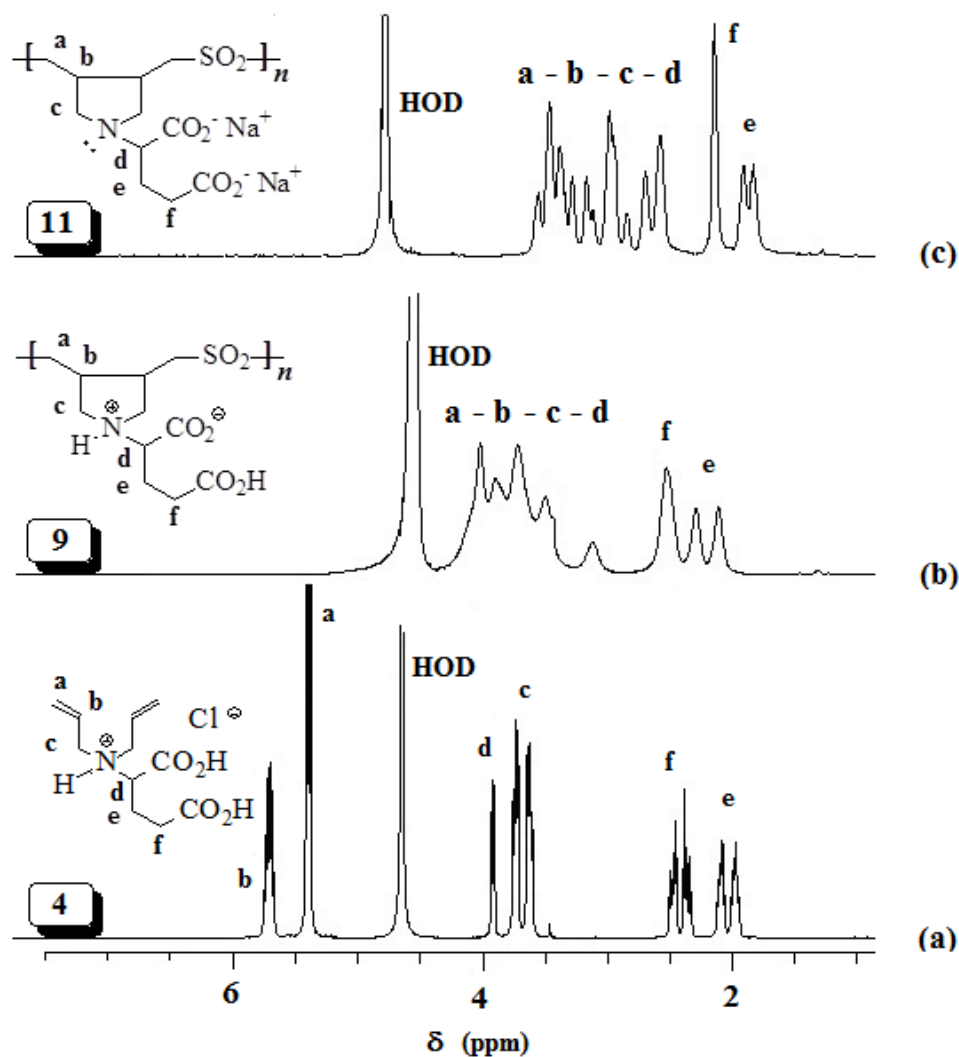


Figure 6.2 ^1H NMR spectra of (a) **4**, (b) **9** (+NaI) and (c) **11** in D_2O (referenced using signal of trimethylsilylpropionate-2,2,3,3- d_4 (TSP) at $\square\square 0$ ppm of as internal standard).

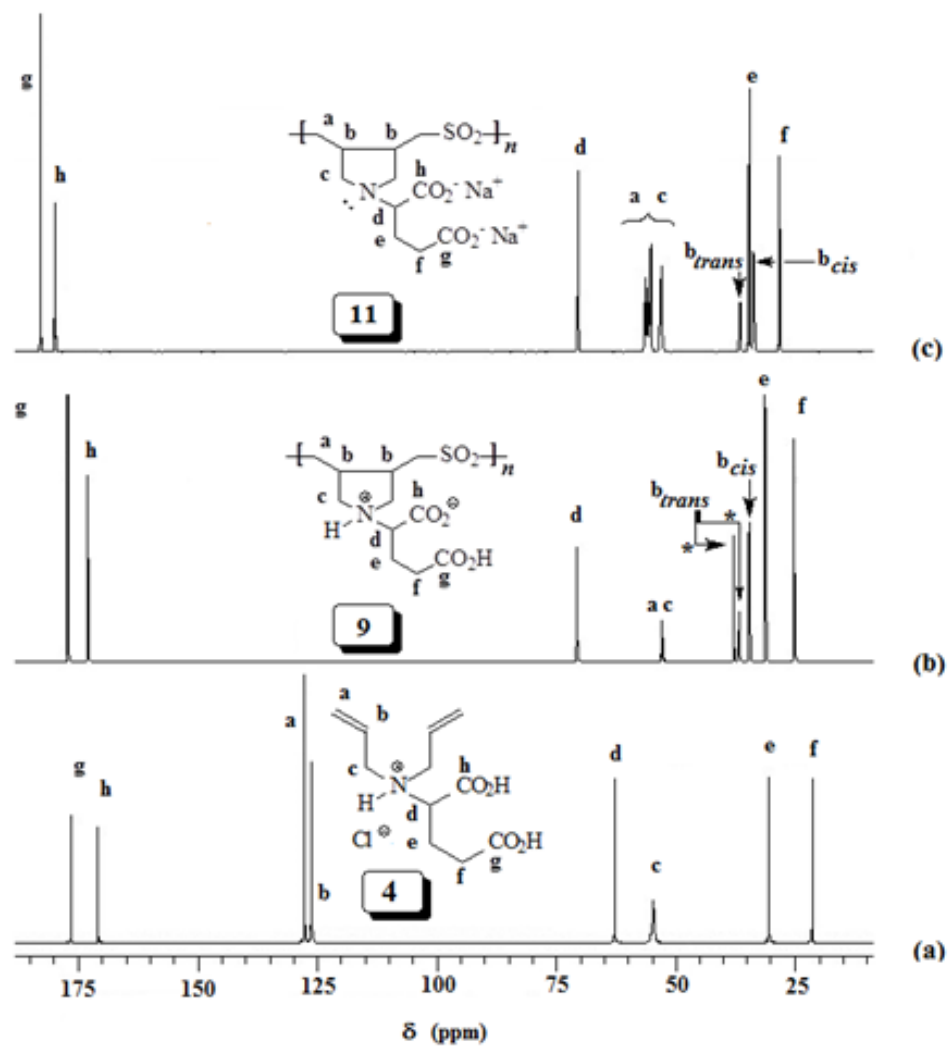


Figure 6.3 ^{13}C NMR spectra of (a) 4, (b) 9 (+NaI) and (c) 11 in D_2O (referenced using $\delta 67.4$ ppm of dioxane as external standard).

6.3.3 Solubility Behavior

Like the majority of known polyelectrolytes [74,118,119], water-insoluble (\pm) **9** becomes soluble with the addition of various salts of small molar masses. For NaBr and NaI, the CSCs at 23 °C were determined to be 2.16 and 0.581 M, respectively. Iodide ions, being the most polarizable (soft), effectively neutralize the positive nitrogens so as to disrupt the intragroup, intra- and interchain ionic crosslinks and thereby, enhance solubility in water [25]. Zwitterionic (\pm) **9** was found to be soluble in 8.59 M HCl as a result of shifting the mobile equilibrium: (\pm) **9** + H⁺ \rightleftharpoons (+) **8** toward right where the zwitterionic interactions required for water-insolubility vanishes. The presence of any concentration of NaCl was not able to disrupt the zwitterionic interactions and promote solubility of polymer (\pm) **9**. This is an interesting solubility behavior which could be exploited in the development of recyclable ATPS (*vide infra*). Polyelectrolytes PZAN **10** and PDE **11** with charge imbalances are found to be water-soluble; anionic portion in (\pm -) **10** overcomes the zwitterionic interactions so as to impart water-solubility. It has been observed during the potentiometric titrations that the polymer solutions become cloudy at pH below \approx 4.6, whereby the polymer backbone is calculated to have a (\pm) **9** / (\pm -) **10** ratio of \approx 80:20. Thus, increasing the zwitterionic portion to more than 80% leads to the polymer's insolubility in deionized water.

6.3.4 Viscosity Measurements

Figure 6.4a,b displays the viscosity plots for (\pm -) **10** and (=) **11** (derived from entry 2, Table 6.1). The viscosity plots for the polymers in deionized water were concave upwards like any polyelectrolytes (Figure 6.4a-i, ii). However, at lower concentration regime, the viscosity values fall off as a result of progressive shifting of the mobile equilibria: [(=) **11**

or $(\pm -)$ **10**] + H₂O \rightleftharpoons [($\pm -$) **10** or (\pm) **9**] + OH⁻ towards right. As per general rule of hydrolysis, the degree of transformation of **11** to **10** (or **10** to **9**) increases with decreasing concentration; overall decrease in the charge imbalance on the polymer chains decreases, thereby leading to lesser electrostatic repulsions hence lesser viscosity values.

The higher viscosity values for zwitterionic/anionic $(\pm -)$ **10** (Figure 6.4a-i) than that of its dianionic counterpart (=) **11** (Figure 6.4a-ii), as confirmed by careful triplicate measurements in deionized water under N₂, is indeed unexpected. The greater repulsion among the (-)ve charges in PDE (=) **11** having the highest degree of charge asymmetry is supposed to impart higher viscosity values. A possible rationale for the higher viscosity of $(\pm -)$ **10** could be attributed to the interchain H-bonding leading to the higher hydrodynamic volume as shown in Scheme 6.3. Note that the more distant negative oxygens of dianions (=) **11** may impart less effective repulsions. However, in 0.1 M NaCl, the interchain hydrogen bonding is discouraged because of the neutralization of the (+)ve charges in $(\pm -)$ **10** by Cl⁻ ions. The viscosity plots in 0.1 M NaCl were found to be in line with the expectation (Fig.4b- i versus ii), whereby the greater charge imbalances in (=) **11** dictating the viscosity values.

6.3.5 Basicity Constants

The pH vs. $\log [(1-\alpha)/\alpha]$ linear regression (Equation 2, Scheme 6.2) furnished the ' n_i ' as the slope and $\log K_i^o$ as the intercept. The basicity constants (K_i) of the anionic centers in the polymers **9-11** is given by Equation 3 (Scheme 6.2) where $\log K_i^o = \text{pH}$ at $\alpha = 0.5$ and $n_i = 1$ for sharp basicity constants. In deionized water, $\log K_1$ of the amine group in (=) **11**, which is the $\text{p}K_1$ of its conjugate acid $(\pm -)$ **10**, and $\log K_2$ of the terminal CO₂⁻ in $(\pm -)$ **10**

(i.e. pK_2 of its conjugate acid (\pm) **9**) were determined to be 9.33 and 5.45, respectively, in deionized water (Table 6.2). $\log K_3$ (i.e. pK_3) involving the equilibrium: **9** (ZH_2^\pm) + H^+ \rightleftharpoons (ZH_3^+) **8** cannot be determined owing to the insolubility of zwitterionic (\pm) **9** (*vide supra*).

The n_i s, which reflect a measure of polyelectrolyte effect, are found to be greater than 1 thereby indicating a gradual decrease of basicity constants (K) with increasing degree of protonation (α) (Table 6.2). The n_1 and n_2 , associated with K_1 and K_2 , respectively, were determined to be 2.07 and 1.44, thereby reflecting a greater polyelectrolyte effect i.e. greater changes in K_1 values during the transformation of (=) **11** to (\pm -) **10**. In deionized water, charge centers in (=) **11** are expected to be more hydrated than in (\pm -) **10**. The higher values of $\log K_1$ and n_1 than $\log K_2$ and n_2 , respectively, are the consequences of the entropy driven protonation step [126]. During protonation, a repeating unit (RU) of (=) **11** would lose greater number of hydrated water molecules than that of (\pm -) **10**. Note that polyzwitterion (\pm) **9**, being the most packed and least hydrated as confirmed by its insolubility in water. As a consequence, during protonation of (=) **11** and (\pm -) **10**, the respective polymer backbones would consist of (=) **11**/ $(\pm$ -) **10** and (\pm -) **10**/ $(\pm$ -) **9** with the former having greater number of water molecules in the hydration shell of each RU. The variations of $\log K_i$ s with α , shown in Figure 6.4c, reflect their “apparent” [125] nature since instead of remaining constant, they decrease with the increase in α . In both cases of protonation, the exothermic enthalpy changes (ΔH^o s) remain constant with increasing α , and the ΔG^o s become less negative as a result of progressive decrease in the (+)ve ΔS^o s. With each protonation, the (-)ve charge density and the hydrated water molecules per RU decrease; as a consequence, a RU being protonated releases less water molecules from its hydration shell than that of the unit protonated in the previous step

[196]. In other words, the continuous decrease of positive ΔS° with α leads to lesser negative ΔG° s, hence a gradual decrease in $\log K$ values.

6.3.6 Viscometric Titrations

The viscosity data of a 0.00858 M (i.e. 0.25 g dL⁻¹) PZA **9** in deionized water in the presence of various concentration of added NaOH at 23 °C is reported using a solid line in Figure 6.4d. The pH values and basicity constants (*vide supra*) were used to construct the distribution curves (dashed lines) of the specie ZH₂[±] (PZA **9**), ZH[±] (PZAN **10**), and Z⁻ (PDE **11**). The reduced viscosity, as expected, increases with the addition upto 1 equivalent of NaOH as a consequence of the transformation of ZH₂[±] to ZH[±]. Maximum viscosity is achieved after the addition of 1 equivalent of NaOH whereby the concentration of ZH₂[±] and ZH[±] reaches the minimum and maximum values, respectively. Further addition of NaOH, which initiates the transformation of ZH[±] to Z⁻, led to a gradual decrease in the reduced viscosities accompanied by an increase in the concentration of the ionic species Z⁻. This unusual viscosity behavior of dianionic **11** (Z⁻) having lower viscosity than its zwitterionic-anionic counterpart **10** (ZH[±]) has also been observed in Figure 6.4a and a rationale for the finding is given (*vide supra*).

6.3.7 Scale inhibition by the synthesized polymer

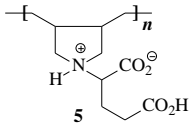
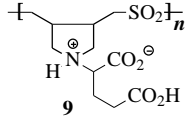
Scaling of inorganic salts like CaSO₄ and CaCO₃ in reverse Osmosis (RO) process damages membranes, thereby impeding their smooth functioning. Excessive presence of the relevant ions in the reject brine leads to their supersaturation and scaling. The percent scale inhibition (PSI) is calculated using Equation 4:

$$\% \text{ Scale Inhibition} = \frac{[Ca^{2+}]_{inhibited(t)} - [Ca^{2+}]_{blank(t)}}{[Ca^{2+}]_{inhibited(t_0)} - [Ca^{2+}]_{blank(t)}} \times 100 \quad (4)$$

where $[Ca^{2+}]$ represents the concentrations in the presence and absence of antiscalant **9** at time zero (t_0) and t .

In the current work, a supersaturated solutions of $CaSO_4$ containing Ca^{2+} (2600 ppm) and SO_4^{2-} (6300 ppm) of in the presence of 0 (blank), 5, 10, 20, and 30 ppm of **9** as an antiscalant were examined by following the conductivity of the solutions versus time. The results of the investigation are given in Table 6.3. In the absence of **9**, a sudden drop in conductivity indicates the precipitation of $CaSO_4$ (Figure 6.5-iv: Blank). To our satisfaction, the presence of **9** at a concentration of 30 ppm imparted a 99% scale inhibition for about 1000 min, while it was 100% at the time of 500 min as calculated using Equation 4 using conductivity values as proportional to the ionic concentrations. Note that the presence of 5, 10, 20, and 30 ppm of the antiscalant was able to register PSI of 94, 98, 99, and 100 %, respectively, at a time of 30 min. These are indeed efficient PSI values since the feed water usually resides for ≈ 30 min. in the osmosis chamber. The time, at which a sharp drop in conductivity happens, signaling the onset of quick precipitation, is known as an induction period (IP). The IPs of 60, 90 and 600 min were observed in the presence of 5, 10 and 20 ppm of **9**, respectively. Note that at the concentration of 30 ppm and the time scale of 1000 min, no induction period was observed; it imparted 99% inhibition. The new antiscalant has demonstrated its efficacy in scavenging metal ions and disrupting the nucleation and crystallization processes [128,198], hence it could be used as a potential antiscalant to minimize membrane fouling by $CaSO_4$ scale.

Table 6.6 Basicity constants K_i and scale efficiency of inhibition of homo- and co-polymer

Polymer	$pK_{NH^+}^a$	$pK_{CO_2H}^a$	$[\eta]^b$ (dL/g)	Scale Inhibition ^c (%)	CSC ^d			
	or $\log K_1$	or $\log K_2$			NaCl (M)	NaBr (M)	NaI (M)	HCl (M)
 5	10.9	5.25	0.160	100	0.548	0.271	0.133	0.0104
 9	9.93	5.45	1.03	77	Insolu- -ble ^e	2.16	0.581	8.59

^a In salt-free water at 23 °C.

^b Intrinsic viscosity of 1-0.0625% polymer **6** (Reference?) and **9** (Table 1, entry 2) treated with 2 equivalents NaOH in 0.1 M NaCl at 30 °C was measured with an Ubbelohde Viscometer ($K=0.005317 \text{ mm}^2/\text{s}^2$).

^c After 500 min using 20 ppm polymer in a supersaturated solution of CaSO_4 (aq) at 40 °C.

^d Critical salt concentration required to promote solubility at 23 °C.

^e Insoluble in the presence of any concentration of NaCl.

6.3.8 Phase diagrams: [PZA **9** + 2 equivs. NaOH] – PEG – H₂O (0.6 M NaCl)

The polymer compositions in the phases, determined by ¹H NMR spectroscopy, were used to construct the tie-lines in the phase diagram (Table 6.4). A small portion of each phase

was taken, and after exchanging H₂O with D₂O the NMR spectra were recorded in the presence of K₂CO₃ which helped to minimize the overlap of PEG signal at δ 3.65 with the signals of PDE **11** (i.e. **9** + 2 equivs. NaOH). The proton spectrum of the bottom phase (system 1, Table 6.4) is displayed in Figure 6.6a; the four Hs marked **e,f** of PDE **11** appeared in the range δ 1.6-2.2 ppm having an area integration of **A**, while the remaining eleven protons marked **a-d** in the range δ 2.4-3.6 ppm integrated for an area of **B**. The mole ratios of the polymers **11/PEG** was determined as **A/C** where **C** is the area of the four-proton signals for PEG at δ 3.65 ppm. For the top phase (Figure 6.6b), where the excessive presence of PEG led to overlapping of its signal with that of PDE **11**, mole ratio of **11/PEG** was calculated as $[(\mathbf{A}+\mathbf{C})-(11\times\mathbf{B}/4)]/\mathbf{B}$, where (A+C) accounts for the combined areas of four-proton PEG and eleven-proton PDE **11** while **C** is equated to $(11\times\mathbf{B}/4)$. The respective molar masses of 291.3 and 44.05 g mol⁻¹ for each RU of **9** and PEG were used for calculation of the weight fractions (*w*) which were used to construct the tie lines as described [195] (Figure 6.7a).

The binodal, constructed using turbidity method, is shown in Figure 6.7a. The tie lines are drawn by connecting A_{total} , A_{top} and A_{bottom} which represents the composition of the total system, PEG-rich top phase and PZA-rich bottom phases, respectively. The ratio of the length of the tie-line segments $(A_{\text{total}}-A_{\text{bot}})/(A_{\text{total}}-A_{\text{top}})$ is equated to $V_{\text{top}}/V_{\text{bottom}}$ where *V* represents the volume of the phases [138]. The composition on a tie-line therefore determines the ratio of the phase volumes.

A single- and two-phase region is demarcated by a binodal curve whose position with respect to the axes determines the economic viability for industrial application. As shown in Figure 6.7a, the binodal for the ATPS is very much closer to the axes requiring only a

total polymer concentrations of $\approx 5\%$ for the separation of the phases. The most beneficial aspect of the environmentally friendly ATPS is the solubility of PDE (\rightleftharpoons) **11** at a higher pH, while it can be recycled [138] at acidic pH by precipitating it in the form of (\pm) **9**. The current ionic ATPS containing the polymer component having pH-triggerable functionalities (N and CO_2^-) of glutamic acid is anticipated to have pH responsive behavior that would impart selectivity in bioseparation.

6.3.9 Correlation of the Phase Diagram

Diamond and Hsu [130] developed Eqs. (5) and (6) based on Florey-Huggins theory to check the consistency of the tie-lines.

$$\ln K_1 = A_1 (w''_1 - w'_1) \quad (5)$$

and

$$\ln K_2 = A_2 (w''_2 - w'_2) \quad (6)$$

where w'' and w' represent the wt% of polymer 1 (PZA **9** + NaOH) and polymer 2 (PEG), in the respective top and bottom phase. The $\ln K - (w''_i - w'_i)$ plots with zero intercept gave the slopes A_1 and A_2 which reflect the effects of molar mass of the polymers and their interactions with water. The partition coefficients K_1 and K_2 of polymer 1 and polymer 2 were determined by their concentration ratio (C_t/C_b) in the top and bottom layer. The straight-line fits in Figure 6.7b certifies the ability of the model to describe the phase behavior. Eq. (7) [131] describes the relationship between the root mean-square deviation (rmsd) with the K_{exp} and K_{cal} :

$$\text{rmsd} = \sqrt{\frac{\sum_{i=1}^N (K_{\text{exp}} - K_{\text{calc}})_i^2}{N-1}} \quad (7)$$

where N represent the number of tie lines (Figure 6.7a). The values of the parameters A_i and $(\text{rmsd})_i$ in Table 6.5 ascertain the usefulness of Equations in correlating the experimental data. In this model, an extensive phase equilibrium determination is avoided, since a single phase composition would suffice to determine A_1 and A_2 .

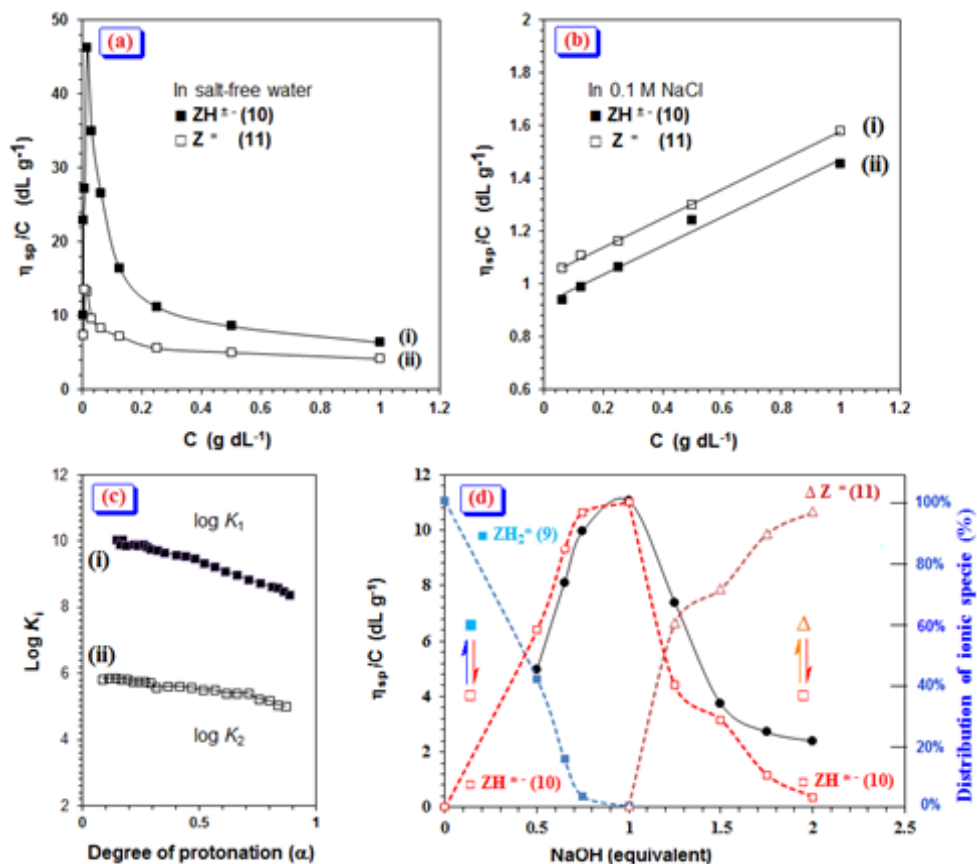


Figure 6.4 (a) The viscosity behavior of sample derived entry 2, Table 1 Utilizing a viscometer, 30 °C: (i) \blacksquare ($\pm -$) 10 and (ii) \square ($=$) 11 in deionized water; (b) (i) \square ($=$) 11 and (ii) \blacksquare ($\pm -$) 10 in 0.1 M NaCl; (c) Plot for the apparent (i) $\log K_1$ versus degree of protonation (α) (entry 3, Table 2) and (ii) $\log K_2$ versus α for PDA 11 (derived from entry 2, Table 1) in deionized water (entry 3, Table 2); (d) Reduced viscosity (η_{sp}/C) at 30 °C of a 0.00858 M (i.e. 0.25 g/dL) solution of polymer PZA 9 (ZH_2^{\pm}) in deionized water (\bullet) versus equivalent of added NaOH. Distribution curves (dashed lines) of the various ionized species [\blacksquare 9 (ZH_2^{\pm}), \square 10 ($\text{ZH}^{\pm-}$), Δ 11 (Z^-)] calculated using eq 2 (Scheme 2) and pH of the solutions in deionized water at 23°C.

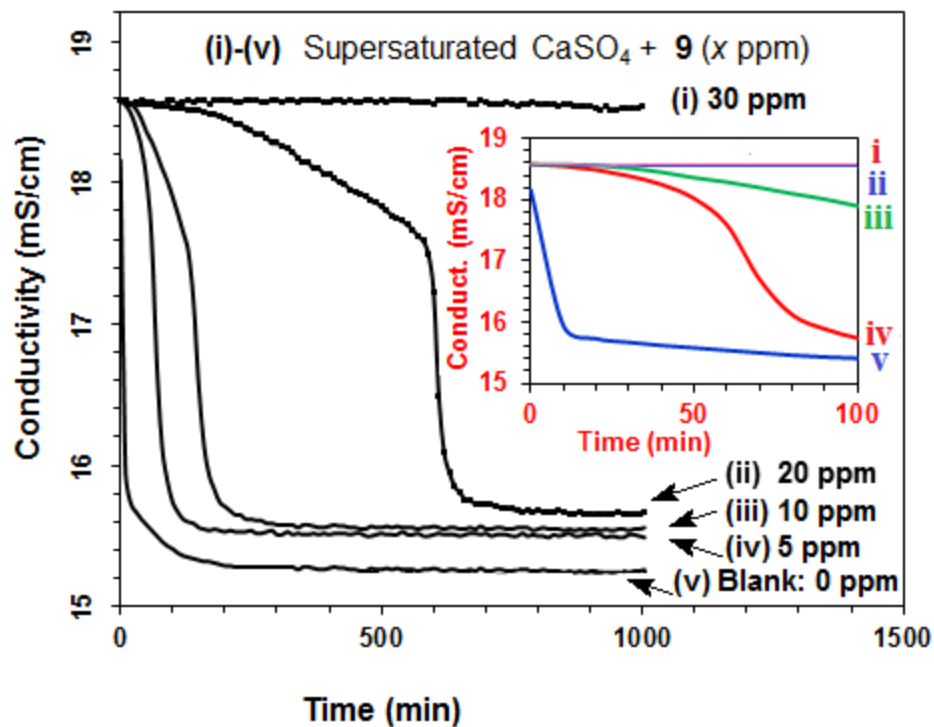


Figure 6.5 Trends in precipitation of a supersaturated solution of CaSO_4 with addition (5, 10, 15, 30 ppm) and absence of PZA 9 (treated with NaHCO_3). Inset showing the precipitation behavior in a shorter time scale of 100 min.

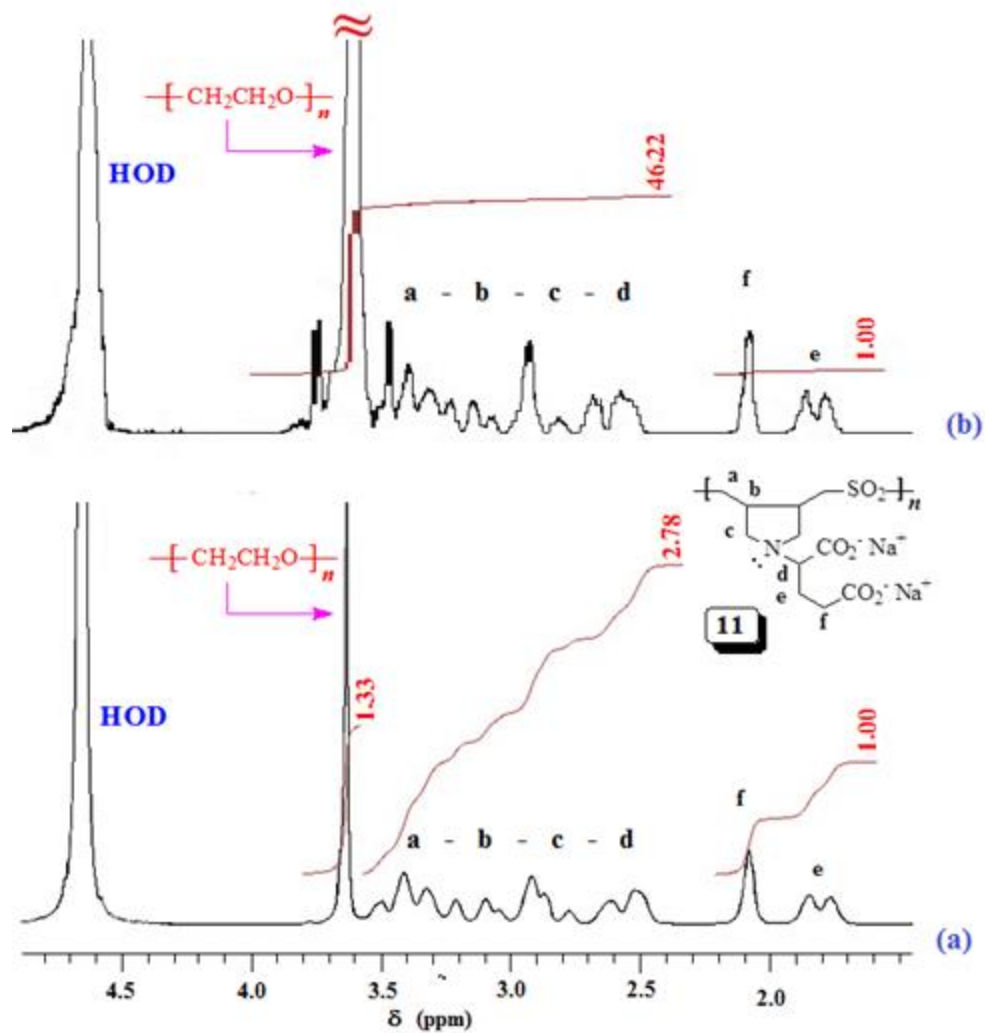


Figure 6.6 ^1H NMR spectrum of (a) bottom layer and (b) top layer of (System 5, Table 4) in D_2O (+ K_2CO_3).

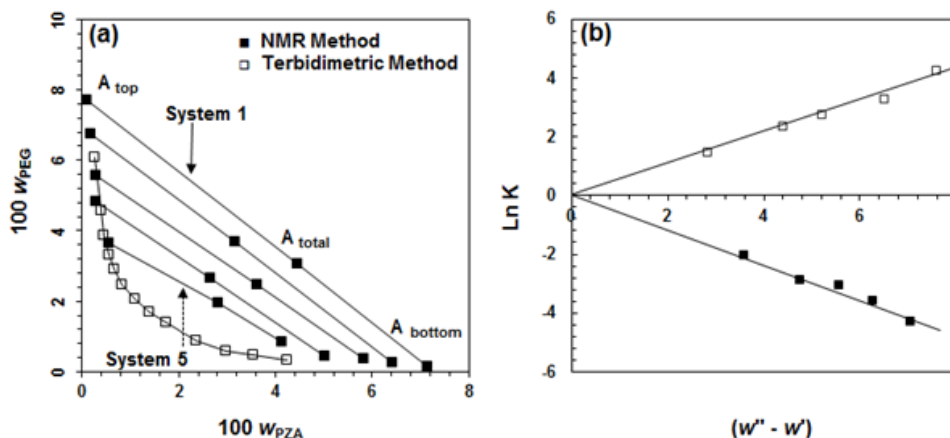


Figure 6.7 (a) Phase diagram [■ and □ represent data obtained by respective NMR and turbidimetric method] at 296 K of 0.6 M NaCl containing PZA 9 (treated with 2 equiv. NaOH)-PEG at 296 K; (b) Correlation of phase diagram of PZA 9 (2 equiv. NaOH)-PEg-H₂O (0.6 M NaCl).

6.3.10 A comparison of homopolymer 5 and copolymer 9:

Several properties of poly(diallylglutamic acid) (**5**) and copolymer poly(diallylglutamic acid-*alt*-SO₂) (**9**) are compared in Table 6.6. The lower basicity constant K_1 of the copolymer **11** is attributed to the electron-withdrawing ability of the SO₂ in its RU. Since $\log K_1 = pK_{NH^+}$, the conjugate acid **10** has thus greater acidity than that of the corresponding homopolymer. Copolymer **11** is found to have much higher intrinsic viscosity (1.03 dL g⁻¹) than its corresponding homopolymer (0.160 dL g⁻¹) (Table 6.6). Homopolymer **5** is found to be a more effective antiscalant than copolymer **9**; in the presence of 20 ppm each of **5** and **9**, the scale inhibition was found to be 100 and 77%, respectively, after the elapse of 500 min. The better performance of the homopolymer **5** may be attributed to its lower molar mass; polymer with a smaller size may interfere more severely with the growth of scale by efficient poisoning of its active sites [89].

The solubility of the polymers differs greatly; the copolymer with much higher CSC values demonstrated stronger zwitterionic interactions (Table 6.6). The greater dispersion of the positive charges in the zwitterionic dipoles of **9** by electron-withdrawing SO₂ makes it less hydrated and thus more attracted to the negative end of the dipole. The solubility behavior of polymer **9** makes it an attractive component in a pH-controlled recyclable ATPS.

6.4 Conclusions

Monomer **4** containing residues of glutamic acid and SO₂ on alternate cyclopolymerization afforded CPE **8** [(i.e. poly(**4**-alt-SO₂))] in excellent yields. CPE **8** on depletion of HCl during dialysis gave water-insoluble PZA **9** whose solubility is promoted by the addition of NaI, NaBr and HCl. PZA (\pm) **9** upon neutralization with 1 and 2 equivalents of NaOH was converted to water-soluble (\pm -) **10** and (=) **11**, which has been used in developing an environmentally friendly recyclable ATPS. The basicity constants K_i for the ligand centres in PDE (=) **11** have been determined. The polymer has demonstrated antiscalant properties and imparted excellent CaSO₄-scale inhibition.

CHAPTER 7

Synthesis and Application of Glutamic Acid-based Resin

Abstract

Inexpensive biogenic glutamic acid has been utilized to synthesize a cross-linked dianionic polyelectrolyte (CDAP) containing metal chelating ligands. Cycloterpolymerization, using azoisobutyronitrile as an initiator, of *N,N*-diallylglutamic acid hydrochloride, sulfur dioxide and a cross-linker afforded a pH-triggerable cross-linked polyzwitterionic acid (CPZA) which upon basification with NaOH was converted into CDAP. The new resin, characterized by a multitude of spectroscopic techniques as well as Scanning Electron Microscopy (SEM) and Brunauer–Emmett–Teller (BET) analyses, was evaluated for the removal of Co(II) as a model case under different conditions. The adsorption capacity of 137 mg g⁻¹ does indeed make the resin as one of the most effective sorbents in recent times. The resin leverages its cheap natural source and ease of regeneration in combination with its high and fast uptake capacities to offer a great promise for wastewater treatment. The resin has demonstrated remarkable efficiency in removing toxic metal ions including arsenic from a wastewater sample.

7.1 Introduction

Water pollution is gaining increasing international awareness since industries are on the upward growth and oftentimes wastes are discharged to the environment without sufficient

precautions. Sources such as mining, metal plating, battery, and paper industries are responsible for introducing these discharges into the environment [212]. Several ions of the heavy metals are not only toxic to living organisms in water but also, cause harmful effects to terrestrial animals. Cobalt is among the common toxic metals that are used extensively in various human endeavors [213]. Excessive levels of cobalt in the body lead to cobalt poisoning; however, in minute amounts, it is an essential component of Vitamin B₁₂ which is needed for the smooth functioning of many important body processes and it is depleted only during pernicious anemia [214]. Chronic exposure to cobalt has numerous deleterious effects on human health [215,216]. Low levels of cobalt exposure have been reported to impact lung function, induce occupational asthma [217,218], vision and hearing problems, especially in patients with hip implants containing cobalt [219,220]. Very recently, the US department of health and human services in its 14th report on carcinogens has classified cobalt and cobalt compounds that release cobalt ions in Vivo as reasonably anticipated to be a human carcinogen [221].

Although different treatment techniques such as precipitation, membrane technology, ion-exchange, electrocoagulation have been reported [222,223] to remove effluents in aqueous media, adsorption [224,225] seems to have a greater potential for such application. Since the adsorption performance is limited by material design and properties, strong efforts have been made in exploring the structural properties of various materials. The use of inorganic materials in combination with polymer hybrid materials for adsorption has been considered as promising, as it is effective, economical as well as environmentally friendly in removing pollutants from the water [226,227].

A recent review described polyglutamic acid (PGA) as an emerging biopolymer of commercial interest because of its prospective wide applications in healthcare, foods and pharmaceuticals [228]. In wastewater treatments, PGA and other poly-amino acids have demonstrated incredible potentials in removing toxic metal ions [229–232]. Poly amino acids remove toxic metal ions through chelation and electrostatic binding [233]. The electrostatic binding of heavy metals by PGA has also been explored for possible treatment of metal intoxication in humans [234,235]. Other researchers have also shown the capability of PGA as a sorbent for removing cationic dyes from waste water [236] thus demonstrating its versatility in removing both inorganic and organic pollutants, especially from aqueous media.

In PGA, two of the three functionalities of the amino acid are involved in the formation of peptide (i.e. amide) bonds thereby keeping only the side chain carboxylate for the purpose of metal exchange. It is our objective to exploit the cheap natural source of the biogenic amino acid and its three metal chelating functional motifs to design and synthesize a polymeric material keeping intact the integrity of all three original chelating functionalities of glutamic acid. This work thus reports the synthesis of such a new glutamic acid-based resin as a sorbent for sequestering Co(II) as a model case from aqueous solution using sorption kinetics and several isotherm models.

7.2 Experimental

7.2.1 Chemical and Materials

L-Glutamic acid, piperazine, allyl chloride, obtained from Fluka Chemie AG, were used as received. Azobisisobutyronitrile (AIBN, Fluka AG) was crystallized from chloroform–ethanol. Dimethylsulfoxide (DMSO) was dried using calcium hydride and then distilled under reduced pressure (64–65°C, 4 mm Hg). Cobalt(II) chloride hexahydrate ($\text{CoCl}_2 \cdot 6\text{H}_2\text{O}$, Fluka AG) was used to prepare the standard which was subsequently diluted to the required concentrations. Sodium hydroxide and nitric acid were purchased from Sigma–Aldrich. Millipore water (18.2 $\text{M}\Omega \cdot \text{cm}$) was used for the adsorption study. For the real wastewater study, the industrial wastewater was collected from an industrial area in Dammam KSA, then, it was filtered to remove the large particles and soils. The pH of the industrial wastewater was determined to be 6.3. The industrial wastewater was spiked with 20 mg/L Co(II) in order to test the performance and efficiency of the analytical method in the real wastewater matrix.

7.2.2 Physical Methods

A Perkin–Elmer 16F PC FTIR spectrometer was utilized to record IR spectra. The proton and carbon-13 spectra were recorded on a JEOL LA 500 MHz spectrometer using HOD signal at 84.65 ppm and dioxane signal at 67.4 ppm as internal and external standards, respectively. The resin surface morphology before and after the cobalt(II) adsorption was examined by Field emission scanning electron microscope (FESEM) and their elemental analyses were determined using Energy-dispersive X-ray spectroscopy (EDX) fitted with a detector model X-Max. A Perkin Elmer 2400 Series II CHNS/O Elemental Analyzer was

used to carry out the elemental analysis. The concentration of Co(II) was monitored using a flames atomic absorption spectrometer (FAAS) (Thermo scientific iCE 3000). TGA was conducted in a thermal analyzer (SDT Q600 from TA instruments, USA). The temperature was raised at a rate of 10°C/min with air flowing at a rate of 100 mL/min. The methods of Brunauer-Emmett-Teller (BET) and Barrett-Joyner-Halenda (BJH) were adopted to determine the resin surface area and its pore size distribution, respectively.

7.2.3 Synthesis of the starting materials

Glutamic acid-derived monomer **1** was prepared as described [209]. The preparation of cross-linker **2** is described elsewhere [82].

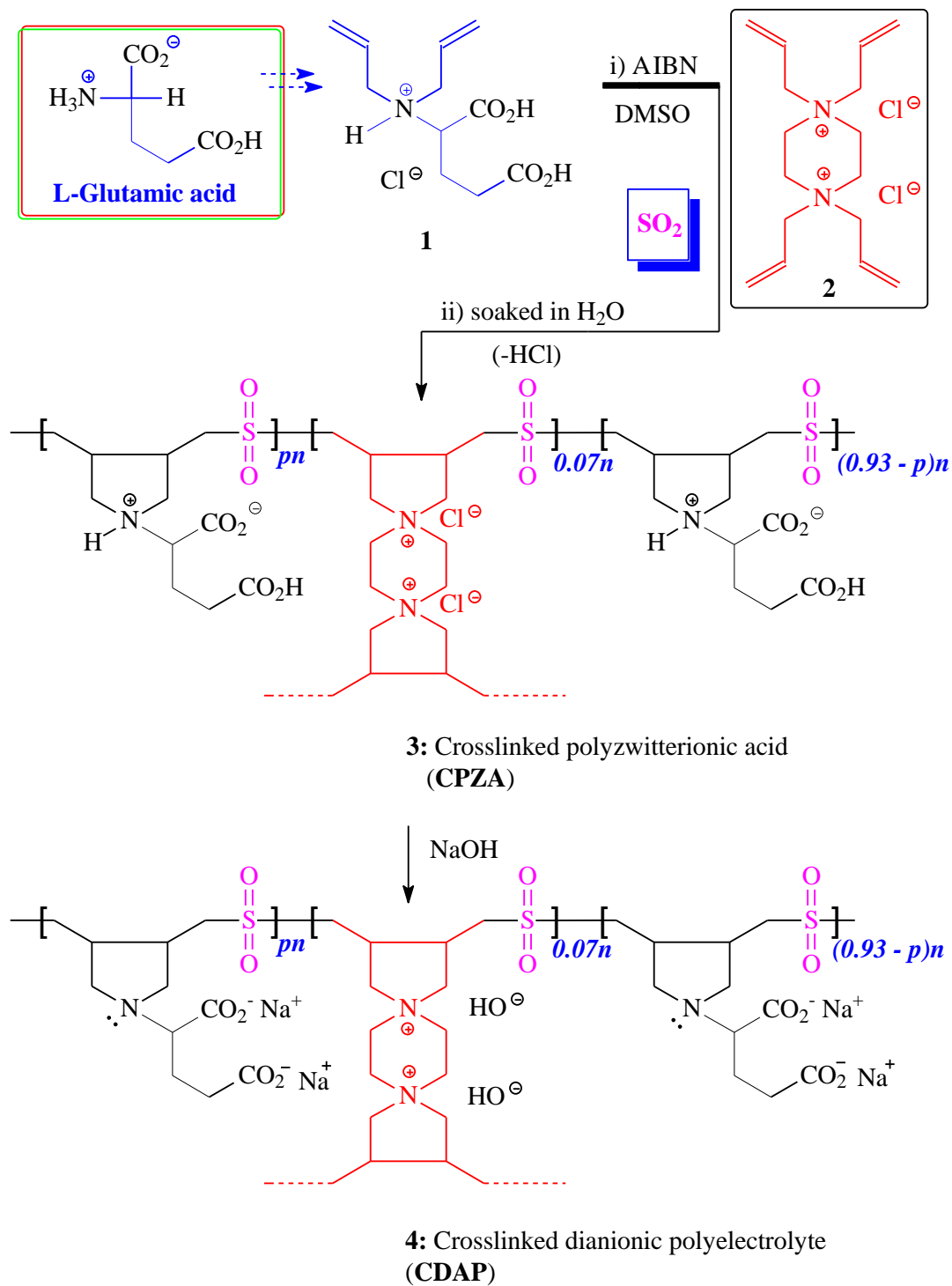
a. Polymerization process

Sulfur dioxide (2.12 g, 34.5 mmol) was absorbed onto a solution of cross-linker **2** (0.721 g, 2.26 mmol) and monomer **1** (7.91 g, 30 mmol) in DMSO (11.3 g) in a Round bottom flask (50 mL). After adding the initiator AIBN (160 mg), the reaction mixture under N₂ was stirred at 60 °C for 48 h. The resultant cross-linked polyzwitterionic acid (CPZA) **3** was soaked in excess water for 24 h, filtered and vacuum-dried at 60 °C to a constant weight (8.94 g, 83%). (Found: C, 44.8; H, 6.1; N, 4.8; S, 10.9%). A terpolymer from monomer **1** (- HCl) (93 mol%), cross-linker **2** (7 mol%) and SO₂ (107 mol %; each cross-linker is expected to react with 2 equivalents of SO₂) requires C, 45.18; H, 5.91; N, 4.91; S, 11.24).

b. Conversion of CPZA **3** to cross-linked dianionic polyelectrolyte (CDAP) **4**

CPZA **3** (8.46 g, 28.2 mmol) in water (150 cm³) was treated with NaOH (1.7 g, 42.5 mmol) at 20 °C for 1 h. A second portion of NaOH (1.7 g, 42.5 mmol) was added, and the mixture was stirred for an additional hour. The resultant resin **4** was filtered and washed

with water and acetone and vacuum-dried at 60°C (9.2 g, 96%). (Found: C, 39.5; H, 4.9; N, 4.2; S, 9.6%). The resin containing the units derived from monomer **1** (93 mol%) and monomer **2** (7 mol%) and SO₂ (107 mol%) requires C, 39.93; H, 4.71; N, 4.36; S, 9.98).



Scheme 7.1 Synthesis of pH-triggerable resin

7.2.4 Co(II) adsorption on CDAP resin

Adsorbent CDAP 4 (30 mg) was added into an aqueous Co(II) solution (20 mL) of specific concentration of 20 or 30 or 50 or 100 mg L⁻¹ and then stirred for a period of 10, 20, 30, 60, 90 and 120 min at 298 K. The filtrate after each time interval was analyzed by AAS to determine the Co(II) uptake. Using an initial Co(II) concentration of 50 mg L⁻¹, the pH dependency of the adsorption process was evaluated at 298 K, while the experiments at 298, 318 and 338 K were performed to determine the kinetic and thermodynamic parameters. The percentage removal of Co(II) is computed using equations 1 and 2:

$$q_t = \frac{(C_i - C_t)V}{W} \quad (1)$$

$$\%Co^{2+} uptake = \left(\frac{C_i - C_t}{C_i} \right) \times 100 \quad (2)$$

where, C_i and C_t represent the initial and final Co(II) concentrations (mg L⁻¹), respectively; V and W denote the solution volume (L) and weight of the resin (g). The adsorption capacity at various times and equilibrium are denoted as q_t and q_e , respectively, where in the case of q_e , the equilibrium concentration C_e is used instead of C_t . The experiments were run in duplicate and each analysis were triplicated. The average value was reported.

7.2.5 Regeneration experiment

Adsorption experiments were carried out by agitating the resin in 50 mg L⁻¹ Co(II) solution for 120 min at the adsorbent dose of 1.5 g L⁻¹. As described above, the amount of Co(II) uptake was determined and the filtered loaded resin (after drying at 60 °C with vacuum) was immersed in a stirring 0.5 M HNO₃ solution for 120 min while keeping

constant the amount of the resin at 1.5 g L^{-1} for the desorption experiment. The amount of desorbed Co(II) was measured in the same manner as the adsorption. The adsorption and desorption procedure was repeated several times.

7.2.6 FTIR spectra

FTIR spectra of the loaded and unloaded resins were recorded. The loaded resin was prepared by immersing the pure resin (60 mg) in 50 mg L^{-1} Co(II) solution (40 mL) for 2 h at a pH of 6.0. It was then filtered and vacuum-dried at $60 \text{ }^{\circ}\text{C}$.

7.3 Results and discussion

7.3.1 Resin synthesis

A solution of glutamic acid-based monomer **1**, piperazine-based cross-linker **2** and SO_2 in DMSO was subjected to undergo cyclopolymerization reaction [24,69,153,237] to generate CPZA **3**, which upon neutralization with NaOH was converted to CDAP **4** in excellent yield (Scheme 7.1). Resin **4** keeps intact all three original functionalities of glutamic acid and as such it can provide a multiple of chelating motifs of unquenched nitrogen valence and carboxylates having differing basicity constants to impound toxic metal ions from contaminated sources.

7.3.2 Characterization of the resins by FT-IR

From the high-frequency end of the IR spectrum of CPZA **3**, is a broad band which centers around 3552 cm^{-1} . It is attributable to the N–H and O–H bands. The IR spectrum of **3** also shows strong bands at 1726 and 1624 cm^{-1} assigned to the unsymmetrical and symmetrical stretching vibrations of $\text{CO}_2^-/\text{COOH}$ groups [137] (Figure 7.1a). Associated with these bands are the moderate C–O–H bending at 1451 cm^{-1} and 1397 cm^{-1} . Absorption

peaks at 1306 and 1127 cm^{-1} were assigned to the unsymmetrical and symmetrical vibrations of sulfone (SO_2) motifs in CPZA **3** [238]. In the unloaded CDAP **4**, the mix N–H and O–H bands at 3552 cm^{-1} are lost because of loss of protons, and the two C=O stretching vibrations collapse into bands at 1573 cm^{-1} and 1408 cm^{-1} for the respective unsymmetrical and symmetrical vibrations of $-\text{COO}^-$ (Figure 7.1b). The SO_2 bands show a slight improvement in intensity. After Co(II) adsorption (Figure 7.1c), the N–H and O–H bands re-emerge at 3427 cm^{-1} , C=O stretching vibrations separate out at 1625 cm^{-1} and 1581 cm^{-1} with improved intensity and the SO_2 bands appear at 1302 cm^{-1} and 1124 cm^{-1} also with improved intensity. The reappearance of these bands at slightly different frequencies after adsorption with Co(II) confirms the bonding interactions of these functional groups with the metal ions. Also, the splitting of the carboxylate bands after Co(II) adsorption suggests the participation of two non-equivalent C=O groups as denoted in Scheme 7.1. Comparison of the IR spectra of both original and used CDAP resins with regenerated resin after three cycles of usage show that the regenerated resin has very similar IR profile as the original resin (Fig. 7.2).

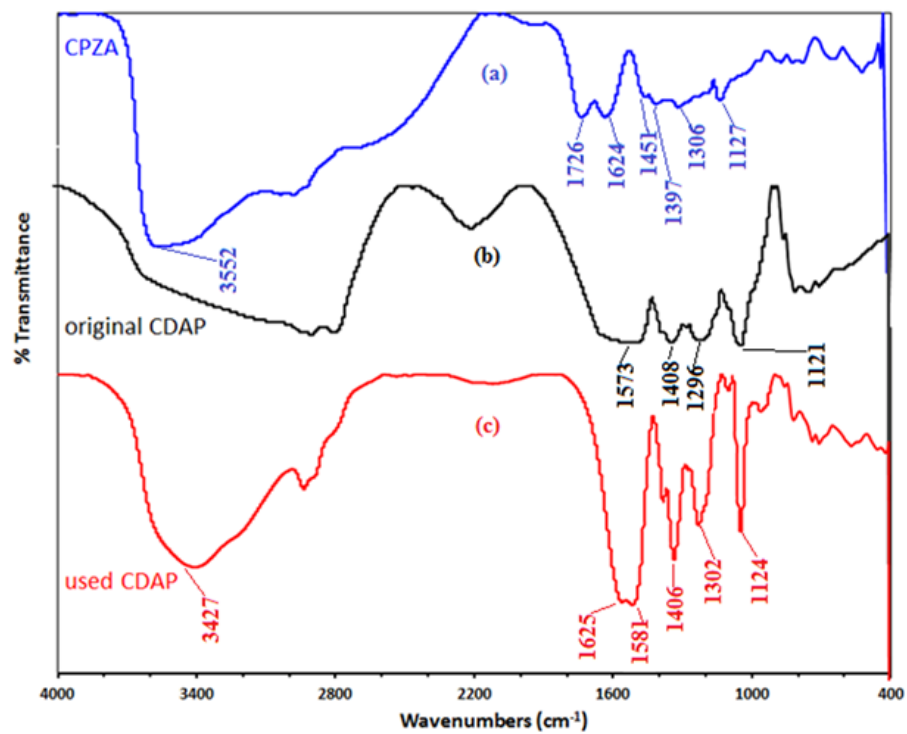


Figure 7.1 IR Spectra of (a) 3 (b) unloaded 4 and (c) Co(II) loaded 4

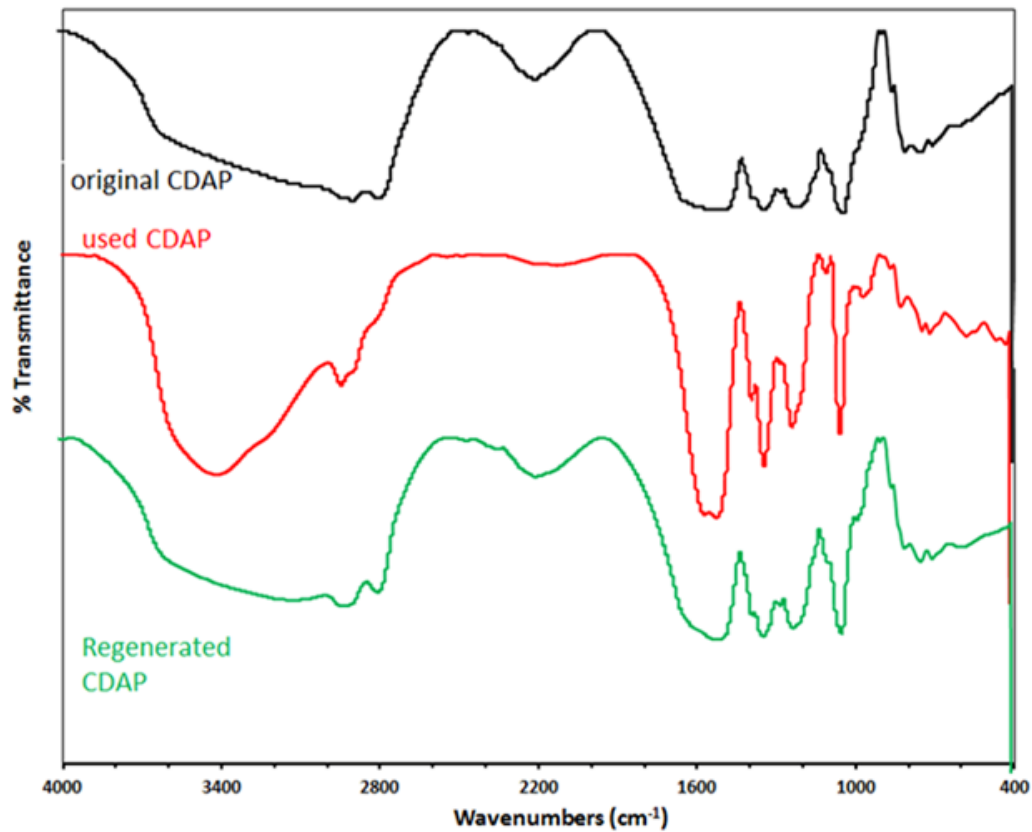


Figure 7.2 IR Spectra of cross-linked resins (a) original (b) used and (c) regenerated CDAP 4

7.3.3 Thermo-gravimetric analysis (TGA)

The TGA curve of CDAP **4** is shown in Figure 7.3. The first weight loss of 11% up to 230 °C is accounted for the removal of moisture and trapped water. The second slow and prolong loss of about 47% in the range 230-700°C is attributed to the loss of SO₂ and CO₂ owing to polymer degradation. The third loss of 20% in the range 700-730°C is attributed to the release of NO_x, CO₂, and H₂O gasses [210]. At 730°C, the residual mass was found to be 22%. Comparison of the TGA profiles of original, used and regenerated resin has shown that the regenerated resin retained the thermal property of the original resin after three cycles of usage (Fig. 7.4).

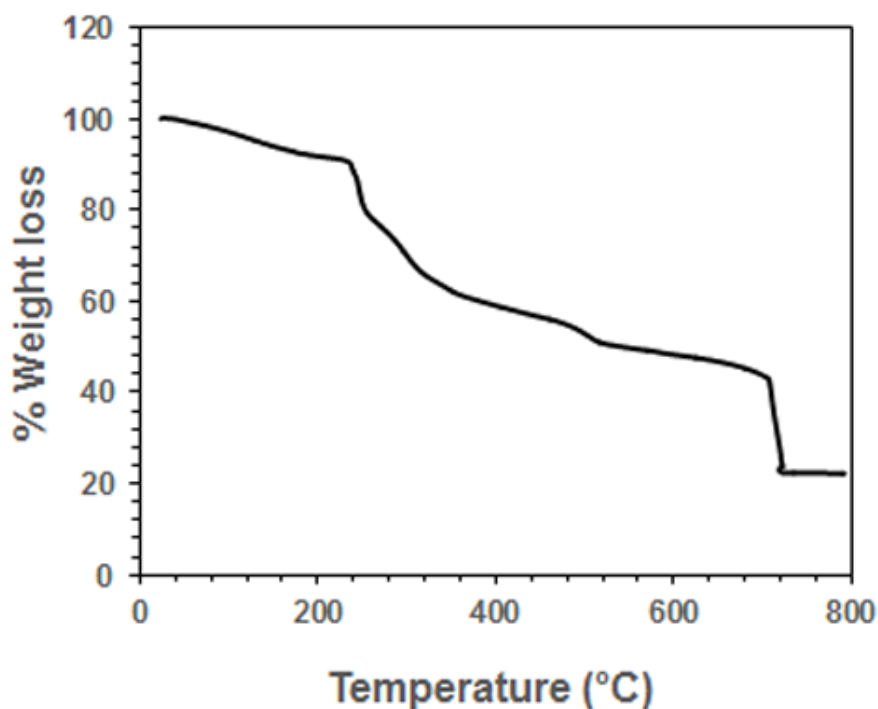


Figure 7.3 TGA curve of resin 4

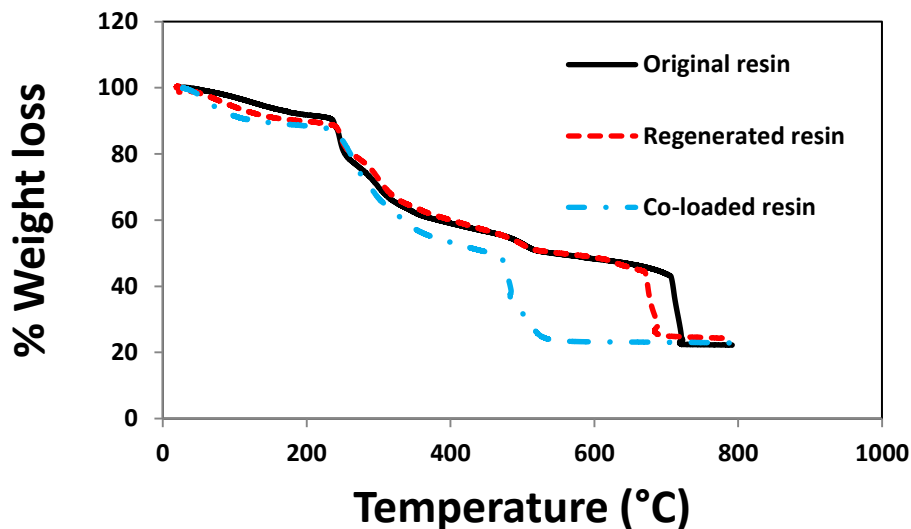


Figure 7.4 TGA curves of original, Co-loaded and regenerated CDAP 4 resin

7.3.4 pH dependency of the adsorption process

The initial pH of the solution *versus* percent Co(II) removal is shown in Figure 7.5. In the pH range 2.5 - 11, the Co(II) uptake was measured after immersing the resin with Co(II) solution (50 mg L^{-1}) for 1 h at 298 K. The adsorption attained its maximum at pH 7. The adsorption process is influenced by the pH-triggerable nature of the amine and carboxylate motifs in the adsorbents and the state of the metal ions in solution.

At lower pH, two factors are at play: (1) All the basic sites on the surface of the resin, CDAP 4, may be protonated and (2) unfavorable competition also occurs between H^+ and Co(II). These two factors do not favor the coordination of the positive Co(II) with the basic sites on the resin as they are now in protonated forms thereby decreasing the adsorption capacity of the resin [239,240]. At higher pH up to 7.5, the degree of protonation decreases; the basic nitrogens and CO_2^- are then available to sequester the metal ions. Beyond pH 7.5,

the increasing basicity has relatively little effect as all the reactive sites are already in the anionic form, Figure 7.5.

In order to determine the optimum pH range for Co(II) adsorption, its speciation over the entire pH range has to be taken into consideration. The distribution of ionic cobalt species as a function of pH, as calculated by visual MINTEQ software [239], is displayed in Fig. 7.6 which shows that there are five cobalt species: Co^{2+} , Co(OH)^+ , Co(OH)_2 , $\text{Co}_4(\text{OH})_4^{4+}$ and Co(OH)_3^- in the pH range 2 to 14 with Co^{2+} being the only species at the pH range 2 to 7. Beyond the pH of 7, the hydrolysis products: Co(OH)^+ , Co(OH)_2 , $\text{Co}_4(\text{OH})_4^{4+}$ and Co(OH)_3^- begin to form and that Co(OH)_2 becomes the dominant species as pH increases up till 12. Evidences from Fig. 7.5, MINTEQ and other literature [240] enabled us to come up with a convenient working pH of 6.0 for Co^{2+} adsorption on this resin.

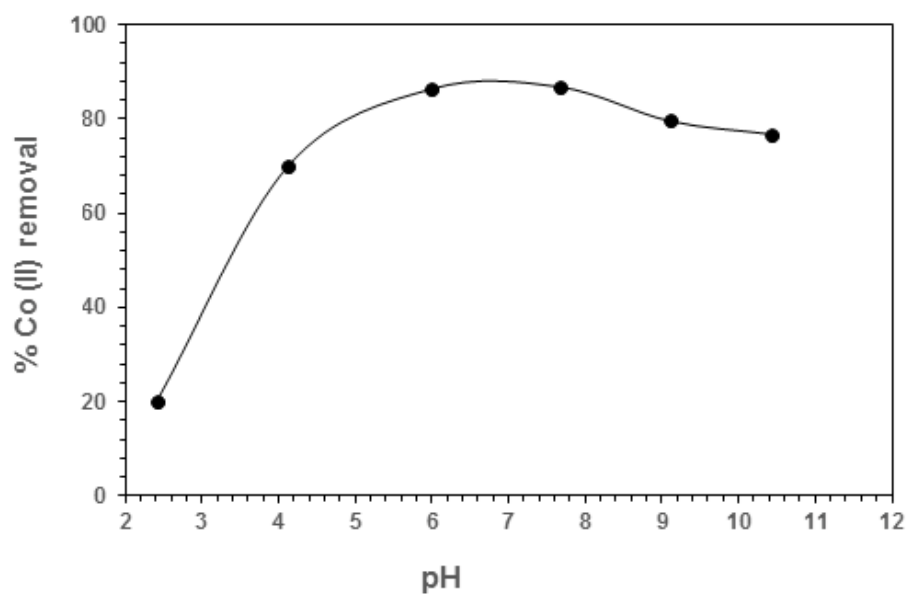


Figure 7.5 Initial pH-dependency of the adsorption of Co(II).

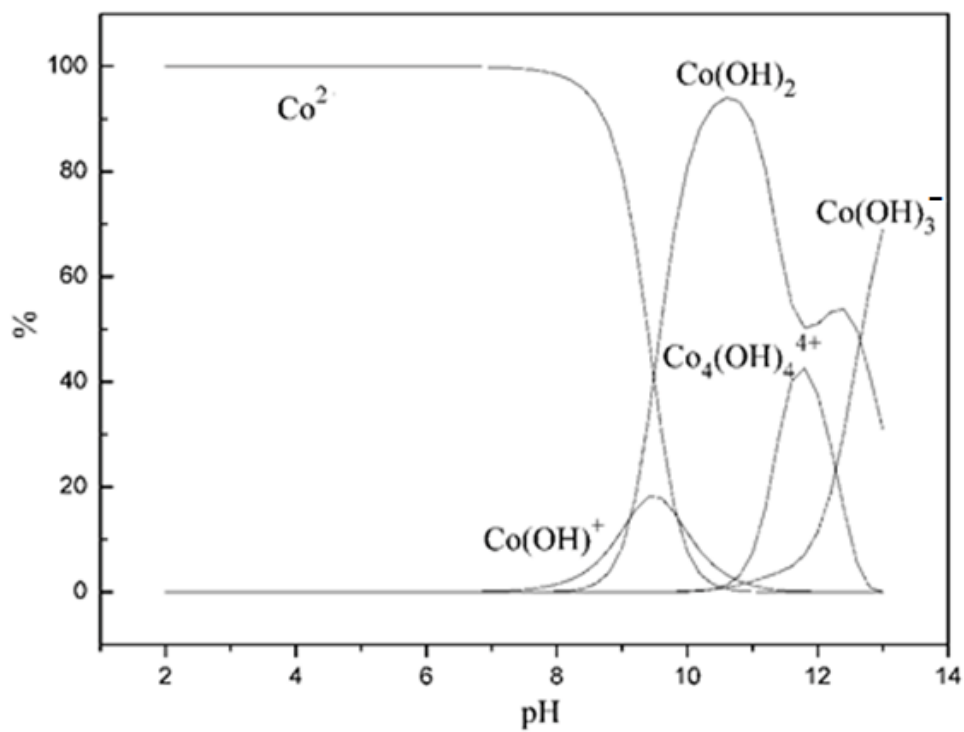


Figure 7.6 Distribution of cobalt ionic species as a function of pH [239]

7.3.5 Initial Co(II) concentration (C_i) versus adsorption capacity

Figure 7.7(a) displays the effect of Co(II) concentrations on its removal by CDAP 4. For a C_i value of 20 mg L^{-1} , it can be seen that the adsorption capacity, q_t , has two distinct parts: the upward slope that reaches the peak rapidly in about 30 min of contact time and the flat section of the plateau where the equilibrium is established slowly. Moving to the C_i value of 30 mg L^{-1} , the initial adsorption capacity increased with time; the entire curve follows the same trend as in the case of 20 mg L^{-1} initial concentration. Similar trend is observed in all other initial concentrations of cobalt ions as depicted in Figure 7.7 (a). The increasing concentration gradient provides the required driving force to overcome the mass transfer effects of Co(II) ions between the aqueous and solid phases [241,242]. The effect of the initial concentration of Co(II) in the range 20 to 100 mg L^{-1} on the equilibrium adsorption capacity, q_e , was examined; it is found to increase with increasing concentrations (Figure 7.7b).

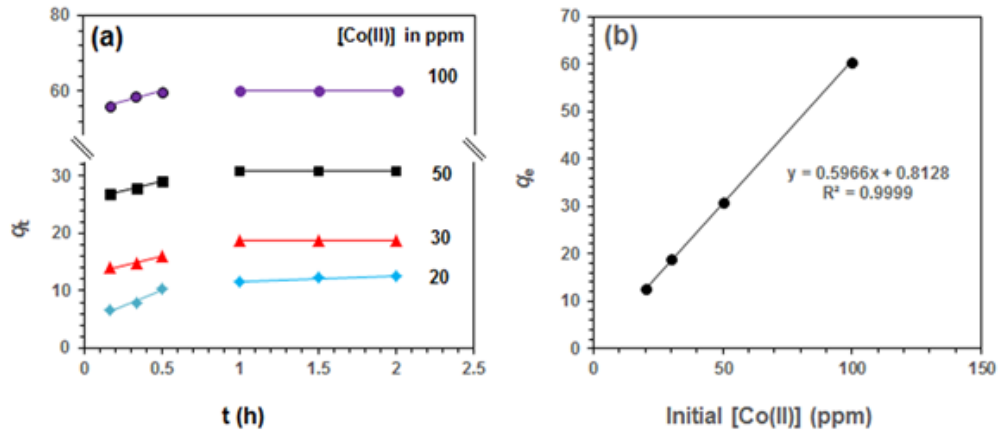


Figure 7.7 (a) Effect of initial Co(II) concentrations on percent Co(II) removal, (b) Effect of initial concentration of Co(II) on the adsorption capacity.

7.3.6 Adsorption energy

The adsorption energy parameters have been computed from experimental data using the well-known kinetic and thermodynamic equations as presented in Table 7.1 (Entries 7 and 8). The activation energy and thermodynamic energy plots are depicted in Fig. 7.8 (a) and (b) respectively, and the parameters extracted therefrom are displayed in Table 7.2. All parameters have their usual meanings. The energy of activation E_a was determined to be 44.8 kJ mol^{-1} ; a negative free energy change, ΔG° , ascertains the favorability of the adsorption process. The negative ΔH° ($-30.6 \text{ kJ mol}^{-1}$) is an indication of the exothermic nature of the adsorption as corroborated by the fact that as the temperature rises from 298 to 338 K, the ΔG° becomes less negative. The negative entropy change ΔS° of $-85.1 \text{ J mol}^{-1} \text{ K}^{-1}$ suggests a decreasing randomness at solid-solution interphase during the adsorption process.

Table 7.1 Mathematical Equations for all the Models used in this Study.

	Linear Form	Eq. no	Plot	Calculated Coefficient
Equilibrium Isotherm Models				
Langmuir	$\frac{C_e}{q_e} = \frac{C_e}{Q_m} + \frac{1}{Q_m b}$	(1)	C_e/q_e vs. C_e	$Q_m = 1/\text{slope}$; $b = \text{slope}/\text{intercept}$
Freundlich	$\log q_e = \log k_f + \frac{1}{n} \log C_e$	(2)	$\log q_e$ vs. $\log C_e$	$n = 1/\text{slope}$; $k_F = 10^{\text{intercept}}$
Tempkin	$q_e = \frac{RT}{b} \ln A + \frac{RT}{b} \ln C_e$	(3)	q_e vs. $\ln C_e$	$b = (RT/\text{slope})$; $A = \exp(\text{intercept}/\text{slope})$
Reaction-based Kinetic Models				
Lagergren Pseudo-first order	$\log(q_e - q_t) = \log q_e - \left(\frac{k_1 t}{2.303}\right)$	(4)	$\log(q_e - q_t)$ vs. t	$k_1 = -2.303 \times \text{slope}$; $q_e = 10^{\text{intercept}}$
Pseudo-second order	$\frac{t}{q_t} = \frac{1}{k_2 q_e^2} + \frac{t}{q_e}$	(5)	t/q_t vs. t	$q_e = 1/\text{slope}$; $k_2 = \text{slope}^2/\text{intercept}$
Diffusion-based Kinetic Models				
Weber–Morris Intraparticle Diffusion	$q_t = k_{id} t^{1/2} + x_i$	(6)	q_t vs. $t^{1/2}$	$k_{id} = \text{slope}$
Kinetic and Thermodynamic Equations				
Activation Energy	$\ln k_2 = -\frac{E_a}{RT} + \text{constant}$	(7)	$\ln k_2$ vs. $1/T$	$\text{Slope} = -\frac{E_a}{R}$
Enthalpy, Entropy and Free Energy Changes	$\ln\left(\frac{q_e}{C_e}\right) = -\frac{\Delta H}{RT} + \frac{\Delta S}{R}$	(8)	$\ln\left(\frac{q_e}{C_e}\right)$ vs. $1/T$	$\text{Slope} = -\frac{\Delta H}{R}$ $\text{Intercept} = \frac{\Delta S}{R}$ $\Delta G = \Delta H - T\Delta S$
Three Parameter Model	Nonlinear form	Parameters		
Langmuir–Freundlich	$q_e = \frac{q_{m_{LF}} (K_{LF} C_e)^{m_{LF}}}{1 + (K_{LF} C_e)^{m_{LF}}}$	where $q_{m_{LF}}$ is the Langmuir–Freundlich maximum adsorption capacity (mg g^{-1}), K_{LF} is the equilibrium constant for a heterogeneous solid, and m_{LF} is the heterogeneity parameter, its value lies between 0 and 1.		
Redlich–Peterson	$q_e = \frac{A C_e}{1 + B C_e^\beta}$	where A is the Redlich–Peterson isotherm constant (L g^{-1}), B is also a constant having unit of $(\text{L mg}^{-1})^\beta$, and β is an exponent that lies between 0 and 1.		
Average Percentage Error	$APE (\%) = \left\{ \frac{\sum_{i=1}^N (q_e)_{\text{experimental}} - (q_e)_{\text{predicted}} }{(q_e)_{\text{experimental}}} \right\} \times 100$ Where N is the number of experimental data			

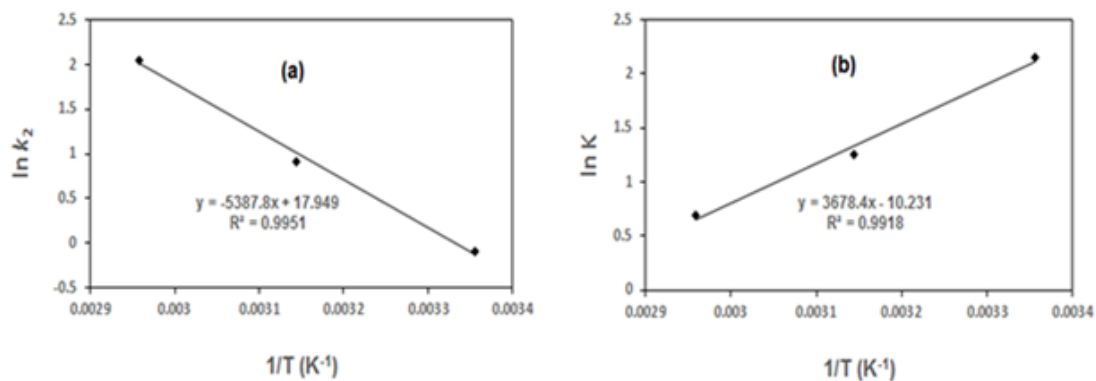


Figure 7.8 (a) Arrhenius and (b) Thermodynamic plots for Co (II) adsorption on CDAP 4

Table 7.2 Thermodynamic and kinetic parameters for Co(II) adsorption on resin 4.

Temp (K)	ΔG° (kJ mol ⁻¹)	ΔH° (kJ mol ⁻¹)	ΔS° (J mol ⁻¹ K ⁻¹)	E_a (kJ mol ⁻¹)
298	-5.23			
318	-3.53	-30.6	-85.1	44.8
338	-1.83			

7.3.7 Data analyses

The experimental data were utilized to identify the best-fit kinetic model from some of the well-known multi-parameter equations. The various equation parameters which often provide insight into the surface properties, the affinity of the adsorbent and even the adsorption mechanism [243] are listed in Table 7.1.

a. Isotherm models

Adsorption isotherms relate the concentration of sorbate in the liquid phase with the amount adsorbed by the adsorbent at a constant temperature. The two-parameter isotherm models used in this study are Langmuir [244], Freundlich [170] and Temkin [171]. Isotherm models tend to shed light on various aspects of the adsorption process such as the nature of adsorption sites as well as its favorability [242].

Experimental data collected were each tested on the linear forms of Langmuir, Freundlich and Temkin model equations (Table 7.1, entries 1-3) and their plots are displayed in Fig. 7.9 (a), (b) and (c), respectively. The various parameters extracted from these models and their average percentage errors (APE %, equation in Table 7.1) are displayed in Table 7.3. Looking at Table 7.3, the R^2 values of 0.9872, 0.9935 and 0.9780 for the two-parameter models of Langmuir, Freundlich and Temkin respectively are too close to make any meaningful distinction between them. However, their average percentage errors (APE %) of 2.21, 4.55 and 9.67, respectively, for Langmuir, Freundlich and Temkin suggest that Langmuir is the best-fit even though it has comparable regression coefficient to Freundlich. The parameter Q_m of 137 mg g⁻¹, obtained from the Langmuir isotherm, is the quantity of adsorbate required to form a monolayer. The dimensionless equilibrium parameter R_L values falling in the range 0.6 - 0.9 suggest the favorability of adsorption process on a homogeneous surface [245].

In order to validate the results of the two parameter models, three-parameter models (Langmuir–Freundlich [246] and Redlich–Peterson [247]) were used to simulate the experimental data using wolfram mathematica version 10 for nonlinear curve fittings. Models with more than two parameters are often employed to minimize the deficiencies of the simple two-parameter models [248,249]. These two nonlinear models were selected

because they are derived from the combined assumptions of the individual Langmuir and Freundlich isotherms whose regression coefficients from linear two parameters plots are comparable as mentioned earlier and shown in Table 7.3. The Langmuir-Freundlich isotherm (equation in Table 7.1) brought together components from both individual isotherms in such a way that at high adsorbate amount, monolayer adsorption capacity characteristic of the Langmuir isotherm can be estimated while at low adsorbate concentrations it is not consistent with Henry's law but reverts to the Freundlich isotherm [246]. On the other hand, the empirical three parameter Redlich–Peterson isotherm equation (Table 7.1) is a hybrid that merges elements from both the Langmuir and Freundlich equations and is not consistent with ideal monolayer adsorption [247].

The q_e and C_e values from the experiments are plugged into the models in order to generate the equations parameters which are then used to predict the variables. Fig. 7.10 displays the curve fittings while the parameters extracted therefrom are shown in Table 7.3. Between the two models, the correlation coefficients are quite comparable with Langmuir–Freundlich (0.9998) having a slight edge over Redlich–Peterson (0.9995). On the basis of Average percentage error (APE%), Langmuir–Freundlich (2.26%) performed better than Redlich–Peterson (3.52%). In fact, Langmuir–Freundlich model effectively predicted adsorption capacity (138 mg g^{-1}) with excellent agreement with two parameter Langmuir monolayer adsorption capacity (137 mg g^{-1}), Table 7.3. This establishes, on one hand, the homogeneity of the surface as in Langmuir two-parameter isotherm but, on the other hand, that the sorption is a cooperative process due to adsorbate–adsorbate interactions at high adsorbate concentrations [246]. Thus, Langmuir adsorption is the predominant mechanism. The current resin's Langmuir adsorption capacity Q_m for Co(II)

is compared with those of the other types of reported adsorbents [149,250–254] in Table 7.4. It is interesting to see that the current resin shows superior performance.

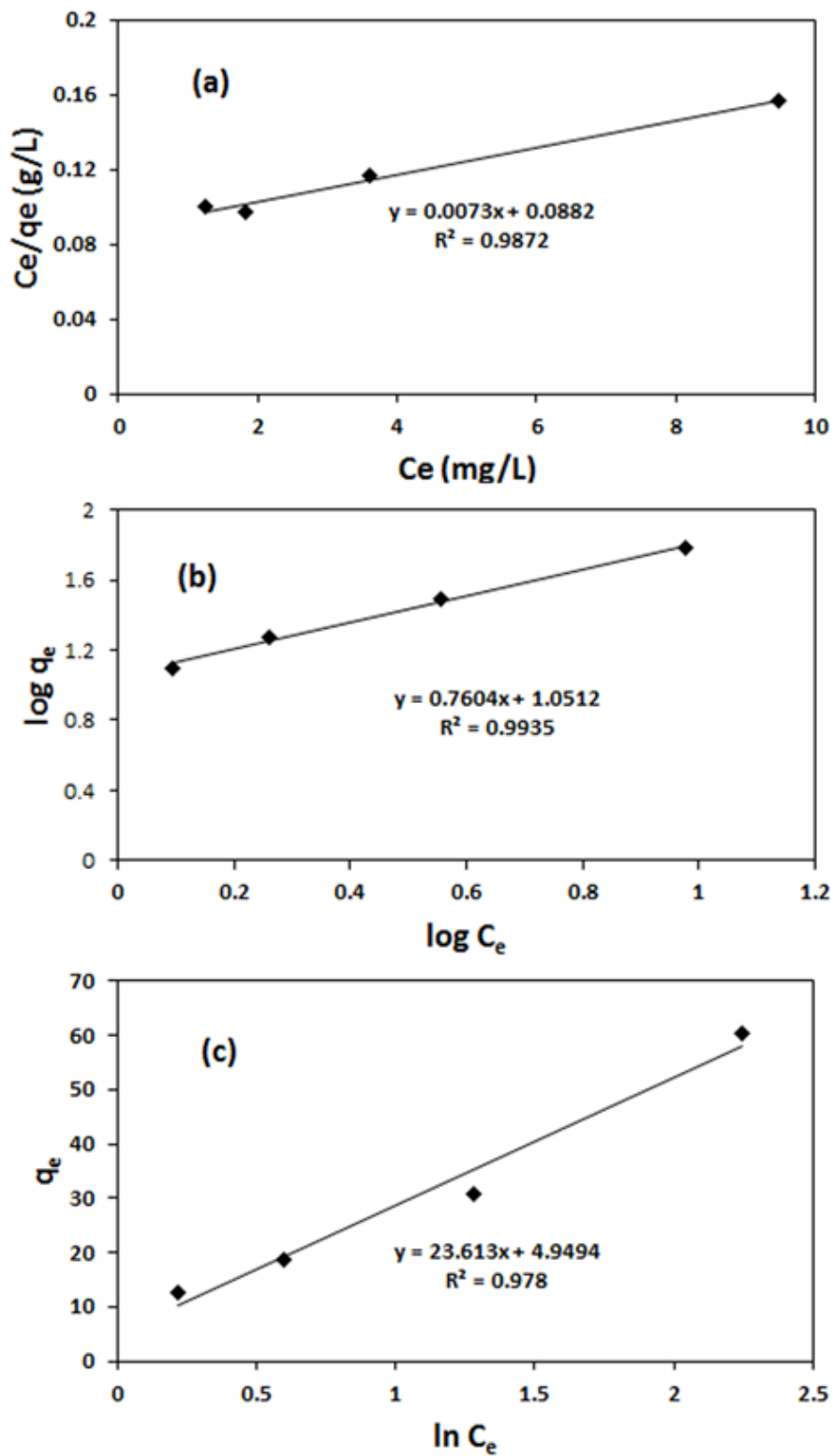


Figure 7.9 (a) Langmuir (b) Freundlich and (c) Temkin adsorption isotherms for Co^{2+} adsorption on CDAP 4 for various initial concentrations at 298K.

Table 7.3 Isotherm parameters for Co(II) adsorption on CDAP 4

Isotherms	Isotherm Parameters		R^2	APE (%)
Langmuir	Q_m	137 mg g ⁻¹	0.9872	2.21
	b	0.0828 L mg ⁻¹		
Freundlich	k_f	11.3	0.9935	4.55
	n	1.32		
Temkin	A	1.23 L g ⁻¹	0.9780	9.67
	b	105 J mol ⁻¹		
Langmuir– Freundlich	q_{mLF}	138 mg g ⁻¹	0.9998	2.26
	K_{LF}	0.0817		
	m_{LF}	1.00		
Redlich–Peterson	A	115	0.9995	3.52
	B	8.74		
	β	0.294		

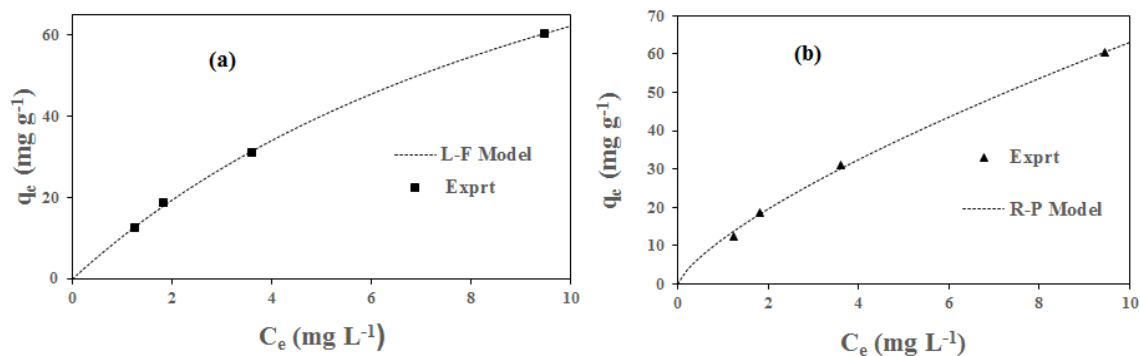


Figure 7.10 Comparison of experimental and predicted adsorption isotherms for Co (II) according to: (a) Langmuir–Freundlich model (b) Redlich–Peterson model

Table 7.4 Comparison of the adsorption capacity of the current resin with that of various adsorbents for Co(II) at 298 K.

Adsorbent	Adsorption Capacity q_m (mg/g)	References
Almond green hull	45.5 at pH 4	[250]
Grafted poly(ethylene terephthalate) fiber	27.2 at pH 4-6	[251]
Clinoptilolite	14.08 at pH 6-7	[149]
Sulphurised activated carbon	40.5 at pH 6	[252]
EDTA-modified silica gel	20.0 at pH 3	[253]
DTPA-modified silica gel	16.1 at pH 3	[253]
Aminated graphene oxide	116.35 at pH 6	[254]
Present polymeric sorbent	137 at pH 6	This study

b. Adsorption kinetics

(i) Reaction-based Kinetic Models

The nature of the interfacial interaction between solid and solution during the metal ion adsorption can be described by kinetic models based on the rate-controlling mechanism involving chemical reaction, mass transfer and diffusion control systems. Lagergren first-order [255] and Pseudo-second-order [163] models have been used to describe the Co(II) adsorption on CDAP **4**. The equations and their parameters are listed in Table 7.1, (Entries 4 and 5). Lagergren pseudo first-order and second-order are used when the rate of occupation of the binding sites is proportional to the number of unoccupied sites on the resin and to its square, respectively [166].

Figure 7.11 (a) and (b) present the plots for first-order and pseudo second-order adsorption process, respectively, at various initial concentrations of Co(II) ions. The parameters calculated from the two kinetic models are given in Table 7.5. The data fit the second-order model, as evinced by the greater proximity of R^2 values to unity (0.9980–1.000) and the better agreement between $q_{e,exp}$ and $q_{e,cal}$. Indeed, the average percentage error (Table 7.5) between the experimental and calculated values also corroborated this claim as pseudo 1st order prediction has more than 100% error (actual 119%) in comparison with Pseudo 2nd order prediction with only a minimal 4.62% error. The better fit of Pseudo 2nd order kinetic suggests that the adsorption process might be chemical in nature [163,210]. As expected, the increasing initial Co(II) concentration resulted in the increase in the initial sorption rate ($h = k_2qe^2$) owing to the increase in the mass transfer to the resin surface [166].

(ii) Diffusion-based Kinetic Models

Weber-Morris intraparticle diffusion model was developed to examine the effect of diffusion of metal ions within the polymer network. The nature of the plot depends on whether the diffusion of the metal ions in the pore of the resin is the rate determining step or there is some influence from mass transfer effects [165,256].

The Weber-Morris equation [164] and its parameters are shown in Table 7.1 (Entry 6). Plots from Weber-Morris equation based on the initial concentration and temperature are shown in Figure 7.11 (c) and (d) and the parameters extracted therefrom are displayed in Table 7.6. Starting with the initial concentration of 30 mg L^{-1} , (Figure 7.11c), the diffusion kinetic curve shows two straight regions -region A (from 10-30 min) and region B (from 60-120 min) for the entire duration of the study. Region A with a steep slope indicates the faster diffusion of Co(II) on the resin surface. However, as the time progresses, the curve flattens out (Region B) indicating a gradual approach to equilibrium. Meanwhile, with an increase in the initial concentration (30, 50 and 100 mg L^{-1}), the values of q_t also increases with increment in the k_{id} (the intraparticle diffusion constant) for region A of the process (Table 7.6). This situation corresponds to a concentration-dependent diffusion process [166,210]. The results agree with the pseudo-second-order kinetic model.

The results of the experiments conducted at 298, 318, and 338 K for C_i of 50 mg L^{-1} show similar behavior, but with a gradual decrease in k_{id} as the temperature increases (see Figure 7.11 (d) and Table 7.6). This is in line with the exothermic nature of the adsorption process which is slowed down with the increase in temperature [210].

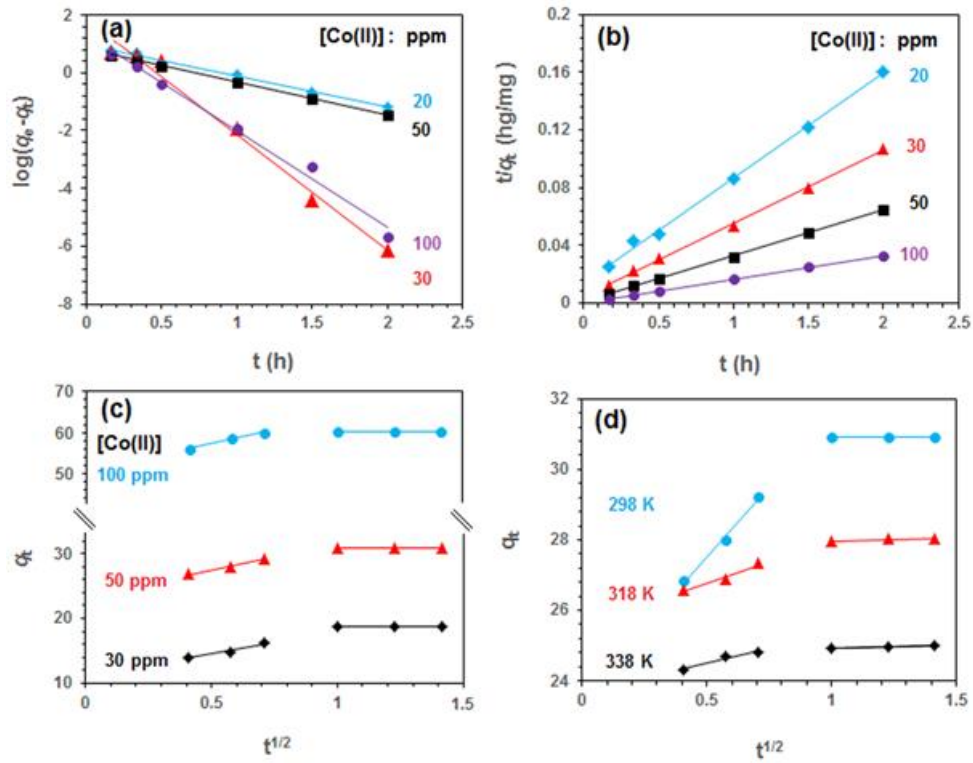


Figure 7.11 For Co (II) adsorption on resin 4 at 298 K: (a) Lagergren first-order plots, (b) Pseudo second-order plots and Weber-Morris intraparticle diffusion plots: (c) at various concentrations (d) temperatures.

Table 7.5 Adsorption kinetic parameters for pseudo first and second order models.

Conc (ppm)	$q_{e,exp}$ (mg g ⁻¹)	Pseudo 1st order			2nd order			
		k_1 (h ⁻¹)	$(q_{e,cal})^b$ (mg g ⁻¹)	R^2	$(q_{e,cal})^c$ (mg g ⁻¹)	k_2 (g mg ⁻¹ h ⁻¹)	h^a (mg g ⁻¹ h ⁻¹)	R^2
20	12.5	2.47	9.14	0.9840	13.8	0.363	0.694×10 ²	0.9980
30	18.8	9.23	76.2	0.9649	19.8	0.569	2.22×10 ²	0.9988
50	30.9	2.65	6.60	0.9782	31.5	0.914	9.09×10 ²	0.9999
100	60.4	7.68	21.2	0.9879	60.7	1.62	59.9×10 ²	1.000

^a Initial adsorption rate, $h = k_2 q_e^2$

^b APE (%) for $q_{e,cal}$ in Pseudo 1st order = 119

^c APE (%) for $q_{e,cal}$ in Pseudo 2nd order = 4.62.

Table 7.6 Intraparticle diffusion parameters.

Conc (mg L ⁻¹)	Temp (K)	k_{id} (mg g ⁻¹ h ⁻¹)	x_i (mg g ⁻¹)	R^2
30	298	7.00	11.0	0.9387
50	298	7.95	23.5	0.9893
	318	2.46	25.5	0.9675
	338	1.68	23.7	0.9599
100	298	13.1	50.9	0.9841

7.3.8 Morphology of fresh and Co-loaded CDAP 4 resin

As determined by BET surface area analyzer, the surface area and the pore size of the fresh CDAP 4 resin were found to be 28.4 m²/g and 19.5 Å, respectively, while the respective values for the regenerated resin were 27.1 m²/g and 17.9 Å. Here, we see a very stable morphology of the resin after regeneration. It suggests that despite clear evidence from IR and EDX of interaction and binding of the cobalt metal ions with the resin, it is quite robust and doesn't suffer distortion in morphology after uses.

The morphology and the structure of the loaded and unloaded resins were examined by SEM and EDX as revealed in Figure 7.12. The EDX spectrum recorded for cobalt-loaded resin (Figure 7.12b) shows the main characteristic peaks for Co(II) at 0.75 and 6.95 keV thereby confirming the binding of Co(II) to the surface of the polymer. Corresponding SEM images are also depicted in Figure 7.12(b).

By the foregoing evidence of interactions from IR (Figure 7.1) and EDX analyses, we now put forward the following proposal in Scheme 7.2 to show the mechanism of the possible interactions between the functional groups on the resin and the cobalt ions during adsorption. Several forms of octahedral complexes of Co(II) are shown in Scheme 7.2. The proposed structures are in line with those proposed for M(II) complexes with amino acid-derived compounds [257–259]. It is important to note that Scheme 7.2 presents only part of the possible interactions of the resin with Co(II) as there is an indication from IR that the resin can undertake further interactions through the SO₂ units in the polymer chain thereby assisting in the sorption process [260]. The formation of these chelating complexes explains the high performance of this resin in cobalt ion removal from the aqueous medium.

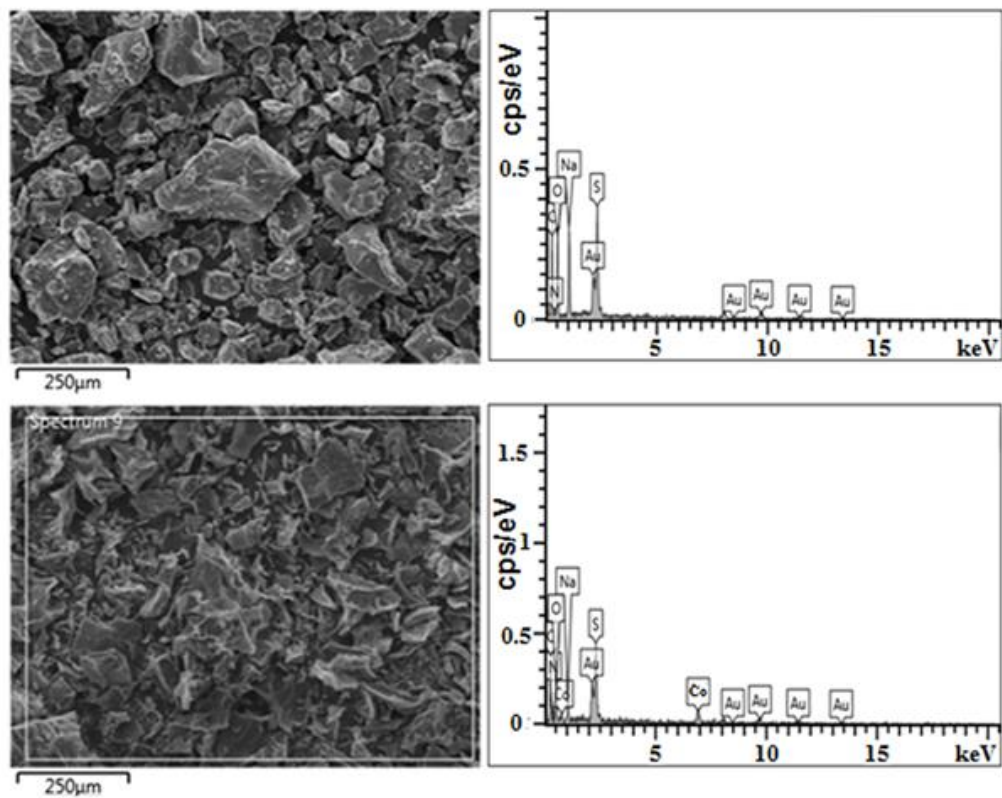
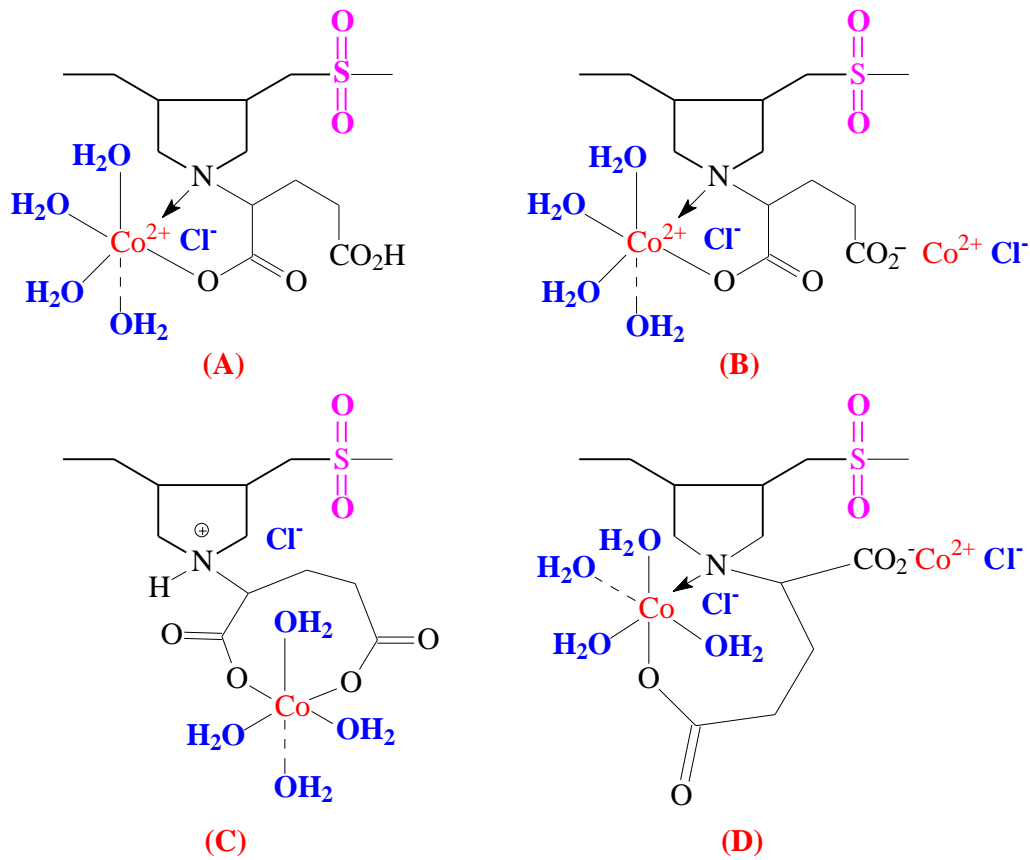


Figure 7.12 SEM image and EDX spectrum of (a) unloaded 4 and (b) Co(II) loaded 4.



Scheme 7.2 Illustration of the resin's latitude in forming complex with Co(II).

7.3.9 Regeneration of the resin

Reusability test was performed on the resin in order to mitigate possible environmental impact after disposal of the spent resin. The results of three (3) cycles of adsorption/desorption procedures are displayed in Fig. 7.13. The performance of the resin is consistent for the removal of Co(II) and the regeneration efficiency of the resin is stable after the three cycles. This underscores a striking balance between its potential economic benefits and its environmental impact. The robust nature of this resin as manifested in its

ease of regeneration has been amply corroborated by data from a surface morphology of the resin (as discussed in section 3.8), IR spectra (Fig. 7.2) and the TGA profiles (Fig. 7.4) where the fresh and the regenerated resins are compared. The results confirmed the reusability of the reported resin.

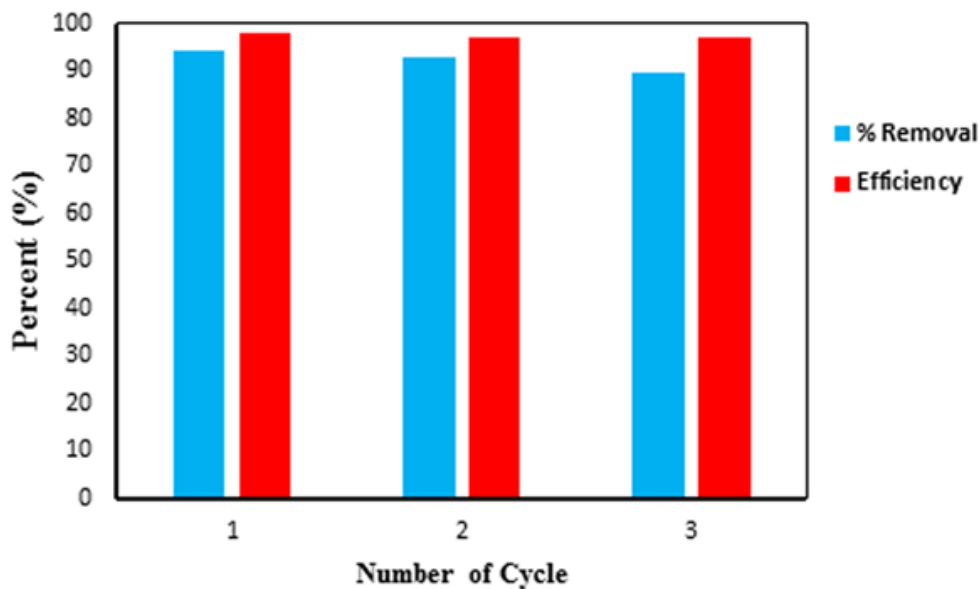


Figure 7.13 Adsorption/desorption with repeated cycles as a measure of performance and efficiency of the resin.

7.3.10 Wastewater treatment

We evaluated the efficacy of the synthesized resin in the removal of the metal ions using a matrix of industrial wastewater having a pH of 6.3. The concentrations of metal ions in the wastewater were determined by Thermo Scientific XSeries 2 Quadrupole Inductively Coupled Plasma Mass Spectrometer (ICP-MS), Germany. 20 mL samples of original wastewater were each treated with the resin (30 mg) and left to equilibrate for 24 h. This treatment was repeated for separate 20 mL samples of original wastewater spiked

with 20 mg/L standard Co^{2+} ions concentration. The analysis of the original wastewater revealed the presence of several metal ions Co, Cd, As, Pb, Cu, Ni, Mn, Cr (Table 7.7). However, after treatment with the resin, the concentrations of all the metal ions notably those of Co, Cr, Cu, As, Pb, and Cu were significantly reduced. Analysis of the spiked wastewater sample, after treatment with the resin, also revealed its excellent efficacy in removing the various metal ions including As, let alone $\approx 99\%$ removal of Co(II). Two forms of arsenic can be found in natural waters: arsenite (AsO_3^{3-}) and arsenate (AsO_4^{3-}), referred to as arsenic (III) and arsenic (V), respectively [261]. Anion-exchange resins having quaternary ammonium groups attached to polymeric matrices have been extensively studied for their ability to remove arsenic [262–264]. It has been found to exhibit a better attraction for divalent species (HAsO_4^{2-}) at the optimum pH in the range 7–9 [262]. It is also reported that resins containing quaternary ammonium motifs are effective in the removal of arsenic in acidic conditions (in the pH range of 3 to 6) [263]. It is worth mentioning that the current resin was able to remove around 90% arsenic. Note that in the entire pH-window, the cross-linker in the resin has positively charged nitrogen centers which can act as anion exchangers to scoop up the negatively charged arsenates from the aqueous solution. The treatment of the wastewater sample proved the potential use of the prepared resin as an industrial adsorbent for wastewater purification.

Table 7.7 Industrial wastewater sample treated with the resin.

Metal ion	Before treatment ($\mu\text{g/L}$)	After treatment with the resin	
		Not Spiked ($\mu\text{g/L}$)	Spiked with 20 ppm Co(II) ($\mu\text{g/L}$)
Co	3.41 ± 0.40	0.152 ± 0.40	1.580 ± 0.40
Cd	0.71 ± 0.20	0.077 ± 0.20	0.084 ± 0.20
As	113 ± 2.1	11.9 ± 2.1	10.8 ± 2.1
Pb	869 ± 0.24	15.3 ± 0.24	16.3 ± 0.24
Cu	39.1 ± 4.2	0.703 ± 4.2	0.508 ± 4.2
Ni	47.9 ± 3.21	14.5 ± 3.21	10.11 ± 3.21
Mn	9.04 ± 2.21	5.70 ± 2.21	4.201 ± 2.21
Cr	135 ± 4.3	21.2 ± 4.3	20.0 ± 4.3

7.4 Conclusion

We report, here, the synthesis of a novel glutamic acid-based cross-linked dianionic polyelectrolyte resin from a relatively inexpensive source. The synthetic approach ensured the preservation of the integrity of all the three original functionalities of the amino acid while incorporating additional basic center through the SO_2 in the polymer network. Besides, the synthesis route also leads to the swelling and expansion of the polymer network, thereby making the numerous basic centers in the polymer chain more available and accessible for cobalt(II) chelation. Application of the polymer resin in the cobalt adsorption from aqueous medium gave a very good adsorption performance with a Langmuir monolayer adsorption capacity of 137 mg g^{-1} which accorded this resin an advantage over other adsorbents previously used for Cobalt(II) adsorptive removal (Table 7.3). The robustness of this resin has also been demonstrated by the relative ease of regeneration of the spent resin- a situation that refreshes the resin and keeps it longer in circulation. With this new glutamic acid-based resin having adsorption activation energy, E_a , of 44.8 kJ mol^{-1} , enthalpy change ΔH° of $-30.6 \text{ kJ mol}^{-1}$ and negative Gibbs free energy change, ΔG° , we are poised to introduce a new dimension in waste water treatments for cobalt and other metal pollutants. The resin has demonstrated remarkable efficiency in removing toxic metal ions including arsenic from a west water sample.

CHAPTER 8

Preparation of Multilayered Polyelectrolyte-coated Silica for the Removal of Toxic Metal Ions and Organic Pollutants

Abstract

In this study the surface modification of mesoporous SBA-15 silica particles is done by coating with alternate polyelectrolytes Poly(diallyldimethylammonium chloride) (PDDA)/Polydianionic Electrolytes (PDE) with and/ or without a hydrophobe. It is a layer-by-layer electrostatic adsorption of polycation/polyanions on the surface or inside the pores of the mesostructured material. In this way, a hybrid multilayered polyelectrolyte-coated silica material retaining much of the properties of each individual organic/inorganic component is designed. The nature of the charge on the surface after modification was verified by Zeta potential measurement. The surface morphology, topography and its textural properties are examined by atomic force microscopy (AFM) and Nitrogen adsorption/desorption respectively. TGA has also been done to ascertain the amount of polymer layer on the silica material. Applications of this material in the areas of adsorption of toxic Cadmium pollutant was tested. Its performance is found to be very impressive in the removal of metal pollutant. The kinetics and thermodynamic parameters for this hybrid adsorbent was studied with the results from cadmium adsorption data. For the material modified with hydrophobe, its dual (+/-) adsorption capacities as evaluated using cationic Methylene Blue (MB) and anionic Eriochrome Black T (EBT) were quite promising.

8.1 Introduction

The growth of modern industries has driven the wide-spread utilization of heavy metals and organic dyes with the concomitant deposition of these toxic materials into the environment. In the case of cadmium, the primary source through which it gets into the human system for non-smoking population is through consumption of agricultural products grown in contaminated environment [265]. Cadmium has not been established to have any known beneficial effects on the human body, yet, its retention in the body systems has been documented and it has been reckoned to lead to kidney damage and other deleterious consequences on the body system. The risk factor considerably increases in smoking population [265]. Recent data tend to suggest that exposure to cadmium could lead significantly to increased risk factors associated with cardiovascular diseases [266]. In this light, every effort must be made to reduce the amount of Cadmium ion in the environment.

On the other hand, dyes are discharged from different industries into the environment resulting into serious health consequences that may ultimately lead to mutagenic or carcinogenic disorders [267]. The complex chemical structures of dyes enable them some stability to oxidation, heat and light and, thus, generally not easily biodegradable except recent report on some specific fungi degradation [268–270]. Owing to their good water solubility, synthetic dyes are prevalent water pollutants. In view of the increasingly strict regulation on the organic content of industrial effluents, there is an urgent need to curtail dyes in the effluent before discharge to the environment.

Till date, so many methods have been used for wastewater treatments but adsorption remains a preferred candidate because of its efficiency and simplicity. As the drive for greater efficiency in wastewater treatments continues, there is increasing need, more than ever before, to design a new adsorbent that will not only meet the requirement of high adsorption and fast uptake capacities but also meet the requirement of high temperature applications as well as operational and mechanical stabilities [210,271].

Mesoporous silica can serve as an adsorbent material of choice as it is hydrothermally stable as well as maintaining such flexibility that allows exquisite tuning of pore structure and surface chemistries. Mesoporous materials with pore size ranging between 2 - 50 nm have offered very interesting characteristics and tremendous opportunities in many fields. The high surface area and the ability to tune the pores are among the most desirable properties of these materials. They have a uniform hexagonal arrangement of pores with size ranging between 1.5 and 10 nm [272].

There is a tremendous interest on mesoporous silica materials because their high specific surface area confers on them large capacity for the adsorption of molecular and ionic species [273]. Furthermore, the well-ordered meso-structures enable fast uptake or capture of small molecules [274]. The product of Self-assembling of monolayers on mesoporous silica has been proven to be an efficient heavy-metal sorbent in aqueous medium, even surpassing other sorbents like activated carbon and polymer resins [275]. Wide range of functional groups can be installed on the surface to optimize the sorbent affinity for target pollutant species [68,276]. The ability to construct such versatile material comprising of intrinsically non-toxic elements (oxygen and Silicon) has rendered its application in biomedical field [277].

The possibility of surface modification of mesoporous silica and the pore tuning is a choice in multilayer formation. Different methods can be applied for materials surface coating [278]. Alternate deposition of polycations and polyanions onto a solid substrate has been proposed as a flexible, reliable, and simple method to construct multilayered polyelectrolyte films on surfaces with good control over composition, thickness, and morphology [279,280]. As a function of the outermost layer, with either negative or positive charges, the films can adsorb large number of different compounds such as dyes and toxic metal particles [275,277,281]. The construction of polyelectrolyte multilayer films by the layer-by-layer (LBL) method impart materials with broad potential applications in many fields including separation and adsorption [277,282,283]. Self-assembly of alternate charged particles in solution takes place due to the formation of reversible electrostatic bond leading to the formation of new/hybrid materials whose properties will depend largely on the incoming chemical substance and its environment.

The aim of this study is to investigate the modifications of the surface properties of some silica particles, by LBL technique. The designed multilayered polyelectrolyte hybrid material will be utilized in the removal of toxic cadmium metal ions and organic dyes (Methylene Blue and Eriochrome Black T) from aqueous solution.

8.2 Experimental

8.2.1 Chemical and Materials

For the synthesis of the polymer, the following materials are used. Diallylamine, dimethyl maleate, and montmorillonite K10 from Fluka AG (Buchs, Switzerland); ammonium persulfate (APS); , 4-phenylphenol, acetonitrile, diethyl ether, potassium

carbonate, were all purchased from Sigma-Aldrich. For dialysis, a membrane (Spectra/Por) with a molecular weight of 6000–8000 was purchased from Spectrum Laboratories, Inc. (Rancho Dominguez, CA, USA).

For the synthesis of mesoporous silica, the following are used: Pluronic-123 [EO₂₀PO₇₀EO₂₀, Aldrich], tetraethylorthosilicate [TEOS, Sigma-Aldrich] and concentrated hydrochloric acid (HCl) were used.

For the layer-by-layer Assembly, the following were used. Cationic Polymer is Poly(diallyldimethylammonium chloride) (PDDA) solution, 20 wt. % in H₂O, Fw 161.7 g/mL, (C₈H₁₆ClN)_n, d 1.04 g/mL. Aldrich. Typical Mw 100000 – 200000. Water purified in a Milli Pore with pH 5.5, R 18.2 MΩ was used in all the experiments. All reagents and solvents used were of analytical grade.

For the adsorption studies, Cadmium nitrate tetrahydrate (Cd(NO₃)₂ · 4H₂O, Molecular Weight 308.48, Aldrich) was used to prepare the standard which was subsequently diluted to the required concentrations. Sodium hydroxide and nitric acid were purchased from Sigma–Aldrich. Millipore water (18.2 MΩ·cm) was used for the adsorption study.

8.2.2 Physical Methods

A Perkin–Elmer 16F PC FTIR spectrometer was utilized to record IR spectra. The proton and carbon-13 spectra were recorded on a JEOL LA 500 MHz spectrometer using HOD signal at 4.65 ppm and dioxane signal at 67.4 ppm as internal and external standards, respectively. The ²⁹Si solid-state nuclear magnetic resonance (NMR) experiments were carried out at a frequency of 400MHz on a Bruker NMR spectrometer. The spectra were

measured at room temperature and the magic-angle spinning (MAS) frequencies were set at 4 kHz. During the experiment, cross-polarization (CP) excitation using a $\pi/2$ pulse length was employed. The Chemical shifts were externally referenced to tetramethylsilane (TMS).

The surface morphology of silica materials was examined by Field emission scanning electron microscope (FESEM) and their elemental analyses were determined using Energy-dispersive X-ray spectroscopy (EDX) fitted with a detector model X-Max. A Perkin Elmer 2400 Series II CHNS/O Elemental Analyzer was used to carry out the elemental analysis. The concentration of Cd(II) was monitored using a flames atomic absorption spectrometer (FAAS) (Thermo scientific iCE 3000). TGA was conducted in a thermal analyzer (SDT Q600 from TA instruments, USA). The temperature was raised at a rate of 10°C/min with air flowing at a rate of 100 mL/min. Nitrogen adsorption–desorption measurements were performed at 77 K on a Micromeritics Tristar II plus analyzer (U.S.A). The methods of Brunauer-Emmett-Teller (BET) and Barrett-Joyner-Halenda (BJH) were adopted to determine the surface area of the material and its pore size distribution, respectively. Chemisorption data was acquired on Micromeritics Autochem II chemisorption analyzer (U. S. A.).

The electrophoretic mobility of investigated samples was determined by means of ZetaSizer Nano ZS (Malvern, UK) operating at the wavelength 633 nm. The results were expressed as the average of at least three independent measurements. Atomic force microscopy (AFM) measurements were done in the AC mode by a MFP-3D device (Asylum Research, USA), using silicon-SPM sensors (BudgetSensors, Bulgaria) with spring constant of ca. 5.7 N/m and tips frequency of ca. 160 kHz, the tip radius being lower than 10 nm. The surface analysis parameters were evaluated by means of the WSxM

Scanning Probe Microscopy Software. To examine the topography of silica particles before and after surface modification, 1 drop of particles dispersions of each sample was dried on mica wafers slides in dust free medium, at room temperature.

8.2.3 Synthesis of the Polymers

Aspartic acid derived polymer was synthesized from its monomer N,N-diallylaspartic acid hydrochloride as previously described in one of our works [137]. The polyzwitterionic acid (PZA) was subsequently modified into poly-di-anionic Electrolyte (PDE) [137] for layer-by-layer adsorption on silica surface. The hydrophobic modification of aspartic acid monomer N,N-diallylaspartic acid hydrochloride (M_1) was done to obtain a second monomer N,N-diallylhexyloxybiphenyl hydrochloride (M_2) according to previously reported protocols [137,284]. Cyclocopolymerization of monomers M_1 and M_2 was done as follows. Appropriate amounts of M_1 (2.71 g, 10.58 mmole) and M_2 (0.130 g, 0.34 mmole) and water (1.17 g) were taken in a round bottom flask and stirred. The initiator APS (429 mg) was then added under N_2 and the closed flask was stirred using a magnetic stir bar at 110° C. An exothermic reaction with minor implosion took place within few seconds after the addition of APS and the reaction was stopped after 5 minutes. The homogenous mixture from polymerization was dialyzed against deionized water. The homogeneous solution became cloudy during dialysis owing to the transformation of polyelectrolyte to polyzwitterionic acid (PZA). The mixture was freeze-dried and then vacuum-dried at 60° C to obtain the product (yield: 1.85 g, 30%).

8.2.4 Synthesis of mesoporous silica SBA-15

Pluronic-123 [EO₂₀PO₇₀EO₂₀, Aldrich] was used as structure directing agent while tetraethylorthosilicate [TEOS, Sigma-Aldrich] was used as silicon precursor. The silica particles were synthesized using the method of Zhao et al [285]. In a typical synthesis, 4g of P123 was dissolved in 80ml of de-ionized water and 15ml of concentrated hydrochloric acid (HCl) at room temperature. The dispersion was stirred at room temperature for about an hour. This was designated as solution A. About 60ml of de-ionized water was added at room temperature to solution A in round-bottom flask while stirring. The system was subsequently transferred to an oil bath at 35°C. Stirring continue for one hour. Appropriate amount of TEOS was added while stirring and the mixture allowed to ripe in a sealed glass for twenty hours (20). The temperature was raised to 95°C and allowed to age for twenty-four hours. The solid product was recovered by filtration and dried overnight at 90°C in an oven. It was subsequently calcined in air at 600°C for four (4) hours at 2°C per minute. About 6g of mesoporous silica was recovered from one synthesis. The synthesis procedure was repeated several times to obtain about 70g of mesoporous silica in order to have enough material for the research work.

8.2.5 Boehm Titration

The amount of acidic oxygen surface functional groups is determined according to Boehm's method [286]. A 0.50g of silica samples were added to beakers each containing 25 mL of the following 0.050 M solutions: NaOH, Na₂CO₃, NaHCO₃ and HCl. The beakers were sealed and shaken for 24 h and then 10 mL of each filtrate was pipetted in an excess of 20ml 0.05M HCl for the determination of acidic functional groups. The filtrate was titrated with 0.050M NaOH using phenolphthalein indicator and the volume required

to reach the endpoint was noted. For Na_2CO_3 reaction base an excess of 30ml 0.05M HCl was added rather than 20ml due to diprotic property of the base to ensure complete reaction with acid. The number of surface basic sites was calculated from the amount of hydrochloric acid required. The number of surface acid sites of each surface group (carboxylic, lactonic, phenolic) were then determined through subtraction of those determined by each reaction base. Finally, the number of surface acid sites was normalized for the amount of silica reacted by dividing by the mass of the silica to determine the mole number of surface acid sites per mass of silica. All titrations were carried out at room temperature (22 ± 3 C). All solutions were made up with 18.2 M Ω water. Additionally, all volumes are based on calibrated pipettes. For ease, the NaHCO_3 , Na_2CO_3 and NaOH bases used to react with the acidic surface functionalities are denoted as reaction bases, and the base used for titration is denoted as the titrator base.

8.2.6 Preparation of polyelectrolyte multilayers on silica

The concentration of polyelectrolytes used for multilayer construction was done in slight excess of the pre-determined number of moles of silica acid sites as determined by boehm titration and chemisorption data. The layer-by-layer coating was done by alternately dipping the silica material in the solution of both cationic and anionic polymers until the desired layer is achieved at the surface. In a typical experiment, Cationic PDDA solution (8mg/mL, pH 7.0-8.0) in 0.1N NaCl was used to soak mesoporous silica SBA-15. After standing for 24 hours, the silica particles were filtered and rinsed three times with Millipore water. It was then freeze-dried and subsequently dried in a vacuum at 45 °C to recover cationic PDDA coated silica particles. For the second coating with anionic polymer, 8mg/mL of PDE (dissolved with mole equivalence of sodium hydroxide) was used to soak

cationic silica particles from the first coating. Similar steps were repeated in order to recover the negatively charged silica particles. In this way, a bilayer consisting first positively charged polymer and second negatively charged polymer outer layer is achieved on the surface of silica. The entire procedure for layer-by-layer coating was repeated for polymer modified with hydrophobe (PDEH).

8.2.7 Cd(II) adsorption on modified Silica adsorbent

The novel silica Adsorbent SBA-15-PDDA-PDE (50 mg) was contacted into an aqueous toxic Cd(II) solution (20 mL) of specific concentration of 20, 40 and 60 mg L⁻¹ and then stirred for a period of 5, 10, 20, 30, 60 and 120 min at 298 K. The filtrate after each time interval was analyzed by AAS to determine the Cd(II) uptake. Using an initial Cd(II) concentration of 50 mg L⁻¹, the pH dependency of the adsorption process was evaluated at 298 K, while the experiments at 298, 313 and 333 K were performed to determine the kinetic and thermodynamic parameters. **Similar procedure was carried out** for the adsorption works on methylene blue and eriochrome black T dyes. For monitoring the concentration of dye left in the filtrate, the absorbance was measured at 665 nm for Methylene blue and 503 nm for EBT on Photo lab 6600 UV-vis spectrophotometer. The readings were recorded in triplicate and the average of the values was taken. The percentage removal of pollutant species is computed using equations 1 and 2:

$$q_t = \frac{(C_i - C_t)V}{W} \quad (1)$$

$$\%Co^{2+}uptake = \left(\frac{C_i - C_t}{C_i} \right) \times 100 \quad (2)$$

where, C_i and C_t represent the initial and final concentrations (mg L^{-1}), respectively; V and W denote the solution volume (L) and weight of the resin (g). The adsorption capacity at various times and equilibrium are denoted as q_t and q_e , respectively, where in the case of q_e , the equilibrium concentration C_e is used instead of C_t . The experiments were run in duplicate and each analysis were triplicated. The average value was reported.

8.3 Results and Discussion

8.3.1 Preparation of polyelectrolyte multilayers on silica

The synthesis of mesoporous silica particles progressed through a templated route using a well-known triblock copolymer pluronic 123 as structure directing agent. The pore channels of the as-synthesized material were liberated after calcination at $600\text{ }^\circ\text{C}$ to obtain ordered porous silica material SBA-15 (Figure 8.1) [287]. The surface of silica has been confirmed to be acidic by Boehm titrations [288] and chemisorption data. And the number of moles of acid sites per gram of silica as determined by Boehm titration and chemisorption measurements are 1.31 mmol/g and 1.224 mmol/g respectively. The construction of polyelectrolyte layers was done with a concentration of polyelectrolyte in excess of the predetermined moles of surface acid sites. The modification of surface of silica particles was performed using the method of consecutive complementary charged layers adsorption in the presence of sodium chloride salt to enhance the charge density on the silica surface [289] and ion exchange process. PDDA used here is frequently used as a linear polycation for electrostatic LBL preparation of multilayer films. The PDE prepared in this work with all the basic centers preserved impacted the anionic outer surface to the

silica particles. The silica surface modification was first followed by Zeta Potential (Z_P) measurements to verify the surface charge.

Taking into account that the as-synthesized silica particles are positively charged due to the acidic medium of the synthesis route, it was first treated with sodium hydroxide of 0.050N prior its use for multilayer experiment. This renders the surface negatively charged and is used subsequently for the multilayer deposition. The incoming polycation may then undergo electrostatic interaction (adsorption) on the silica surface. When negatively charged PDE/PDEH is contacted with the positive end silica particles, further electrostatic adsorption between the silica surface and negative function on the PDE/PDEH (COO⁻ and basic Nitrogen) creates additional layer of negative charges on the surface of silica (Figure 8.2). The outer layer of modified silica particles is expected to retain all three original functionalities of aspartic acid and as such it can provide a multiple chelating motifs of unquenched nitrogen valence and carboxylates having differing basicity constants [137] to remove toxic metal ions and organic pollutants from contaminated sources.

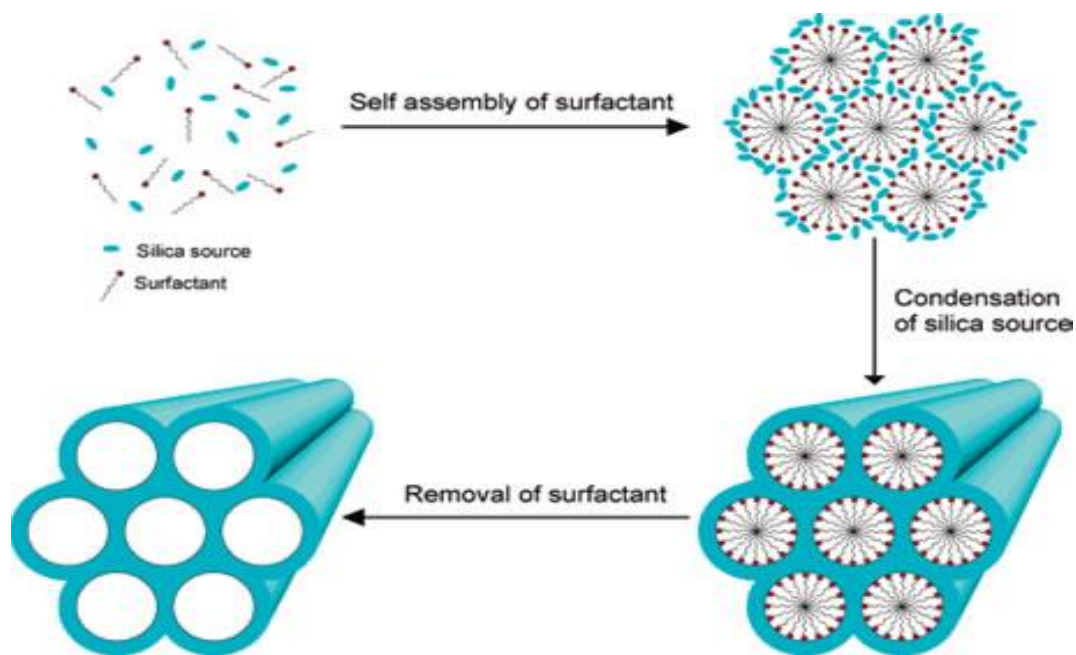


Figure 8.1 **Synthesis of mesoporous materials through cooperative self-assembly.**
(Reproduced from Canadian J Chem 90:1015–1031 (2012))

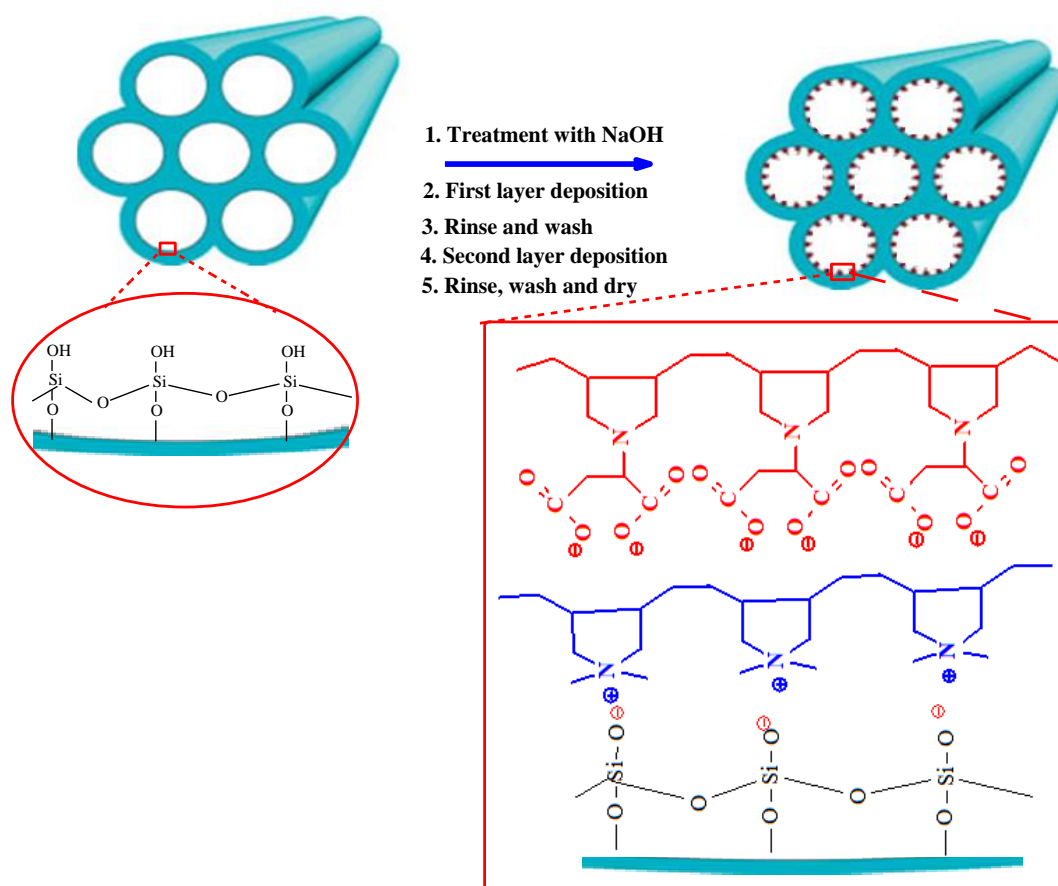


Figure 8.2 Modification scheme of SBA 15 mesoporous-silica with PDDA and PDE

8.3.2 Zeta Potential

Zeta potential (Z_p) values for all the synthesized silica materials are displayed in Table 8.1. Beginning with -13.02 mV in SBA-15 for the starting silica material, the Z_p changes to 13.86 mV in SBA-15-PDDA after modification with PDDA. Additional layer of the poly-di-anionic electrolyte (PDE) reverses the charge with a Z_p of -18.16 mV for SBA-15-PDDA-PDE. Similar trend was observed for PDEH. This is an indication of the success of the multilayer polyelectrolyte deposition on the surface of silica SBA-15.

Table 8.1 Pore diameters (D_p), pore volumes (P_v), surface areas (S_{BET}) and zeta potentials (Z_p) for the mesoporous SBA-15 and its surface modified forms

Silica	D_p	P_v	S_{BET}	Z_p
	(Å)	(cm ³ /g)	(m ² /g)	(mV)
SBA-15	58.1	0.60	694	-13.02
SBA-15-PDDA	70.4	0.54	595	13.86
SBA-15-PDDA-PDE	93.2	0.39	456	-18.16
SBA-15-PDDA-PDEH	71.7	0.51	605	-17.56

8.3.3 ²⁹Si CP-MAS NMR Experiments

In order to determine the nature of interaction between the layers and silica surface, the modification of SBA-15 materials was examined with solid state NMR spectroscopy. For ¹³C NMR, no resonance was observed for both original and modified SBA-15. This is probably due to low amount of polyelectrolyte layers on the silica material as only two layers were deposited. The ²⁹Si MAS NMR spectroscopy became the only suitable method for probing the surface species of Silica and the Si coordination environments in the modified silica material. Without cross polarization, the silica surface chemical species can be separated into three: the siloxane group (Q₄) forming the bulk of the material; the single hydroxyl silanol group (Q₃); and the geminal hydroxyl silanol group (Q₂) [290–293]. Their resonances with respect to TMS appear at around -91, -101 and -110 ppm for Q₂, Q₃ and Q₄ respectively [290]. However, in cross polarization experiment, contributions from

atoms of silicon deep in the lattice are highly improbable because of their long Si-H distances [294]. Interestingly, the CP MAS spectrum for our unmodified SBA-15 material shows conspicuously a resonance at about -100 ppm which corresponds to Q₃ (Figure 8.3). It has been established that with cross polarization the whole siloxane group is not observed (because the proton is too far from these silicon sites) and only a fraction of geminal hydroxyl silanol sites can be deduced from the evolution of the spectra versus contact time [295]. In the case of our SBA-15 material, the absence of resonance corresponding to Q₂ may mean that this sample contains a very small number of germinal hydroxyl silanol groups [293]. On moving to the modified sample SBA-15-PDDA (after deposition of one layer of PDDA on SBA-15), there is gradual evolution of Q₄ resonance indicated by a shoulder at 110 ppm (Figure 8.3). This becomes more distinct after the second layer deposition of PDE in SBA-15-PDDA-PDE. The separation of Q₄ resonance in CP MAS experiment which corresponds to the siloxane group is a strong evidence of some sort of bonding interaction between the layers and siloxane group. By extension, the emergence of Q₄ and the significant change of the intensity of the Q₃ signal [296,297] with respect to its signal in the spectrum of unmodified SBA-15 confirm that the multilayer formation is successful and that it is achieved through chemical bonds [298].

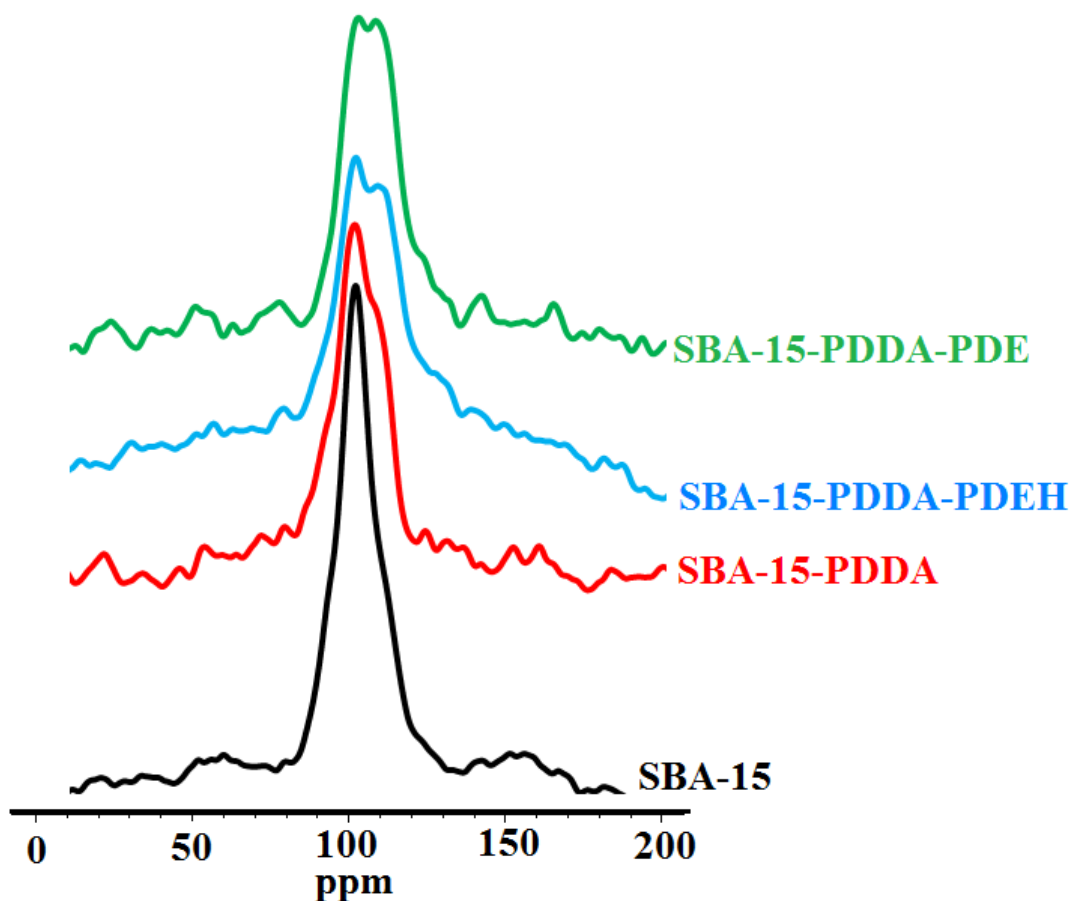


Figure 8.3 ^{29}Si CP-MAS NMR spectra of the SBA-15 and its modified forms: SBA-15-PDDA and SBA-15-PDDA-PDE

8.3.4 Scanning electron microscopy (SEM) Study

Figure 8.4 show the SEM images of silica materials before and after modification by LBL deposition. The shape of SBA-15 particles in Figure 8.4(a) is hexagonal due to the method of synthesis [285,287] and the surface of individual silica particle is smooth. In Figure 8.4(b), there is a clear evidence for the successful deposition of first layer of PDDA on the surface of SBA-15 particles as the surface has become rough with occurrence of tiny

particles on the surface. Such a rough surface subsequently serves as an anchor for further LbL deposition. As shown in Figure 8.4(c), after the deposition of second LbL cationic PDE layer, the surface roughness has increased and the growing surface particles has become more obvious. This completes the multilayer formation on the surface of silica SBA-15 for our application. Figure 8.4(d) is 200 nm deeper view of Figure 8.4(c) for better visualization of the particles. It is expected that this growth of polyelectrolyte charges on the surface of the mesoporous silica will enhance its performance in toxic metal ions capture.

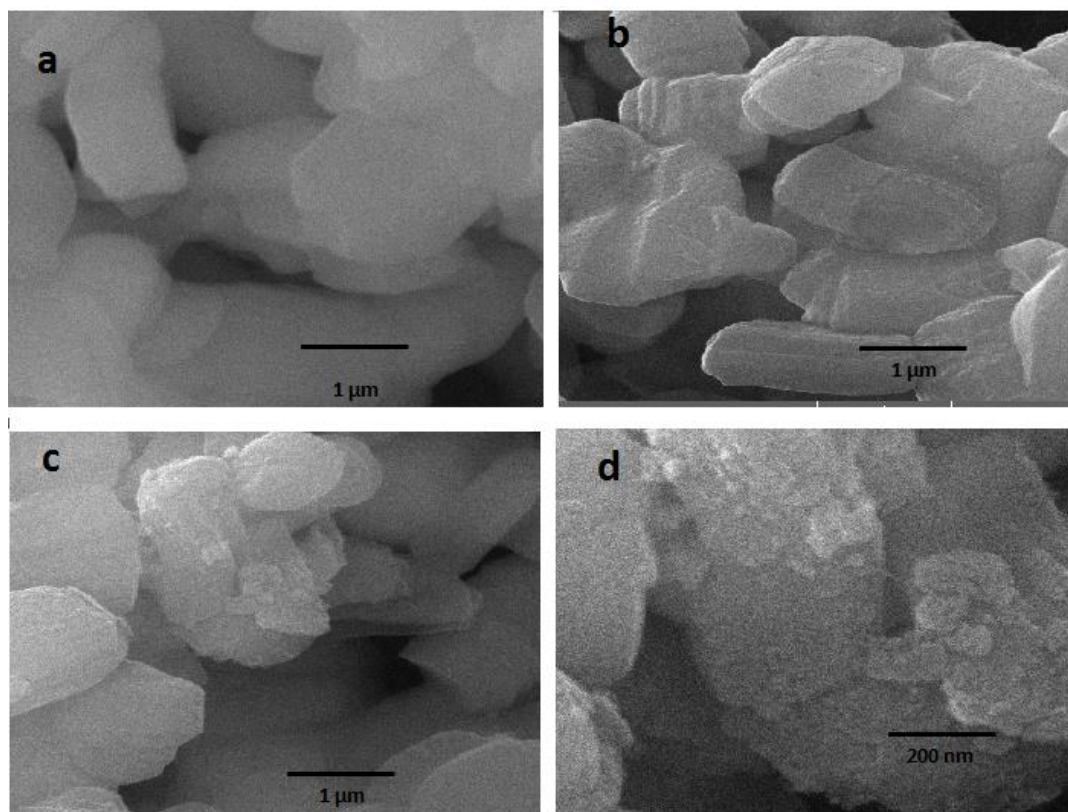


Figure 8.4 SEM images of the SBA-15 and its modified forms: (a) as-fabricated; (b) after first LbL deposition of PDDA; (c) after second LbL deposition of PDE on (b); and (d) 200 nm view of the silica particles in (c).

8.3.5 Atomic Force Microscopy (AFM) Examination

Figure 8.5 shows the AFM surface images of as-synthesized SBA-15 and after the deposition of polyelectrolyte layers of PDDA/PDE. The surface of the as-synthesized silica is smooth as can be seen from Figure 8.5a. which after the deposition of two layers of alternate cationic and anionic polyelectrolyte becomes rough. The multilayer conformation may be influenced by the method of surface modification and the nature of polyelectrolytes [279].

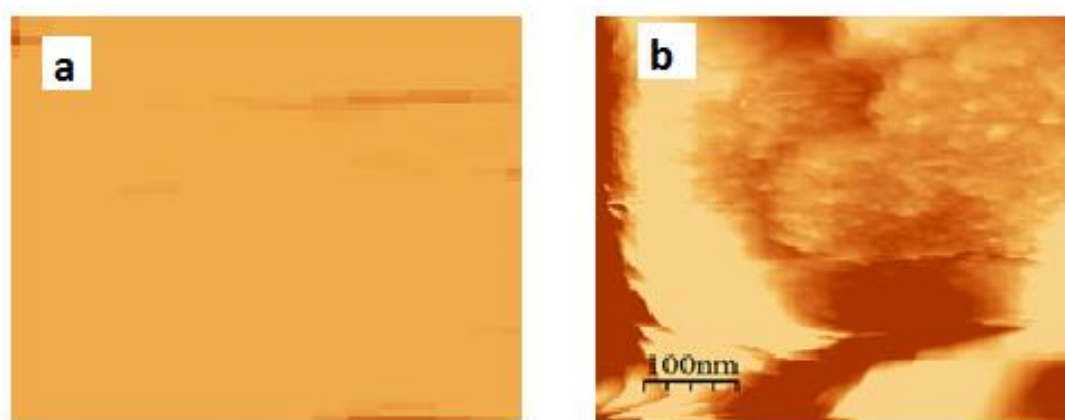


Figure 8.5 AFM tapping mode images of (a) as-synthesized SBA-15 material; (b) SBA-15 material after LBL deposition of PDDA/PDE

8.3.6 Nitrogen adsorption-desorption

The Nitrogen adsorption-desorption isotherms acquired at 77K for SBA-15 and its modified forms are shown in Figure 8.6. The shape of the isotherms is irreversible type-IV, according to the IUPAC classification which includes most of the mesoporous materials. The H1-type hysteresis loop, typical of SBA-15 materials, is also clearly evident,

and the sharp steep in the adsorption branch of the isotherms indicates narrow pore size distribution which is typical of a well ordered mesostructured material.

After the modification with first layer in SBA-15-PDDA, there is no significant change in the shape of the hysteresis loop except in the starting and closing points where there is a slight change in relative higher pressure. This is an indication of the widening of the mesopores due to deposition of cationic PDDA layer on the pore wall. This trend continues in SBA-15-PDDA-PDE as additional layer of anionic PDE is added. The P/P^0 position of the inflexion points is related to the diameter in the mesoporous range. Interestingly, the shape of the hysteresis loop for SBA-15-PDDA-PDE is somewhat divided into two cavities with a narrow path (almost like a forced closure) between them. This seems to have occurred in the desorption branch and it could be due to the narrowing of the mesopores in some regions as the additional layer of PDE is deposited on the pore wall. It could also be due to the pore network effects as larger pores are emptied into the smaller pores during desorption [299]. The evidence of pore narrowing suggests that the deposited layers may be inside the pores rather than on the surface. The BJH pore size distributions of the SBA-15 and its modified forms is shown in Figure 8.7. It can be seen that narrow pore size distribution is obtained in all cases even after modification of SBA-15 but with a decreasing pore volumes as the polyelectrolytes layers are attached to the pore walls. The distribution of pore sizes for all samples is in the mesoporous range.

Other textural properties are shown in Table 8.1. The BET surface area shrinks from 694 m^2/g for SBA-15 to 456 m^2/g in SBA-15-PDDA-PDE after the second layer on SBA-15. This is due to the filling of the pore and the coverage of the surface of the support by the

charge alternating polyelectrolytes PDDA and PDE. The pore volume shows the same trend as the area while the pore diameter expands as expected (Table 8.1).

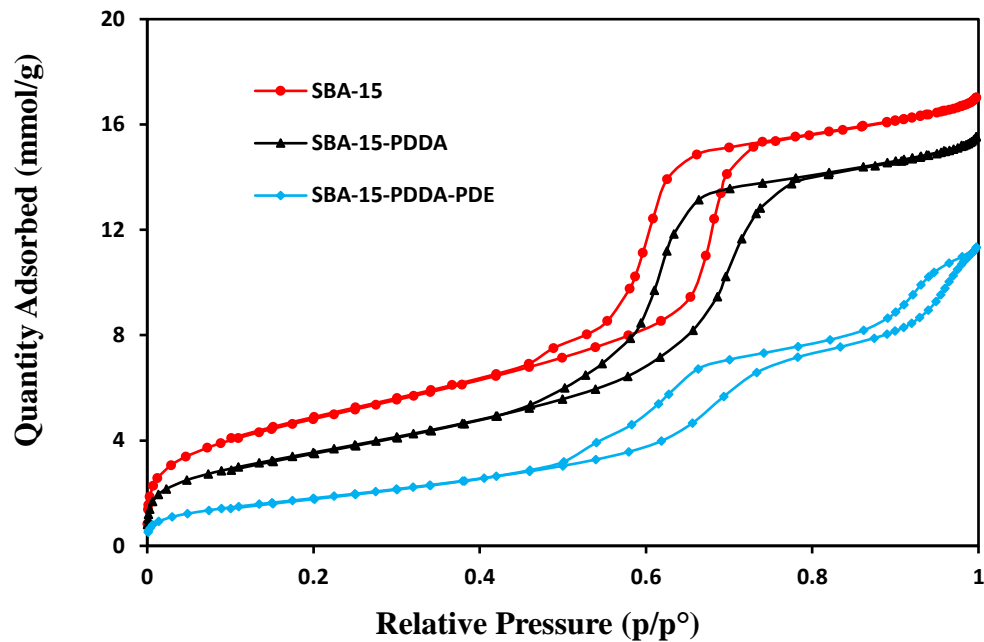


Figure 8.6 Nitrogen adsorption–desorption isotherms of SBA-15 and LBL-modified SBA-15

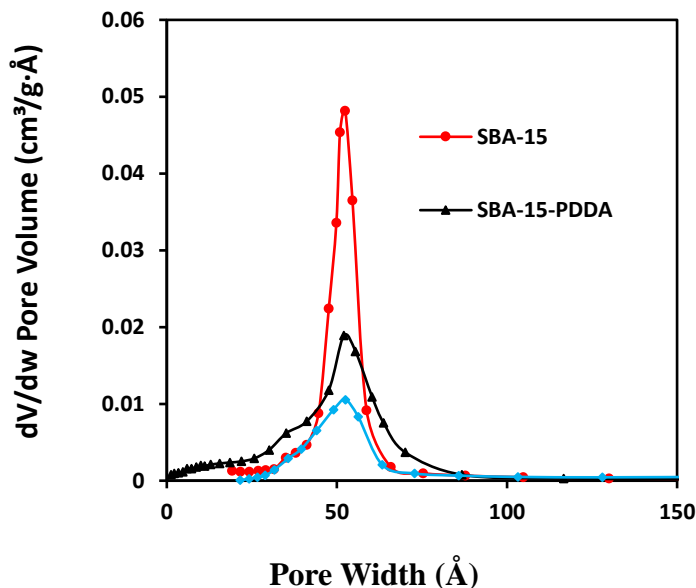


Figure 8.7 BJH desorption pore size distributions of SBA-15 and LBL-modified SBA-15

8.3.7 Thermo-gravimetric Analysis (TGA)

The polyelectrolyte uptake of silica materials was monitored by TG measurements as shown in Figure 8.8. The TG curve for the original SBA-15 exhibits two distinct weight loss regions: i) a dramatic weight loss of about 10% from room temperature up to 80 °C which is attributed to desorption of physically adsorbed water molecules from silica surface [300] and ii) a slow gradual weight loss of about 7% from 80 – 790 °C attributed to silanol condensation [301]. The residual mass at 790 °C is 83%. The TGA curve for the SBA-15-PDDA with a layer of PDDA differs significantly from that for the unmodified SBA-15. While the initial weight loss due to removal of water molecules is significantly extended beyond 25 – 80 °C range, there is additional weight loss region between 100 - 430 °C. which corresponds to the degradation temperature of PDDA layer on silica surface. The residual mass at 790 °C for SBA-15-PDDA is 79 %. Thermal profile for SBA-15-PDDA-

PDE also show additional curve convolution in the temperature range leading up to 600 °C. The complexity of SBA-15-PDDA-PDE is understood to be due to the additional layer of anionic PDE and the multilayer polyelectrolyte interaction. The residual mass at 790 °C for SBA-15-PDDA-PDE is 77 %. Starting from the unmodified SBA-15, the decreasing residual weight percent of 83, 79 and 77% corresponding to SBA-15, SBA-15-PDDA, and SBA-15-PDDA-PDE, respectively, is an indication of the fraction of the polyelectrolyte layer on the surface of original SBA-15 which are burnt off. This is a direct gravimetric evidence of the success of the multilayer formation as the decreasing residual silicas correspond to increasing polymer incorporation as the multilayer formation progresses.

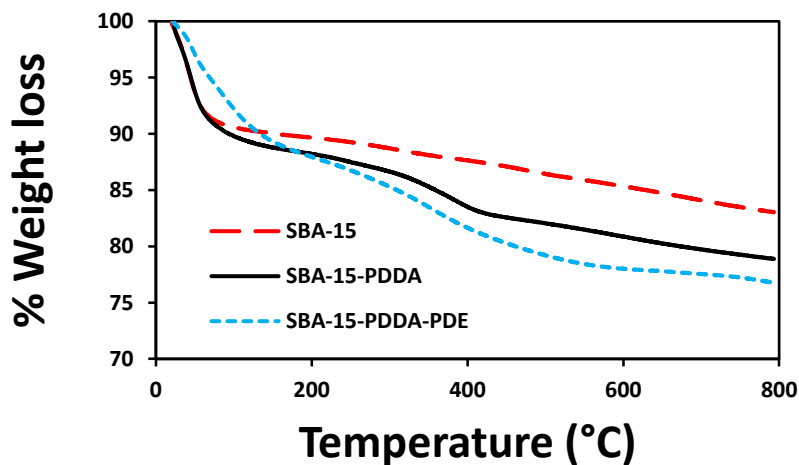


Figure 8.8 TGA profiles of SBA-15 and LBL-modified SBA-15

8.3.8 Initial concentration (C_i) versus adsorption capacity

Figure 8.9 displays the effect of Cd(II) concentrations on its removal by SBA-15-PDDA-PDE. For a C_i value of 20 mg L^{-1} , it can be seen that the adsorption capacity, q_t , has two separate parts: the upward slope that reaches the peak rapidly in about 0.5hr of contact time and the flat section of the plateau where the equilibrium is established slowly. Moving to the C_i value of 40 mg L^{-1} , the initial adsorption capacity increased with time; the entire curve follows the same trend as in the case of 20 mg L^{-1} initial concentration. Similar trend is observed for 60 mg L^{-1} concentrations of cadmium ions as depicted in Figure 8.9. The increasing concentration gradient gives the required driving force to overcome the mass transfer effects of Cd(II) ions between the aqueous and solid phases [241,242]. The effect of the initial concentration of Cd(II) in the range 20 to 60 mg L^{-1} on the equilibrium adsorption capacity, q_e , was examined; it is found to increase with increasing concentrations (Figure 8.10). The performance of this adsorbent as a function of initial concentration of Cd(II) has been compared with pure SBA-15 as shown in Table 8.2. It is obvious from Table 8.2 that unmodified SBA-15 could only take up about 4% of the initial concentration of 60 mg L^{-1} Cd (II) after a contact time of 12 hours. This dramatically increased to 99% with modified SBA-15-PDDA-PDE adsorbent for the same experimental conditions. Higher concentrations were also tested and the results are quite promising as shown in Table 8.2. The adsorption capacity in mg per gram of the adsorbent also shows similar trend.

For the silica particles modified by polymer with hydrophobe (SBA-15-PDDA-PDEH) in order to interact with organic dyes, its dual cation/anionic performance in the removal of Methylene Blue and Eriochrome Black T is depicted in table 8.3. Starting with 50 mg, the

unmodified SBA-15 material show minimal uptake of the organic dyes (2.5% and 1.0% for MB and EBT respectively). After modification, the hybrid adsorbent show dramatic performance for 3 mg L⁻¹ of both cationic and anionic dye pollutants (100% for MB and 99% for EBT). Higher concentrations of the organic dyes up till 30 mg L⁻¹ were also tested with impressive results. The dual cationic/anionic activity of this hybrid sorbent underscores its great potential in wastewater remediation.

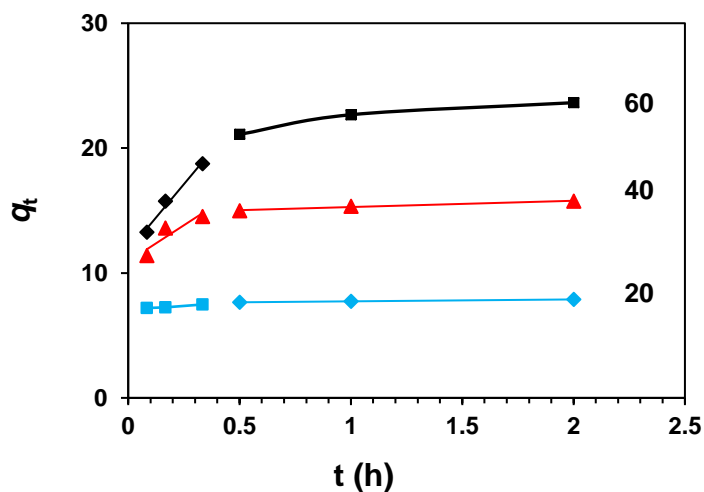


Figure 8.9 Effect of initial Cd(II) concentrations on Cd(II) adsorption capacity

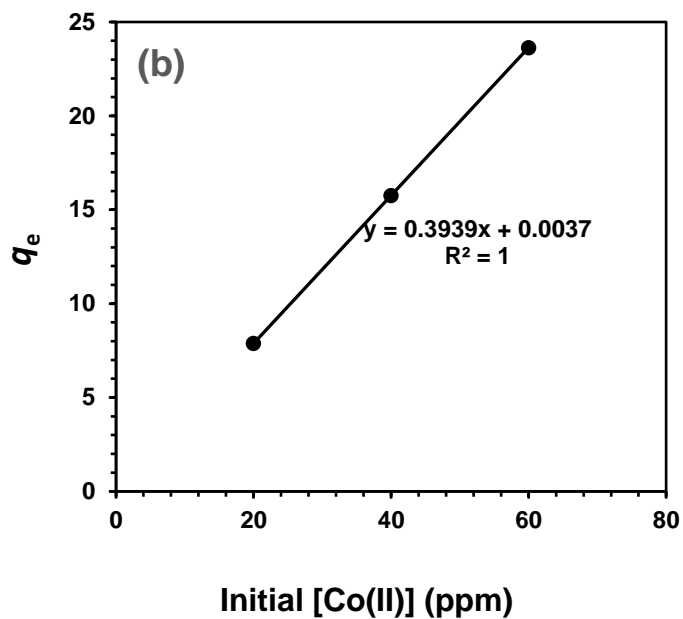


Figure 8.10 Effect of initial concentration of Cd(II) on the adsorption capacity

Table 8.2 Comparison of Cd(II) adsorption performance of SBA-15/SBA-15-PDDA-PDE for 12hrs contact time with 50mg adsorbent

Sample	C_o (mg L^{-1})	Cd(II) uptake (%)	q_t (mg g^{-1})
SBA-15	60	3.52 ± 0.21	0.85 ± 0.05
SBA-15-PDDA-PDE	5	100 ± 0.05	2.00 ± 0.001
	60	98.5 ± 0.05	23.6 ± 0.01
	300	85.6 ± 0.04	114 ± 0.06
	1000	80.0 ± 0.06	320 ± 0.06

Table 8.3 Dual Cation/anionic Performance of SBA-15/SBA-15-PDDA-PDEH for Organic Pollutants

Sample	C_0 (mg L ⁻¹)	MB uptake (%)	EBT uptake (%)
SBA-15	3	2.50	1.00
SBA-15-PDDA-PDEH	3	100	99.1
	30	99.2	97.3

8.3.9 Energy paramters

The adsorption energy parameters have been computed from experimental data using the well-known kinetic and thermodynamic equations as presented in Table 8.4. The activation energy and thermodynamic energy plots are depicted in Figure 8.11 and the parameters extracted therefrom are displayed in Table 8.5. The energy of activation E_a was determined to be 45.4 kJ mol⁻¹; a negative free energy change, ΔG° , ascertains the favorability of the adsorption process. The negative ΔH° (-64.3 kJ mol⁻¹) is an indication of the exothermic nature of the adsorption as corroborated by the fact that as the temperature rises from 298 to 333 K, the ΔG° becomes less negative. The negative entropy change ΔS° of -189 J mol⁻¹ K⁻¹ suggests a decreasing randomness at solid-solution interphase during the adsorption process.

Table 8.4 Mathematical equations for all the models used in this study

Name	Linear Form	Plot	Calculated Coefficient
Equilibrium Isotherm Models			
Langmuir	$\frac{C_e}{q_e} = \frac{C_e}{Q_m} + \frac{1}{Q_m b}$	C_e/q_e vs. C_e	$Q_m = 1/\text{slope}$; $b = \text{slope}/\text{intercept}$
Freundlich	$\log q_e = \log k_f + \frac{1}{n} \log C_e$	$\log q_e$ vs. $\log C_e$	$n = 1/\text{slope}$; $k_F = 10^{\text{intercept}}$
Tempkin	$q_e = \frac{RT}{b} \ln A + \frac{RT}{b} \ln C_e$	q_e vs. $\ln C_e$	$b = (RT/\text{slope})$; $A = \exp(\text{intercept}/\text{slope})$
Reaction-based Kinetic Models			
Lagergren Pseudo-first order	$\log(q_e - q_t) = \log q_e - \left(\frac{k_1 t}{2.303}\right)$	$\log(q_e - q_t)$ vs. t	$k_1 = -2.303 \times \text{slope}$; $q_e = 10^{\text{intercept}}$

Pseudo-second order	$\frac{t}{q_t} = \frac{1}{k_2 q_e^2} + \frac{t}{q_e}$	t/q_t vs. t	$q_e = 1/\text{slope};$ $k_2 = \text{slope}^2/\text{intercept}$
Kinetic and Thermodynamic Equations			
Activation Energy	$\ln k_2 = -\frac{E_a}{RT} + \text{constant}$	$\ln k_2$ vs. $1/T$	Slope = $-\frac{E_a}{R}$
Enthalpy, Entropy and Free Energy Changes	$\ln\left(\frac{q_e}{C_e}\right) = -\frac{\Delta H}{RT} + \frac{\Delta S}{R}$	$\ln\left(\frac{q_e}{C_e}\right)$ vs. $1/T$	Slope = $-\frac{\Delta H}{R}$ Intercept = $\frac{\Delta S}{R}$ $\Delta G = \Delta H - T\Delta S$
Average Percentage Error	<p>APE (%)</p> $= \left\{ \frac{\sum_{i=1}^N ((q_e)_{\text{experimental}} - (q_e)_{\text{predicted}}) / (q_e)_{\text{experimental}} }{N} \right\} \times 100$ <p>Where N is the number of experimental data</p>		

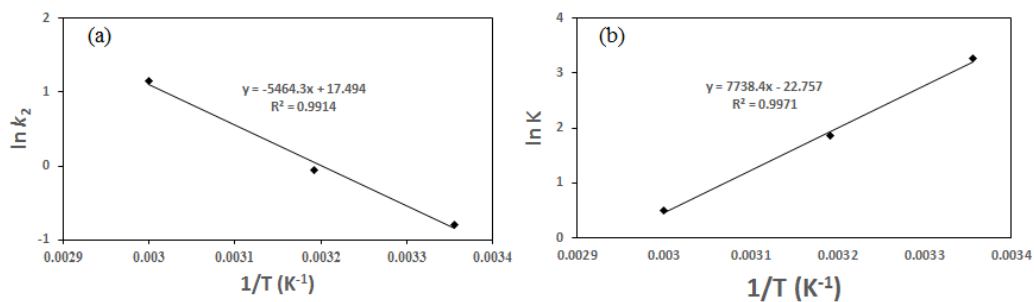


Figure 8.11 (a) Activation (b) Thermodynamic Energy plots for the hybrid adsorbent

Table 8.5 Thermodynamic and kinetic parameters for Cd(II) adsorption

Temp (K)	ΔG° (kJ mol ⁻¹)	ΔH° (kJ mol ⁻¹)	ΔS° (J mol ⁻¹ K ⁻¹)	E_a (kJ mol ⁻¹)
298	-7.95			
313	-5.06	-64.3	-189	45.4
333	-1.28			

8.3.10 Data analyses

Data from the experiments have been utilized to identify the best-fit kinetic model from some of the established many parameter equations. These equation parameters which could provide insight into the surface properties, the affinity of the adsorbent and even the adsorption mechanism [243] are listed in Table 8.4.

a. Isotherm models

The two-parameter isotherm models used in this study are Langmuir [244], Freundlich [170] and Temkin [171]. Isotherm models usually shed light on the nature of adsorption sites as well as its favorability [242].

Experimental data obtained were each plugged onto the linear forms of Langmuir, Freundlich and Temkin model equations (Table 8.4). Their various plots are shown in Figure 8.12 with the parameters obtained from them displayed in Table 8.6. Among the three models explored, Freundlich isotherm showed the best fit with $R^2 = 1.000$ and least average percentage error (APE%) of 0.1% (Table 8.5). This is suggesting that the adsorption of Cd(II) on the SBA-15-PDDA-PDE surface is multilayer as well as linear with the value of $1/nF$ approaching unity (0.98) [242]. Between the other two linear isotherm models used, Langmuir fits the experimental data better than Temkin (Table 8.6). With $R^2 = 0.9996$ and an APE of 2.88% for Langmuir, there is a good chance that some of the adsorption sites on the surface of the multilayered adsorbent are homogenous and that the adsorption process is not exclusively multilayer. The good fit of the Langmuir model has allowed us to estimate the monolayer adsorption capacity Q_m to be 833 mg g⁻¹. The dimensionless equilibrium parameter R_L values falling in the range 0.97 - 0.99 (approaching unity) also suggest that adsorption is a linear process [245]. The comparable

regression coefficients between Freundlich and Langmuir models suggests the possibility of a generalized Langmuir-Freundlich model that allows us to estimate the monolayer adsorption capacity at high adsorbate concentration while reverting to Freundlich's form at low adsorbate concentration [246,302]. The current hybrid adsorbent's Langmuir adsorption capacity for Cd(II) is compared with the values for other types of adsorbents used for Cd(II) [303–309] in Table 8.7. It is obvious that our current sorbent shows superior performance.

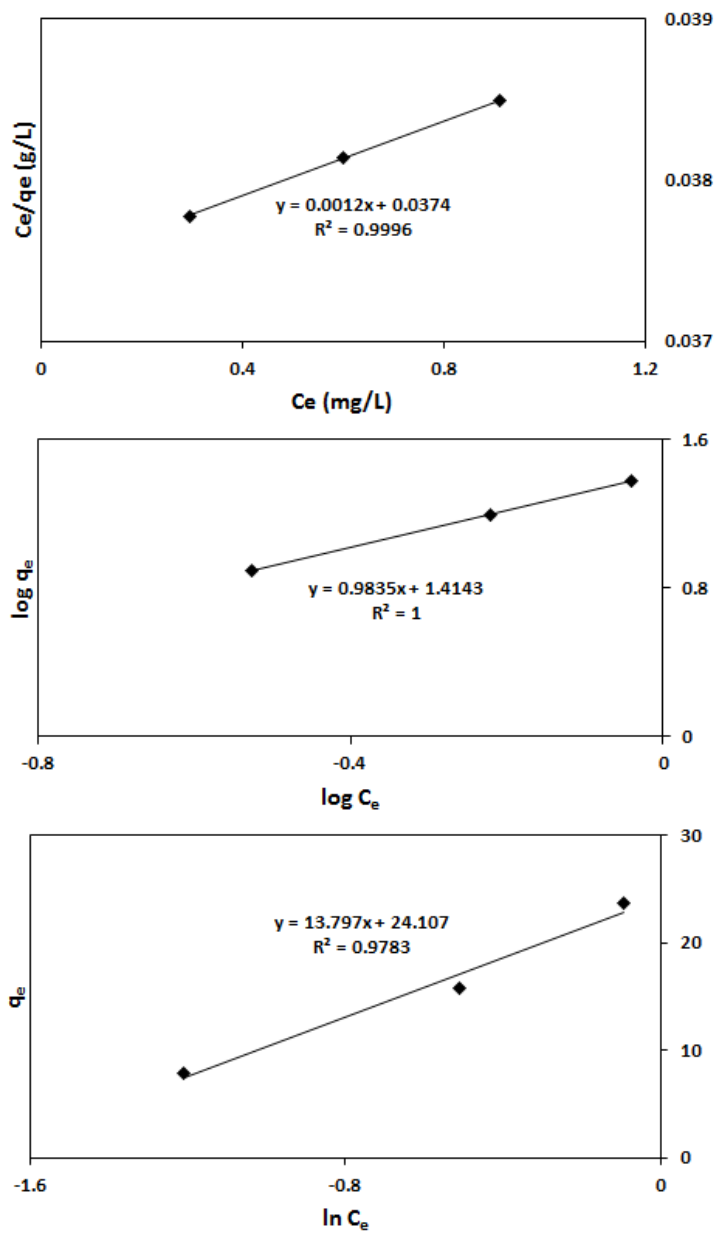


Figure 8.12 (a) Langmuir (b) Freundlich and (c) Temkin adsorption isotherms for Cd(II) adsorption

Table 8.6 Isotherm parameters for Cd(II) adsorption

Isotherms	Isotherm Parameters		R^2	APE (%)
Langmuir	Q_m	833 mg g ⁻¹	0.9996	2.88
	b	0.0321 L mg ⁻¹		
Freundlich	k_f	26.0	1.000	0.091
	n	1.02		
Temkin	A	5.74 L g ⁻¹	0.9783	6.06
	b	180 J mol ⁻¹		

Table 8.7 Comparison of the adsorption capacity of the current adsorbent with that of various adsorbents for Cd(II) at 298 K

Adsorbent	Adsorption Capacity q_m (mg/g)	References
MgO-SiO ₂	94.05 at pH ~7	[303]
Agricultural Waste Rice Polish	9.72 at pH 8.6	[304]
Zinc oxide	387 at pH 5.5	[305]
Aluminum oxide (Al ₂ O ₃)	83.33 at pH 5.0	[306]
Maghemite	94.33 at pH 6.0	[310]
Magnetite nanorods (Fe ₃ O ₄)	88.39 at pH 5.5	[308]
Shellac coated iron oxide nanoparticle	18.80 at pH 8.0	[309]
Present hybrid Silica sorbent	833 at pH 6.0	This study

b. Adsorption kinetics: Reaction-based kinetic models

The nature of the interfacial interaction between solid and solution during the metal ion adsorption can be described by kinetic models based on the rate-controlling mechanism involving chemical reaction, mass transfer and diffusion control systems. Lagergren first-order [255] and Pseudo-second-order [163] models have been used to describe the Cd(II) adsorption on this adsorbent. The equations and their parameters are displayed in Table 8.4. Lagergren pseudo first-order and second-order are used when the rate of occupation

of the binding sites is proportional to the number of unoccupied sites on the resin and to its square, respectively [166].

The plots of these kinetic models are shown in Figure 8.13 and the parameters extracted from the two kinetic models are given in Table 8.8. The data fit the second-order model, as seen by the greater closeness of R^2 values to unity (0.9998–1.000) and the better agreement between $q_{e,exp}$ and $q_{e,cal}$. In fact, the average percentage error (Table 8.8) between the experimental and calculated values also corroborated this claim as pseudo 1st order prediction has about 71% error in comparison with Pseudo 2nd order prediction with only a minimal 2% error. The better fit of Pseudo 2nd order kinetic suggests that the adsorption process might be chemical in nature [163,210].

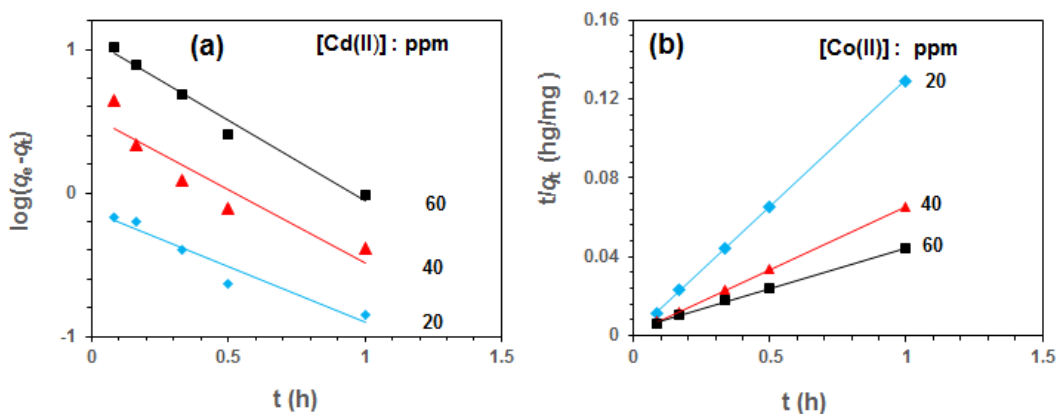


Figure 8.13 (a) Lagergren first-order plots and (b) Pseudo second-order plots at 298 K for various initial concentrations

Table 8.8 Adsorption kinetic parameters for pseudo first and second order models

Conc (ppm)	$q_{e,exp}$ (mg g ⁻¹)	Pseudo 1st order			2nd order			
		k_1 (h ⁻¹)	$(q_{e,cal})^a$ (mg g ⁻¹)	R^2	$(q_{e,cal})^b$ (mg g ⁻¹)	k_2 (g mg ⁻¹ h ⁻¹)	h^c (mg g ⁻¹ h ⁻¹)	R^2
20	7.88	1.78	1.34	0.9352	7.92	7.58	4.76×10 ²	0.9999
40	15.8	2.36	3.46	0.8795	16.0	1.86	4.76×10 ²	1.000
60	23.6	2.60	11.7	0.9797	24.7	0.46	2.78×10 ²	0.9998

^a APE (%) for $q_{e,cal}$ in Pseudo 1st order = 70.5

^b APE (%) for $q_{e,cal}$ in Pseudo 2nd order = 2.18

^c Initial adsorption rate, $h = k_2 q_e^2$

8.4 Conclusion

Here, we report the use of aspartic acid-based polydianionic Polyelectrolyte (PDE) synthesized in our laboratory for the multilayer formation on mesoporous silica substrate. The synthesis approach ensured that the integrity of all the original amino acid functionalities in aspartic acid are preserved. The electrostatic layer adsorption was achieved by LBL alternate deposition of PDDA and PDE. Application of the hybrid polymer-silica adsorbent on Cd(II) adsorption from aqueous medium gave a very impressive adsorption performance with a Langmuir monolayer adsorption capacity of 833 mg g⁻¹ which accorded this adsorbent a prestigious place among other adsorbents previously used for Cd(II) removal. Furthermore, hydrophobic modification of the aspartic

acid polymer prior to layer-by-layer coating was equally examined with a very promising result in the simultaneous removal of both cationic and anionic dye pollutants.

References

- [1] M.F. Hamoda, Water strategies and potential of water reuse in the south Mediterranean countries, *Desalination*. 165 (2004) 31–41.
doi:10.1016/j.desal.2004.06.004.
- [2] United Nations, ECONOMIC AND SOCIAL COMMISSION FOR WESTERN ASIA (ESCWA), ‘The Role of Desalinated Water in Augmentation of the Water Supply in selected ESCWA Member Countries, New York, 2001.
- [3] K. Frenken, Food and Agriculture Organization of the United Nations., Irrigation in the Middle East Region in figures : AQUASTAT survey - 2008, Food and Agriculture Organization of the United Nations, 2009.
<http://www.fao.org/docrep/012/i0936e/i0936e00.htm> (accessed March 4, 2017).
- [4] US Department of the Interior Bureau of Reclamation and Sandia National Laboratories, Desalination and Water Purification Technology Roadmap, *Water Purification Res. Dev. Progr.* 95 (2003) 1–83.
- [5] U.-S.A.B. Council, Public-Private Agreements Upgrade Saudi Water Infrastructure, *US-Saudi Bus. Br.* (2010) 9–10.
- [6] K. Kadirvelu, Removal of heavy metals from industrial wastewaters by adsorption onto activated carbon prepared from an agricultural solid waste, *Bioresour. Technol.* 76 (2001) 63–65. doi:10.1016/S0960-8524(00)00072-9.
- [7] W. Wirojanagud, N. Tantemsapya, P. Tantriratna, Precipitation of heavy metals by lime mud waste of pulp and paper mill, *Songklanakarin J. Sci. Technol.* 26 (2004)

45–53.

- [8] D. TEI Kavalas., A. Davidis, K. Dermentzis, A. Christoforidis, K. Ouzounis, *Journal of engineering science and technology review.*, Kavala Institute of Technology, 2009. <https://doaj.org/article/0d8996a8dd344cb9ace1b09e1d778b3d> (accessed March 4, 2017).
- [9] A. Wójtowicz, A. Stokłosa, *Polish journal of environmental studies.*, HARD, n.d. <http://journals.indexcopernicus.com/abstract.php?icid=6816> (accessed March 4, 2017).
- [10] T. Bakalár, Milan Búgel and Lucia Gajdošová, Heavy metal removal using reverse osmosis, *Acta Montan. Slovaca.* 14 (2009) 250–253.
- [11] K.A. Matis, N.K. Lazaridis, A.I. Zouboulis, G.P. Gallios, V. Mavrov, A hybrid flotation—microfiltration process for metal ions recovery, *J. Memb. Sci.* 247 (2005) 29–35. doi:10.1016/j.memsci.2004.07.031.
- [12] A.K. Sengupta, *Environmental separation of heavy metals : engineering processes*, Lewis Publishers, 2002. <https://www.crcpress.com/Environmental-Separation-of-Heavy-Metals-Engineering-Processes/SenGupta/p/book/9781566768849> (accessed March 4, 2017).
- [13] E. F. S. Vieira, J. de A. Simoni, C. Airoidi, Interaction of cations with SH-modified silica gel: thermochemical study through calorimetric titration and direct extent of reaction determination, *J. Mater. Chem.* 7 (1997) 2249–2252. doi:10.1039/A704286H.
- [14] L. Mercier, C. Detellier, Preparation, Characterization, and Applications as Heavy Metals Sorbents of Covalently Grafted Thiol Functionalities on the Interlamellar

Surface of Montmorillonite, *Environ. Sci. Technol.* 29 (1995) 1318–1323.
doi:10.1021/es00005a026.

- [15] A. Bibby, L. Mercier, Mercury(II) Ion Adsorption Behavior in Thiol-Functionalized Mesoporous Silica Microspheres, *Chem. Mater.* 14 (2002) 1591–1597. doi:10.1021/cm0112082.
- [16] R.I. Nooney, M. Kalyanaraman, G. Kennedy, E.J. Maginn, Heavy Metal Remediation Using Functionalized Mesoporous Silicas with Controlled Macrostructure, *Langmuir.* 17 (2001) 528–533. doi:10.1021/la000720j.
- [17] Y. Mori, T.J. Pinnavaia, Optimizing organic functionality in mesostructured silica: direct assembly of mercaptopropyl groups in wormhole framework structures, *Chem. Mater.* 13 (2001) 2173–2178.
- [18] A. Stein, B.J. Melde, R.C. Schroden, Hybrid Inorganic–Organic Mesoporous Silicates—Nanoscopic Reactors Coming of Age, *Adv. Mater.* 12 (2000) 1403–1419. doi:10.1002/1521-4095(200010)12:19<1403::AID-ADMA1403>3.0.CO;2-X.
- [19] R.M. Allen-King, P. Grathwohl, W.P. Ball, New modeling paradigms for the sorption of hydrophobic organic chemicals to heterogeneous carbonaceous matter in soils, sediments, and rocks, *Adv. Water Resour.* 25 (2002) 985–1016. doi:10.1016/S0309-1708(02)00045-3.
- [20] S.E. Bailey, T.J. Olin, R.M. Bricka, D.D. Adrian, A review of potentially low-cost sorbents for heavy metals, *Water Res.* 33 (1999) 2469–2479. doi:10.1016/S0043-1354(98)00475-8.
- [21] J.J. Pignatello, B. Xing, Mechanisms of Slow Sorption of Organic Chemicals to

Natural Particles, Environ. Sci. Technol. 30 (1996) 1–11. doi:10.1021/es940683g.

- [22] F. Veglio', F. Beolchini, D. Barba, Experimental Study and Simulation on the Biosorption of Copper(II) in Membrane Reactors: A Preliminary Study, Ind. Eng. Chem. Res. 39 (2000) 2480–2484. doi:10.1021/ie990786d.
- [23] P. Pajunen, Hard chrome bath purification and recovery using ion exchange, Met. Finish. (1987) 40–45.
- [24] G.B. Butler, Cyclopolymerization and Cyclocopolymerization, Marcel Dekker, New York, 1992.
- [25] S. Kudaibergenov, W. Jaeger, A. Laschewsky, Polymeric betaines: Synthesis, characterization, and application, 2006. doi:10.1007/12_078.
- [26] P.K. Singh, V.K. Singh, M. Singh, Zwitterionic polyelectrolytes: A review, E-Polymers. (2007).
- [27] G. Decher, Polyelectrolyte Multilayers, an Overview, in: Multilayer Thin Film., Wiley-VCH Verlag GmbH & Co. KGaA, Weinheim, FRG, n.d.: pp. 1–46. doi:10.1002/3527600574.ch1.
- [28] G. Decher, J.D. Hong, J. Schmitt, Buildup of ultrathin multilayer films by a self-assembly process: III. Consecutively alternating adsorption of anionic and cationic polyelectrolytes on charged surfaces, Thin Solid Films. 210–211 (1992) 831–835. doi:10.1016/0040-6090(92)90417-A.
- [29] G. Decher, J.-D. Hong, Buildup of ultrathin multilayer films by a self-assembly process, 1 consecutive adsorption of anionic and cationic bipolar amphiphiles on charged surfaces, Makromol. Chemie. Macromol. Symp. 46 (1991) 321–327.

doi:10.1002/masy.19910460145.

- [30] S.A. Sukhishvili, E. Kharlampieva, V. Izumrudov, Where Polyelectrolyte Multilayers and Polyelectrolyte Complexes Meet, *Macromolecules*. 39 (2006) 8873–8881. doi:10.1021/ma061617p.
- [31] A.F. Thünemann, M. Müller, H. Dautzenberg, J.-F. Joanny, H. Löwen, Polyelectrolyte Complexes, in: M. Schmidt (Ed.), *Polyelectrolytes with Defin. Mol. Archit. II*, Springer Berlin Heidelberg, Berlin, Heidelberg, 2004: pp. 113–171. doi:10.1007/b11350.
- [32] T. Iwatsubo, S.P. Kusumocahyo, T. Shinbo, Water/ethanol pervaporation performance of asymmetric polyelectrolyte complex membrane constructed by the diffusion of poly(acrylic acid) in chitosan membrane, *J. Appl. Polym. Sci.* 86 (2002) 265–271. doi:10.1002/app.10949.
- [33] S.-G. Kim, G.-T. Lim, J. Jegal, K.-H. Lee, Pervaporation separation of MTBE (methyl tert-butyl ether) and methanol mixtures through polyion complex composite membranes consisting of sodium alginate/chitosan, *J. Memb. Sci.* 174 (2000) 1–15. doi:10.1016/S0376-7388(00)00339-2.
- [34] S. Dumitriu, E. Chornet, Immobilization of Xylanase in Chitosan–Xanthan Hydrogels, *Biotechnol. Prog.* 13 (1997) 539–545. doi:10.1021/bp970059i.
- [35] F. Mi, Drug release from chitosan–alginate complex beads reinforced by a naturally occurring cross-linking agent, *Carbohydr. Polym.* 48 (2002) 61–72. doi:10.1016/S0144-8617(01)00212-0.
- [36] N. Makita, K. Yoshikawa, Proton concentration (pH) switches the higher-order structure of DNA in the presence of spermine, *Biophys. Chem.* 99 (2002) 43–53.

doi:10.1016/S0301-4622(02)00110-2.

- [37] Y. Wang, J.Y. Gao, P.L. Dubin, Protein Separation via Polyelectrolyte Coacervation: Selectivity and Efficiency, *Biotechnol. Prog.* 12 (1996) 356–362. doi:10.1021/bp960013+.
- [38] J. Choi, M.F. Rubner, Influence of the Degree of Ionization on Weak Polyelectrolyte Multilayer Assembly, *Macromolecules.* 38 (2005) 116–124. doi:10.1021/ma048596o.
- [39] M.A.J. Mazumder, N.A.D. Burke, F. Shen, M.A. Potter, H.D.H. Stöver, Core-Cross-Linked Alginate Microcapsules for Cell Encapsulation, *Biomacromolecules.* 10 (2009) 1365–1373. doi:10.1021/bm801330j.
- [40] H.-B. Li, H. Jiang, C.-Y. Wang, C.-M. Duan, Y. Ye, X.-P. Su, Q.-X. Kong, J.-F. Wu, X.-M. Guo, Comparison of two types of alginate microcapsules on stability and biocompatibility in vitro and in vivo, *Biomed. Mater.* 1 (2006) 42. <http://stacks.iop.org/1748-605X/1/i=1/a=007>.
- [41] R. Vinodh, R. Padmavathi, D. Sangeetha, Separation of heavy metals from water samples using anion exchange polymers by adsorption process, *Desalination.* 267 (2011) 267–276. doi:10.1016/j.desal.2010.09.039.
- [42] J. Liu, Y. Ma, Y. Zhang, G. Shao, Novel negatively charged hybrids. 3. Removal of Pb²⁺ from aqueous solution using zwitterionic hybrid polymers as adsorbent, *J. Hazard. Mater.* 173 (2010). doi:10.1016/j.jhazmat.2009.08.097.
- [43] G. Camci-Unal, N.L.B. Pohl, Quantitative determination of heavy metal contaminant complexation by the carbohydrate polymer chitin, *J. Chem. Eng. Data.* 55 (2009) 1117–1121.

- [44] W.U. Hong, J.I.N. Yan, L.U.O. Mingbiao, B.I. Shuping, A simple and sensitive flow-injection on-line preconcentration coupled with hydride generation atomic fluorescence spectrometry for the determination of ultra-trace lead in water, wine, and rice, *Anal. Sci.* 23 (2007) 1109–1112.
- [45] S.J. Central Institute for Labour Protection., M. Khadem, F. Golbabaie, A. Rahimi-Froushan, M.R. Ganjali, P. Norouzi, *International journal of occupational safety and ergonomics : JOSE.*, n.d.
<http://journals.indexcopernicus.com/abstract.php?icid=902575> (accessed March 4, 2017).
- [46] T. Chakrabarty, M. Kumar, V. K., *Chitosan Based Membranes for Separation, Pervaporation and Fuel Cell Applications: Recent Developments*, in: *Biopolymers*, Sciyo, 2010. doi:10.5772/10263.
- [47] S. Chatterjee, S.H. Woo, The removal of nitrate from aqueous solutions by chitosan hydrogel beads, *J. Hazard. Mater.* 164 (2009) 1012–1018.
doi:10.1016/j.jhazmat.2008.09.001.
- [48] R. Yao, F. Meng, L. Zhang, D. Ma, M. Wang, Defluoridation of water using neodymium-modified chitosan, *J. Hazard. Mater.* 165 (2009) 454–460.
doi:10.1016/j.jhazmat.2008.10.052.
- [49] P. MONVISADE, P. SIRIPHANNON, Chitosan intercalated montmorillonite: Preparation, characterization and cationic dye adsorption, *Appl. Clay Sci.* 42 (2009) 427–431. doi:10.1016/j.clay.2008.04.013.
- [50] L. Qi, Z. Xu, Lead sorption from aqueous solutions on chitosan nanoparticles, *Colloids Surfaces A Physicochem. Eng. Asp.* 251 (2004) 183–190.
doi:10.1016/j.colsurfa.2004.10.010.

- [51] M.S. Mauter, M. Elimelech, Environmental Applications of Carbon-Based Nanomaterials, *Environ. Sci. Technol.* 42 (2008) 5843–5859. doi:10.1021/es8006904.
- [52] Y. Tao, L. Ye, J. Pan, Y. Wang, B. Tang, Removal of Pb(II) from aqueous solution on chitosan/TiO₂ hybrid film, *J. Hazard. Mater.* 161 (2009) 718–722. doi:10.1016/j.jhazmat.2008.04.012.
- [53] C.S. Chuang, M.-K. Wang, C.-H. Ko, C.-C. Ou, C.-H. Wu, Removal of benzene and toluene by carbonized bamboo materials modified with TiO₂, *Bioresour. Technol.* 99 (2008) 954–958. doi:10.1016/j.biortech.2007.03.003.
- [54] G.P. Kumar, P.A. Kumar, S. Chakraborty, M. Ray, Uptake and desorption of copper ion using functionalized polymer coated silica gel in aqueous environment, *Sep. Purif. Technol.* 57 (2007) 47–56. doi:10.1016/j.seppur.2007.03.003.
- [55] J. Liu, Y. Ma, T. Xu, G. Shao, Preparation of zwitterionic hybrid polymer and its application for the removal of heavy metal ions from water, *J. Hazard. Mater.* 178 (2010). doi:10.1016/j.jhazmat.2010.02.041.
- [56] W.-J. Liang, C.-P. Wu, C.-Y. Hsu, P.-L. Kuo, Synthesis, characterization, and proton-conducting properties of organic–inorganic hybrid membranes based on polysiloxane zwitterionomer, *J. Polym. Sci. Part A Polym. Chem.* 44 (2006) 3444–3453. doi:10.1002/pola.21455.
- [57] K. Riedelsberger, W. Jaeger, Polymeric aminomethylphosphonic acids - 1. Synthesis and properties in solution, *Des. Monomers Polym.* 1 (1998) 387–407. doi:10.1163/156855598X00233.
- [58] E. Álvarez-Ayuso, Purification of metal electroplating waste waters using zeolites,

Water Res. 37 (2003) 4855–4862. doi:10.1016/j.watres.2003.08.009.

- [59] C. Lu, Y.-L. Chung, K.-F. Chang, Adsorption of trihalomethanes from water with carbon nanotubes, *Water Res.* 39 (2005) 1183–1189. doi:10.1016/j.watres.2004.12.033.
- [60] F.H. Yang, A.J. Lachawiec, R.T. Yang, Adsorption of Spillover Hydrogen Atoms on Single-Wall Carbon Nanotubes, *J. Phys. Chem. B.* 110 (2006) 6236–6244. doi:10.1021/jp056461u.
- [61] X. Cheng, A.T. Kan, M.B. Tomson, Naphthalene Adsorption and Desorption from Aqueous C60 Fullerene, *J. Chem. Eng. Data.* 49 (2004) 675–683. doi:10.1021/je030247m.
- [62] Z. Wang, M.A. Al-Daous, E.R. Kiesel, F. Li, A. Stein, Design and synthesis of 3D ordered macroporous ZrO₂/Zeolite nanocomposites, *Microporous Mesoporous Mater.* 120 (2009) 351–358.
- [63] Y. Zhao, Q. Gao, T. Tang, Y. Xu, D. Wu, Effective NH₂-grafting on mesoporous SBA-15 surface for adsorption of heavy metal ions, *Mater. Lett.* 65 (2011) 1045–1047. doi:10.1016/j.matlet.2010.12.047.
- [64] C. Yang, Z. Wang, X. Zhou, X. Tian, Z. Pi, Y. Wang, A mesoporous Pt-SBA-15 nano architecture with catalytic functions on oxidation of CO, *J. Porous Mater.* 18 (2011) 31–35. doi:10.1007/s10934-010-9353-9.
- [65] K.F. Lam, H. Kassab, M. Pera-Titus, K.L. Yeung, B. Albel, L. Bonneviot, MCM-41 “LUS”: Alumina Tubular Membranes for Metal Separation in Aqueous Solution, *J. Phys. Chem. C.* 115 (2011) 176–187. doi:10.1021/jp1065874.

- [66] S.A. Idris, C.M. Davidson, C. McManamon, M.A. Morris, P. Anderson, L.T. Gibson, Large pore diameter MCM-41 and its application for lead removal from aqueous media, *J. Hazard. Mater.* 185 (2011) 898–904.
doi:10.1016/j.jhazmat.2010.09.105.
- [67] E.-Y. Jeong, M.B. Ansari, Y.-H. Mo, S.-E. Park, Removal of Cu(II) from water by tetrakis(4-carboxyphenyl) porphyrin-functionalized mesoporous silica, *J. Hazard. Mater.* 185 (2011) 1311–1317. doi:10.1016/j.jhazmat.2010.10.047.
- [68] A. Walcarius, L. Mercier, Mesoporous organosilica adsorbents: nanoengineered materials for removal of organic and inorganic pollutants, *J. Mater. Chem.* 20 (2010) 4478–4511. doi:10.1039/B924316J.
- [69] M.S. P. K. Singh, V. K. Singh, No Title, *E-Polymers.* 30 (2007) 1–34.
- [70] S.. Ali, M.. Saeed, Synthesis and corrosion inhibition study of some 1,6-hexanediamine-based N,N-diallyl quaternary ammonium salts and their polymers, *Polymer (Guildf).* 42 (2001) 2785–2794. doi:10.1016/S0032-3861(00)00665-0.
- [71] N.Y. Abu-Thabit, I.W. Kazi, H.A. Al-Muallem, S.A. Ali, Phosphonobetaine/sulfur dioxide copolymer by Butler's cyclopolymerization process, *Eur. Polym. J.* 47 (2011). doi:10.1016/j.eurpolymj.2011.02.004.
- [72] S.A. Ali, N.Y. Abu-Thabit, H.A. Al-Muallem, Synthesis and solution properties of a pH-responsive cyclopolymer of zwitterionic ethyl 3-(N,N-diallylammonio)propanephosphonate, *J. Polym. Sci. Part A Polym. Chem.* 48 (2010) 5693–5703. doi:10.1002/pola.24363.
- [73] P. Anton, A. Laschewsky, Zwitterionic polysoaps with reduced density of surfactant side groups, *Die Makromol. Chemie.* 194 (1993) 601–624.

doi:10.1002/macp.1993.021940221.

- [74] T.A. Wielema, J.B.F.N. Engberts, Zwitterionic polymers—I. Synthesis of a novel series of poly(vinylsulphobetaines). Effect of structure of polymer on solubility in water, *Eur. Polym. J.* 23 (1987) 947–950. doi:10.1016/0014-3057(87)90038-3.
- [75] S.A. Ali, M.A.J. Mazumder, H.A. Al-Muallem, Synthesis and solution properties of a new pH-responsive polymer containing amino propanesulfonic acid residues, *J. Polym. Sci. Part A Polym. Chem.* 41 (2003) 172–184. doi:10.1002/pola.10565.
- [76] H.A. Al-Muallem, M.I.M. Wazeer, S.A. Ali, Synthesis and solution properties of a new pH-responsive polymer containing amino acid residues, *Polymer (Guildf)*. 43 (2002). doi:10.1016/S0032-3861(02)00251-3.
- [77] S.A. Ali, Y. Umar, B.F. Abu-Sharkh, H.A. Al-Muallem, Synthesis and comparative solution properties of single-, twin-, and triple-tailed associating ionic polymers based on diallylammonium salts, *J. Polym. Sci. Part A Polym. Chem.* 44 (2006). doi:10.1002/pola.21624.
- [78] S.A. Ali, Y. Umar, B.F. Abu-Sharkh, Amphiphilic cycloterpolymers of diallyldimethylammonium chloride, diallyloctadecylammonium chloride, and sulfur dioxide, *J. Appl. Polym. Sci.* 97 (2005) 1298–1306. doi:10.1002/app.21819.
- [79] S.A. Ali, H.A. Al-Muallem, N.Y. Abu-Thabit, Synthesis and solution properties of amphiphilic cyclopolymers and terpolymers of 4-methoxycarbonyl-1,1-diallylpiperidinium chloride, diallyloctadecylammonium chloride, and sulfur dioxide, *J. Appl. Polym. Sci.* 118 (2010) 2951–2958. doi:10.1002/app.32653.
- [80] S.A. Ali, H.A. Al-Muallem, N.Y. Abu-Thabit, Synthesis and solution properties of amphiphilic cycloterpolymers of 1,1-diallyl-4-formylpiperizinium chloride,

diallyloctadecylammonium chloride and sulfur dioxide, *Eur. Polym. J.* 45 (2009) 131–140. doi:10.1016/j.eurpolymj.2008.10.003.

- [81] Y. Chang, C.L. McCormick, Water-soluble copolymers: 57. Amphiphilic cyclocopolymers of diallylalkoxybenzyl-methylammonium chloride and diallyl-dimethylammonium chloride, *Polymer (Guildf)*. 35 (1994) 3503–3512. doi:10.1016/0032-3861(94)90916-4.
- [82] S.A. Ali, S.Z. Ahmed, E.Z. Hamad, Cyclopolymerization studies of diallyl- and tetraallylpiperazinium salts, *J. Appl. Polym. Sci.* 61 (1996) 1077–1085. doi:10.1002/(SICI)1097-4628(19960815)61:7<1077::AID-APP2>3.0.CO;2-J.
- [83] S.A. Ali, O.C.S. Al Hamouz, N.M. Hassan, Novel cross-linked polymers having pH-responsive amino acid residues for the removal of Cu²⁺ from aqueous solution at low concentrations, *J. Hazard. Mater.* 248–249 (2013) 47–58. doi:10.1016/j.jhazmat.2012.12.052.
- [84] S.A. Ali, S.A. Haladu, A novel cross-linked polyzwitterion/anion having pH-responsive carboxylate and sulfonate groups for the removal of Sr²⁺ from aqueous solution at low concentrations, *React. Funct. Polym.* 73 (2013) 796–804. doi:10.1016/j.reactfunctpolym.2013.03.011.
- [85] O.C.S. Al Hamouz, S.A. Ali, Removal of heavy metal ions using a novel cross-linked polyzwitterionic phosphonate, *Sep. Purif. Technol.* 98 (2012) 94–101. doi:10.1016/j.seppur.2012.07.019.
- [86] O.C.S. Al Hamouz, S.A. Ali, Novel Cross-Linked Polyphosphonate for the Removal of Pb²⁺ and Cu²⁺ from Aqueous Solution, *Ind. Eng. Chem. Res.* 51 (2012) 14178–14187. doi:10.1021/ie301231k.

- [87] S.M. Thombre, B.D. Sarwade, Synthesis and biodegradability of polyaspartic acid: A critical review, *J. Macromol. Sci. - Pure Appl. Chem.* 42 A (2005) 1299–1315. doi:10.1080/10601320500189604.
- [88] Commercial poly (aspartic acid) and its uses, *Glas. JE Hydrophilic Polym. Adv. Chem.* 248. (1996).
- [89] D. Hasson, H. Shemer, A. Sher, State of the art of friendly “green” scale control inhibitors: A review article, *Ind. Eng. Chem. Res.* 50 (2011) 7601–7607. doi:10.1021/ie200370v.
- [90] M.J. Zohuriaan-Mehr, A. Pourjavadi, H. Salimi, M. Kurdtabar, Protein- and homo poly(amino acid)-based hydrogels with super-swelling properties, *Polym. Adv. Technol.* 20 (2009) 655–671. doi:10.1002/pat.1395.
- [91] K. Wahid, M. Saravanan, F. Shady, K. Neeraj, J.D. Abraham, No Title, *Macromol. Biosci.* 11 (2011) 1625–1636.
- [92] B. Gyarmati, E. Krisch, A. Szilágyi, In situ oxidation-induced gelation of poly(aspartic acid) thiomers, *React. Funct. Polym.* 84 (2014) 29–36. doi:10.1016/j.reactfunctpolym.2014.08.007.
- [93] R.A. Gross, B. Kalra, Biodegradable polymers for the environment, *Science* (80-.). 297 (2002) 803–807. doi:10.1126/science.297.5582.803.
- [94] K.W. Rusenko, J.E. Donachy, A.P. Wheeler, C.S. Sikes, A.P. Wheeler, Purification and characterization of a shell matrix phosphoprotein from the american oyster, *Surf. React. Pept. Polym. ACS Symp. Ser.* 444. ACS. (1991) 107–124.

- [95] Z. Quan, Y. Chen, X. Wang, C. Shi, Y. Liu, C. Ma, Experimental study on scale inhibition performance of a green scale inhibitor polyaspartic acid, *Sci. China, Ser. B Chem.* 51 (2008) 695–699. doi:10.1007/s11426-008-0063-y.
- [96] H. Montgomerie, P. Chen, T. Hagen, R. Wat, O.M. Selle, No Title, *Well Treat. Comprising A Polym. Form. from A Diallyl Ammonium Salt A Scale Inhib.* US 8101554 B2. (2012).
- [97] S.A.A. Sajadi, Metal ion-binding properties of l-glutamic acid and l-aspartic acid, a comparative investigation, *Nat. Sci.* 2 (2010) 85–90.
- [98] J.A. Gould, M.J. Rosseinsky, S.A. Moggach, Tuning the coordination chemistry of a Cu(ii) complex at high-pressure, *Dalt. Trans.* 41 (2012) 5464–5467. doi:10.1039/c2dt12302a.
- [99] Y.Z. Hamada, N. Bayakly, M. Shafi, S. Painter, V. Taylor, J. Greene, K. Rosli, No Title, *Complex Met.* 1 (2014) 46–51.
- [100] V. Kora, S.M. Nair, R. Duraiswamy, S. Muchi, No Title, *J. Chem. Soc. Dalt. Trans.* 2 (1982) 291.
- [101] J. I owska, L. Chruściński, Potentiometric studies on complexes in Cr(III)-l-aspartic acid-dl-methionine or dl-ethionine systems, *Polyhedron.* 5 (1986) 1131–1134. doi:10.1016/S0277-5387(00)84313-2.
- [102] G. Anderegg, F. Arnaud-Neu, R. Delgado, J. Felcman, K. Popov, Critical evaluation of stability constants of metal complexes of complexones for biomedical and environmental applications (IUPAC Technical Report), *Pure Appl. Chem.* 77 (2005) 1445–1495. doi:10.1351/pac200577081445.

- [103] S.A. Haladu, S.A. Ali, A pH-responsive cyclopolymer having phospho- and sulfopropyl pendants in the same repeating unit: Synthesis, characterization, and its application as an antiscalant, *J. Polym. Sci. Part A Polym. Chem.* 51 (2013) 5130–5142. doi:10.1002/pola.26945.
- [104] S.A. Ali, H.A. Al-Muallem, O.C.S.O. Al-Hamouz, M.K. Estaitie, Synthesis of a novel zwitterionic bisphosphonate cyclopolymer containing residues of alendronic acid, *React. Funct. Polym.* 86 (2015) 80–86. doi:10.1016/j.reactfunctpolym.2014.11.011.
- [105] P. Albertsson, Partition of cell particles and macromolecules in polymer two-phase systems, *Adv. Protein Chem.* 24 (1970) 309–341. doi:10.1016/S0065-3233(08)60244-2.
- [106] S.M. Waziri, B.F. Abu-Sharkh, S.A. Ali, Protein partitioning in aqueous two-phase systems composed of a pH-responsive copolymer and poly(ethylene glycol), *Biotechnol. Prog.* 20 (2004) 526–532. doi:10.1021/bp0342349.
- [107] M.M. Nasef, M. Nallappan, Z. Ujang, Polymer-based chelating adsorbents for the selective removal of boron from water and wastewater: A review, *React. Funct. Polym.* 85 (2014) 54–68. doi:10.1016/j.reactfunctpolym.2014.10.007.
- [108] S. Emik, Preparation and characterization of an IPN type chelating resin containing amino and carboxyl groups for removal of Cu(II) from aqueous solutions, *React. Funct. Polym.* 75 (2014) 63–74. doi:10.1016/j.reactfunctpolym.2013.12.006.
- [109] T. V Dokichev, D.R. Latypova, R.R. Shakirov, R.Z. Biglova, R.F. Talipov, Catalyzed synthesis of β -amino acids esters, *Russ. J. Org. Chem.* 46 (2010) 755–757. doi:10.1134/S107042801005026X.

- [110] S.A. Ali, S.A. Haladu, H.A. Al-Muallem, Bis[3-(diethoxyphosphoryl)propyl]diallylammonium chloride: Synthesis and use of its cyclopolymer as an antiscalant, *J. Appl. Polym. Sci.* 131 (2014). doi:10.1002/app.40615.
- [111] S.A. Ali, I.W. Kazi, N. Ullah, Construction of aqueous two-phase systems of the cyclopolymer of (diallylamino)propylphosphonate and its sulfur dioxide copolymer with polyoxyethylene using ¹H NMR spectroscopy, *J. Chem. Eng. Data.* 59 (2014) 3863–3872. doi:10.1021/je500767z.
- [112] J.F. Pearson, M.A. Slifkin, The infrared spectra of amino acids and dipeptides, *Spectrochim. Acta Part A Mol. Spectrosc.* 28 (1972) 2403–2417. doi:10.1016/0584-8539(72)80220-4.
- [113] G.B. Butler, R.T. Angelo, Preparation and polymerization of unsaturated quaternary ammonium compounds. VIII. A proposed alternating intramolecular-intermolecular chain propagation, *J. Am. Chem. Soc.* 79 (1957) 3128–3131.
- [114] R.M. Pike, R.A. Cohen, Organophosphorus polymers. I. Peroxide-initiated polymerization of diethyl and diisopropyl vinylphosphonate, *J Polym Sci.* 44 (1960) 531.
- [115] S.A. Ali, A. Rasheed, M.I.M. Wazeer, Synthesis and solution properties of a quaternary ammonium polyampholyte, *Polymer (Guildf).* 40 (1999) 2439–2446. doi:10.1016/S0032-3861(98)00448-0.
- [116] V. De Vynck, E.J. Goethals, Synthesis and polymerization of N,N-diallylpyrrolidinium bromide, *Macromol. Rapid Commun.* 18 (1997) 149–156.
- [117] F. Rullens, M. Devillers, A. Laschewsky, New regular, amphiphilic

poly(ampholyte)s: Synthesis and characterization, *Macromol. Chem. Phys.* 205 (2004) 1155–1166. doi:10.1002/macp.200400081.

- [118] J.C. Salamone, W. Volksen, A.P. Olson, S.C. Israel, Aqueous solution properties of a poly(vinyl imidazolium sulphobetaine), *Polymer (Guildf)*. 19 (1978) 1157–1162. doi:10.1016/0032-3861(78)90064-2.
- [119] M. Yoshizawa, H. Ohno, Molecular brush having molten salt domain for fast ion conduction, *Chem. Lett.* (1999) 889–890.
- [120] K. Nishida, K. Kaji, T. Kanaya, N. Fanjat, Determination of intrinsic viscosity of polyelectrolyte solutions, *Polymer (Guildf)*. 43 (2002) 1295–1300. doi:10.1016/S0032-3861(01)00682-6.
- [121] P.G. Higgs, J.-F. Joanny, Theory of polyampholyte solutions, *J. Chem. Phys.* 94 (1991) 1543–1554.
- [122] F. Candau, J.F. Joanny, Polyampholytes (Properties in Aqueous Solution), *Polym. Mater. Encycl.* 7 (1996) 5476–5488.
- [123] J. Wittmer, A. Johner, J.F. Joanny, Random and alternating polyampholytes, *EPL*. 24 (1993) 263–268. doi:10.1209/0295-5075/24/4/005.
- [124] R. Everaers, A. Johner, J.-F. Joanny, Complexation and precipitation in polyampholyte solutions, *Europhys. Lett.* 37 (1997) 275–280. doi:10.1209/epl/i1997-00143-x.
- [125] R. Barbucci, M. Casolaro, N. Danzo, V. Barone, P. Ferruti, A. Angeloni, Effect of different shielding groups on the polyelectrolyte behavior of polyamines, *Macromolecules*®. 16 (1983) 456–462.

- [126] R. Barbucci, M. Casolaro, P. Ferruti, M. Nocentini, Spectroscopic and calorimetric studies on the protonation of polymeric amino acids, *Macromolecules*. 19 (1986) 1856–1861.
- [127] H. David, S. Hilla, S. Alexander, No Title, *Ind. Eng. Chem. Res.* 50 (2011) 7601–7607.
- [128] R.J. Davey, ROLE OF ADDITIVES IN PRECIPITATION PROCESSES., in: *Ind. Cryst. Proc. Symp.*, 1982: pp. 123–135.
- [129] P.A. Albertsson, No Title, *Partit. Cell Part. Macromol.* (1986).
- [130] A.D. Diamond, J.T. Hsu, Correlation of polymer partitioning in aqueous two-phase systems, in: *AIChE Symp. Ser.*, 1992: pp. 105–111.
- [131] S. Shahriari, S.G. Doozandeh, G. Pazuki, Partitioning of cephalexin in aqueous two-phase systems containing poly(ethylene glycol) and sodium citrate salt at different temperatures, *J. Chem. Eng. Data*. 57 (2012) 256–262.
doi:10.1021/je201033f.
- [132] H.A. Krebs, P.D.J. Weitzman, No Title, *Krebs' Citric Acid Cycle Half A Century Still Turn.* (1987).
- [133] S. Roweton, S.J. Huang, G. Swift, Poly(aspartic acid): Synthesis, biodegradation, and current applications, *J. Environ. Polym. Degrad.* 5 (1997) 175–181.
- [134] W. Joentgen, N. M \ddot{u} ller, A. Mitschker, H. Schmidt, Polyaspartic acids. In: *Fahnestock S, Steinb \ddot{u} chel A (eds) Polyamides and complex proteinaceous materials I. Biopolymers 7.* Wiley-VCH. pp 175–179, ISBN 9783527302222. (2004).

- [135] M. Liu, L. Wang, H. Su, H. Cao, T. Tan, PH-sensitive IPN hydrogel based on poly (aspartic acid) and poly (vinyl alcohol) for controlled release, *Polym. Bull.* 70 (2013) 2815–2827. doi:10.1007/s00289-013-0990-4.
- [136] S.A. Ali, S.M.J. Zaidi, A.M.Z. El-Sharif, A.A. Al-Taq, Cyclopolymers from N,N-diallyl-N-propargyl-(12-N'-formylamino)-1-dodecylammonium chloride and their use as inhibitors for mild steel corrosion, *Polym. Bull.* 69 (2012) 491–507. doi:10.1007/s00289-012-0765-3.
- [137] Z.A. Jamiu, H.A. Al-Muallem, S.A. Ali, Aspartic acid in a new role: Synthesis and application of a pH-responsive cyclopolymer containing residues of the amino acid, *React. Funct. Polym.* 93 (2015) 120–129. doi:10.1016/j.reactfunctpolym.2015.06.006.
- [138] P.A. Albertsson, No Title, *Partit. Cell Part. Macromol.* (1986).
- [139] S.A. Ali, H.A. Al-Muallem, M.A.J. Mazumder, Coexistence curves of aqueous two-phase systems of some pH-responsive homo-and copolymers of 3-(diallylammonio)propane-1-sulfonate and urethanized poly(ethanol) or poly(oxyethylene), *J. Chem. Eng. Data.* 58 (2013) 2574–2585. doi:10.1021/je400465q.
- [140] B.A. Andrews, J.A. Asenjo, Theoretical and experimental evaluation of hydrophobicity of proteins to predict their partitioning behavior in aqueous two phase systems: A review, *Sep. Sci. Technol.* 45 (2010) 2165–2170. doi:10.1080/01496395.2010.507436.
- [141] A. Laschewsky, Structures and synthesis of zwitterionic polymers, *Polymers (Basel)*. 6 (2014) 1544–1601. doi:10.3390/polym6051544.

- [142] Y. Zhang, Y. Zhou, C. Liu, Structure and properties of novel blend films from alginate and quaternized poly(4-vinyl-N-carboxymethylpyridine) containing zwitterion structure units, *Polym. Bull.* 71 (2014) 1909–1918. doi:10.1007/s00289-014-1163-9.
- [143] A. Heidari, H. Younesi, Z. Mehraban, Removal of Ni(II), Cd(II), and Pb(II) from a ternary aqueous solution by amino functionalized mesoporous and nano mesoporous silica, *Chem. Eng. J.* 153 (2009). doi:10.1016/j.cej.2009.06.016.
- [144] Environmental Pollution Control Alternatives: Drinking Water Treatment for Small Communities, Cincinnati, Ohio, 1990. doi:(EPA/625/5-90/025).
- [145] M. -q. Jiang, Q. -p. Wang, X. -y. Jin, Z. -l. Chen, Removal of Pb(II) from aqueous solution using modified and unmodified kaolinite clay, *J. Hazard. Mater.* 170 (2009). doi:10.1016/j.jhazmat.2009.04.092.
- [146] M.M. Rao, D.K. Ramana, K. Seshiah, M.C. Wang, S.W.C. Chien, Removal of some metal ions by activated carbon prepared from Phaseolus aureus hulls, *J. Hazard. Mater.* 166 (2009). doi:10.1016/j.jhazmat.2008.12.002.
- [147] M. Ghaedi, M.N. Biyareh, S.N. Kokhdan, S. Shamsaldini, R. Sahraei, A. Daneshfar, S. Shahriyar, Comparison of the efficiency of palladium and silver nanoparticles loaded on activated carbon and zinc oxide nanorods loaded on activated carbon as new adsorbents for removal of Congo red from aqueous solution: Kinetic and isotherm study, *Mater. Sci. Eng. C.* 32 (2012). doi:10.1016/j.msec.2012.01.015.
- [148] J.M. Dias, M.C.M. Alvim-Ferraz, M.F. Almeida, J. Rivera-Utrilla, M. Sánchez-Polo, Waste materials for activated carbon preparation and its use in aqueous-phase treatment: A review, *J. Environ. Manage.* 85 (2007).

doi:10.1016/j.jenvman.2007.07.031.

- [149] E. Erdem, N. Karapinar, R. Donat, The removal of heavy metal cations by natural zeolites., *J. Colloid Interface Sci.* 280 (2004) 309–14.
doi:10.1016/j.jcis.2004.08.028.
- [150] J. Liu, X. Wang, T. Xu, G. Shao, Novel negatively charged hybrids. 1. copolymers: Preparation and adsorption properties, *Sep. Purif. Technol.* 66 (2009).
doi:10.1016/j.seppur.2008.11.005.
- [151] M. Cegłowski, G. Schroeder, Preparation of porous resin with Schiff base chelating groups for removal of heavy metal ions from aqueous solutions, *Chem. Eng. J.* 263 (2015). doi:10.1016/j.cej.2014.11.047.
- [152] W. Jaeger, J. Bohrisch, A. Laschewsky, Synthetic polymers with quaternary nitrogen atoms-Synthesis and structure of the most used type of cationic polyelectrolytes, *Prog. Polym. Sci.* 35 (2010).
doi:10.1016/j.progpolymsci.2010.01.002.
- [153] S.A. Ali, O.C.S. Al-Hamouz, Comparative solution properties of cyclocopolymers having cationic, anionic, zwitterionic and zwitterionic/anionic backbones of similar degree of polymerization, *Polymer (Guildf)*. 53 (2012) 3368–3377.
doi:10.1016/j.polymer.2012.05.034.
- [154] G.B.B. Butler, Cyclopolymerization, *J. Polym. Sci. Part A Polym. Chem.* 38 (2000) 3451–3461.
- [155] F.C. McGrew, Structure of synthetic high polymers, *J. Chem. Educ.* 35 (1958).
- [156] H. Silvia Martínez-Tapia, A. Cabeza, S. Bruque, P. Pertierra, S. García-Granda,

M.A.G. Aranda, Synthesis and structure of $\text{Na}_2[(\text{HO})_3\text{PCH}_2)_3\text{NH}]1.5\text{H}_2\text{O}$: The first alkaline triphosphonate, *J. Solid State Chem.* 151 (2000).
doi:10.1006/jssc.2000.8634.

- [157] D. Kołodyńska, Z. Hubicki, S. Pasieczna-Patkowska, FT-ir/pas studies of cu(II)-EDTA complexes sorption on the chelating ion exchangers, *Acta Phys. Pol. A.* 116 (2009).
- [158] W. Plazinski, W. Rudzinski, Modeling the effect of pH on kinetics of heavy metal ion biosorption. A theoretical approach based on the statistical rate theory, *Langmuir.* 25 (2009). doi:10.1021/la803075k.
- [159] W.D.S. and D.C. McAvoy, MINEQL+: a chemical equilibrium program for personal computers, *Environmental Research Software*, (2001).
- [160] W.-J. Liu, F.-X. Zeng, H. Jiang, X.-S. Zhang, Adsorption of lead (Pb) from aqueous solution with *Typha angustifolia* biomass modified by SOCl_2 activated EDTA, *Chem. Eng. J.* 170 (2011). doi:10.1016/j.cej.2011.03.020.
- [161] M.K. Aroua, S.P.P. Leong, L.Y. Teo, C.Y. Yin, W.M.A.W. Daud, Real-time determination of kinetics of adsorption of lead(II) onto palm shell-based activated carbon using ion selective electrode, *Bioresour. Technol.* 99 (2008).
doi:10.1016/j.biortech.2007.10.010.
- [162] Y.S. Ho, G. McKay, Comparative sorption kinetic studies of dye and aromatic compounds onto fly ash, *J. Environ. Sci. Heal. - Part A Toxic/Hazardous Subst. Environ. Eng.* 34 (1999).
- [163] Y.S. Ho, G. McKay, Pseudo-second order model for sorption processes, *Process*

Biochem. 34 (1999) 451–465. doi:10.1016/S0032-9592(98)00112-5.

- [164] W.J.W. and J.C. Morris, Intraparticle diffusion during the sorption of surfactants onto activated carbon, Eng. Div. Am. Soc. Civ. Eng. 89 (1963) 31–60.
- [165] G. ANNADURAI, R.-S. JUANG, D.-J. LEE, Use of cellulose-based wastes for adsorption of dyes from aqueous solutions, J. Hazard. Mater. 92 (2002) 263–274. doi:10.1016/S0304-3894(02)00017-1.
- [166] I. Vergili, G. Soltobaeva, Y. Kaya, Z.B.B. Gönder, S. Çavuş, G. Gürdağ, Study of the Removal of Pb(II) Using a Weak Acidic Cation Resin: Kinetics, Thermodynamics, Equilibrium, and Breakthrough Curves, Ind. Eng. Chem. Res. 52 (2013) 9227–9238. doi:10.1021/ie400630d.
- [167] F.-C. Wu, R.-L. Tseng, R.-S. Juang, Adsorption of dyes and phenols from water on the activated carbons prepared from corncob wastes, Environ. Technol. 22 (2001).
- [168] S. Rengaraj, J.-W. Yeon, Y. Kim, Y. Jung, Y.-K. Ha, W.-H. Kim, Adsorption characteristics of Cu(II) onto ion exchange resins 252H and 1500H: Kinetics, isotherms and error analysis, J. Hazard. Mater. 143 (2007). doi:10.1016/j.jhazmat.2006.09.064.
- [169] I. Langmuir, The adsorption of gases on plane surfaces of glass, mica and platinum, J. Am. Chem. Soc. 40 (1918).
- [170] H.M.F. Freundlich, Über die adsorption in lösungen, Z. Phys. Chem. 57 (1906) 385–471.
- [171] V.P. M.J. Tempkin, Kinetics of ammonia synthesis on promoted iron catalysts, Acta Physicochim. (1940) 217–256.

- [172] R.R. Sheha, A.A. El-Zahhar, Synthesis of some ferromagnetic composite resins and their metal removal characteristics in aqueous solutions, *J. Hazard. Mater.* 150 (2008). doi:10.1016/j.jhazmat.2007.05.042.
- [173] N. Chiron, R. Guilet, E. Deydier, Adsorption of Cu(II) and Pb(II) onto a grafted silica: Isotherms and kinetic models, *Water Res.* 37 (2003). doi:10.1016/S0043-1354(03)00156-8.
- [174] S.K. Ouki, M. Kavannagh, Performance of natural zeolites for the treatment of mixed metal- contaminated effluents, *Waste Manag. Res.* 15 (1997). doi:10.1006/wmre.1996.0094.
- [175] P.C. Mishra, R.K. Patel, Removal of lead and zinc ions from water by low cost adsorbents, *J. Hazard. Mater.* 168 (2009). doi:10.1016/j.jhazmat.2009.02.026.
- [176] Z. Li, Y. Ge, L. Wan, Fabrication of a green porous lignin-based sphere for the removal of lead ions from aqueous media, *J. Hazard. Mater.* 285 (2015). doi:10.1016/j.jhazmat.2014.11.033.
- [177] W. Shen, S. Chen, S. Shi, X. Li, X. Zhang, W. Hu, H. Wang, Adsorption of Cu(II) and Pb(II) onto diethylenetriamine-bacterial cellulose, *Carbohydr. Polym.* 75 (2009). doi:10.1016/j.carbpol.2008.07.006.
- [178] S.M. Musyoka, J.C. Ngila, B. Moodley, L. Petrik, A. Kindness, Synthesis, characterization, and adsorption kinetic studies of ethylenediamine modified cellulose for removal of Cd and pb, *Anal. Lett.* 44 (2011). doi:10.1080/00032719.2010.539736.
- [179] Z. Li, Y. Kong, Y. Ge, Synthesis of porous lignin xanthate resin for Pb²⁺ removal from aqueous solution, *Chem. Eng. J.* 270 (2015). doi:10.1016/j.cej.2015.01.123.

- [180] K. Rout, M. Mohapatra, S. Anand, 2-Line ferrihydrite: Synthesis, characterization and its adsorption behaviour for removal of Pb(ii), Cd(ii), Cu(ii) and Zn(ii) from aqueous solutions, *Dalt. Trans.* 41 (2012). doi:10.1039/c2dt11651k.
- [181] I. Anastopoulos, I. Massas, C. Ehaliotis, Composting improves biosorption of Pb²⁺ and Ni²⁺ by renewable lignocellulosic materials. Characteristics and mechanisms involved, *Chem. Eng. J.* 231 (2013). doi:10.1016/j.cej.2013.07.028.
- [182] N.-C. Feng, X.-Y. Guo, Characterization of adsorptive capacity and mechanisms on adsorption of copper, lead and zinc by modified orange peel, *Trans. Nonferrous Met. Soc. China (English Ed.)* 22 (2012). doi:10.1016/S1003-6326(11)61309-5.
- [183] S. Liang, X. Guo, Q. Tian, Adsorption of Pb²⁺ and Zn²⁺ from aqueous solutions by sulfured orange peel, *Desalination*. 275 (2011). doi:10.1016/j.desal.2011.03.001.
- [184] L. Yu, R. Zou, Z. Zhang, G. Song, Z. Chen, J. Yang, J. Hu, A Zn²⁺GeO₄-ethylenediamine hybrid nanoribbon membrane as a recyclable adsorbent for the highly efficient removal of heavy metals from contaminated water, *Chem. Commun.* 47 (2011). doi:10.1039/c1cc14159g.
- [185] R. Sapolsky, No Title, *Biol. Hum. Behav. Neurol. Orig. Individ.* (2005) 19–20.
- [186] W.J. McEntee, T.H. Crook, Glutamate: its role in learning, memory, and the aging brain, *Psychopharmacology (Berl.)* 111 (1993) 391–401. doi:10.1007/BF02253527.
- [187] M.G. Erlander, A.J. Tobin, The structural and functional heterogeneity of glutamic acid decarboxylase: A review, *Neurochem. Res.* 16 (1991) 215–226. doi:10.1007/BF00966084.

- [188] I. Bajaj, R. Singhal, Poly (glutamic acid) - An emerging biopolymer of commercial interest, *Bioresour. Technol.* 102 (2011) 5551–5561.
doi:10.1016/j.biortech.2011.02.047.
- [189] C. Li, D.-F. Yu, R.A. Newman, F. Cabral, L.C. Stephens, N. Hunter, L. Milas, S. Wallace, Complete regression of well-established tumors using a novel water-soluble poly(L-glutamic acid)-paclitaxel conjugate, *Cancer Res.* 58 (1998) 2404–2409.
- [190] S. Murakami, N. Aoki, Bio-based hydrogels prepared by cross-linking of microbial poly(γ -glutamic acid) with various saccharides, *Biomacromolecules.* 7 (2006) 2122–2127. doi:10.1021/bm0600264.
- [191] J.M. Buescher, A. Margaritis, Microbial biosynthesis of polyglutamic acid biopolymer and applications in the biopharmaceutical, biomedical and food industries, *Crit. Rev. Biotechnol.* 27 (2007) 1–19.
doi:10.1080/07388550601166458.
- [192] A.E. Martel, Critical stability constants of metal complexes, *Crit. Stab. Constants Met. Complexes.* (2006) 26.
- [193] A. Mehta, S.J.S. Flora, Possible role of metal redistribution, hepatotoxicity and oxidative stress in chelating agents induced hepatic and renal metallothionein in rats, *Food Chem. Toxicol.* 39 (2001) 1029–1038. doi:10.1016/S0278-6915(01)00046-1.
- [194] M.R. Vakili, S. Zahmatkesh, M.J. Panahiyan, T. Jafarizadeh, Poly(amide-hydrazide-imide)s containing L-aspartic acid: Synthesis, characterization, and their applications in removal of heavy metal ions, *Des. Monomers Polym.* 18 (2015) 315–322. doi:10.1080/15685551.2014.999463.

- [195] F.H. Butt, F. Rahman, U. Baduruthamal, Pilot plant evaluation of advanced vs. conventional scale inhibitors for RO desalination, *Desalination*. 103 (1995) 189–198. doi:10.1016/0011-9164(95)00072-0.
- [196] R. Barbucci, M. Casolaro, M. Nocentini, S. Corezzi, P. Ferruti, V. Barone, Acid-base and metal ion complex formation properties of polymers containing amino acid residues, *Macromolecules*. 19 (1986) 37–42.
- [197] A. Fini, M. Casolaro, M. Nocentini, R. Barbucci, M. Laus, No Title, *Makromol Chem*. 188 (1987).
- [198] H. David, S. Hilla, S. Alexander, No Title, *Ind. Eng. Chem. Res.* 50 (2011) 7601–7607.
- [199] K. Riedelsberger, Polymeric aminomethylphosphonic acids - 2. Polychelatogenes for separation of transition metal ions by membrane filtration, *Des. Monomers Polym.* 3 (2000) 35–53.
- [200] B.S. Meldrum, Glutamate as a neurotransmitter in the brain: Review of physiology and pathology, *J. Nutr.* 130 (2000) 1007S–1015S.
- [201] I. Ali, W.A. Wani, K. Saleem, M.-F. Hsieh, Anticancer metallodrugs of glutamic acid sulphonamides: In silico, DNA binding, hemolysis and anticancer studies, *RSC Adv.* 4 (2014) 29629–29641. doi:10.1039/c4ra02570a.
- [202] A. Ogunleye, A. Bhat, V.U. Irorere, D. Hill, C. Williams, I. Radecka, Poly- γ -glutamic acid: Production, properties and applications, *Microbiol. (United Kingdom)*. 161 (2015) 1–17. doi:10.1099/mic.0.081448-0.
- [203] I.-L.I.-L. Shih, Y.-T. Van, The production of poly-(γ -glutamic acid) from

microorganisms and its various applications, *Bioresour. Technol.* 79 (2001) 207–225. doi:10.1016/S0960-8524(01)00074-8.

- [204] T. Tsujimoto, J. Kimura, Y. Takeuchi, H. Uyama, C. Park, M.-H. Sung, Chelation of calcium ions by poly(γ -glutamic acid) from *Bacillus subtilis* (chungkookjang), *J. Microbiol. Biotechnol.* 20 (2010) 1436–1439. doi:10.4014/jmb.1004.04043.
- [205] C. Park, Y.-H. Choi, H.-J. Shin, H. Poo, J.J. Song, C.-J. Kim, M.-H. Sung, Effect of high-molecular-weight poly(γ -glutamic acid) from *Bacillus subtilis* (chungkookjang) on Ca solubility and intestinal absorption, *J. Microbiol. Biotechnol.* 15 (2005) 855–858.
- [206] X. Wen, E.F. Jackson, R.E. Price, E.E. Kim, Q. Wu, S. Wallace, C. Charnsangavej, J.G. Gelovani, C. Li, Synthesis and characterization of poly(L-glutamic acid) gadolinium chelate: A new biodegradable MRI contrast agent, *Bioconjug. Chem.* 15 (2004) 1408–1415. doi:10.1021/bc049910m.
- [207] Z. Yu, C. Peng, Y. Luo, J. Zhu, C. Chen, M. Shen, X. Shi, Poly(γ -glutamic acid)-stabilized iron oxide nanoparticles: Synthesis, characterization and applications for MR imaging of tumors, *RSC Adv.* 5 (2015) 76700–76707. doi:10.1039/c5ra15814a.
- [208] Y.C. Rajan, B.S. Inbaraj, B.H. Chen, Synthesis and characterization of poly(γ -glutamic acid)-based alumina nanoparticles with their protein adsorption efficiency and cytotoxicity towards human prostate cancer cells, *RSC Adv.* 5 (2015) 15126–15139. doi:10.1039/c4ra10445e.
- [209] S.A.A. Z. A. Jamiu, H. A. Al-Muallem, A glutamic acid-based polymer keeping intact the integrity of all the three original functionalities of the amino acid, *Des. Monomers Polym.* 5551 (2015). doi:10.1080/15685551.2015.1124320.

- [210] Z.A. Jamiu, T.A. Saleh, S.A. Ali, Synthesis of a unique cross-linked polyzwitterion/anion with an aspartic acid residue and its use for Pb²⁺ removal from aqueous solution, *RSC Adv.* 5 (2015) 42222–42232. doi:10.1039/C5RA05447H.
- [211] S.A. Ali, I.W. Kazi, N. Ullah, New Chelating Ion-Exchange Resin Synthesized via the Cyclopolymerization Protocol and Its Uptake Performance for Metal Ion Removal, *Ind. Eng. Chem. Res.* 54 (2015) 9689–9698. doi:10.1021/acs.iecr.5b02267.
- [212] S.-Y. Wang, M.-H. Tsai, S.-F. Lo, M.-J. Tsai, Effects of manufacturing conditions on the adsorption capacity of heavy metal ions by Makino bamboo charcoal., *Bioresour. Technol.* 99 (2008) 7027–33. doi:10.1016/j.biortech.2008.01.014.
- [213] B. Alyüz, S. Veli, Kinetics and equilibrium studies for the removal of nickel and zinc from aqueous solutions by ion exchange resins., *J. Hazard. Mater.* 167 (2009) 482–8. doi:10.1016/j.jhazmat.2009.01.006.
- [214] J.D. Donaldson, D. Beyersmann, Cobalt and Cobalt Compounds, in: *Ullmann's Encycl. Ind. Chem.*, Wiley-VCH Verlag GmbH & Co. KGaA, 2005. doi:10.1002/14356007.a07_281.pub2.
- [215] O.M. Faroon, H. Abadin, S. Keith, M. Osier, L. Chappell, G. Diamond, G. Sage, Toxicological Profile for Cobalt, *Agency Toxic Subst. Dis. Regist.* (2004) 486. <http://www.atsdr.cdc.gov/toxprofiles/tp33.pdf>.
- [216] U.S. Department of Health and Human Services. Hazardous Substances Data Bank (HSDB, online database). National Toxicology Information Program, National Library of Medicine, Bethesda, MD. 1993., (n.d.). <http://toxnet.nlm.nih.gov/cgi-bin/sis/search2/f?./temp/~7RVjkL:1> (accessed December 19, 2015).

- [217] G.I. Walters, V.C. Moore, A.S. Robertson, C.B.S.G. Burge, A.-D. Vellore, P.S. Burge, An outbreak of occupational asthma due to chromium and cobalt, *Occup. Med.* . 62 (2012) 533–540. doi:10.1093/occmed/kqs111.
- [218] P. Rehfisch, M. Anderson, P. Berg, E. Lampa, Y. Nordling, M. Svartengren, H. Westberg, L.-G. Gunnarsson, Lung function and respiratory symptoms in hard metal workers exposed to cobalt., *J. Occup. Environ. Med.* 54 (2012) 409–13. doi:10.1097/JOM.0b013e31824d2d7e.
- [219] A. Mendy, J. Gasana, E.R. Vieira, Urinary heavy metals and associated medical conditions in the US adult population., *Int. J. Environ. Health Res.* 22 (2012) 105–18. doi:10.1080/09603123.2011.605877.
- [220] P. Apostoli, S. Catalani, A. Zaghini, A. Mariotti, P.L. Poliani, V. Vielmi, F. Semeraro, S. Duse, A. Porzionato, V. Macchi, A. Padovani, M.C. Rizzetti, R. De Caro, High doses of cobalt induce optic and auditory neuropathy., *Exp. Toxicol. Pathol. Off. J. Gesellschaft Für Toxikologische Pathol.* 65 (2013) 719–27. doi:10.1016/j.etp.2012.09.006.
- [221] U.S. Department of Health and Human Services, Cobalt and Cobalt Compounds That Release Cobalt Ions In Vivo, 2016.
http://ntp.niehs.nih.gov/ntp/roc/monographs/cobalt_final_508.pdf.
- [222] O.O. of A.Q.P. and S. US EPA, Cobalt Compounds | Technology Transfer Network Air Toxics Web site | US EPA, (n.d.).
<http://www3.epa.gov/airtoxics/hlthef/cobalt.html> (accessed December 28, 2015).
- [223] M. Mohsen-Nia, P. Montazeri, H. Modarress, Removal of Cu²⁺ and Ni²⁺ from wastewater with a chelating agent and reverse osmosis processes, *Desalination.* 217 (2007) 276–281. doi:10.1016/j.desal.2006.01.043.

- [224] A.K. Meena, K. Kadirvelu, G.K. Mishra, C. Rajagopal, P.N. Nagar, Adsorptive removal of heavy metals from aqueous solution by treated sawdust (*Acacia arabica*), *J. Hazard. Mater.* 150 (2008) 604–11.
doi:10.1016/j.jhazmat.2007.05.030.
- [225] T. Saleh, Isotherm, kinetic, and thermodynamic studies on Hg(II) adsorption from aqueous solution by silica- multiwall carbon nanotubes, *Environ. Sci. Pollut. Res.* 22 (2015) 16721–16731. doi:10.1007/s11356-015-4866-z.
- [226] H. Bai, C. Li, G. Shi, Functional Composite Materials Based on Chemically Converted Graphene, *Adv. Mater.* 23 (2011) 1089–1115.
doi:10.1002/adma.201003753.
- [227] Y. XU, A. Rosa, X. LIU, D. SU, Characterization and use of functionalized carbon nanotubes for the adsorption of heavy metal anions, *New Carbon Mater.* 26 (2011) 57–62. doi:10.1016/S1872-5805(11)60066-8.
- [228] I. Bajaj, R. Singhal, Poly (glutamic acid)--an emerging biopolymer of commercial interest., *Bioresour. Technol.* 102 (2011) 5551–61.
doi:10.1016/j.biortech.2011.02.047.
- [229] B.S. Inbaraj, J.S. Wang, J.F. Lu, F.Y. Siao, B.H. Chen, Adsorption of toxic mercury(II) by an extracellular biopolymer poly(γ -glutamic acid), *Bioresour. Technol.* 100 (2009) 200–207. doi:10.1016/j.biortech.2008.05.014.
- [230] D. Bhattacharyya, J.. Hestekin, P. Brushaber, L. Cullen, L.. Bachas, S.. Sikdar, Novel poly-glutamic acid functionalized microfiltration membranes for sorption of heavy metals at high capacity, *J. Memb. Sci.* 141 (1998) 121–135.
doi:10.1016/S0376-7388(97)00301-3.

- [231] S.M.C. Ritchie, K.E. Kissick, L.G. Bachas, S.K. Sikdar, C. Parikh, D. Bhattacharyya, Polycysteine and other polyamino acid functionalized microfiltration membranes for heavy metal capture, *Environ. Sci. Technol.* 35 (2001) 3252–3258. doi:10.1021/es010617w.
- [232] S.M.. Ritchie, D. Bhattacharyya, Membrane-based hybrid processes for high water recovery and selective inorganic pollutant separation, *J. Hazard. Mater.* 92 (2002) 21–32. doi:10.1016/S0304-3894(01)00370-3.
- [233] E. Gutierrez, T.C. Miller, J.R. Gonzalez-Redondo, J.A. Holcombe, Characterization of Immobilized Poly- l -aspartate as a Metal Chelator, *Environ. Sci. Technol.* 33 (1999) 1664–1670. doi:10.1021/es981166r.
- [234] F.Y. Siao, J.F. Lu, J.S. Wang, B.S. Inbaraj, B.H. Chen, In Vitro Binding of Heavy Metals by an Edible Biopolymer Poly(γ -glutamic acid), *J. Agric. Food Chem.* 57 (2009) 777–784. doi:10.1021/jf803006r.
- [235] T.L. Wang, T.H. Kao, B.S. Inbaraj, Y.T. Su, B.H. Chen, Inhibition Effect of Poly(γ -glutamic acid) on Lead-Induced Toxicity in Mice, *J. Agric. Food Chem.* 58 (2010) 12562–12567. doi:10.1021/jf1034509.
- [236] B. Stephen Inbaraj, C.P. Chiu, G.H. Ho, J. Yang, B.H. Chen, Removal of cationic dyes from aqueous solution using an anionic poly- γ -glutamic acid-based adsorbent, *J. Hazard. Mater.* 137 (2006) 226–234. doi:10.1016/j.jhazmat.2006.01.057.
- [237] A.L. S. Kudaibergenov, W. Jaeger, No Title, *Adv. Polym. Sci.* 201 (2006) 157–224.
- [238] B.C. Smith, *Infrared Spectral Interpretation: A Systematic Approach*, Taylor &

Francis, 1998. <https://books.google.com.sa/books?id=Ywzf4GyoUaoC>.

- [239] M. He, Y. Zhu, Y. Yang, B. Han, Y. Zhang, Adsorption of cobalt(II) ions from aqueous solutions by palygorskite, *Appl. Clay Sci.* 54 (2011) 292–296. doi:10.1016/j.clay.2011.09.013.
- [240] H. Yüzer, M. Kara, E. Sabah, M.S. Çelik, M.S. Celik, Contribution of cobalt ion precipitation to adsorption in ion exchange dominant systems., *J. Hazard. Mater.* 151 (2008) 33–7. doi:10.1016/j.jhazmat.2007.05.052.
- [241] M. Abbas, S. Kaddour, M. Trari, Kinetic and equilibrium studies of cobalt adsorption on apricot stone activated carbon, *J. Ind. Eng. Chem.* 20 (2014) 745–751. doi:10.1016/j.jiec.2013.06.030.
- [242] F. Gimbert, N. Morin-Crini, F. Renault, P.-M. Badot, G. Crini, Adsorption isotherm models for dye removal by cationized starch-based material in a single component system: error analysis., *J. Hazard. Mater.* 157 (2008) 34–46. doi:10.1016/j.jhazmat.2007.12.072.
- [243] Y.S. Ho, J.F. Porter, G. Mckay, Divalent Metal Ions Onto Peat : Copper , Nickel and Lead Single Component Systems, *Water, Air, Soil Pollut.* 141 (2002) 1–33. doi:10.1023/A:1021304828010.
- [244] I. Langmuir, THE CONSTITUTION AND FUNDAMENTAL PROPERTIES OF SOLIDS AND LIQUIDS. PART I. SOLIDS., *J. Am. Chem. Soc.* 38 (1916) 2221–2295. doi:10.1021/ja02268a002.
- [245] K.Y. Foo, B.H. Hameed, Insights into the modeling of adsorption isotherm systems, *Chem. Eng. J.* 156 (2010) 2–10. doi:10.1016/j.cej.2009.09.013.

- [246] R. Sips, On the Structure of a Catalyst Surface, *J. Chem. Phys.* 16 (1948) 490.
doi:10.1063/1.1746922.
- [247] O. Redlich, D. Peterson, A useful adsorption isotherm, *J. Physic Chem.* 63 (1959) 1024. doi:10.1021/j150576a611.
- [248] B. Özkaya, Adsorption and desorption of phenol on activated carbon and a comparison of isotherm models, *J. Hazard. Mater.* 129 (2006) 158–163.
doi:10.1016/j.jhazmat.2005.08.025.
- [249] K. Vijayaraghavan, T.V.N. Padmesh, K. Palanivelu, M. Velan, Biosorption of nickel(II) ions onto *Sargassum wightii*: Application of two-parameter and three-parameter isotherm models, 2006. doi:10.1016/j.jhazmat.2005.10.016.
- [250] A. Ahmadpour, M. Tahmasbi, T.R. Bastami, J.A. Besharati, Rapid removal of cobalt ion from aqueous solutions by almond green hull., *J. Hazard. Mater.* 166 (2009) 925–30. doi:10.1016/j.jhazmat.2008.11.103.
- [251] R. Coşkun, C. Soykan, M. Saçak, Adsorption of copper(II), nickel(II) and cobalt(II) ions from aqueous solution by methacrylic acid/acrylamide monomer mixture grafted poly(ethylene terephthalate) fiber, *Sep. Purif. Technol.* 49 (2006) 107–114. doi:10.1016/j.seppur.2005.09.002.
- [252] K.A. Krishnan, T.S. Anirudhan, Kinetic and equilibrium modelling of cobalt(II) adsorption onto bagasse pith based sulphurised activated carbon, *Chem. Eng. J.* 137 (2008) 257–264. doi:10.1016/j.cej.2007.04.029.
- [253] E. Repo, T.A. Kurniawan, J.K. Warchol, M.E.T. Sillanpää, Removal of Co(II) and Ni(II) ions from contaminated water using silica gel functionalized with EDTA and/or DTPA as chelating agents, *J. Hazard. Mater.* 171 (2009) 1071–1080.

doi:10.1016/j.jhazmat.2009.06.111.

[254] F. Fang, L. Kong, J. Huang, S. Wu, K. Zhang, X. Wang, B. Sun, Z. Jin, J. Wang, X.-J. Huang, J. Liu, Removal of cobalt ions from aqueous solution by an amination graphene oxide nanocomposite, *J. Hazard. Mater.* 270 (2014) 1–10.
doi:10.1016/j.jhazmat.2014.01.031.

[255] V. S. Lagergren, K.S., No Title, *Handl.* 24 (1898) 1–39.

[256] B.K. Singh, N.S. Rawat, Comparative sorption kinetic studies of phenolic compounds on fly ash and impregnated fly ash, *J. Chem. Technol. Biotechnol.* 61 (1994) 57–65. doi:10.1002/jctb.280610109.

[257] Z.H. Chohan, M. Arif, M.A. Akhtar, C.T. Supuran, Metal-Based Antibacterial and Antifungal Agents: Synthesis, Characterization, and In Vitro Biological Evaluation of Co(II), Cu(II), Ni(II), and Zn(II) Complexes with Amino Acid-Derived Compounds, *Bioinorg. Chem. Appl.* 2006 (2006) 1–13.
doi:10.1155/BCA/2006/83131.

[258] A.S.A. Zidan, A.I. El-Said, M.S. El-Meligy, A.A.M. Aly, O.F. Mohammed, Mixed Ligand Complexes of 5-arylazo-8-hydroxyquinoline and α -amino Acids with Co(II), Ni(II) and Cu(II), *J. Therm. Anal. Calorim.* 62 (2000) 665–679.
doi:10.1023/A:1026761007006.

[259] C.S. Bürgisser, A.T. Stone, Determination of EDTA, NTA, and Other Amino Carboxylic Acids and Their Co(II) and Co(III) Complexes by Capillary Electrophoresis, *Environ. Sci. Technol.* 31 (1997) 2656–2664.
doi:10.1021/es970080f.

[260] C.H. Langford, P.O. Langford, Sulfone Ligands in Cobalt(II) Complexes, *Inorg.*

Chem. 1 (1962) 184–185. doi:10.1021/ic50001a037.

- [261] S. Amrose, A. Gadgil, V. Srinivasan, K. Kowolik, M. Muller, J. Huang, R. KostECKI, 6. Arsenic removal from groundwater using iron electrocoagulation: effect of charge dosage rate., *J. Environ. Sci. Health. A. Tox. Hazard. Subst. Environ. Eng.* 48 (2013) 1019–30. doi:10.1080/10934529.2013.773215.
- [262] G.G. Clifford DA, Metal-Oxide Adsorption, Ion Exchange, and Coagulation–Microfiltration for Arsenic Removal from Water. In: Frankenberger WT (ed) *Environmental Chemistry of Arsenic*, First, Marcel Dekker, Inc., New York, n.d.
- [263] L. Dambies, R. Salinaro, S.D. Alexandratos, Immobilized N-methyl-D-glucamine as an arsenate-selective resin, *Environ. Sci. Technol.* 38 (2004) 6139–6146. doi:10.1021/es040312s.
- [264] L. Toledo, R. BL, U. BF, J. Sanchez, Novel N-methyl-D-glucamine-based water-soluble polymer and its potential application in the removal of arsenic, *Sep. Purif. Technol.* 103 (2013) 1–7. doi:10.1016/j.seppur.2012.10.022.
- [265] L. Järup, A. Åkesson, Current status of cadmium as an environmental health problem, *Toxicol. Appl. Pharmacol.* 238 (2009) 201–208. doi:10.1016/j.taap.2009.04.020.
- [266] J.L. Peters, T.S. Perlstein, M.J. Perry, E. McNeely, J. Weuve, Cadmium exposure in association with history of stroke and heart failure, *Environ. Res.* 110 (2010) 199–206. doi:10.1016/j.envres.2009.12.004.
- [267] Z. Carmen, S. Daniel, Textile Organic Dyes – Characteristics, Polluting Effects and Separation/Elimination Procedures from Industrial Effluents – A Critical Overview, in: *Org. Pollut. Ten Years After Stock. Conv. - Environ. Anal. Updat.*,

InTech, 2012. doi:10.5772/32373.

- [268] Y. Fu, T. Viraraghavan, Fungal decolorization of dye wastewaters: a review, *Bioresour. Technol.* 79 (2001) 251–262. doi:10.1016/S0960-8524(01)00028-1.
- [269] M.A.M. Martins, N. Lima, A.J.D. Silvestre, M.J. Queiroz, Comparative studies of fungal degradation of single or mixed bioaccessible reactive azo dyes, *Chemosphere.* 52 (2003) 967–973. doi:10.1016/S0045-6535(03)00286-8.
- [270] Y.-C. Toh, J.J.L. Yen, J.P. Obbard, Y.-P. Ting, Decolourisation of azo dyes by white-rot fungi (WRF) isolated in Singapore, *Enzyme Microb. Technol.* 33 (2003) 569–575. doi:10.1016/S0141-0229(03)00177-7.
- [271] S.K. Das, X. Wang, M.M. Ostwal, Z. Lai, A highly stable microporous covalent imine network adsorbent for natural gas upgrading and flue gas CO₂ capture, *Sep. Purif. Technol.* 170 (2016) 68–77. doi:10.1016/j.seppur.2016.06.016.
- [272] J.S. Beck, J.C. Vartuli, W.J. Roth, M.E. Leonowicz, C.T. Kresge, K.D. Schmitt, C.T.W. Chu, D.H. Olson, E.W. Sheppard, S.B. McCullen, J.B. Higgins, J.L. Schlenker, A new family of mesoporous molecular sieves prepared with liquid crystal templates, *J. Am. Chem. Soc.* 114 (1992) 10834–10843. doi:10.1021/ja00053a020.
- [273] X. Feng, G.E. Fryxell, L.-Q. Wang, A.Y. Kim, J. Liu, K.M. Kemner, Functionalized Monolayers on Ordered Mesoporous Supports, *Science* (80-.). 276 (1997) 923 LP-926. <http://science.sciencemag.org/content/276/5314/923.abstract>.
- [274] C. Delacôte, F.O.M. Gaslain, B. Lebeau, A. Walcarius, Factors affecting the reactivity of thiol-functionalized mesoporous silica adsorbents toward mercury(II), *Talanta.* 79 (2009) 877–886. doi:10.1016/j.talanta.2009.05.020.

- [275] B.E. Johnson, P.H. Santschi, R. Shane Addleman, M. Douglas, J.D. Davidson, G.E. Fryxell, J.M. Schwantes, Collection of fission and activation product elements from fresh and ocean waters: A comparison of traditional and novel sorbents, *Appl. Radiat. Isot.* 69 (2011) 205–216.
doi:10.1016/j.apradiso.2010.07.025.
- [276] T. Sangvanich, V. Sukwarotwat, R.J. Wiacek, R.M. Grudzien, G.E. Fryxell, R.S. Addleman, C. Timchalk, W. Yantasee, Selective capture of cesium and thallium from natural waters and simulated wastes with copper ferrocyanide functionalized mesoporous silica, *J. Hazard. Mater.* 182 (2010) 225–231.
doi:10.1016/j.jhazmat.2010.06.019.
- [277] W. Yantasee, R.D. Rutledge, W. Chouyyok, V. Sukwarotwat, G. Orr, C.L. Warner, M.G. Warner, G.E. Fryxell, R.J. Wiacek, C. Timchalk, R.S. Addleman, Functionalized Nanoporous Silica for the Removal of Heavy Metals from Biological Systems: Adsorption and Application, *ACS Appl. Mater. Interfaces.* 2 (2010) 2749–2758. doi:10.1021/am100616b.
- [278] S.J. Netzer L, ω -Hexadecenyltrichlorosilane has proven to be a useful, modifiable, siloxy-anchored amphiphile, *J Am Chem Soc.* 105 (1983) 674–676.
- [279] M. Mihai, S. Schwarz, A. Janke, C.A. Ghiorghiță, E.S. Drăgan, Silica microparticles surface coating by layer-by-layer or polyelectrolyte complex adsorption, *J. Polym. Res.* 20 (2013). doi:10.1007/s10965-013-0089-5.
- [280] S.M. Mahltig B, Gohy J-F, Jérôme R, Pfütze G, Desorption behaviour of regular adsorbed polyampholytic layers, *J Polym Res.* 10 (2003) 69–77.
- [281] E.S. Dragan, S. Schwarz, K.-J. Eichhorn, Specific effects of the counterion type and concentration on the construction and morphology of polycation/azo dye

multilayers, *Colloids Surfaces A Physicochem. Eng. Asp.* 372 (2010) 210–216.
doi:10.1016/j.colsurfa.2010.10.023.

- [282] N. Joseph, P. Ahmadiannamini, R. Hoogenboom, I.F.J. Vankelecom, Layer-by-layer preparation of polyelectrolyte multilayer membranes for separation, *Polym. Chem.* 5 (2014) 1817–1831. doi:10.1039/C3PY01262J.
- [283] P.T. Hammond, Form and Function in Multilayer Assembly: New Applications at the Nanoscale, *Adv. Mater.* 16 (2004) 1271–1293. doi:10.1002/adma.200400760.
- [284] A. Yamaguchi, Y. Maeda, H. Yokoyama, A. Yoshizawa, Self-assembly of amphiphilic liquid-crystalline oligomers possessing a semiperfluorinated alkyl chain, *Chem. Mater.* 18 (2006) 5704–5710. doi:10.1021/cm061606a.
- [285] D. Zhao, Q. Huo, J. Feng, B.F. Chmelka, G.D. Stucky, Tri-, Tetra-, and Octablock Copolymer and Nonionic Surfactant Syntheses of Highly Ordered, Hydrothermally Stable, Mesoporous Silica Structures, *J. Am. Chem. Soc.* 120 (1998) 6024–6036. doi:Doi 10.1021/Ja974025i.
- [286] B. HP, Chemical identification of surface groups., in: Eley, W.P.B. DD, Pines Herman (Eds.), *Adv. Catal.*, Academic Press, 1966: pp. 179–274.
- [287] D. Zhao, J. Feng, Q. Huo, N. Melosh, G.H. Fredrickson, B.F. Chmelka, G.D. Stucky, Triblock Copolymer Syntheses of Mesoporous Silica with Periodic 50 to 300 Angstrom Pores, *Science* (80-.). 279 (1998) 548 LP-552.
<http://science.sciencemag.org/content/279/5350/548.abstract>.
- [288] Boehm H. P., Some aspects of the surface-chemistry of carbonblacks and other carbons, *Carbon N. Y.* 32 (1994) 759–69.

- [289] A. Salis, D.F. Parsons, M. Boström, L. Medda, B. Barse, B.W. Ninham, M. Monduzzi, Ion specific surface charge density of SBA-15 mesoporous silica, *Langmuir*. 26 (2010) 2484–2490. doi:10.1021/la902721a.
- [290] S. Leonardelli, L. Facchini, C. Fretigny, P. Tougne, A.P. Legrand, Silicon-29 NMR study of silica, *J. Am. Chem. Soc.* 114 (1992) 6412–6418. doi:10.1021/ja00042a018.
- [291] D.W. Sindorf, G.E. Maciel, Silicon-29 CP/MAS NMR studies of methylchlorosilane reactions on silica gel, *J. Am. Chem. Soc.* 103 (1981) 4263–4265. doi:10.1021/ja00404a055.
- [292] G.E. Michael, D.W. Sindorf, V.J. Bartuska, Characterization of silica-attached systems by ²⁹Si and ¹³C cross-polarization and magic-angle spinning nuclear magnetic resonance, 1981. doi:10.1016/S0021-9673(00)82673-4.
- [293] A.P. Legrand, H. Hommel, H. Taïbi, J.L. Miquel, P. Tougne, Contribution of solid state NMR spectroscopy to the characterization of materials, *Colloids and Surfaces*. 45 (1990) 391–411. doi:10.1016/0166-6622(90)80039-7.
- [294] G.E. Maciel, D.W. Sindorf, Silicon-29 NMR study of the surface of silica gel by cross polarization and magic-angle spinning, *J. Am. Chem. Soc.* 102 (1980) 7606–7607. doi:10.1021/ja00545a056.
- [295] D.W. Sindorf, G.E. Maciel, Silicon-29 NMR study of dehydrated/rehydrated silica gel using cross polarization and magic-angle spinning, *J. Am. Chem. Soc.* 105 (1983) 1487–1493. doi:10.1021/ja00344a012.
- [296] T. Yasmin, K. Müller, Synthesis and characterization of surface modified SBA-15 silica materials and their application in chromatography, *J. Chromatogr. A*. 1218

(2011) 6464–6475. doi:10.1016/j.chroma.2011.07.035.

- [297] A. Sakthivel, J. Zhao, F.E. Kühn, Grafting of the η^5 -CpMo(CO)₃ moiety on pure and surface modified SBA-15 molecular sieves, *Microporous Mesoporous Mater.* 86 (2005) 341–348. doi:10.1016/j.micromeso.2005.07.042.
- [298] A. Grünberg, X. Yeping, H. Breitzke, G. Buntkowsky, Solid-state NMR characterization of Wilkinson's catalyst immobilized in mesoporous SBA-3 silica., *Chemistry*. 16 (2010) 6993–8. doi:10.1002/chem.200903322.
- [299] J.C. Groen, L.A. Peffer, J. Pérez-Ramírez, Pore size determination in modified micro- and mesoporous materials. Pitfalls and limitations in gas adsorption data analysis, *Microporous Mesoporous Mater.* 60 (2003) 1–17. doi:10.1016/S1387-1811(03)00339-1.
- [300] C. Jaroniec, R. Gilpin, M. Jaroniec, Adsorption and thermogravimetric studies of silica-based amide bonded phases, *J. Phys.* 44242 (1997) 6861–6866. doi:10.1021/jp964002a J.
- [301] R.K. Iler, *The Chemistry of Silica: Solubility, Polymerization, Colloid and Surface Properties and Biochemistry of Silica*, John Wiley, New York, n.d.
- [302] Z.A. Jamiu, T.A. Saleh, S.A. Ali, Biogenic glutamic acid-based resin: Its synthesis and application in the removal of cobalt(II), *J. Hazard. Mater.* 327 (2017) 44–54. doi:10.1016/j.jhazmat.2016.12.041.
- [303] F. Ciesielczyk, P. Bartczak, T. Jesionowski, Removal of cadmium(II) and lead(II) ions from model aqueous solutions using sol--gel-derived inorganic oxide adsorbent, *Adsorption*. 22 (2016) 445–458. doi:10.1007/s10450-015-9703-7.

- [304] K.K. Singh, R. Rastogi, S.H. Hasan, Removal of cadmium from wastewater using agricultural waste “rice polish,” *J. Hazard. Mater.* 121 (2005) 51–58.
doi:10.1016/j.jhazmat.2004.11.002.
- [305] T. Sheela, Y.A. Nayaka, R. Viswanatha, S. Basavanna, T.G. Venkatesha, Kinetics and thermodynamics studies on the adsorption of Zn (II), Cd (II) and Hg (II) from aqueous solution using zinc oxide nanoparticles, *Powder Technol.* 217 (2012) 163–170. doi:10.1016/j.powtec.2011.10.023.
- [306] B.H. Afkhami A, Tehrani MS, Simultaneous removal of heavy metal ions in wastewater samples using nano-alumina modified with 2,4-dinitrophenylhydrazine., *J Hazard Mater.* 1–3 (2010) 836–844.
- [307] A. Roy, J. Bhattacharya, A binary and ternary adsorption study of wastewater Cd(II), Ni(II) and Co(II) by γ -Fe₂O₃ nanotubes, *Sep. Purif. Technol.* 115 (2013) 172–179. doi:10.1016/j.seppur.2013.05.010.
- [308] H. Karami, Heavy metal removal from water by magnetite nanorods, *Chem. Eng. J.* 219 (2013) 209–216. doi:10.1016/j.cej.2013.01.022.
- [309] J. Gong, L. Chen, G. Zeng, F. Long, J. Deng, Q. Niu, X. He, Shellac-coated iron oxide nanoparticles for removal of cadmium(II) ions from aqueous solution, *J. Environ. Sci.* 24 (2012) 1165–1173. doi:10.1016/S1001-0742(11)60934-0.
- [310] A. Roy, J. Bhattacharya, A binary and ternary adsorption study of wastewater Cd (II), Ni (II) and Co (II) by γ -Fe₂O₃ nanotubes, *Sep. Purif. Technol.* 115 (2013) 172–179. doi:10.1016/j.seppur.2013.05.010.

Vitae

Name :Zakariyah Abdulkareem Jamiu

Nationality :Nigerian

Date of Birth :5/6/1980

Email :gurfatan@gmail.com

Address :Click here to enter text.

Academic Background :

PhD **Chemistry**, King Fahd University of Petroleum & Minerals 2012 –2017

Dissertation: Multilayered Polyelectrolyte-coated Silica for the Removal of Toxic Metal Ions and Organic Contaminants: A Novel Protocol

MSc. **Chemistry**, King Fahd University of Petroleum & Minerals 2009 –2012

Dissertation: Preparation, Characterization and Hydrodesulfurization (HDS) activity of Mo-SBA-15 catalyst with increased and well dispersed Mo species

BSc. **Applied Chemistry**, University of Jos, Jos- Nigeria. 1999 -2004

Dissertation: Investigation of Anti-oxidative and free radical scavenging properties of two local medicinal plants used in the cure of Jaundice

List of Publications

1. **Z. A. Jamiu**, H. A. Al-muallem & S. A. Ali, Aspartic acid in a new role: Synthesis and application of a pH-responsive cyclopolymer containing residues of the amino acid, **Reactive and Functional Polymers** 93 (2015) 120–129.
2. **Z. A. Jamiu**, T. A. Saleh & S. A. Ali, Synthesis of a unique cross-linked polyzwitterion/anion with an aspartic acid residue and its use for Pb²⁺ removal from aqueous solution, **RSC Adv.**, 2015, 5, 42222-42232.
3. Ali, S.A. & **Jamiu, Z.A**, Poly(N,N-diallylaspartic acid-alt-sulfur dioxide): its synthesis and application, **Polym. Bull.** (2016) 73: 2179. doi:10.1007/s00289-016-1602-x.
4. **Z. A. Jamiu**, H. A. Al-Muallem & S. A. Ali, A glutamic acid-based polymer keeping intact the integrity of all the three original functionalities of the amino acid, **Designed Monomers and Polymers**, 2016, (19) 2, 128-137.
5. **Z. A. Jamiu**, S. A. Ali, Alternate cyclopolymer of diallylglutamic acid and sulfur dioxide, **RSC Adv.**, 2016, **6**, 31019-31030.
6. **Z. A. Jamiu**, T. A. Saleh, S. A. Ali, Biogenic Glutamic Acid-based Resin: Its Synthesis and Application in the Removal of Cobalt(II), **Journal of Hazardous Materials**. 327 (2017) 44–54.

Patent

Z. A. Jamiu, T. A. Saleh & S. A. Ali. 2016. Crosslinked polyzwitterion/anion with aspartic acid residue for Pb^{2+} sorption from aqueous solution. US Patent 9,480,979 B1, **issued** Nov. 1, 2016.

Conference

Z. A. Jamiu, S. A. Ali, (2016, Nov.). New Glutamic Acid-derived Resin: Its Synthesis and Application in Remediation of a Model Cobalt Wastewater. Oral session presented at “The 10th International Conference and Exhibition on Chemistry in Industry”, Environmental Issues & Solutions, ChemIndix 2016, Manama, Bahrain|